CAPACI OCCASIO
FOUNDED 1894

SAIMM

THE SOUTHERN AFRICAN INSTITUTE OF MINING AND METALLURGY

VOLUME 121 NO. 5 MAY 2021

ELBROC
MINING PRODUCTS (PTY) LTD

TH ARCH SUPPORT SYSTEMS

PROFILE SETS

Ring Set

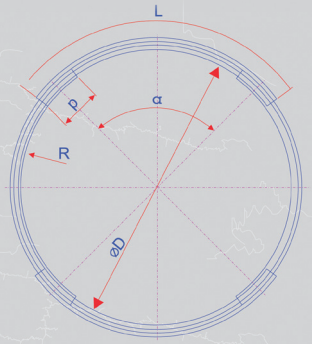

Semi Arch Set

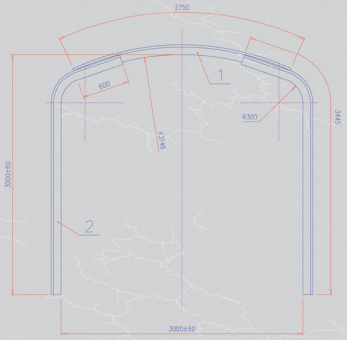

Half Arch Set

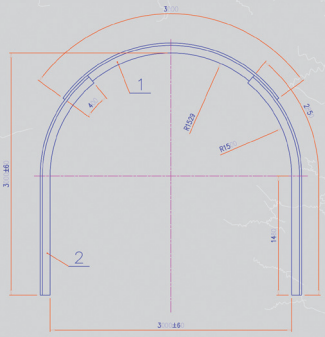

PRODUCTION CAPABILITIES:

- Standard arch lengths from 1.8m to 5.5m
- Minimal curvature R 1000mm, at R 1200mm at R 1600mm

APPLICATIONS

- Tunnel junctions
- Over and under ore passes
- Haulage
- Incline shaft portals
- Active support through bad ground conditions, dykes, faults, friable ground

BENEFITS

- Simple and fast installation
- High load carrying capacity
- Long operational life
- Suitable for tunnels from 4.15m to 5.5m wide
- Upright support beams cater for tunnel heights from 3.1 to 6.5m
- Cost effective
- Dimensional and design flexibility

OMNI 150

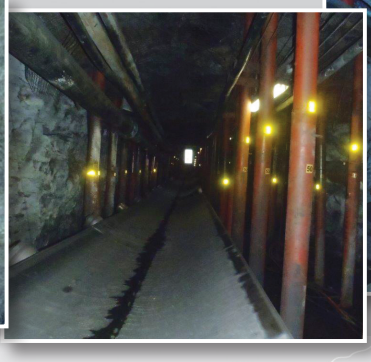

APPLICATIONS

- Tunnel support
- Pillar rehabilitation
- Set construction on friable ground
- Active blast on support
- Used with backfill
- Travelling ways, mono ways and winch chambers

BENEFITS AND FEATURES

- Provides active roof support with controlled yielding
- Working load set to customer requirements (8 to 45 ton)
- Resilient in rockburst conditions
- Superb energy absorption
- Can accommodate numerous seismic events
- Constant and consistent support resistance
- Light, easy and quick to install
- Safe remote installation
- Cannot be over extended
- Reusable versions available on request
- Standard lengths available to 6 meters
- Longer lengths available on request

SABS ISO 9001

a member of the rbh royal bafokeng holdings

TO VIEW OUR FULL RANGE OF TUNNEL SUPPORT PLEASE VISIT OUR WEBPAGE

Tel: +27 010 534 5174 • sales@elbroc.co.za
www.elbroc.co.za

mogs

OFFICE BEARERS AND COUNCIL FOR THE 2020/2021 SESSION

Honorary President

Mxolisi Mgojo
President, Minerals Council South Africa

Honorary Vice Presidents

Gwede Mantashe
Minister of Mineral Resources, South Africa

Ebrahim Patel
Minister of Trade, Industry and Competition, South Africa

Blade Nzimande
Minister of Higher Education, Science and Technology, South Africa

President

V.G. Duke

President Elect

I.J. Geldenhuys

Senior Vice President

Z. Botha

Junior Vice President

W.C. Joughin

Incoming Junior Vice President

E Matinde

Immediate Past President

M.I. Mthenjane

Co-opted to Office Bearers

S. Ndlovu
G.R. Lane

Honorary Treasurer

W.C. Joughin

Ordinary Members on Council

B. Genc
G.R. Lane
K.M. Letsoalo
T.M. Mmola
G. Njowa
S.J. Ntsoelengoe
S.M. Rupprecht
N. Singh
A.G. Smith
M.H. Solomon
A.J.S. Spearing
S.J. Tose
M.I. van der Bank
A.T. van Zyl
E.J. Walls

Co-opted Members

Z. Fakhraei

Past Presidents Serving on Council

N.A. Barcza
R.D. Beck
J.R. Dixon
H.E. James
R.T. Jones
A.S. Macfarlane
C. Musingwini
S. Ndlovu
J.L. Porter
S.J. Ramokgopa
M.H. Rogers
D.A.J. Ross-Watt
G.L. Smith
W.H. van Niekerk

G.R. Lane–TPC Mining Chairperson
Z. Botha–TPC Metallurgy Chairperson

S.F. Manjengwa–YPC Chairperson
A.T. Chinhava–YPC Vice Chairperson

Branch Chairpersons

Johannesburg D.F. Jensen
Namibia N.M. Namate
Northern Cape I. Lute
Pretoria S. Uludag
Western Cape A.B. Nesbitt
Zambia D. Muma
Zimbabwe C.P. Sadomba
Zululand C.W. Mienie

PAST PRESIDENTS

*Deceased

* W. Bettel (1894–1895)
* A.F. Crosse (1895–1896)
* W.R. Feldtmann (1896–1897)
* C. Butters (1897–1898)
* J. Loevy (1898–1899)
* J.R. Williams (1899–1903)
* S.H. Pearce (1903–1904)
* W.A. Caldecott (1904–1905)
* W. Cullen (1905–1906)
* E.H. Johnson (1906–1907)
* J. Yates (1907–1908)
* R.G. Bevington (1908–1909)
* A. McA. Johnston (1909–1910)
* J. Moir (1910–1911)
* C.B. Saner (1911–1912)
* W.R. Dowling (1912–1913)
* A. Richardson (1913–1914)
* G.H. Stanley (1914–1915)
* J.E. Thomas (1915–1916)
* J.A. Wilkinson (1916–1917)
* G. Hildick-Smith (1917–1918)
* H.S. Meyer (1918–1919)
* J. Gray (1919–1920)
* J. Chilton (1920–1921)
* F. Wartenweiler (1921–1922)
* G.A. Watermeyer (1922–1923)
* F.W. Watson (1923–1924)
* C.J. Gray (1924–1925)
* H.A. White (1925–1926)
* H.R. Adam (1926–1927)
* Sir Robert Kotze (1927–1928)
* J.A. Woodburn (1928–1929)
* H. Pirow (1929–1930)
* J. Henderson (1930–1931)
* A. King (1931–1932)
* V. Nimmo-Dewar (1932–1933)
* P.N. Lategan (1933–1934)
* E.C. Ranson (1934–1935)
* R.A. Flugge-De-Smidt (1935–1936)
* T.K. Prentice (1936–1937)
* R.S.G. Stokes (1937–1938)
* P.E. Hall (1938–1939)
* E.H.A. Joseph (1939–1940)
* J.H. Dobson (1940–1941)
* Theo Meyer (1941–1942)
* John V. Muller (1942–1943)
* C. Biccard Jeppe (1943–1944)
* P.J. Louis Bok (1944–1945)
* J.T. McIntyre (1945–1946)
* M. Falcon (1946–1947)
* A. Clemens (1947–1948)
* F.G. Hill (1948–1949)
* O.A.E. Jackson (1949–1950)
* W.E. Gooday (1950–1951)
* C.J. Irving (1951–1952)
* D.D. Stitt (1952–1953)
* M.C.G. Meyer (1953–1954)
* L.A. Bushell (1954–1955)
* H. Britten (1955–1956)
* Wm. Bleloch (1956–1957)
* H. Simon (1957–1958)
* M. Barcza (1958–1959)
* R.J. Adamson (1959–1960)
* W.S. Findlay (1960–1961)
* D.G. Maxwell (1961–1962)
* J. de V. Lambrechts (1962–1963)
* J.F. Reid (1963–1964)
* D.M. Jamieson (1964–1965)
* H.E. Cross (1965–1966)
* D. Gordon Jones (1966–1967)
* P. Lambooy (1967–1968)
* R.C.J. Goode (1968–1969)
* J.K.E. Douglas (1969–1970)
* V.C. Robinson (1970–1971)
* D.D. Howat (1971–1972)
* J.P. Hugo (1972–1973)
* P.W.J. van Rensburg (1973–1974)
* R.P. Plewman (1974–1975)
* R.E. Robinson (1975–1976)
* M.D.G. Salamon (1976–1977)
* P.A. Von Wielligh (1977–1978)
* M.G. Atmore (1978–1979)
* D.A. Viljoen (1979–1980)
* P.R. Jochens (1980–1981)
* G.Y. Nisbet (1981–1982)
  A.N. Brown (1982–1983)
* R.P. King (1983–1984)
  J.D. Austin (1984–1985)
  H.E. James (1985–1986)
  H. Wagner (1986–1987)
* B.C. Alberts (1987–1988)
* C.E. Fivaz (1988–1989)
* O.K.H. Steffen (1989–1990)
* H.G. Mosenthal (1990–1991)
  R.D. Beck (1991–1992)
* J.P. Hoffman (1992–1993)
* H. Scott-Russell (1993–1994)
  J.A. Cruise (1994–1995)
  D.A.J. Ross-Watt (1995–1996)
  N.A. Barcza (1996–1997)
* R.P. Mohring (1997–1998)
  J.R. Dixon (1998–1999)
  M.H. Rogers (1999–2000)
  L.A. Cramer (2000–2001)
* A.A.B. Douglas (2001–2002)
  S.J. Ramokgopa (2002-2003)
  T.R. Stacey (2003–2004)
  F.M.G. Egerton (2004–2005)
  W.H. van Niekerk (2005–2006)
  R.P.H. Willis (2006–2007)
  R.G.B. Pickering (2007–2008)
  A.M. Garbers-Craig (2008–2009)
  J.C. Ngoma (2009–2010)
  G.V.R. Landman (2010–2011)
  J.N. van der Merwe (2011–2012)
  G.L. Smith (2012–2013)
  M. Dworzanowski (2013–2014)
  J.L. Porter (2014–2015)
  R.T. Jones (2015–2016)
  C. Musingwini (2016–2017)
  S. Ndlovu (2017–2018)
  A.S. Macfarlane (2018–2019)
  M.I. Mthenjane (2019–2020)

Honorary Legal Advisers
MH Attorneys

Auditors
Genesis Chartered Accountants

Secretaries
The Southern African Institute of Mining and Metallurgy
Fifth Floor, Minerals Council South Africa
5 Hollard Street, Johannesburg 2001 • P.O. Box 61127, Marshalltown 2107
Telephone (011) 834-1273/7 • Fax (011) 838-5923 or (011) 833-8156
E-mail: journal@saimm.co.za

Typeset and Published by

The Southern African Institute of Mining and Metallurgy
P.O. Box 61127
Marshalltown 2107
Telephone (011) 834-1273/7
Fax (011) 838-5923
E-mail: journal@saimm.co.za

Printed by

Camera Press, Johannesburg

Advertising Representative

Barbara Spence
Avenue Advertising
Telephone (011) 463-7940
E-mail: barbara@avenue.co.za

ISSN 2225-6253 (print)
ISSN 2411-9717 (online)

SAIMM
JOURNAL OF THE SOUTHERN AFRICAN INSTITUTE OF MINING AND METALLURGY

VOLUME 121 NO. 5 MAY 2021

Contents

PROFESSIONAL TECHNICAL AND SCIENTIFIC PAPERS

This paper presents three technological scenarios for the recovery of a marketable product (iron-containing pellets) from gangue stored in the tailings dam at Kremikovtzi metallurgical plant in Bulgaria, using various combinations of flotation, magnetic separation, magnetic flocculation, and roasting. The iron concentrate from each process was subjected to pelletizing in a laboratory-scale pelletizer. Each technology was assessed with respect to the mass yield of concentrate, iron recovery, and the iron, lead, and zinc contents of the concentrate in order to establish the most effective route.

Silicon Smelters (Pty) Ltd (South Africa) consumes more than 80 000 t/a of wood derived charcoal as carbon reductant in the production of silicon metal. More than 10% of this material is discarded as fines (<6 mm) due to abrasion during processing. Charcoal fines residue (<650 µm) and polyvinyl alcohol (PVA) binder were used in this study to produce mechanically strong charcoal briquettes for metallurgical application. Key properties were investigated, and the results compared with metallurgical grade coarse charcoal. The produced briquettes were found to have a lower resistance to abrasion and drop-shattering than the coarse charcoal, but better compressive strength and water resistance.

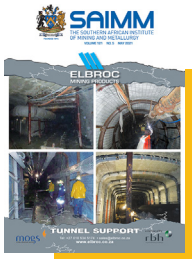

PROFESSIONAL TECHNICAL AND SCIENTIFIC PAPERS

Leaders who rescue projects from destruction

Foreign-based companies now control most of South Africa's largest mining and metallurgical projects. This has had both positive and negative consequences. The success of Anglo American's Kumba iron ore project is one example of the contribution which foreign-based firms can bring to the South African mining industry, and Vedanta's revival of the moribund Gamsberg zinc project is another.

However, when companies are owned offshore it is inevitable that foreign interests must prevail over South African interests. Foreign-owned companies are subject to the dictates of their shareholders and, as a consequence, they decide what their core businesses are and in which countries and in which projects they are prepared to invest. Thus, when Anglo American decided that their core business was mining and, therefore, they needed to dispose of all their South African industrial assets, it had a devastating effect on the local and national economy.

It has been left to dedicated leaders to save what remains of projects that have been abandoned by foreign-owned companies. These people and domestically owned companies seldom receive the recognition they deserve – they are the true heroes of South Africa's mining and metallurgical industries.

Two outstanding examples are the restart of the mill at Highveld Steel after the former Anglo American company had been sold to Russian-owned Evraz and was subsequently liquidated after many years of losses, and Manganese Metal Company, which was sold by BHP Billiton and continues to survive – and thrive as world leader – despite being based on a highly power-intensive process.

Let us salute and support the leaders whose patriotic commitment and passion have saved valuable national projects from destruction despite all the odds stacked against them.

I. Robinson

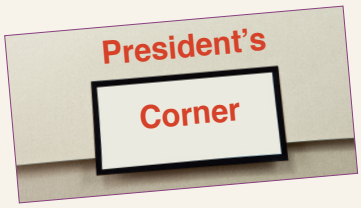

Are we facing a long-term commodity boom?

'The truth is never pure and rarely simple' – Oscar Wild

The S&P GSCI Industrial Metals Index has increased by over 86% since March 2020. The London Metal Exchange (LME) Index, which comprises aluminium (42.8%), copper (31.2%), zinc (14.8%), lead (8.2%), nickel (2%), and tin (1%), is also up by some 90% over the same periodsince March 2020. These are large jumps and one can see why our media have been speculating on the prospects of a 'super-cycle'.

A super-cycle could be described as a period of demand that remains above the overall trend for a material amount of time, and which producers find difficult to meet. Commodity prices then increase, and this can last for many years before oversupply kicks in as a consequence of miners producing more.

These types of cycles are uncommon, and only four appear to have occurred since the early 1900s.

- The first was a consequence of the industrialization in the USA over a relatively short period following 1910.
- The second started with countries re-arming prior to and during the Second World War, and continued during the rebuilding of both Europe and Japan during the 1950s and 1960s.
- The third cycle followed in the early 1970s in response to strong economic growth and increased prices for materials through to the early 1980s. Demand was high, but supply was disrupted as mines were nationalized and new investments dried up.
- The fourth and latest super-cycle started in the early 2000s when China began to modernize its economy after joining the World Trade Organization. Industrialization occurred on an unprecedented scale, together with a building boom as workers migrated to cities.

Each of the above phenomena can be linked to a large shift in global economics, and today a combination of the 2008 financial crises, Covid-19 pandemic, and fourth industrial revolution (4IR) could be the reason for the current debate.

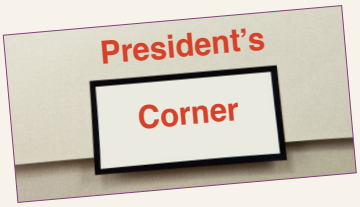

Are we facing a long-term commodity boom? *(continued)*

The financial crisis of 2008 disrupted the fourth super-cycle when cash was suddenly pulled out of the system. Some of the money, already committed to projects underway, was released, but most was held back as further investments were curtailed. In addition, economic stimulus by China supported demand for only a little longer before prices started to fall again around 2012.

Capacity had, however, already increased by 2008 when we saw a build-up in inventories. Markets then traded sideways for a long time. Excess stock was consumed and we are now once again seeing a situation where above average demand is outstripping supply.

We often see commodity prices rising with inflation. Zero interest rates and low inflation have prevailed since 2008, but now fiscal stimulus and a weaker US dollar are likely to again fuel inflation. This may cause investors to hedge their positions by turning to commodities.

Then along came the Covid-19 pandemic, which may well be the catalyst for the next super-cycle. It has significantly accelerated the rate at which 4IR is changing the way we work and live around the globe. At the same time, it has impeded production globally. Covid-19 is also behind the significant economic stimulation packages recently announced. Large portions of this money will be used to support pledges by governments and private companies around the globe to strive for a net-zero carbon economy by the middle of this century (the green energy revolution). This expenditure is likely to occur over an extended period of time.

High demand, and these disruptions, could arguably drive certain commodity prices well into the future. Copper and other base metals will be needed for green energy infrastructure, while nickel, cobalt, lithium (for high-performance batteries), and aluminium (to reduce weight) will benefit from the continued rollout of electric vehicles. Of particular interest to our members is the role that PGMs and vanadium are destined to play in our re-engineered future, with the Bushveld Complex hosting one of the world's treasure troves of these great metals.

On the other hand, uncertainty prevails. The recent and dramatic increases in demand for commodities may well last for only a short period. Any increase in the cost of transporting commodities to market would reduce prices, and cash flow volatility is always a concern. Recent cash flows into gold have already started to reverse, and this shows how quickly cash can flow back out again.

Clarity and understanding come with hindsight, and this is also true for super-cycles. Increased demand, fiscal stimulus, and government spending may well support a super-cycle, but many of my associates believe that it is simply too early to call and that we won't really know until after the fact.

The only certainty is uncertainty. As our Chinese friends say: 'may you live in interesting times'. Brace yourselves, dear colleagues, for the rollercoaster ride of your lives!

V.G. Duke
President, SAIMM

Technological research on converting iron ore tailings into a marketable product

I. Mitov[1], A. Stoilova[1,2], B. Yordanov[1], and D. Krastev[1]

Affiliation:
[1] University of Chemical Technology and Metallurgy, Sofia, Bulgaria.
[2] Institute of Optical Materials and Technology – Bulgarian Academy of Sciences, Sofia, Bulgaria.

Correspondence to:
A. Stoilova

Email:
ani_st@web.de

Dates:
Received: 12 Jul. 2020
Revised: 7 Feb. 2021
Accepted: 10 Feb. 2021
Published: May 2021

How to cite:
Mitov, I., Stoilova, A., Yordanov, B., and Krastev, D. 2021 Technological research on converting iron ore tailings into a marketable product. Journal of the Southern African Institute of Mining and Metallurgy, vol. 121, no. 5, pp. 181–186.

DOI ID:
http://dx.doi.org/10.17159/2411-9717/1273/2021

ORCID
A. Stoilova
https://orchid.org/ 0000-0001-8357-3303

Synopsis

We present three technological scenarios for the recovery of valuable components from gangue, stored in the tailings dam at Kremikovtzi metallurgical plant in Bulgaria, into marketable iron-containing pellets. In the first approach the iron concentrate was recovered through a two-stage flotation process, desliming, and magnetic separation. In the second proposed process, the iron concentrate was subjected to four sequential stages of magnetic separation coupled with selective magnetic flocculation. The third route entails the not very common practice of magnetizing roasting, followed by selective magnetic flocculation, desliming, and magnetic separation. The iron concentrate was pelletized in a laboratory-scale pelletizer. Each technology has been assessed with regard to the mass yield of iron concentrate, the iron recovery. and the iron, lead, and zinc content in order to identify the most effective route.

Keywords
tailings reprocessing, magnetizing roasting, pelletization.

Introduction

Tailings are the commercially worthless fractions of an ore. Usually, they are stored in the most cost-effective way possible to meet specific environmental regulations. Converting tailings, through reprocessing, into a valuable material represents a profitable field for technological research for mining companies and a viable solution to environmental issues.

Here we used three technological scenarios for the recovery of valuable components from gangue, stored in the tailings dam at Kremikovtzi ore dressing plant in Bulgaria, into marketable iron-containing pellets. The tailings storage facility of the company, which has been closed down, was used for disposal of waste material originating from various manufacturing processes, such as granulated blast-furnace slag, coal-fired power station ash and slag, steelmaking slag, and by-products from ferroalloy and fuel production.

Many approaches have been developed for recovering iron from tailings (Ajaka, 2009; Rao and Narasimhan, 1985; Sakthivel *et al.*, 2010; Li *et al.*, 2010). Usually they couple magnetic separation with selective flocculation. Another method for the beneficiation of the iron ore tailings is magnetizing roasting, which is an energy-intensive process and as such seldom used. However, it offers the advantage of reduction of paramagnetic haematite to ferromagnetic magnetite, which can be recovered by wet low-intensity magnetic separation (Da Corte, Bergmann, and Woollacott, 2019). As shown below, magnetizing roasting could be very helpful if the extracted iron concentrate will be subjected to pelletizing.

Another technology that is being developed for iron recovery from tailings is the production of electrolytic iron. This appears to be an attractive way to produce iron with lower associated CO_2 emissions (Maihatchi *et al.*, 2020). It has the advantage of producing a product of extreme purity, and further of utilizing ores which are not suitable for smelting. The high production cost is a disadvantage, however.

The direct reduction of iron ore to iron using as reductant gas instead of coal is another potential process. The reduction of iron oxides using hydrogen produced via renewable energy has been intensively investigated as a future alternative to the commonly used carbon reducing agents. (Spreitzer and Schenk, 2019). A method for microbial recovery of iron from solid industrial waste has been patented (Hoffmann, Arnold, and Stephanopoulos, 1989). However, none of the 'green' technologies mentioned above can yet match the advantages of the popular blast-furnace technology for recovering iron from mine tailings.

Technological research on converting iron ore tailings into a marketable product

Many researchers have investigated the utilization of iron tailings for production of building materials such as bricks, ceramic tiles, cement, or concrete, microcrystalline glasses, and underground backfill materials (Kuranchie, 2015; Sun, Ren, and Lu, 2010; Das, Kumar, and Ramachandrarao, 2000; Das *et al.*, 2012; Tang *et al.*, 2019, Li and Wang, 2008; Li *et al.*, 2010). A little information about using iron ore tailings for pellet making can be found in the literature. Güngör, Atalay, and Sivrikaya (2011) describe the extraction of magnetite concentrate from tailings through low-intensity magnetic separation, which meets the specifications for pellet making, but the agglomeration process itself has been not carried out. Roy, Das, and Mohanty (2007) present a technology for beneficiating low-grade iron ore slime, sampled in Chitradurga, India, for producing pellet-grade concentrate, together with a detailed investigation of the mineralogical and microstructural characteristics of the iron ore bulk sample and the flotation concentrate. However, pelletizing was not included in the work. In this paper, we aim to present a complete study on processing mine tailings to marketable iron-containing pellets. Three different technological scenarios have been investigated so that the most suitable route can be identified.

Materials and methods

Raw material from the upper 2.5 m horizon of the tailings was sampled, dried at 105°C, classified by hand sieving at 2 mm aperture, and analysed for chemical (Tables I) and mineralogical composition (Figure 1). The chemical composition of the sample, the intermediate products, and the final iron concentrate from each of the three process flow sheets were characterized using classical chemical analytical methods.

Mineralogical characterization

The main mineral constituents of the iron ore tailings, were determined using XRD with a Cu radiation source. The analytical parameters were step size 0.05°, scan time step size 43.6 seconds, and angle interval 5–95° 2θ. As shown in Figure 1, the main minerals in the tailings were magnetite, haematite. and calcite.

Recovery of iron concentrates through two stages of flotation, desliming, and magnetic separation

The first flow sheet applied for processing the tailings comprised sample grinding, flotation of lead, zinc, silver, and organic components, a second (reverse) process of flotation, desliming, and separation of the iron particles at 1800 G magnetic field intensity into an iron concentrate. The sample was milled for 12 minutes to less than 40 µm. The contents of iron, lead, zinc, silver, and carbon in the sample after each operation are shown in Figure 2.

Table I

Chemical composition of the head sample

(a)		(b)	
Component	**Amount**	**Component**	**Amount**
Iron	45.72 (wt.%)	Total organic carbon	5.98 (wt.%)
Lead	1.75 (wt.%)	Total inorganic carbon	1.39 (wt.%)
Silver	53.00 (g/t)	Petroleum products	56.00 (mg/kg)
Zinc	0.84 (wt.%)		

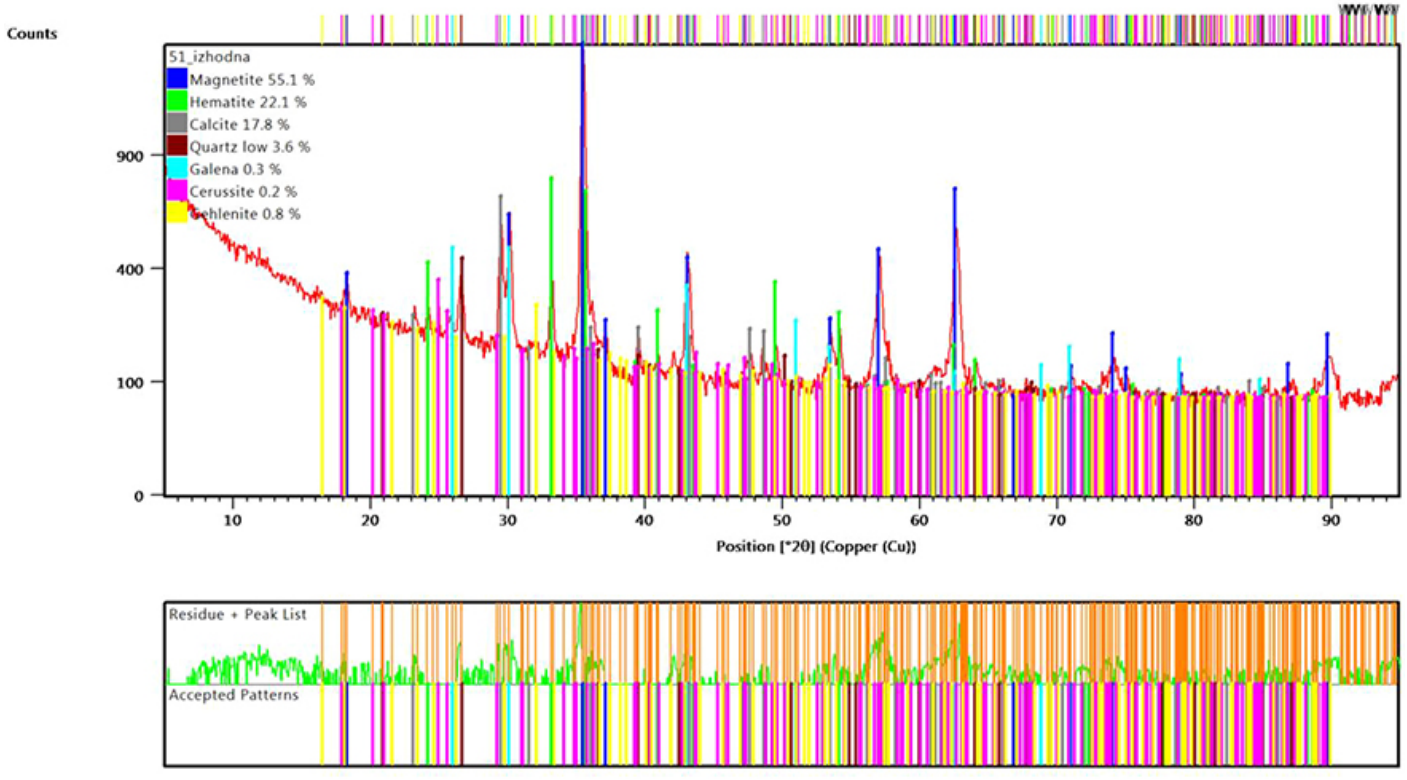

Figure 1—XRD pattern of the iron ore tailings

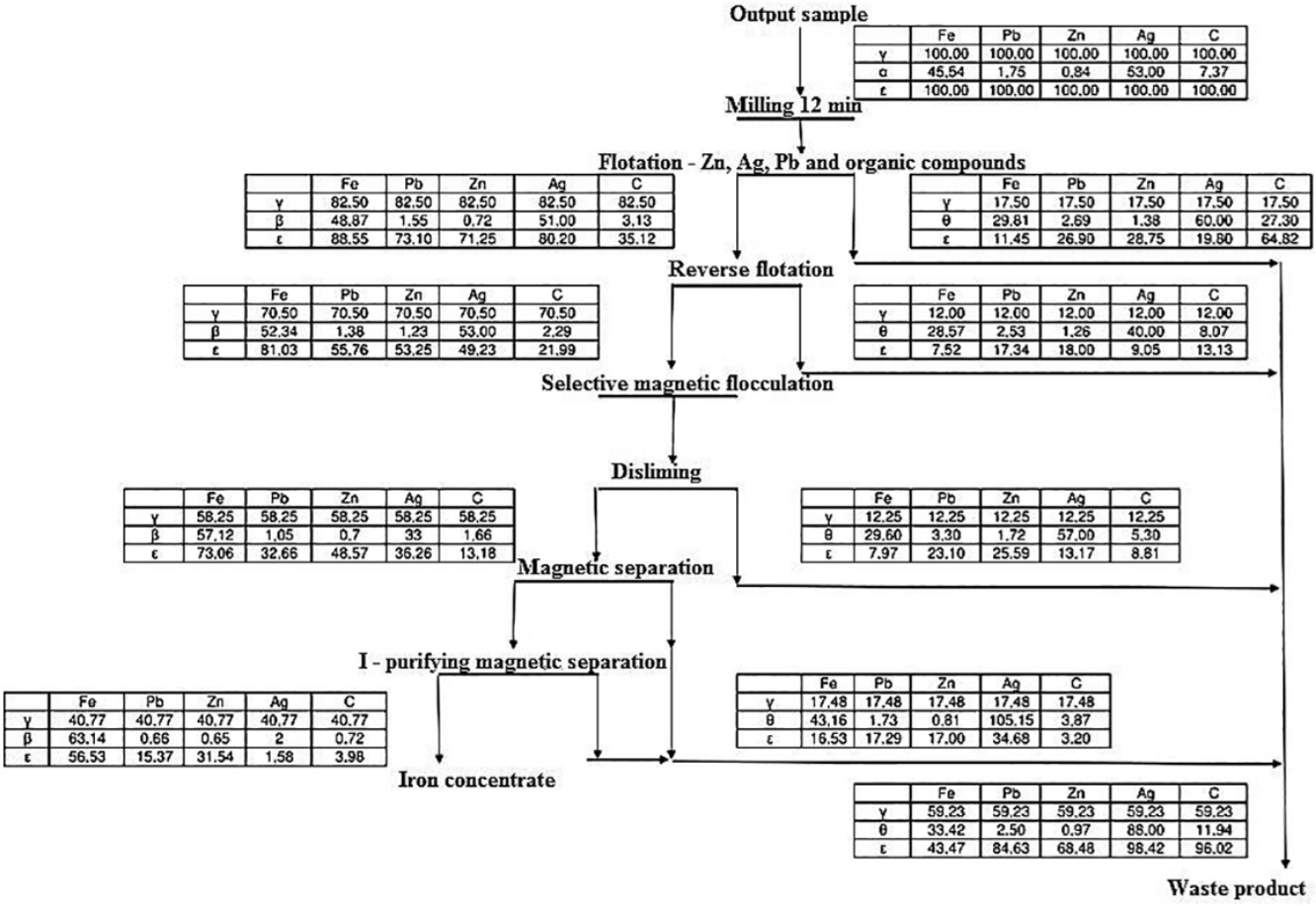

	Fe	Pb	Zn	Ag	C
γ	100.00	100.00	100.00	100.00	100.00
α	45.54	1.75	0.84	53.00	7.37
ε	100.00	100.00	100.00	100.00	100.00

	Fe	Pb	Zn	Ag	C
γ	82.50	82.50	82.50	82.50	82.50
β	48.87	1.55	0.72	51.00	3.13
ε	88.55	73.10	71.25	80.20	35.12

	Fe	Pb	Zn	Ag	C
γ	17.50	17.50	17.50	17.50	17.50
θ	29.81	2.69	1.38	60.00	27.30
ε	11.45	26.90	28.75	19.80	64.82

	Fe	Pb	Zn	Ag	C
γ	70.50	70.50	70.50	70.50	70.50
β	52.34	1.38	1.23	53.00	2.29
ε	81.03	55.76	53.25	49.23	21.99

	Fe	Pb	Zn	Ag	C
γ	12.00	12.00	12.00	12.00	12.00
θ	28.57	2.53	1.26	40.00	8.07
ε	7.52	17.34	18.00	9.05	13.13

	Fe	Pb	Zn	Ag	C
γ	58.25	58.25	58.25	58.25	58.25
β	57.12	1.05	0.7	33	1.66
ε	73.06	32.66	48.57	36.26	13.18

	Fe	Pb	Zn	Ag	C
γ	12.25	12.25	12.25	12.25	12.25
θ	29.60	3.30	1.72	57.00	5.30
ε	7.97	23.10	25.59	13.17	8.81

	Fe	Pb	Zn	Ag	C
γ	40.77	40.77	40.77	40.77	40.77
β	63.14	0.66	0.65	2	0.72
ε	56.53	15.37	31.54	1.58	3.98

	Fe	Pb	Zn	Ag	C
γ	17.48	17.48	17.48	17.48	17.48
θ	43.16	1.73	0.81	105.15	3.87
ε	16.53	17.29	17.00	34.68	3.20

	Fe	Pb	Zn	Ag	C
γ	59.23	59.23	59.23	59.23	59.23
θ	33.42	2.50	0.97	88.00	11.94
ε	43.47	84.63	68.48	98.42	96.02

Figure 2—Recovery of iron concentrate through two stages of flotation, coupled with desliming and magnetic separation. (α) Concentration of the corresponding component in the output sample in weight %, (γ) mass yield of the corresponding product in weight %, (β_ concentration of the valuable component in the concentrate in weight %, (θ) concentration of the corresponding component in the waste product in weight %, (ε) recovery of the corresponding component in the extracted concentrate in weight %

Recovery of iron concentrate through four stages of magnetic separation, coupled with selective magnetic flocculation in impulse magnetic field

The second technology used for processing the tailings is presented on Figure 3. The flow diagram includes four stages of magnetic separation with selective magnetic flocculation after the second separation stage.

Recovery of iron concentrates after beneficiation by magnetizing roasting

Magnetizing roasting was applied to beneficiate the iron ore tailings, followed by selective magnetic flocculation, desliming, and magnetic separation. The raw material was initially milled for 12 minutes in a ball mill and then subjected to a magnetizing roast (Figure 4). Figure 5 presents the flow sheet.

Process conditions

Flotation was carried out at a pulp solids concentration of 33% and pulp pH in the range 8.5–9.0, adjusted using water glass. Potassium isobutyl xanthate was used as the collector for the first flotation stage, and potassium oleate for the second (reverse) flotation.

Magnetic separation was performed at 0.18 T field strength.

The magnetizing roasting was carried out for 60 minutes at temperature of 700°C in the presence of coals as a reducing agent.

Pelletizing experiments

A lot of experimental work has been done to establish the optimal conditions under which iron pellets with an iron content over 60.00%, a lead content less than 0.01%, and zinc content of 0.09% or less can be produced. Initially, the pellets were produced manually by varying the size of the pellets, the binder concentration (bentonite), the firing temperature, the concentration and type of the coal used as a reducing agent, and the roasting time. A laboratory-scale pelletizer disc was used to form the pellets under the following operating parameters: iron concentrate moisture 12.5 wt.%, bentonite concentration 2.5 wt.%, pellets size 9–16 mm, pelletizer disc rotation speed 15 r/min, pelletizer disc inclination 60°, coal content 25 wt.%. After firing at 1100°C in a high-temperature furnace for 40 minutes, the pellets were cooled to 700°C in a reducing environment.

Results

The iron concentrate obtained *via* the first flow sheet (two stages of flotation, desliming, and magnetic separation) contained 63.14 wt.% iron, 0.66 wt.% lead, 0.65 wt.% zinc, 2 g/t silver, 2.15 wt.% silicon dioxide, 2.40 wt.% lime, 1.6 wt.%, manganese, 0.74 wt.% magnesium oxide, 0.046 wt.% copper, 0.50 wt.% alumina (aluminum trioxide), and 0.72 wt.% total carbon. The mass yield of the concentrate was 40.77 wt.%. The iron content meets the requirements for producing pellets with customized

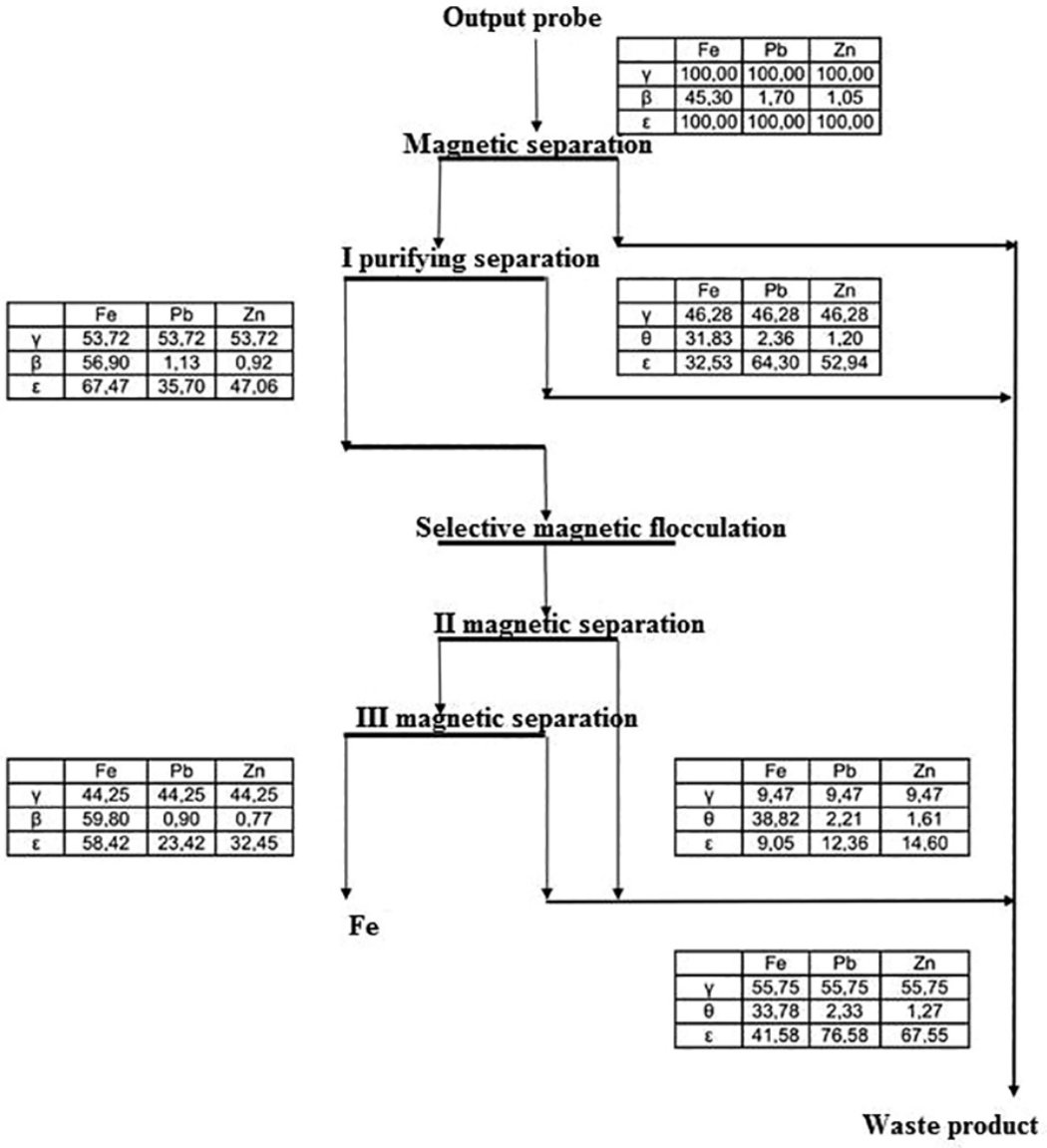

Figure 3—Extraction of iron concentrate after four stages of magnetic separation coupled with selective magnetic flocculation

properties. We tried to extract the non-ferrous bearing minerals as a separate marketable product through further flotation experiments. Unfortunately, the results from the laboratory analysis have shown that a very small proportion of the silver-, lead-, and zinc-bearing minerals is in a form that can be successfully floated (Table II).

The mass yield of the iron concentrate after applying the second proposed approach was slightly higher than with the first one – 44.25 wt.% *vs.* 40.77 wt.% – but it contained less iron (59.80 wt.%), more lead (0.90 wt.%), and more zinc (0.77 wt.%). The iron recovery was 58.24 wt.%. The results show that magnetic separation coupled with selective magnetic flocculation yields an iron concentrate of good quality suitable for pelletizing. Furthermore, this technology is much easier to apply in industry than that presented in Figure 1.

Processing the tailings in accordance with the third proposed technological scenario resulted in a mass yield to the concentrate of 74.42 wt.% and an iron recovery of 88.00 wt.%. The concentrate contained 59.98 wt.% iron, 1.50 wt.% Pb, and 1.19 wt.% Zn. After desliming the waste product contained 16.11 wt.% iron, which is significantly lower than that obtained by the first approach (29.60 wt.%). Compared to the second scenario (γ = 44.25 wt.%, β = 59.80 wt.%, ε = 58.42 wt.%) the yield of the iron concentrate was 28.15 wt.% higher and the iron recovery to the concentrate 29.58 wt.% higher. The lead and zinc contents were almost double those obtained via the other two technologies. Since during pelletizing the concentrate will be subjected to firing at 1000°C in the presence of a reducing agent, in our case the carbon in the concentrate, the higher contents of lead and the zinc will be reduced.

The pellets produced from the iron concentrate obtained by magnetizing roasting (Figure 4) had an iron content of 68.0 wt.%, 0.007 wt.% lead, and 0.09 wt.% zinc. The chemical composition of the pellets is given in Table III.

Conclusion

The tailings stored at the Kremikovtzi ore dressing plant in Bulgaria can be reprocessed by one of three proposed flow sheets so as to produce metallized pellets of good quality. The first technology, which couples two-stage flotation with desliming,

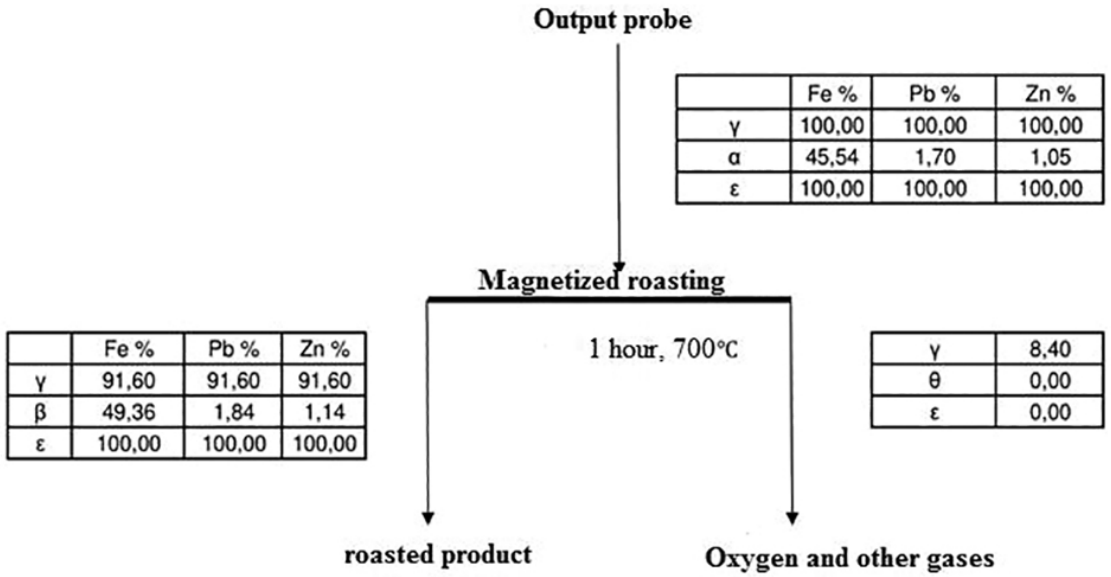

	Fe %	Pb %	Zn %
γ	100,00	100,00	100,00
α	45,54	1,70	1,05
ε	100,00	100,00	100,00

	Fe %	Pb %	Zn %
γ	91,60	91,60	91,60
β	49,36	1,84	1,14
ε	100,00	100,00	100,00

γ	8,40
θ	0,00
ε	0,00

Figure 4—Beneficiation by magnetizing roasting

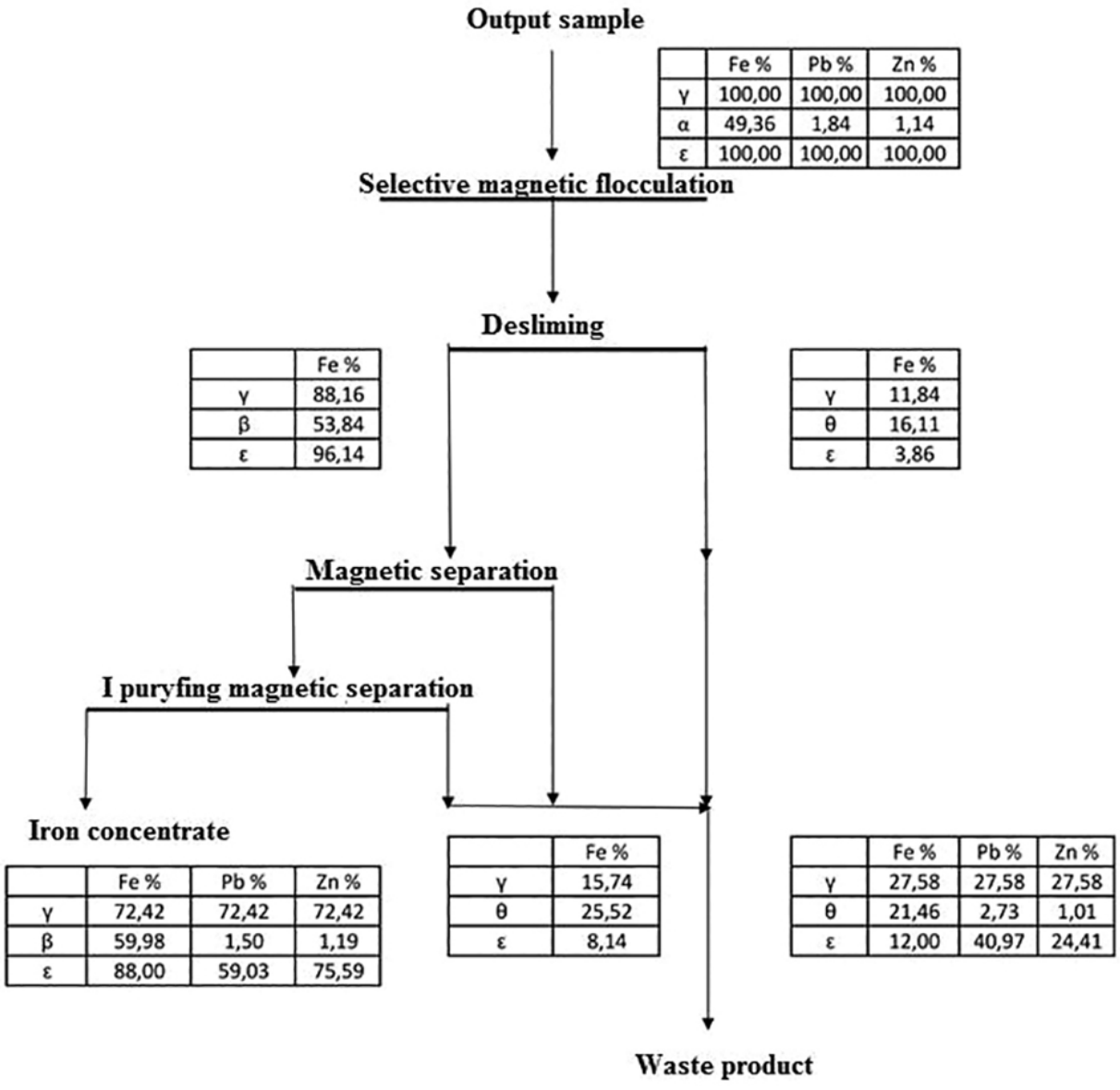

	Fe %	Pb %	Zn %
γ	100,00	100,00	100,00
α	49,36	1,84	1,14
ε	100,00	100,00	100,00

	Fe %
γ	88,16
β	53,84
ε	96,14

	Fe %
γ	11,84
θ	16,11
ε	3,86

	Fe %	Pb %	Zn %
γ	72,42	72,42	72,42
β	59,98	1,50	1,19
ε	88,00	59,03	75,59

	Fe %
γ	15,74
θ	25,52
ε	8,14

	Fe %	Pb %	Zn %
γ	27,58	27,58	27,58
θ	21,46	2,73	1,01
ε	12,00	40,97	24,41

Figure 5—Recovery of iron concentrate after beneficiation by magnetizing roasting

Table II

Chemical composition of the waste product after additional flotation experiments

Element	Amount
Ag	40 wt.%
C	8.07 wt.%
Pb	2.53 wt.%
Zn	1.26 wt%

Table III

Chemical composition of the pellets produced from iron concentrate obtained by magnetizing roasting

Component	Amount
Ag	25 g/t
C	0.19 wt.%
Cu	0.04 wt.%
Fe	68.00 wt.%
MgO	1.53 wt.%
Mn	2.02 wt.%
CaO	7.92 wt.%
Pb	0.007 wt.%
SiO_2	8.10 wt.%
Zn	0.09 wt.%

selective magnetic flocculation, and magnetic separation, offers the lowest iron recovery, and would be more complicated to apply on an industrial scale in comparison to the other two routes. Moreover, only the iron with strong magnetic properties can be extracted. The second technology, which couples four stages of magnetic separation with selective magnetic flocculation, can be used for production of pellet-grade concentrate, but it has the same disadvantage as the first route, namely only the iron with strong magnetic properties can be extracted. The third scenario offers a combination of magnetizing roasting followed by magnetic separation and desliming. This technology enables the recovery of iron with weak magnetic properties, but is more complex, more expensive, and would be more difficult to implement. The chemical composition analysis of the fired pellets shows that the contents of arsenic, copper, sulphur, phosphorus, chlorine, and fluorine are well below the standards. After further processing, the dust collected in the bag filters during pelletizing, which is rich in zinc and lead, can also used as a feed in nonferrous metals manufacturing. As further experiments, we plan to subject the product beneficiated through magnetizing roasting, to dry magnetic separation, and to fire the pellets in a rotary tube furnace.

References

Ajaka, E.O. 2009. Recovering fine iron minerals from Itakpe iron ore process tailing. *Journal of Engineering and Applied Sciences*, vol. 4, no. 9. pp. 17–28. http://citeseerx.ist.psu.edu/viewdoc/download?doi=10.1.1.536.2410&rep=rep1&type=pdf

Da Corte, C., Bergmann, C., and Woollacott, L. 2019. Improving the separation efficiency of Southern African hematite from slimes through selective flocculation coupled with magnetic separation. *Journal of the Southern African Institute of Mining and Metallurgy*, vol. 119, no. 11. pp. 963–972. http://dx.doi.org/10.17159/2411-9717/646/2019

Das, S.K., Ghosh, J., Mandal, A.K., Singh, N., and Gupta, S. 2012. Iron ore tailing: A waste material used in ceramic tile compositions as alternative source of raw materials. *Transactions of the Indian Ceramic Society*, vol. 71. pp. 21–24. http://dx.doi.org/10.1080/0371750X.2012.689507

Das, S.K., Kumar, S., and Ramachandrarao, P. 2000. Exploitation of iron ore tailing for the development of ceramic tiles. *Waste Management*, vol. 20, no. 8. pp. 725–729. http://dx.doi.org/10.1016/S0956-053X(00)00034-9

Güngör, K., Atalay, M.Ü., and Sivrikaya, O. 2011. Production of magnetite concentrate from iron ore tailings. *Proceedings of the XIV Balkan Mineral Processing Congress*, Tuzla, Bosnia and Herzegovina, 14–16 June 2011. Faculty of Mining, Geology and Civil Engineering in Tuzla and Faculty in Maining in Prijedor. pp. 331–337.

Hoffmann, M.R., Arnold, R.G. and Stephanopoulos, G. 1989. Microbial reduction of iron ore. US patent 4880740 A.

Kuranchie, F. 2015. Characterisation and applications of iron ore tailings in building and construction projects, PhD thesis, Edith Cowan University, Australia.

Li, C., Sun, H., Bai, J., and Li, L. 2010. Innovative methodology for comprehensive utilization of iron ore tailings: Part 1. The recovery of iron from iron ore tailings using magnetic separation after magnetizing roasting. *Journal of Hazardous Materials*, vol. 174, no. 1–3. pp. 71–77. http://dx.doi.org/10.1016/j.jhazmat.2009.09.018

Li, C., Sun, H., Yic, Z., and Li, L. 2010. Innovative methodology for comprehensive utilization of iron ore tailings: Part 2: The residues after iron recovery from iron ore tailings to prepare cementitious material. *Journal of Hazardous Materials*, vol. 174, no. 1–3. pp. 78–83. http://dx.doi.org/10.1016/j.jhazmat.2009.09.019

Li, J., Wang, Q., Liu, J., and Peng, L. 2009. Synthesis process of forsterite refractory by iron ore tailings. *Journal of Environmental Sciences*, vol. 21, sup. 1. pp. 592–595. http://dx.doi. org/10.1016/S1001-0742(09)60046-2

Maihatchi A., Pons M.-N., Ricoux Q., Goettmann F., and Lapicque F. 2020. Electrolytic iron production from alkaline suspensions of solid oxides: compared cases of hematite, iron ore and iron-rich Bayer process residues. *Journal of Electrochemical Science and Engineering*, vol.10, no. 2. pp. 95–102. http://dx.doi.org/10.5599/jese.751

Rao, K.H. and Narasimhan, K.S. 1985. Selective flocculation applied to Barsuan iron ore tailings. *International Journal of Mineral Processing*, vol. 14. pp. 67–75. https://doi.org/10.1016/0301-7516(85)90015-8.

Roy, S., Das, A., and Mohanty, M.K. 2007, Feasibility of producing pellet grade concentrate by beneficiation of iron ore slime in India. *Separation Science and Technology*, vol. 42, no. 14. pp. 3271–3287. https://doi.org/10.1080/01496390701514824

Sakthivel, R., Vasumathi, N., Sahu, D., and Mishra, B.K. 2010. Synthesis of magnetite powder from iron ore tailings. Powder Technology, vol. 201, no. 2. pp. 187–190. https://doi.org/10.1016/j.powtec.2010.03.005

Sun, T., Ren, J., and Lu, L. 2010. Study of sintering perforated brick technology using iron ore tail. *Metal Mine*, vol. 5. pp. 186–188. http://dx.doi.org/10.1109/ICEEE.2010.5661200

Spreitzer D. and Schenk J. 2019. Reduction of iron oxides with hydrogen—A review, *Steel Research International*, vol. 90, no. 10. 1900108.

Tang, C., Li, K., Ni, W., and Fan, D. 2019. Recovering iron from iron ore tailings and preparing concrete composite admixtures. *Minerals*, vol. 9, no. 4. pp. 232–244; https://doi.org/10.3390/min9040232

The Iron Platform. Not dated. REACH registration for iron and iron substances: Iron ores agglomerates (pellets) SIEF. https://www.iron-consortium.org/iron-ore-pellets-sief.html ◆

Evaluation of the mechanical properties of wood-derived charcoal briquettes for use as a reductant

N.W. Makgobelele[1], R.K.K. Mbaya[1], J.R. Bunt[2], N.T. Leokaoke[2], and H.W.J.P. Neomagus[2]

Affiliation:
[1] Department of Metallurgy and Chemical Engineering, Faculty of Engineering and the Built Environment, Tshwane University of Technology, South Africa.
[2] Centre of Excellence in Carbon-based fuels, Faculty of Engineering, North West University, Potchefstroom, South Africa.

Correspondence to:
N.W. Makgobelelea

Email:
walt.makg@gmail.com

Dates:
Received: 29 Aug. 2019
Revised: 16 Mar. 2021
Accepted: 19 Mar. 2021
Published: May 2021

How to cite:
Makgobelele, N.W., Mbaya, R.K.K., Bunt, J.R., Leokaoke, N.T., and Neomagus, H.W.J.P. 2021
Evaluation of the mechanical properties of wood-derived charcoal briquettes for use as a reductant.
Journal of the Southern African Institute of Mining and Metallurgy, vol. 121, no. 5, pp. 187–192.

DOI ID:
http://dx.doi.org/10.17159/2411-9717/903/2021

ORCID
N.W. Makgobelele
https://orchid.org/0000-0003-2071-0950
R.K.K. Mbaya
https://orchid.org/0000-0003-4012-748X
J.R. Bunt
https://orchid.org/0000-0003-3051-2528
N.T. Leokaoke
https://orchid.org/0000-0002-0178-210X
H.W.J.P. Neomagus
https://orchid.org/0000-0002-8683-9725

Synopsis

Silicon Smelters consumes more than 80000 t/a of wood-derived charcoal as carbonaceous reductant in the production of silicon metal. More than 10% of this material is discarded as fines (<6 mm) generated due to abrasion during processing. Charcoal fine residues (<650 µm) and polyvinyl alcohol (PVA) binder were used in this study to produce mechanically strong charcoal briquettes for metallurgical application as carbonaceous reductant. The PVA binder was added in mass percentages of 1, 3, and 5 wt% to the charcoal fines. The compressive strength, abrasion resistance index (ARI), drop shatter resistance (SRI), and water resistance index (WRI) were measured as functions of curing for up to 7 days under atmospheric conditions, and the results compared with metallurgical grade coarse charcoal. The ash content of the produced briquettes was found to be high (6.6–8.0%) compared with the coarse charcoal (1–3%). The 3 and 5 wt% PVA-bound briquettes were found to be the strongest, with compressive strengths of 40 and 115 kg/cm^2 respectively, with WRI values of 75 and 73% respectively. The produced briquettes were found to have lower ARI and SRI values compared to the coarse charcoal. Future work should include beneficiation of the fine charcoal discards prior to briquetting, and an increase in binder addition to above 6 wt% to improve the ARI and SRIn.

Keywords
wood charcoal, fines, briquettes, reductant, polyvinyl alcohol binder, compressive strength, water resistance, curing time.

Introduction

In 2015, South Africa's production and processing of wood-derived charcoal resulted in the generation of more than 5.2 Mt of charcoal fines (<6 mm) due to abrasion and attrition during transport and handling, which were discarded as a residue (FAO, 2017). Coarse charcoal (CC) with particle sizes (6–60 mm) is widely used in the metallurgical industry as a carbonaceous reductant because of its low level of impurities compared to coal, and ease of handling. More than 10% of the charcoal fines less than 6 mm in size is discarded into stockpiles as residue. In this research, different polyvinyl alcohol (PVA) binder solution concentrations were used with charcoal fines to produce charcoal briquettes for metallurgical utilization. The mechanical properties of the briquettes produced were evaluated in relation to coarse charcoal.

Literature review

Wood-derived charcoal is a carbonaceous product with low ash, moisture, and volatile contents, obtained by a pyrolysis process at temperatures ranging between 400 and 600°C (Basu, 2010). With the exception of particle size and moisture differences, the charcoal fines have similar characteristics as the coarse charcoal. Beneficiation of charcoal residue gives briquettes a charcoal-like appearance; hence the terms 'charcoal briquettes' or 'biocoal' (McDougall, 1991). Briquetting of charcoal fines is the process of converting the low-density pulverized charcoal matter from the biomass material to high-density and energy-concentrated charcoal briquettes, often with the aid of a suitable chemical binder material (Zubairu and Gana, 2014). Briquetting technology has been used successfully in many countries to amalgamate loose biomass into hard solids of regular shapes such as briquettes, pellets, or cubes, depending on the densification equipment employed.

Charcoal briquette properties depend on the type of wood from which the charcoal is derived, as well as the carbonization process used (Sahajwalla, 2004). The earliest industrial use of charcoal was as carbonaceous reductant for iron smelting to reduce iron oxide to metallic iron. With the development of the chemical industry and increasing legislative requirements for the preservation of the environment, the application of charcoal for purification of industrial wastes has grown markedly. Some metallurgical

applications of charcoal in various industries are smelting and sintering of iron ores, production of ferrosilicon and silicon metal, case hardening of steel, as a purification agent in smelting non-ferrous metals, a fuel in foundry cupolas, and electrodes (FAO, 1985). The earliest coal briquettes were made in hand-filled brick moulds using clay and cow dung as binders. These briquettes had poor mechanical properties (compressive strength, abrasion resistance, shatter resistance, and water resistance) which made them unsuitable for transportation over long distances (Venter and Naude, 2015).The acceptable compressive strength for coal briquettes in the industry is 3.8 kg/cm^2 (Richards, 1990). Increased strength reduces absorption of atmospheric moisture and thus increases the briquette durability. Different parameters affect the compaction pressure, *e.g.* feedstock, temperature of the pressing chamber, dimensions (length and diameter), the shape of the pressing chamber, and the compacting procedure (Kaur, Roy, and Kundu, 2017).

Briquettes undergo various degrees of mechanical degradation during conveying over short distances and long-distance haulage. This arises from breakage due to compression and abrasion while the briquettes are in contact with each other and the walls of the transportation vehicle. The falling of the briquettes during conveyer belt transfers, from chutes to bins, and off trucks onto the ground may also enhance their degradation. Impact-shatter is defined as breaking violently into pieces from a sudden impact. Impact-shatter forces are encountered when briquettes drop during stockpiling, at conveyor transfer points, and from bins and chutes. The measurement of this parameter can be used to indicate the extent to which briquettes will remain intact during handling, transportation, and storage. Water resistance shows the resistance of solid fuel briquettes to moisture or water penetration during transport or storage. High water resistance is a desirable quality which enables briquettes to remain impermeable to water for a long period before losing their integrity (Prasityousil and Muenjina, 2013).

Materials and method

Charcoal fines discard (<6 mm) from Silicon Smelters (Pty) Ltd (Polokwane, South Africa) and polyvinyl alcohol $(CH_2CHOH)_n$ (PVA 17-99) from Chem System (Pty) Ltd (Kempton Park, South Africa) were used in this study. The produced charcoal briquettes were characterized and compared with the metallurgical-grade coarse charcoal used as a reductant in electric-arc furnaces.

Charcoal fines preparation

The charcoal fines were milled in a stainless steel ball mill. The particle size distribution was determined using a Malvern Mastersizer 2000, and 90% of the milled sample was found to be below 650 µm. The milled charcoal was air-dried and a representative sample was taken for proximate and ultimate analyses.

Proximate and ultimate analyses

The inherent moisture content was determined by mass loss. The air-dried charcoal sample was placed in an oven which was thermostatically controlled with forced air ventilation, maintaining a temperature of 105°C for 3 hours. The ash and volatile matter contents on an air-dried basis (adb) were determined by means of the ISO 1171 (2010) and ISO 562 (2010) standards using a muffle furnace. The percentage of fixed carbon (FC) was calculated as the difference between 100% and the sum of the percentages of inherent moisture (IM), ash, and volatile matter (VM) contents on an air-dry basis using Equation [1].

$$FC_{adb} = 100 - (\%IM + \%Ash + \%VM) \quad [1]$$

The ultimate analysis was determined by Bureau Veritas based on the ISO 12902 standard to determine the percentage carbon, hydrogen, and nitrogen. Sulphur was determined using the (ISO 19576 (2006) standard. The oxygen content was calculated by difference, using Equation [2]:

$$\%O = (100 - \%C - \%H - \%N - \%S) \quad [2]$$

The ash composition was determined based on the ASTM D4326-04 92004) standards by X-ray fluorescence (XRF) using fusion beads. Table I shows the obtained proximate, ultimate, and ash composition analyses of the discard charcoal fines.

The proximate and ash analyses indicate an ash content of 7.7 wt% and a high silica content in the ash, of 72 wt%.

Polyvinyl alcohol (PVA) binder preparation

The 1, 3, and 5 wt% PVA solutions were prepared using a Labotec 105 magnetic heater stirrer, glass beaker, and thermocouple. Three 100 g aqueous solutions were prepared containing 1, 3, and 5 g of PVA powder. Water, in a beaker, was placed on the heated stirrer and heated to a maximum temperature of 92–98°C, at a heating rate of 2°C/min and stirring rate of 100 r/min. The fully solubilized solution was then allowed to cool to a temperature less than 30°C. The PVA solutions produced were then sealed in bottles and stored in an air-conditioned laboratory.

Charcoal briquetting

A 25 g aliquot of PVA solution was gradually dosed into 475 g of fine charcoal and homogenized using a pestle and mortar, to give a total mixture mass of 500 g. To produce the binderless and the PVA-bound briquettes, a mixture of charcoal fines with PVA solution was fed into a single-die mould machine to produce a compacted cylindrical agglomerate of size 13 × 10 mm. The fines

Table I

Proximate, ultimate and ash analyses of the charcoal fines

Proximate analysis, wt % (adb)	
Inherent moisture	15.6
Ash	7.7
Volatile matter	21.0
Fixed carbon (by difference)	55.7
Ultimate analysis, wt % (adb)	
Carbon	52.2
Hydrogen	2.0
Nitrogen	0.6
Oxygen (by difference)	21.9
Total sulphur	0.1
Ash Composition, %wt	
SiO_2	71.8
Al_2O_3	8.5
CaO	6.5
Fe_2O_3	4.4
Na_2O	2.5
K_2O	2.2
MgO	0.8
SO_3	1.9
TiO_2	0.4
P_2O_5	0.3

were compacted with a Chatillon Amatek TCD200 press (Figure 1), with a force of 1000 N at a constant speed of 120 mm/min to produce high-density briquettes. The briquettes were stored in an air-conditioned room for further proximate and physical analyses. Charcoal lumps of dimensions 13 × 10 mm were selected from the coarse sample (+6 –60 mm) for comparison with the briquettes.

Mechanical analysis

The coarse charcoal, binderless, and PVA–bound briquettes were tested for compressive strength (CS) (kg/cm^2), drop shatter resistance (SRI), abrasion resistance (ARI), and water resistance (WRI) as a function of curing time. The charcoal briquettes were cured in an air-conditioned laboratory at 24°C, 40% relative humidity, and tested on days zero (as produced), 3, 5, and 7.

Drop shatter resistance index

The drop shatter index is a measurement of the particle's resistance to mechanical impact, which mainly happens during transportation and handling of the briquettes. Weighed samples, each containing 20 particles of coarse or agglomerated charcoal, were dropped twice from a 2 m height. For each sample, the shattered pieces were screened using a 2 mm aperture screen and weighed to determine the mass of the retained sample, which was recorded as the final weight. Percentage mass loss of charcoal and briquettes was determined from the difference between the initial mass and final mass. The %SRI was calculated using Equation [3] (Ajiboye *et al.*, 2016):

$$\%\ SRI = 100 - \%\ Mass\ loss \quad [3]$$

Figure 1—Chatillon Amatek press

Compressive strength

A Chatillon Amatek DFE II instrument was used to measure the compressive strength of the coarse charcoal and charcoal briquettes. A sample was placed on the flat horizontal surface of the instrument, and slowly pressed between two parallel flat metal plates with facial areas greater than the projected area of the sample (20 and 50 mm diameters for the lower and upper plates, respectively). The cross-sectional area (A_c) of the particle was determined and the maximum length of the peak was horizontally displayed on the instrument as the fractural load (F_i) as the plate was vertically compressing the particle. The compressive strength of the sample was calculated using Equation [4] (Mangena *et al.*, 2004):

$$Compresssive\ strength = \frac{F_i(N)}{A_c(m^2)} \quad [4]$$

Abrasion resistance index

ARI was measured by tumbling five weighed particles of charcoal or charcoal briquettes in a cylindrical drum of 70 × 35 mm ID at 50 r/min for 2 minutes. During tumbling, the cylindrical briquettes were abraded along the edges and became pillow-shaped. The load was then screened with a 2 mm aperture screen and the mass of the retained sample determined. Percentage mass loss of charcoal and briquettes was determined from the difference between the initial mass and final mass. The %ARI was calculated using Equation [5] (Venter and Naude, 2015):

$$\%\ ARI = 100 - \%\ Mass\ loss \quad [5]$$

Water resistance index

The method for WRI determination was described in a study by Mangena *et al.* (2004). A single weighed sample was submerged in a beaker of cold water for 2 hours and inspected for disintegration, weighed, and then dried at atmospheric conditions for more than 6 hours with repeated weighing until no further significant mass loss was observed. The difference between initial and final mass of the particle sample was used to calculate the percentage water absorbed, and the WRI was calculated using Equation [6]:

$$WRI = 100 - \%\ Water\ absorbed \quad [6]$$

Results and discussion

Proximate analysis

Table II shows the results for proximate analysis of the metallurgical grade, coarse charcoal (CC), and charcoal briquettes with mass concentrations of zero (binderless briquettes), 1, 3, and 5 wt% PVA binder. It was observed that the metallurgical-grade coarse charcoal had a low ash yield (below 3%), with a fixed carbon content of 66%. The PVA-bound briquettes, on the

Table II

Proximate analysis of charcoal briquettes (adb)

Specification	CC	0%wt	1%wt	3%wt	5%wt
Moisture	12.2	15.6	10.9	7.0	10.2
Ash	2.5	7.7	8.0	7.7	6.6
Volatile matter	19.2	21.0	22.8	22.0	20.6
Fixed carbon (by difference)	66.1	55.7	58.3	63.3	62.6

other hand, yielded more ash (ranging between 6.5 and 8%) due to the high silica content of the ash, which was found to be 72%. The percentage fixed carbon for the produced charcoal briquettes with PVA ranged between 56 and 63%, while the volatile matter ranged between 20 and 23%. According to (Narjord (2017) these char characteristics are acceptable for metallurgical utilization in the production of steel. Table II indicates an increase in fixed carbon content with the addition of PVA.

Briquette mechanical analysis

Figure 2 shows the moisture content as a function of curing time for coarse charcoal, binderless, and 1, 3, and 5 wt% PVA-bound briquettes.

For the binderless briquette, the moisture content reduced from 14.7% on day zero to 4.1% on day 7, while in that curing period the 1 wt% PVA-bound briquette experienced an inherent moisture reduction of 4.4%. The 3 and 5 wt% PVA-bound briquettes had inherent moisture contents of 7.0% and 10.2%, respectively on day zero, which decreased to 4.0% on day 7. It was observed that moisture of the charcoal briquettes decreased with curing time to less than 4.5%. The mechanical properties of the CC, 0, 1, 3 and 5 wt% PVA briquettes as a function of curing time in relation with the decrease in moisture are depicted in Figures 3, 4, and 5.

Compressive strength

Figure 3 shows the briquette compressive strength as a function of curing time.

The binderless and 1 wt% PVA-bound briquettes failed to meet the mean compressive strength of 31 kg/cm^2 obtained for the coarse charcoal. It appears that briquettes produced with less than 3 wt% PVA were not amenable to compression, even if they were naturally dried for an extended period. This was probably due to weaker cohesion and adhesion forces between the low concentration PVA binder and the charcoal fines. According to Rousset *et al.* (2011), the mean compressive strength for charcoal ranges between 10 and 80 kg/cm^2, with an ash content in the range of 2–5%, When the ash content ranged between 1 and 1.5%, the charcoal compressive strength was between 50 and 100 kg/cm^2. Both the 3 and 5 wt% PVA-bound briquettes attained the minimum required mean compressive strength after 3 days of natural curing, which ranged between 28 to 40 kg/cm^2 for the 3 wt% PVA-bound briquettes, and 64 to 115 kg/cm^2 for the 5 wt% PVA-bound briquettes.

Abrasion resistance

Figure 4 shows the briquette abrasion resistance as a function of curing time. The obtained results were compared with the coarse charcoal lumps.

It can be observed that the ARI for binderless briquettes continues to decrease with curing time, from 22% to 3% between days zero and 7. An initial 50% decrease in the ARI, from 20% to 10%, was observed in the 1 wt% PVA-bound briquettes between days zero and 3, followed by an increase to 15%. The decrease in ARI for both the binderless briquettes and the 1 wt% PVA-bound briquettes could be attributed to the low adhesion forces between charcoal fines and PVA binder at zero or low binder concentrations. For the 3 and 5 wt% briquettes the ARI increased to 80 and 84%, respectively, after 3 days of curing. Between 3 and 7 days of curing, the average ARI for both the 3 and 5 wt% PVA-bound briquettes was 82% with a standard deviation of 0.3. The ARI obtained for the coarse charcoal was 96%, which was not attained by the manufactured briquettes. According to Mangena (2001), a 25% fines content may be tolerated, therefore 75% ARI was chosen in this study as the minimum target value for abrasion resistance.

Drop shatter resistance

Figure 5 shows the effect of briquette curing time on SRI, with the SRI of coarse charcoal for comparison.

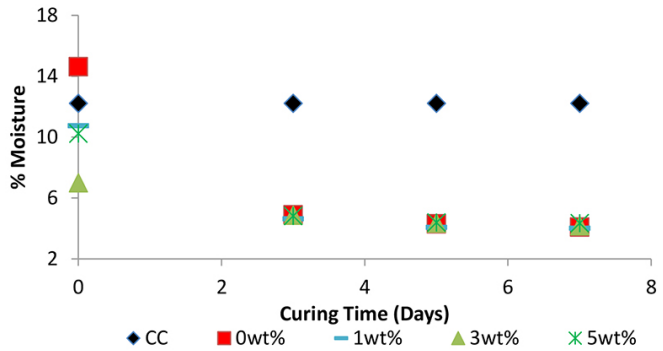

Figure 2—Percentage moisture as a function of curing time

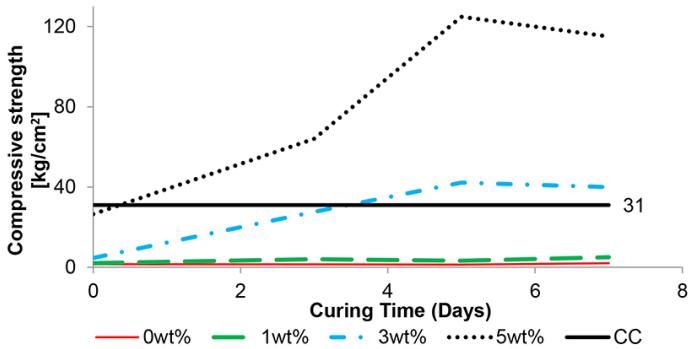

Figure 3—Compressive strength as a function of curing time

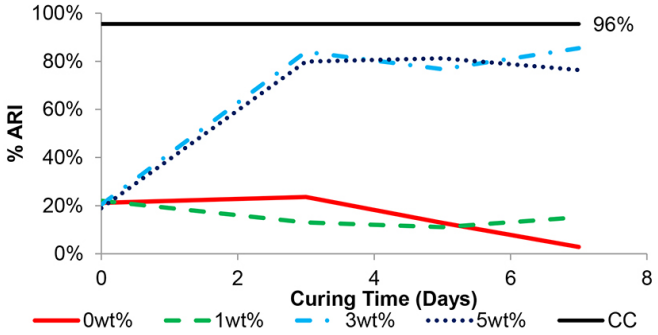

Figure 4—Abrasion resistance as a function of curing time

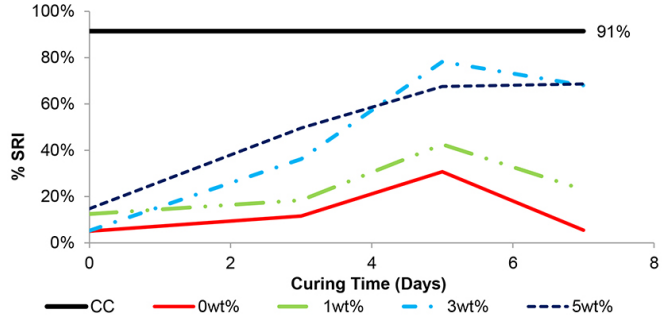

Figure 5—Shatter resistance as a function of curing time

In the first five days of curing, the SRI increased for all briquettes. It was observed that from days 5 to 7 of curing, a continuous decrease in SRIs of the charcoal briquettes resulted, with the briquettes becoming more brittle and breaking easily. The lower SRI for the binderless briquettes and the 1 wt% PVA-bound briquettes (SRI 5 and 23%, respectively) were obtained at inherent moisture contents of less than 4.4%, after 7 days of curing. The results obtained for both the 3 and 5 wt% PVA-bound briquettes (averaging 70%) were low compared to the shatter resistance of 91% for the coarse charcoal.

Water resistance

Table III shows the water resistance index (WRI) results obtained for all briquettes, along with the coarse charcoal, submerged in water for more than 2 hours.

The binderless briquettes and the 1 wt% PVA-bound briquettes disintegrated within a few seconds in the presence of water, which proved that the briquettes were not water resistant. Both the 3 and 5 wt% PVA-bound briquettes yielded a water resistance index between 73 and 75%. According to (Richards (1990), a WRI greater than 95% should be obtainable after 2 hours. Although lower than the suggested minimum acceptable WRI proposed by Richards, the WRI results obtained for the 3 and 5 wt% PVA-bound briquettes were higher than for the coarse charcoal. This was attributed to the high concentration of PVA binder on the surface of the briquettes. The wet compressive strength was also tested over a 9-day period at 3-day intervals, in order to determine the effect of PVA binder on the briquettes under rainy conditions. The results are shown in Figure 6.

It was observed that the wet compressive strength increased with curing time for the first 5 days. The insignificant increase in wet compressive strength observed for the coarse charcoal (from 20 to 32 kg/cm^2 over the 9-day period) was attributed to the charcoal's large surface area and high porosity. On day zero, the wet compressive strength for the 3 wt% briquette was

Table III

Water resistance analysis

Sample	% Water absorbed	% WRI
CC	42	58
0%wt	100	0
1%wt	100	0
3%wt	25	75
5%wt	27	73

2 kg/cm^2, increasing to 36 kg/cm^2 due to natural curing for 5 days. After day 5, the compressive strength of the 3 wt% PVA-bound briquettes decreased to 32 kg/cm^2. The compressive strength of 5 wt% PVA-bound briquettes, with an initial value of 12 kg/cm^2, increased significantly to 83 kg/cm^2, but subsequently decreased to 78 kg/cm^2 after 7 days of curing. The results indicate that the rainy seasons will have a greater effect on the mechanical properties of the lower concentration PVA-bound briquettes, which will therefore require care in handling and storage on site. Table IV shows a summary of the mechanical properties for the binderless and PVA-bound briquettes compared to the coarse charcoal after 7 days of curing.

From Table IV it is clear that the mechanical properties of the binderless and 1 wt% PVA-bound briquettes are inferior to those of the coarse charcoal (CC). On the other hand, the 3 and 5 wt% PVA-bound briquettes showed superior performance compared to the raw charcoal in terms of compressive strength and water resistance. The abrasion resistance and shatter resistance of the 3 and 5 wt% PVA bound-briquettes were slightly inferior to the coarse charcoal. The increase in binder concentration may have improved these results, to produce agglomerates comparable to coarse charcoal.

Conclusions

This study showed that charcoal briquettes produced from wood

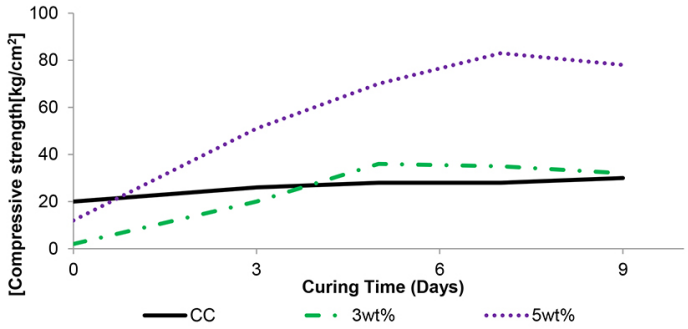

Figure 6—Wet compressive strength as a function of curing time

Table IV

Mechanical properties as a function of curing time (days)

	CC	0wt%	1wt%	3wt%	5wt%
CS(kg/cm²)	31	2	5	40	115
ARI, %	96	3	15	85	76
SRI, %	91	5	23	68	69
WRI, %	58	0	0	75	73

charcoal fines with a PVA binder concentration of 3 wt% and higher have suitable compressive strength and water resistance properties for metallurgical application as a carbonaceous reductant. The binderless and the low concentration (1 wt%) PVA-bound briquettes, on the other hand, exhibited poor mechanical properties. The mechanical properties of the briquettes with 3 wt% PVA binder i improved with curing time, with the compressive strength increasing from 5 to 42 kg/cm² after 5 days of curing. The 5 wt% PVA-bound briquette yielded the highest compressive strength, which increased from 26 to 125 kg/cm² after 5 days of curing. This is more than a 300% increase in compressive strength compared to the coarse charcoal at 31 kg/cm². The 3 and 5 wt% PVA-bound briquettes yielded water resistance indices of 75 and 73%, respectively, compared with the benchmark of 58% set by the coarse charcoal.

The results show that the charcoal fines will require an appropriate storage facility to avoid contamination. The 3 and 5 wt% PVA-bound briquettes will also require a storage facility in order to avoid water damage during prolonged rainy periods. Based on the proximate and physical analyses obtained for the 3 and 5 wt% PVA briquettes, in comparison to the coarse charcoal, the results show that the briquettes can be used as a carbonaceous reductant for metallurgical applications. Future work should include an increase in binder concentration to above 6 wt% to improve the ARI and SRI. Beneficiation to remove extraneous sand/debris from the discarded charcoal fines should also be investigated to reduce the ash content before briquetting.

Acknowledgement

The information presented in this paper is based on research which is financially supported by the South African Research Chairs Initiative (SARChI) of the Department of Science and Technology and National Research Foundation of South Africa (Coal Research Chair Grant No. 86880). Any opinion, finding, or conclusion or recommendation expressed in this material is that of the author(s) and the NRF does not accept any liability in this regard. Facets of the study have been presented at the North West University, Potchefstroom campus and the Tshwane University of Technology.

References

Ajiboye, T.K., Abdulkareem, S., and Anibijuwon, A.O. 2016. Investigation of mechanical properties of briquette product of sawdust-charcoal as a potential domestic energy source. *Journal of Applied Sciences and Environmental Management*, vol. 20, no. 4. pp. 1179–1188. doi: 10.4314/jasem.v20i4.34

ASTM D4326-04. 2004. Major and minor elements in coal and coke ash by X-ray fluorescence. 26 May. ASTM International, West Conshohocken, PA. pp. 1–4.

Basu, P. 2010. Biomass Gasification and Pyrolysis; Practical Design and Theory. 2nd edn. Elsivier, Kidlington, Oxford.

FAO. 1985. Charcoal utalization and marketing. Industrial Charcoal Making. Food and Agriculture Organization, Rome.

FAO. 2017. 'The Charcoal Transition. Food and Agriculture Organization, Rome. pp. 1–184.

ISO 1171. 2010. Solid mineral fuel - Determination of ash. Internatioanal Organization for Standardization, Geneva. pp. 1–7.

ISO 12902. 2001. Determination of total carbon, hydrogen and nitrogen - Instrumental methods. Internatioanal Organization for Standardization, Geneva. pp. 1–3.

ISO 19576. 2006. Solid mineral fuels - Determination of sulfur by IR spectrometry. Internatioanal Organization for Standardization, Geneva. pp. 1–4.

ISO 562. 2010. Hard coal and coke - Determination of volatile matter. Internatioanal Organization for Standardization, Geneva. pp. 1–16.

Kaur, A., Roy, M., and Kundu, K. 2017. Densification of biomass by briquetting. *International Journal of Recent Scientific Research*, vol. 8. pp. 20561–20568.

Mangena, S.J., de Korte, G.J., McCrindle, R.I., and Morgan, D.L. 2004. The ameneability of some South African bituminous coal to binderless briquetting. *Fuel Prcessing Technology*, vol. 85. pp. 1647–1662.

Mangena, S.J., de Korte, G.J., McGrindle, R.I., and Morgan, D.L. 2004. The amenability of some Witbank bituminous ultra fine coals to binderless briquetting. *Fuel Processing Technology*, vol. 85, no. 15. pp. 1647–1662.

McDougall, G.J. 1991. The physical nature and manufacturing of activated carbon. *Journal of the South African Institution of Mining and Metallurgy*, vol. 91. pp. 109–120.

Narjord, H.B. 2017. Theoretical study of mechanical stability of charcoal from biomass resources. MSc thesis, Norwegian University of Science and Technology, Trondheim. http://hdl.handle.net/11250/2458484

Prasityousil, J. and Muenjina, A. 2013. Properties of solid fuel briquettes produced from rejected material of municipal waste composting. *SUSTAIN 2012. Proceedings of the 3rd International Conference on Sustainable Future for Human Security*. pp. 603–610. https://core.ac.uk/download/pdf/82105259.pdf

Richards, S.R. 1990. Physical testing of fuel briquettes. *Fuel Processing Technology*, vol. 25, no. 2. pp. 89–100.

Rousset, P., Caldeira-Pires, A., Sablowski, A., and Rodrigues, T. 2011. LCA of eucolyptus wood charcoal briquettes. *Journal of Cleaner Production*, vol. 19, no. 14. pp. 1647–1653.

Sahajwalla, V.D.K.R. 2004. Reductant characterisation and selection: Implications of ferroalloys processing. *INFACON X: Proceedings of the Tenth International Ferroalloy Congress*, Cape Town, South Africa, 1–4 February 2004. South African Institute of Mining and Metallurgy, Johannesburg. pp. 351–362.

Venter, P. and Naude, N. 2015, Evaluation of some optimum moisture and binder conditions for coal fines for briquetting. *Journal of the Southern African Institution of Mining and Metallurgy*, vol. 115. pp. 329–333.

Zubairu, A. and Gana, S.A. 2014. Production and characteristics of briquette charcoal by carbonization of agro-waste. *Energy and Power*, vol. 4, no. 2. pp. 41–47. doi: 10.5923/j.ep.20140402.03

A new grade-capping approach based on coarse duplicate data correlation

R.V. Dutaut[1] and D. Marcotte[1]

Affiliation:
[1] École Polytechnique, Montréal, Québec, Canada.

Correspondence to:
R.V. Dutaut

Email:
raphael.dut@wanadoo.fr

Dates:
Received: 10 Sep. 2020
Revised: 14 Feb. 2021
Accepted: 18 Feb. 2021
Published: May 2021

How to cite:
R.V. Dutaut and D. Marcotte. 2021
A new grade-capping approach based on coarse duplicate data correlation.
Journal of the Southern African Institute of Mining and Metallurgy, vol. 121, no. 5, pp. 193–200.

DOI ID:
http://dx.doi.org/10.17159/2411-9717/1379/2021

ORCID
R.V. Dutaut
https://orchid.org/0000-0001-7474-2574
D. Marcotte
https://orchid.org/0000-0002-5784-9115

Synopsis

In most exploration or mining grade data-sets, the presence of outliers or extreme values represents a significant challenge to mineral resource estimators. The most common practice is to cap the extreme values at a predefined level. A new capping approach is presented that uses QA/QC coarse duplicate data correlation to predict the real data coefficient of variation (*i.e.*, error-free CV). The cap grade is determined such that the capped data has a CV equal to the predicted CV. The robustness of the approach with regard to original core assay length decisions, departure from lognormality, and capping before or after compositing is assessed using simulated data-sets. Real case studies of gold and nickel deposits are used to compare the proposed approach to the methods most widely used in industry. The new approach is simple and objective. It provides a cap grade that is determined automatically, based on predicted CV, and takes into account the quality of the assay procedure as determined by coarse duplicates correlation.

Keywords
geostatistics, outliers, capping, duplicates, QA/QC, lognormal distribution.

Introduction

Outliers or extreme values are present in most mining grade data-sets. They can reflect true small-scale spatial variability and/or sampling and analytical errors introduced by procedures. Extreme values are deemed undesirable in kriging as they could propagate assay errors over significant ore tonnages. It is common practice in the mining industry to reduce these grade values to (or cap them at) a lower top-cut value (Leuangthong and Nowak, 2015). Cap value determination is not straightforward and often remains subjective, especially for highly skewed distributions found in precious metal deposits.

Numerous methods have been proposed to address cap value determination, including the following:

- Top percentile (Rossi and Deutsch, 2013): Most likely the simplest method, where the cap value is a high percentile of the distribution, generally between the 99th and 99.9th percentile. Sometimes the cap value is based on historical practices, such as capping at 1 ounce of gold per ton (this practice was common in northern Quebec, Canada). Although simple, the choice of cap percentile is arbitrary and subjective, and it does not take into account the quality of the assays.
- Parrish capping (Parrish, 1997): The cap grade is selected such that the post-cap metal content of the assays above the 90th percentile represents less than 40% of the total metal and/or that of the assays above the 99th percentile represents less than 10% of the total. Although this method is repeatable, it can define overly conservative (*i.e.*, very low) cap grades, especially for highly skewed deposits. In addition, the percentiles and the proportions used are arbitrary, and the method does not take into account the quality of the assay procedure.
- Log probability (Rossi and Deutsch, 2013): A cumulative log probability plot, or more simply a data histogram, is used to identify a change in slope or a gap in the tail of the distribution. This is one of the most commonly used methods in the industry. It is relatively easy to interpret, but there are often multiple breaks/gaps in the distribution that make the choice of cap value subjective. In addition, the method is sensitive to the amount of data. For small data-sets, the cap value tends to be fairly low. When more data is available, the gap generally appears at a much higher value. The method also does not take into account the quality of the assay procedure.
- Cutting curves (Roscoe, 1996): The average grade for different cap values is plotted and an inflection point is visually selected by the practitioner. This method is fairly arbitrary, and the choice of inflection point is subjective.

- Central variation error from the cross-validation of simulated local average (Babakhani, 2014): A local cap value is selected from a volume of influence (determined based on data spacing and kriging parameters) such that the interpolated block average within the volume is equal to the simulated median. A given high grade can be capped at different values depending on the neighbouring data. The method is complex as it requires kriging and conditional simulation, both of which need a variogram, on raw data for kriging and on Gaussian grades for simulation. The raw data variogram is itself sensitive to extreme values. The Gaussian transform required for simulation is also sensitive to extreme values. Furthermore, the results are likely to be sensitive to the choice of neighbourhood for both kriging and conditional simulation. In addition, this method requires coordinates, so it can't be used for conveyor, truck, or grab samples, for example.
- Metal risk analysis using simulations (Parker, reported in Rossi and Deutsch, 2013): Monte Carlo simulations are used to simulate the high-grade distribution. This method makes it possible to generate a confidence level for a predefined (*e.g.*, yearly) metal production volume. This simulation method suffers from basically the same shortcomings as the method of Babakhani (2014).

It is worth noting that some authors have proposed alternative methods to avoid capping (David, 1977; Parker, 1991; Rivoirard, 2013; Maleki, Madani, and Emery, 2014). Although these methods are interesting from a theoretical point of view, they are rarely used in mining applications, where the capping of extreme values is still perceived as a best practice.

In this research, we propose the use of the correlation of the coarse duplicates to determine the cap value. The use of duplicates is now mandatory according to QA/QC guidelines and routine in the mining industry. Although Abzalov (2011) and Rossi and Deutsch (2013) describe various uses for duplicate samples, helping the determination of the cap level is not one of them. A rarely documented and supplementary question in resource assessments is whether capping should be performed before or after compositing.

Using a multiplicative lognormal error model, it is possible to determine the coefficient of variation of the true (unobserved) grades from the correlation between original and duplicate values (see later). We propose to determine the cap grade such that the newly capped population has the same CV as the CV determined from correlation between original and duplicate pairs.

After describing the multiplicative lognormal error model, the link between the lognormal parameters of the true grades, those of the errors, and the theoretical correlation between duplicates is derived. From this correlation, the predicted theoretical coefficient of variation of the grades is obtained and established as the target to be reached when determining the cap grade. The robustness to the sample length and the lognormal assumption is then assessed and the effects of capping before or after compositing is also analysed. Finally, case studies of a gold and a nickel deposit are presented, and cap grades obtained using the proposed approach are compared to those obtained using some traditional methods.

Methods

This section presents the multiplicative lognormal error model and the main results that are derived from it. Synthetic case studies are used to assess the method's robustness with regard to some assumptions and to measure the effects of capping before or after compositing.

Theoretical background

Assuming the following model (Marcotte and Dutaut, 2020) is valid:

$$Z_o(x) = Z_v(x).t \quad [1]$$

where Z_o is the observed value at the x position, Z_v is the true value, and t is the multiplicative error of the analysis (in this study both Z_v and t are assumed to be lognormal, a reasonable assumption for most precious and base metal deposits). Equation [1] can be written:

$$Z_o(x) = \exp(\log(Z_v(x)) + \log(t)) \quad [2]$$

$$E[Z_o(x)] = e^{(\alpha+\mu+\frac{\beta^2+\sigma^2}{2})} \quad [3]$$

$$Var[Z_o(x)] = (e^{\beta^2+\sigma^2}-1).e^{2(\alpha+\mu)+\beta^2+\sigma^2} \quad [4]$$

where α and β are the logarithmic mean and standard deviation of Z_v respectively, and μ and σ are the logarithmic mean and standard deviation of t respectively. Note that in the multiplicative lognormal error model, σ^2 is related to the variance of the duplicates' log-ratio:

$$\sigma^2 = \frac{1}{2} Var\left(log\left(\frac{Z_o}{Z_o'}\right)\right) \quad [5]$$

where Z_o and Z_o' are the observed original and duplicate assays (in short, duplicates values). Hence, σ^2 can be estimated directly from the duplicates independently of the other parameters (α, β, μ). This result is not used hereinafter but is presented for the sake of completeness.

If quality assurance and quality control (QA/QC) is performed and sampling theory guidelines are followed, there should be no or limited bias on mean grade. From Equation [4] this implies:

$$\mu = -\frac{\sigma^2}{2} \quad [6]$$

Correlation between duplicates

The theoretical correlation between duplicates in the multiplicative model is given by:

$$\rho_{dup} = \frac{\left(e^{\beta^2}-1\right)}{\left(e^{\beta^2+\sigma^2}-1\right)} = \frac{CV_v^2}{CV_o^2} \quad [7]$$

The first equality comes from $\frac{Var(Z_o)}{m^2} = \frac{Var(Z_o')}{m^2} = \left(e^{\beta^2+\sigma^2}-1\right)$ for the denominator and $\frac{Cov\,(Z_o,Z_o')}{m^2} = \left(e^{\beta^2}-1\right)$ in the numerator. The last equality in Equation [7] comes directly from the definition of coefficient of variation and Equations [3] and [4] for the denominator and the same equations with $\sigma^2 = 0$, for the numerator. With σ^2 estimated from Equation [5] and correlation between duplicates, it is possible to estimate β using Equation [7] and then α using Equation [3]. Better yet, from Equation [7], the squared coefficients of variation of true and observed values are directly related to the duplicates' coefficient of correlation by:

$$CV_v^2 = \rho_{dup}.CV_o^2 \quad [8]$$

where CV_v is the (unobserved) coefficient of variation of Z_v and CV_o is the (observed) coefficient of variation of Z_o. Hence, it is

possible to estimate the coefficient of variation of the true grades using only the correlation between duplicates and CV_o computed with all available samples.

Figure 1a shows the curve defined by Equation [8], with $\beta = 1$, and simulated results. Figure 1b illustrates Equation [8] for different β values.

Figure 2 compares the theoretical error-free coefficient of variation $CV_{theo} = \sqrt{(exp(\beta)^2 - 1)}$ defined by β to CV_{pred} predicted using duplicates correlation ρ_{dup} and CV_{dup} in Equation [8]. Each point represents a different lognormal distribution with parameters uniformly drawn in intervals described in Table I. As the number of duplicates increases, the spread of the points and the skewness of the conditional distribution of $CV_{pred} \mid CV_{theo}$ diminish. The number of duplicates required to estimate CV_{theo} to a given precision increases with CV value. Note that in Table I, the minimum and maximum theoretical CV are $\sqrt{(exp(0.5)^2 - 1)} = 0.53$ and $\sqrt{(exp(1.5)^2 - 1)} = 2.91$, which cover most practical cases. Also, $\sigma \leq \beta$ and using Equation [8], the minimum and maximum theoretical ρ_{dup} are 0.42 and 0.957 respectively. Using Equations [3] and [4], the minimum and maximum theoretical CV_o are 0.54 and 4.51 respectively, which cover most practical cases.

Capping based on correlation between duplicates

Equation [8] indicates that the coefficient of variation of the observed duplicate grades is inflated by sampling errors. This suggests the following capping criterion: choose the threshold providing $CV_{cap} = CV_{pred}$ determined experimentally from the correlation between duplicates and the coefficient of variation computed using all available samples (original and duplicates) using Equation [8]. This criterion, although arbitrary, has the advantage of being objective, repeatable, and simple to compute. It takes into account the quality of the assay procedure in determining the cap value, contrary to existing methods. Moreover, it does not require localization of the samples, contrary to the methods of Babakhani (2014) and Parker (1991).

Figure 3 shows the cap percentile applied to the distribution of Z_o that provides $CV_{cap} = CV_{pred}$ as a function of ρ_{dup} for different values of β. All curves are computed by numerical integration

Table I

Sampled intervals and definitions for parameters of the lognormal distributions of Z_v and t

Parameter	Interval or definition
α	[–0.5, 0.5]
β	[0.5, 1.5]
f	[0.2, 0.6]
σ	βf
μ	$-\sigma^2/2$

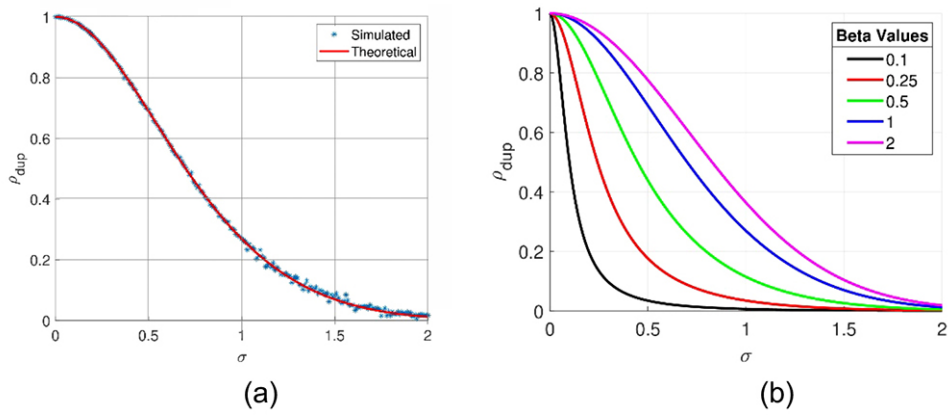

Figure 1—(a) Theoretical (red line, Equation [7]) and simulated (n = 1 000 000 duplicates with 200 blue dots) ρ_{dup} against σ for $\beta = 1$. (b) Theoretical ρ_{dup} against σ for various β values

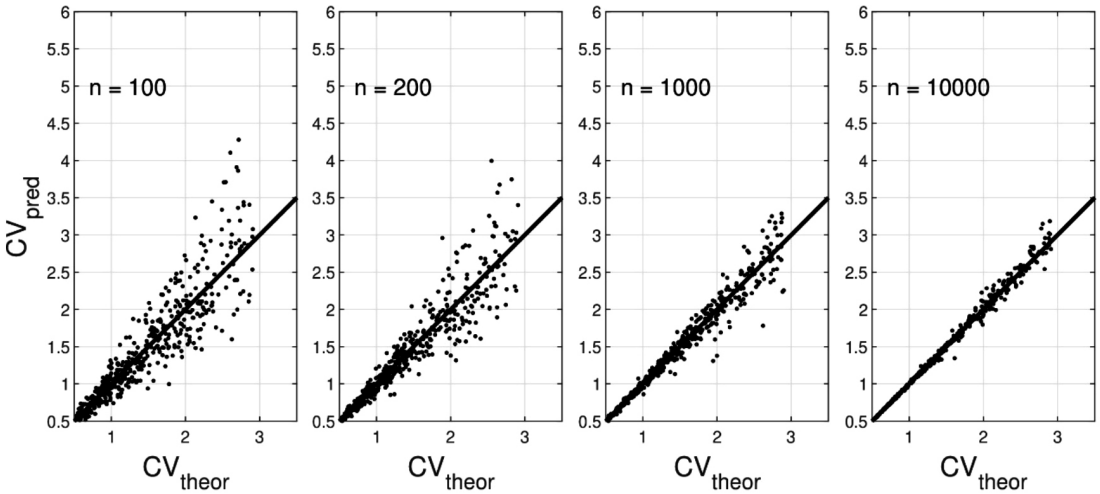

Figure 2 – Theoretical and predicted CV using Equation [8] for different lognormal parameters and an increasing number of duplicates (n = 100, 200, 1 000, 10 000)

of the truncated lognormal distribution. As expected, the cap percentile for each curve increases with the duplicates correlation, indicating that large error variances (lower duplicates correlation) require a lower cap value to obtain the desired coefficient of variation. Also, for a given correlation, the cap threshold increases with β, indicating a lower cap value is required for less skewed distributions of Z_v. Note that parameter α has no influence on determining the cap percentile.

Effects of variable assay supports

The results obtained so far assume the duplicate assays were on samples with identical supports. However, this might be not the case in practice for a variety of reasons (geological contacts, different sampling campaigns, technical drilling difficulties, *etc.*). It is therefore important to assess the effects of support variations on the statistics ρ_{dup} and β used to determine the cap percentile. Note that σ is the standard deviation of the error due to sample preparation and analysis; hence, it is not related to the support. Only β varies with the support.

If the point variogram is available, it is possible to compute the variance of the regularized support for any support. Assuming that distribution remains lognormal with the same mean, it is possible to compute β_s, the logarithmic standard deviation associated with support *s*. The beta corresponding to a given support can be computed using classical geostatistical relations as:

$$\beta_s = \left\{ log\left(\frac{\tau_s^2}{m^2} + 1\right)\right\}^{1/2} \quad [9]$$

where $\tau_s^2 = \tau_0^2 - \bar{\gamma}(s,s)$, $m = \exp(\alpha + \frac{\beta_0^2}{2})$, $\tau_0^2 = m^2(\exp(\beta_0^2)-1)$, β_0^2 is the logarithmic variance at point support, and $\bar{\gamma}(s,s)$ is the average variogram value within support *s*.

Example

Consider a typical gold deposit case with $\alpha = 0$, $\beta_0 = 1$, the mean $m = \exp(0.5) = 1.65$ ppm, the point true grade variance $\tau_0 = m^2(\exp(1)-1) = 4.67$ ppm^2 and a spherical variogram with correlation range 20 m. The assay supports are half cores of lengths varying between 1 m and 5 m. The corresponding variances of core grades are 4.5 ppm^2 and 4.1 ppm^2 for 1 m and 5 m lengths respectively, corresponding to $\beta_{1m} = 0.99$ and $\beta_{5m} = 0.96$. Further computing duplicates correlation using Equation [7] and $\sigma = 0.5$ for the two supports gives values of 0.69 and 0.68 respectively. Other values of σ provide similar differences in correlation and α has no impact on determining β and ρ_{dup}. As seen in this example, the effects of the support on β and ρ_{dup} are negligible when compared to the precision of the estimates of duplicates correlation and coefficient of variation.

Effects of departing from the lognormal assumption

Figure 3 indicates that realistic cap percentiles should be obtained for the lognormal case when the distributions are skewed (large β and CV) and the correlation between duplicates is high. When the skewness is low, the cap percentile tends to decrease, meaning that a significant percentage of the samples will be capped unless this is compensated for by a higher duplicates correlation corresponding to a better sampling preparation procedure in real deposits.

The lognormal assumption is realistic for many low-grade skewed distributions, which are typically encountered in precious- and base metal deposits. To get an idea of the sensitivity of the proposed approach to the lognormal assumptions, five different cases were simulated with a large quantity of data (1 million). Table II describes the five simulated cases. Figure 4 shows the duplicates' scattergrams and the histograms of the error-free simulated Z_v and the observed Z_o. Despite the strong departure from lognormality and small CV_v of each case, the five cap values determined by our approach appear reasonable in terms of percentile of the observed grades. Moreover, the CV of the capped values matches very well in each case with the CV of the error-free Z_v, indicating that Equation [8] also approximates the true CV in the non-lognormal case well.

Capping after or before compositing?

Some practitioners favour capping before compositing, others advocate doing so after. The argument of the 'before' camp is that possible outliers are averaged in the compositing process and can thus pass undetected, especially when the assay length is related to the presence or absence of visible mineralization. On the other hand, the 'after' camp maintains that assays over longer supports are already diluted, so it seems reasonable to dilute the outliers obtained on shorter supports to treat them like all other segments of the boreholes. But in fact, does it really matter?

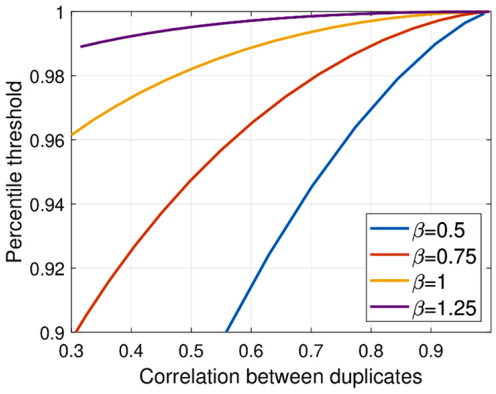

Figure 3—Percentile threshold against ρ_{dup} to have $CV_{cap}^2 = CV_v^2$ for various β values

Table II

Cases considered to evaluate the robustness of the approach

	Case 1	Case 2	Case 3	Case 4	Case 5
Description	Z_v lognormal, *t* normal	Z_v normal, *t* t normal	Z_v normal, *t* lognormal	Z_v two lognormal, *t* lognormal	Z_v two lognormal, *t* normal, contamination
ρ_{dup}	0.87	0.78	0.67	0.75	0.77
Cap grade	49.4	5.0	8.7	5.3	4.9
Perc. cap	0.9996	0.946	0.935	0.940	0.940
Error-free CV	1.31	0.69	0.73	0.63	0.89
Capped CV	1.31	0.69	0.74	0.63	0.87

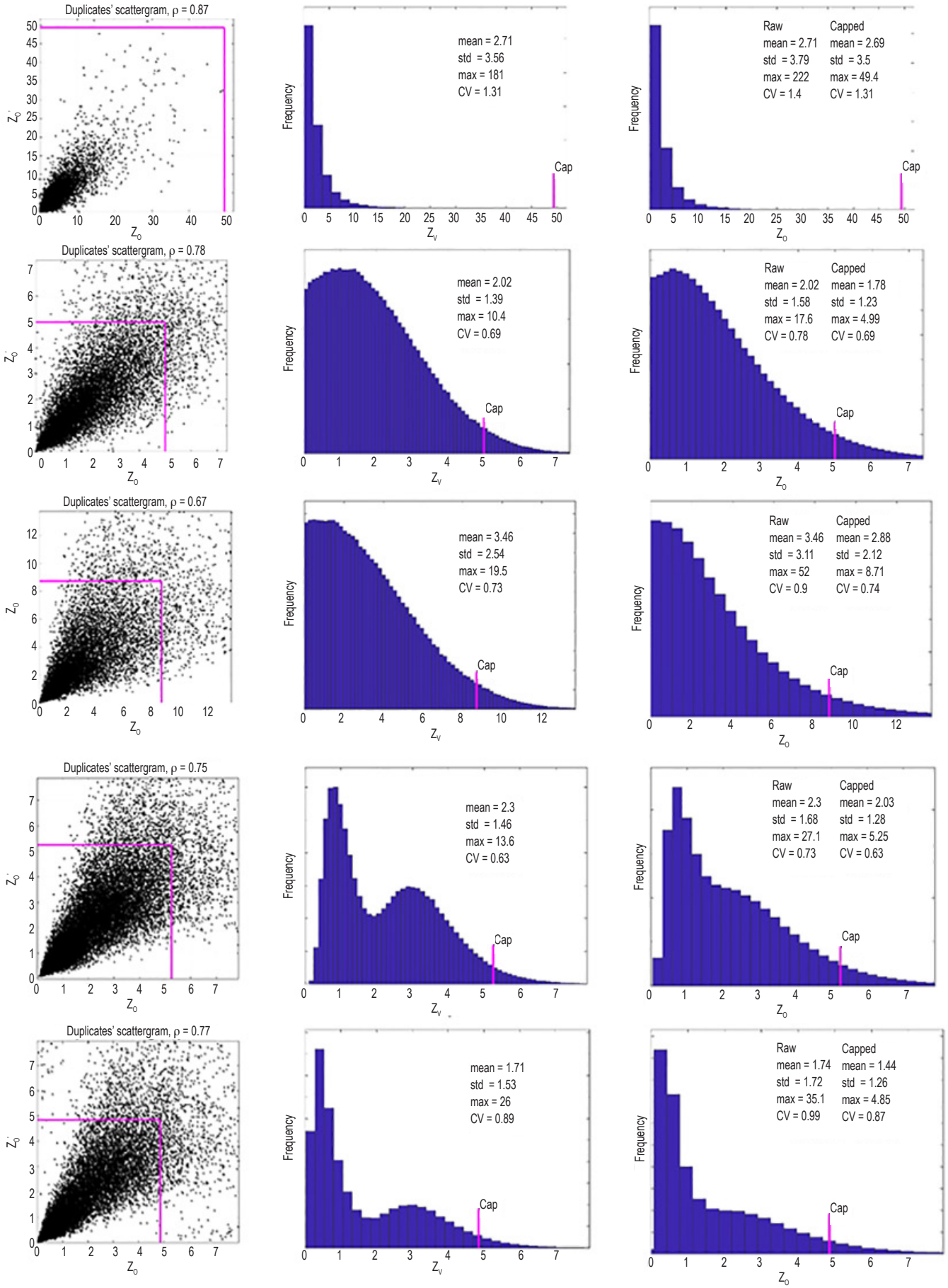

Figure 4—Duplicates' scattergrams (left column), error-free histograms (middle), and observed values histograms (right column) for cases 1 (top) to 5 (bottom) described in Table II

A new grade-capping approach based on coarse duplicate data correlation

A simple experiment

A series of synthetic boreholes totalling 300 000 m are simulated at every 10 cm. The variogram model is spherical with range 20 m. The distribution is lognormal with $\alpha = 0$ and $\beta = 1$. Synthetic grades on variable lengths are computed according to the grade of the first 10 cm. The length is set to 0.5 m when $Z(x) > Q_{90}$ (where Q_{90} is the quantile 0.9 of the simulated distribution), 3 m when $v(x) > Q_{75}$, and 1.5 m otherwise. This scenario mimics preferential sampling of visible mineralization. The 'true' assays Z_v are obtained on the specified lengths by averaging the simulated values. Then a multiplicative error t (drawn from a lognormal distribution with $\sigma = 0.8$) is applied to each assay to form the set of observed assays Z_o.

In the 'before' case, a series of potential cap values is applied to observed assay grades. Then regular 3 m composites are formed using the capped assays. In the 'after' case, the 3 m composites are formed using the raw assays and then the cap values are applied to the composites. The target CV_v for both cases is computed using the simulated Z_v at each 10 cm regularized over the variable length (in the 'before' case) or the composite length (in the 'after' case). Compositing is done on capped values for the 'before' case. The bias on mean in % (relative to simulated uncapped data) after capping the composites is computed. Results are shown in Figure 5. The 'after' case presents slightly less bias on the mean for any given CV_{cap} than the 'before' case. Similar results (not shown) were obtained for different cases by varying the composite lengths, the variogram range, and parameters α, β and σ.

Work flow

To summarize, we propose to apply the following work flow to objectively determine the cap value based on duplicates:

- Compute correlation between coarse duplicates
- Compute the observed coefficient of variation (CV_o) using all data available
- Estimate CV_v, the target coefficient of variation of the error-free composites' grades, using Equation [8]
- Experimentally determine the cap value to apply to the composites to obtain $CV_{cap} = CV_v$.

Case studies

In the following section, two real duplicate data-sets were used to compare the proposed capping strategy to some of the industry's most widely used methods.

Gold case

The first case study is on gold duplicates. Duplicate samples were obtained from 5 m blast-holes (diameter 96 mm) using sampling of the cuttings in the cone around the drill string. Sample preparation consisted of pre-crushing 5 kg of cuttings to 2 mm and then pulverizing 250 g to 75 µm. Fire assaying was done on 30 g aliquots with an atomic absorption (FA-AA) finish. The data-set contains 1 786 samples for a total of 3 572 duplicate assays. The gold duplicates' scattergram (Figure 6) shows $\rho = 0.27$ indicates an important overall sampling error. The artifact below 10^{-2} for both duplicate assays reflects the limits of detection used by the assay laboratory. It is also seen in the spike at low levels in the probability plot. This low correlation is

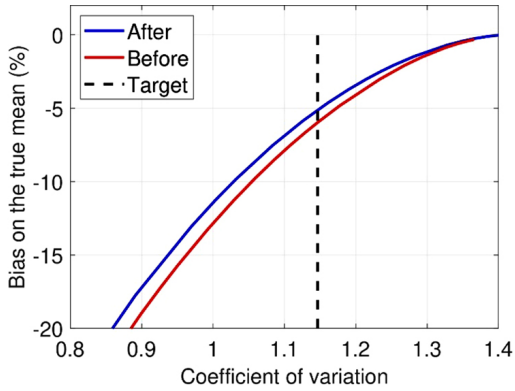

Figure 5—Effect of capping before or after compositing. Bias on the mean against CV for 3 m composites using assays on 0.5 m, 1.5 m, and 3 m; α = 0, β = 1 and σ = 0.8 ; Target CV obtained from error-free composites

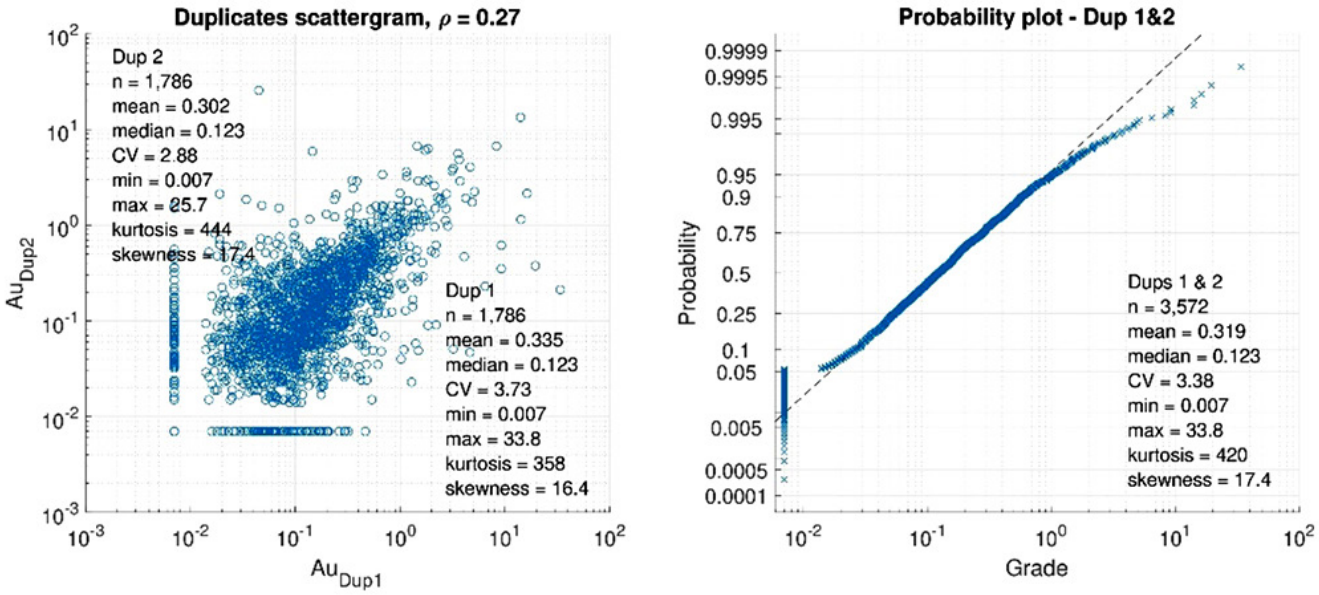

Figure 6—Gold duplicates' scattergram (left) and log probability plot for duplicates 1 and 2 (right)

Table III

Gold case cap results - The target CV (Equation [8]) is 1.76

Capping method	Percentile	Capped level	Capped CV value	Capped mean	Capped STD
Uncap data	n/a	n/a	3.38	0.32	1.08
99th percentile	0.990	3.11	1.67	0.27	0.45
Parrish	0.981	1.91	1.43	0.25	0.36
Log probability plot	0.995	4.49	1.92	0.28	0.53
Duplicates	0.992	3.69	1.76	0.28	0.49

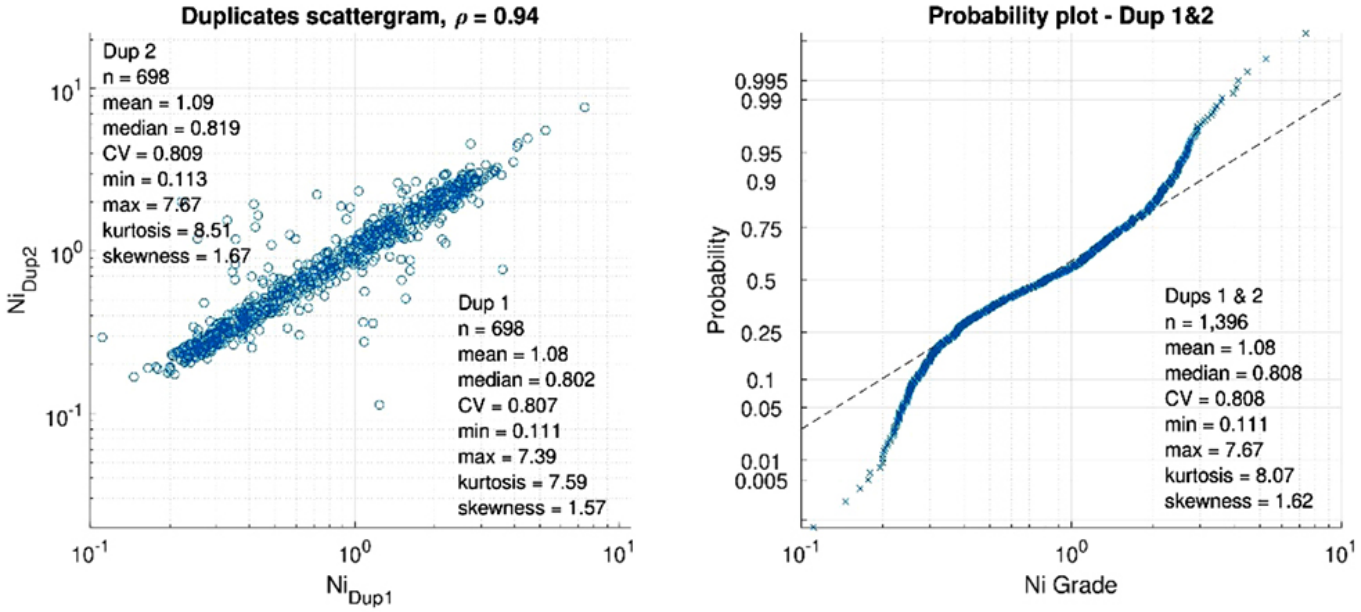

Figure 7—Nickel duplicates' scattergram (left) and log probability plot for duplicates 1 and 2 (right)

Table IV

Nickel case cap results - The target *CV* (Equation [8]) is 0.783

Capping method	Percentile	Capped level	Capped CV value	Capped mean	Capped STD
Uncap data	n/a	n/a	0.81	1.080	0.87
99th percentile	0.990	3.56	0.76	1.07	0.82
Parrish	0.90	2.32	0.70	1.02	0.72
Log probability plot	0.99	3.60	0.76	1.07	0.82
Duplicates	0.996	4.59	0.78	1.08	0.84

undesirable but sadly common in practice, especially in blast-hole samples. The log probability plot shows a gap in the upper tail around the 0.995 percentile value, which was retained as the log probability plot capping level.

Table III presents the cap results obtained using the different methods tested. The cap grades vary from 1.91 g/t to 4.49 g/t. The proposed method shows the second highest cap value at 3.69 g/t. The theoretical CV based on Equation [8] is 1.76. By design, the proposed method returns the same CV. The 99th percentile method returns the next closest one. The log probability plot and Parrish methods suggest cap values that result in a strong overestimation and underestimation, respectively, of the target CV value.

Nickel case

Drilling was done using the air core (AC) technique and 6 kg duplicates were created from the chips using a riffle splitter. Then 500 g of material were crushed to 2 mm and 250 g were pulverized to 75 µm. Fire assaying was done on 20 g aliquots with an XRF finish. The data-set contains 698 samples. Each sample provided two coarse duplicates for a total of 1396 duplicate assays.

The nickel duplicates present similar basic statistics (Figure 7), with a much lower kurtosis value than for the gold data-set. The high duplicates correlation coefficient ($\rho = 0.94$) indicates good reproducibility of the assays, as expected for a base metal deposit.

Table IV shows the cap results obtained using the different methods. The proposed method presents the highest recommended cap value as a result of strong duplicates correlation. All other methods underestimate the target CV (0.783), a consequence of selecting an overly low cap value.

Discussion

In mining applications, extreme values can often be encountered and must be controlled to avoid spreading high grade to large areas. The capping strategy can significantly impact the results of geostatistical and economic studies. In the exploration phase, an unduly low cap value can lead to an overly conservative resource estimate, possibly resulting in project rejection. On the other hand, too high a cap value may lead to an overly optimistic economic valuation and serious losses for mining companies. Various methods have been proposed in the past and are routinely used in the industry to determine cap values. Most are based on rather arbitrary empirical rules or on a subjective graphical interpretation of the cumulative distribution function. None use the important and mandatory coarse duplicate data to help determine a reasonable cap value that takes into account the quality of the assay procedure.

The proposed approach fills this gap. An unbiased multiplicative lognormal error model was used to derive the relationship between the observed and true grade CVs. The two CVs are simply linked through the duplicates correlation coefficient (see Equation [8]). One can predict the unobserved true CV from the observed CV with an estimate of the duplicates correlation. The proposed capping strategy is simple: select the cap value such that the CV of the capped samples is equal to the predicted true CV value.

Simulated data-sets showed that Equation [8] is unbiased for the true CV, even with a relatively small amount of duplicate data (Figure 2). They also showed that the analysed length has a limited impact on the proposed method, as both ρ and CV_o are relatively robust in response to this factor. Finally, Figure 4 illustrates the good stability of the method relative to different departures from the lognormal assumption.

The question of capping before or after compositing was also examined. Simulated data-sets with a preferential re-sampling approach (*i.e.*, the intersections of high grade are analysed on shorter lengths than low grade) were used. The differences between the 'before' and 'after' cases are rather small but systematic. The 'before' case leads to more bias on the mean than the 'after' case for all CVs. We therefore recommend capping after compositing to minimize the bias on the mean.

The proposed approach was compared to some of the methods most widely used in the industry using two real data-sets, one for gold and the other for nickel, where coarse duplicates were available. With the proposed approach, the CV computed using capped data was equal to the predicted true CV by design. Interestingly, the proposed approach had the highest cap value of all the methods tested when reproducible duplicate data was available (nickel case, $\rho = 0.94$) but not for duplicate data with low correlation (gold case, $\rho = 0.27$). This illustrates that the capping strategy of the proposed method, contrary to other methods, takes into account the quality and reliability of assay data measured by duplicates correlation. Other advantages of the proposed approach are its simplicity and objectivity, as it can easily be computed automatically from assays and duplicate data-sets without requiring variogram modelling, kriging, simulation, or cdf plotting and gap/break interpretation like some of the other methods.

When following QA/QC recommendations, thousands of duplicates are typically obtained even before the prefeasibility study. Hence, enough data is available to reliably estimate the correlation coefficient between duplicates. In earlier stages, when only a smaller quantity of duplicates is available, it might be interesting to consider a robust estimator of duplicates correlation. Many such robust estimators are described in the statistical literature. Further study is required to assess the influence of using different correlation robust estimators on the proposed method. Robust estimators of CV_o could also be considered but this appears less necessary as much more data is available for CV_o estimation.

Conclusions

A new capping strategy based on the correlation coefficient between coarse duplicates is proposed. It incorporates the idea that the higher the correlation coefficient between duplicates, the greater the confidence level of the assay value, and accordingly the higher the cap value should be. The method proved to be robust to variations in sample support (assay length), departure from lognormality, and capping before or after compositing. When applied to gold and nickel deposit data, the proposed approach provided cap grades that reflected the reliability of the assays and were generally higher than those obtained with the other methods tested. The proposed approach is simple, objective, and repeatable. It makes it possible to automatically determine the cap grade from duplicate data.

References

Abzalov, M. 2011. Sampling errors and control of assay data quality in exploration and mining geology. *Applications and Experiences of Quality Control*. Intech Open.

Babakhani, M. 2014. Geostatistical modeling in presence of extreme values. Master's thesis, University of Alberta, Canada.

David, M. 1977. Geostatistical Ore Reserve Estimation. Elsevier.

Leuangthong, O. and Nowak, M. 2015. Dealing with high-grade data in resource estimation. *Journal of the Southern African Institute of Mining and Metallurgy*, vol. 115, no. 1. pp. 27–36.

Maleki, M., Madani, N., and Emery, X. 2014. Capping and kriging grades with long-tailed distributions. *Journal of the Southern African Institute of Mining and Metallurgy*, vol. 114, no. 3. pp. 255–263.

Marcotte, D. and Dutaut, R. 2020. Linking Gy's formula to QA/QC duplicates statistics. *Mathematical Geosciences*. September. pp. 1–13, https://doi.org/10.1007/s11004-020-09894-x

Parker, H. 1991. Statistical treatment of outlier data in epithermal gold deposit reserve estimation. *Mathematical Geology*, vol. 23. pp. 175–199.

Parrish, O. 1997. Geologist's gordian knot: To cut or not to cut. *Mining Engineering*, vol. 49. pp. 45–49.

Rivoirard, J., Demange, C., Freulon, X., Lécureuil, A., and Bellot, N. 2013. A top-cut model for deposits with heavy-tailed grade distribution. *Mathematical Geosciences*, vol. 45. pp. 967–982.

Roscoe, W. 1996. Cutting curves for grade estimation and grade control in gold mines. *Proceedings of the 98th Annual General Meeting*, Edmonton, Alberta, 29 April. Canadian Institute of Mining, Metallurgy and Petroleum, Montreal.

Rossi, M.E. and Deutsch, C.V. 2013. Mineral Resource Estimation. Springer Science & Business Media. ◆

A review of the role of underground measurements in the historical development of rock engineering in South Africa

D.F. Malan[1] and J.A.L. Napier[1]

Affiliation:
[1] Department of Mining Engineering, University of Pretoria.

Correspondence to:
D.F. Malan

Email:
francois.malan@up.ac.za

Dates:
Received: 1 Dec. 2020
Revised: 19 Mar. 2021
Accepted: 19 Mar. 2021
Published: May 2021

How to cite:
Malan, D.F. and Napier, J.A.L. 2021
A review of the role of underground measurements in the historical development of rock engineering in South Africa. Journal of the Southern African Institute of Mining and Metallurgy, vol. 121, no. 5, pp. 201–216.

DOI ID:
http://dx.doi.org/10.17159/2411-9717/1443/2021

ORCID
D.F. Malan
https://orchid.org/0000-0002-9861-8735

Synopsis

This paper describes some important aspects associated with historical underground measurements in South African gold and coal mines. Deformation measurements were used to confirm the use of elastic theory to simulate the rock mass behaviour in the Witwatersrand gold mines in the 1960s. Although a prominent time-dependent component of stope closure was measured as early as the 1930s, it was ignored owing to the benefit of adopting elastic theory. Neglecting the time-dependent response of the rock for many decades resulted in important aspects such as the effect of mining rate, the effect of advance per blast, and the need for enhanced design criteria not being explored. Recent work is only now starting to address this gap in knowledge. *In-situ* measurements of large coal specimens in the 1960s and 1970s indicated that a linear formula may possibly be a better approximation of coal pillar strengths. This alternative formulation was never adopted, however, as the power law strength formula was already deeply entrenched in the industry at that stage. In spite of these apparent failures to continuously generate and adopt new knowledge, a key lesson learnt is that major advances in rock mechanics will not be possible without careful monitoring of the rock mass behaviour in experimental sites. Areas requiring further research, such as pillar strength formulae for the Bushveld Complex and enhanced design criteria for the gold mines, can only be developed using extensive underground monitoring programmes.

Keywords
rock engineering, underground monitoring, elastic theory, time-dependence, pillar strength.

Introduction

Even after many decades of research, a number of key rock mechanics questions remain unanswered. Jooste and Malan (2020) recently highlighted the need for additional research in the area of layout design criteria for deep gold mines. Two popular design criteria are currently used in the deep gold mines of South Africa, namely average pillar stress (APS) and energy release rate (ERR). The introduction of these criteria assisted greatly in reducing areas of high stress concentrations, but both criteria are of limited use. It is, for example, not clear what the maximum value of APS on remnants and pillars should be for safe extraction, and it is questionable whether numerical modelling programs calculate this parameter correctly in areas where inelastic rock behaviour is prominent. Elastic ERR has a significant drawback as no dissipative mechanisms are incorporated to allow for failure of the rock mass. Improved methods to estimate the risk when mining pillars and remnants in the deep gold mines are therefore urgently required.

As a second example, the difficulties in estimating the strength of pillars in bord and pillar layouts in the Bushveld Complex are well known (Malan and Napier, 2011). Empirical power-law strength formulae nevertheless remain popular and this is the standard method to determine pillar strength in the hard rock South African platinum and chrome mining industry. The typical form of the formula is well known:

$$\sigma_s = K \frac{w^{\alpha}}{h^{\beta}} \qquad [1]$$

In industry, it is commonly accepted that K reflects the fitted 'strength' of the *in-situ* rock, w is the width of the (square) pillar, h is the height in metres, and α and β are dimensionless constants. Bieniawski and van Heerden (1975) made the interesting comment that K given in Equation [1] has the dimensions of (MPa·m$^{\alpha-\beta}$). Only if $\alpha = \beta$ does K have the meaning of the strength of a cube of rock with unit side length. This subtlety is ignored in industry and it is simply assigned the units of MPa.

The parameters α and β are equal to 0.46 and 0.66 respectively in the well-known Salamon and Munro (1967) coal pillar strength formula. For the Hedley and Grant (1972) formula used in the

Bushveld Complex, $\alpha = 0.5$ and $\beta = 0.75$. The *K*-value is typically taken as between a third and two thirds of the laboratory UCS strength of the rock. A significant effort to develop a new pillar strength formula for the Bushveld Complex was undertaken by the PlatMine research programme (Ryder, Watson, and Kataka, 2005). From this study, it was proposed that $K = 67$ MPa, $\alpha = 0.67$, and $\beta = 0.32$. A new strength formula was also derived for the Merensky Reef pillars (Watson *et al.*, 2008). For the Merensky formula, $K = 86$ MPa, $\alpha = 0.76$, and $\beta = 0.36$.

For the new UG2 and Merensky pillar strength formulae, note that $\alpha > \beta$. This is in contrast to the Hedley and Grant and Salamon and Munro formulae where $\alpha < \beta$. The implications of this can be examined by writing Equation [1] in its alternative form. As pillar volume is given by $V = w^2h$ and defining the width to height ratio, $R = w/h$, Equation [1] can be expressed as:

$$\sigma_s = KV^{(\alpha-\beta)/3}R^{(\alpha+2\beta)/3} \quad [2]$$

It can be seen from Equation [2] that if $\alpha = \beta$, the pillar strength is independent of the pillar volume whereas if $\alpha > \beta$, as in the Salamon and Munro and Hedley and Grant formulations, the pillar strength is predicted to decrease as the pillar volume is increased even if the pillar shape is unchanged. The pillar strength for the Merensky and UG2 formulations, $\alpha > \beta$, will increase as the pillar volume is increased. This is illustrated in Figure 1. It is not clear whether the increase in pillar strength for an increase in volume predicted by the Merensky formula is an appropriate representation of underground pillar strength. Note that the results in the graph are for a cube with a constant width to height ratio (R = 1) where only the volume of the cube is increased. It is expected intuitively that as the volume of rock increases, more discontinuities may be present that may weaken the volume of rock. Bieniawski and van Heerden (1975) emphasised the need for *in-situ* large-scale tests (Figure 2). They stated that for the small laboratory specimens, fewer discontinuities are present and therefore small specimens are stronger than larger specimens.

An objection raised by Bieniawski (1992) is that, according to the Salamon and Munro power law formulation, the cube strength ($w = h$, R = 1) would continue to decrease indefinitely with side length. This is considered unreasonable (Hustrulid, 1976). Most laboratory and field data indicates that the *w:h* strengthening curve has a zero or positively upwards curvature

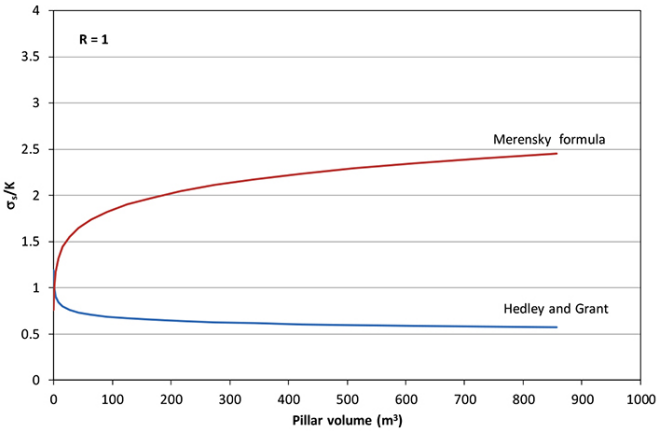

Figure 1—Effect of pillar volume on pillar strength for a constant width to height ratio of 1 (for a cube)

(Ryder and Jager, 2002). The power law formula with $\beta > \alpha$ predicts downward curvature, in contrast. An alternative 'linear' equation, with no volumetric size effect, was therefore proposed and it directly expresses the strengthening effect of the *w:h* ratio (Bieniawski, 1992).

$$\sigma_s = K\left(A + B\frac{w}{h}\right) \quad [3]$$

where *K* (MPa) is the '*in-situ*' strength of a large block (*w:h* = 1) of pillar material and A and B are dimensionless strengthening parameters such that A + B = 1.

It is of interest to note that the original form of the Salamon-Munro pillar strength formulation (Equation [1]) is quoted in the later paper by Salamon, Ozbay, and Madden (1998) in the form

$$\sigma_{Pwr} = K\left(\frac{W}{W_0}\right)^{\alpha}\left(\frac{M}{M_0}\right)^{\beta}, \quad [4]$$

where it is stated that 'the multiplier *K* is the compressive strength of a reference block of coal of height M_0 and width W_0'. Equation [4] is a more satisfactory formulation of the power law relationship but does not include any physical insights into the controlling mechanisms of failure in the pillar system. There would seem to be considerable merit in investigating a non-dimensional strength formula which would include a fundamental length scale that can be related, for example, to a characteristic joint spacing as well as the inclusion of some measure of the fundamental strength of the intact pillar material.

It is clear from these examples that additional research is required regarding the behaviour of the rock mass in the Witwatersrand and Bushveld Complex mines. Owing to the difficulty of many of these investigations, many modern studies are office-based, typically using computer simulations, with little or no comparison to underground observations or measurements. The objective of this paper is to review some historical *in-situ* measurements at experimental sites and to highlight how these had a profound effect on the development of rock engineering in South Africa. The intention is to stimulate renewed interest in the value of these *in-situ* measurements and illustrate the urgent need for more experimental data. Of particular interest are the

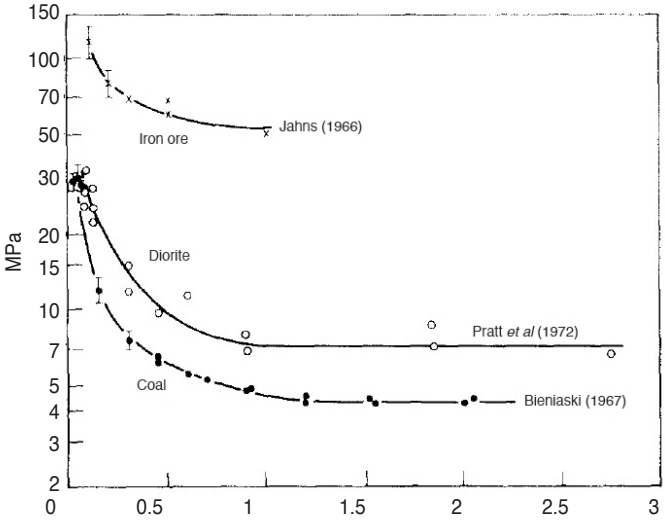

Figure 2—Bieniawski and van Heerden (1975) emphasised that rock strength asymptotically approaches a constant value when conducting large-scale testing

valuable convergence measurements taken before the 1960s and how these revealed an 'inconvenient truth' that was ignored with the widespread adoption of elastic theory. As seismic data and ejection velocities for rockburst support design in the South African mines are extensively described in a number of papers (*e.g.* see Durrheim, 2010; Malan and Napier, 2018), this topic is excluded from this study, as are laboratory tests on small-scale samples.

Franklin (1975) emphasised the role of monitoring in rock engineering. He stated that '*One solution for design based on uncertain data is to adopt a conservative approach with correspondingly high factors of safety. A better alternative is to recognize that much of the design work must be done in the course of execution of the project based on observations of actual rock conditions and on the records obtained by monitoring*.' This is particularly relevant to the pillar strength problem in South Africa as it is suspected that the methodology of using a Hedley and Grant formulation, with a substantially downgraded value of *K*, leads to a conservative approach. As the depth increases in these mines, carefully designed experimental work and monitoring will be required to develop more appropriate strength formulae. Szwedzicki (1989) refers to 'geotechnical assessment deficiencies', which is the difference between prediction and the actual performance of the rock mass. This may lead to collapses and other rock engineering disasters. To minimize these potential problems, site characterization and geotechnical analysis should be carefully planned to understand how the various parameters control the behaviour of the rock mass.

The following sections illustrate the interesting history of stope deformation monitoring and how the adoption of elastic theory eventually leads to geotechnical assessment deficiencies.

Early deformation measurements

Some of the earliest references to closure measurements in South African gold mines can be found in papers by Altson (1933) and Mickel (1935). A report on closure measurements (termed 'hangingwall sag') by R.K. Bradley was published as part of the discussion of the paper by Mickel. Some of his continuous closure profiles are depicted in Figure 3. The detail of his closure measuring instrument is shown in Malan, Napier, and Janse van Rensburg (2007). It is interesting to note that the prominent time-dependent closure between blasts was already recorded in 1935.

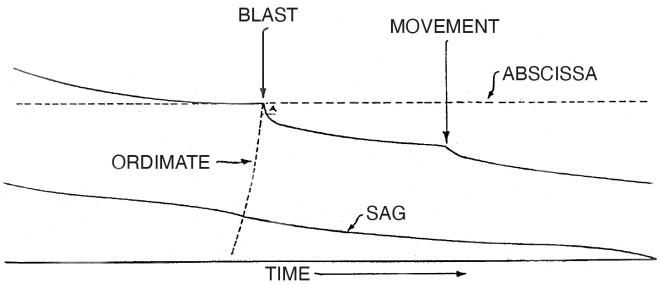

Figure 3—Continuous closure measurements recorded at Crown Mines (after Mickel, 1935). Note that the closure increases downwards on the vertical axis

The National Mechanical Engineering Research Institute of the CSIR conducted deformation measurements at Harmony Gold Mine from 1955 to 1957 (Barcza and von Willich, 1958; CSIR, 1958). Measurements were taken in the ventilation shaft, in two haulages, and closure measurements were taken in stopes. Figure 4 illustrates the layout indicating that early mining of the ventilation shaft pillar occurred, which is why measurements in this shaft were of particular interest. For the period during which the area around the ventilation shaft could be considered as 2D (1957), attempts were made to find a relationship between maximum closure and stope span. This is shown in Figure 5. In

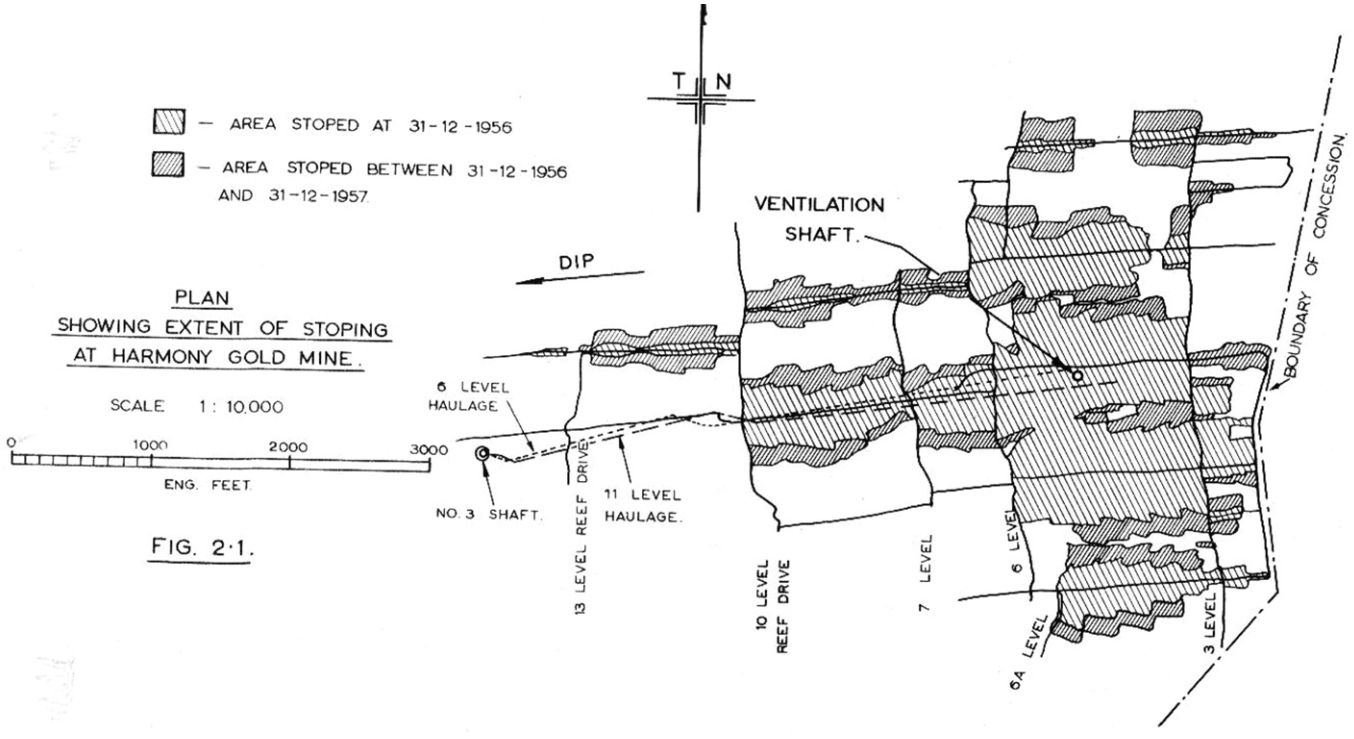

Figure 4—Mining layout at Harmony Gold Mine during December 1957 (after CSIR, 1958)

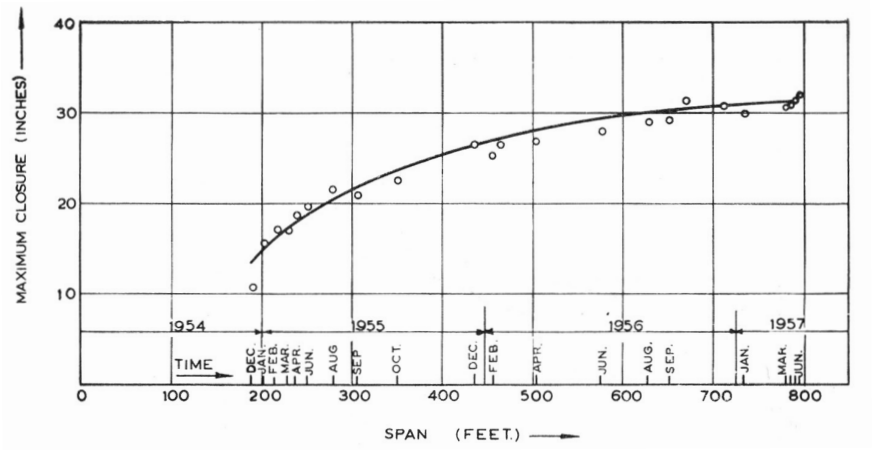

Figure 5—Relationship between maximum closure and stope span at Harmony Gold Mine (Barcza and von Willich, 1958)

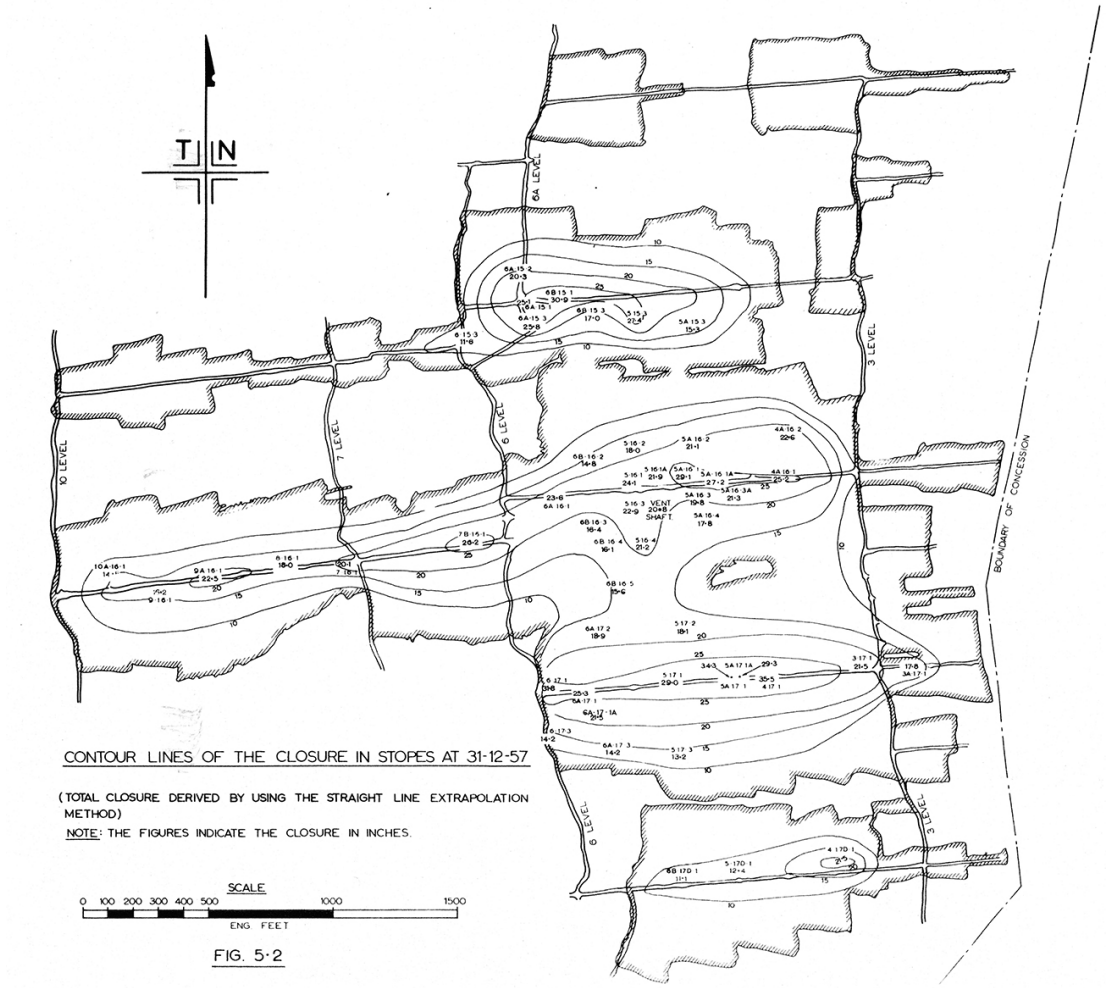

Figure 6—Contour lines of closure in the stope at Harmony Gold Mine during December 1957 (after CSIR, 1958)

1958, the geometry became more complex and as elastic analysis methods for complex layout geometries were not yet available, the CSIR report mentioned that '*In view of the fact that the excavation is of a more irregular shape during the year under review, it was not possible to relate the extent of movement to any variable factor such as stoping span*.' The results nevertheless indicated that the zone of movement and fracturing around the ventilation shaft became progressively larger as the excavated area increased in size. An important finding was that points above a stoping excavation move downwards while points below the excavation move upwards. This was important evidence for the adoption of elastic theory to simulate the behaviour of the intact rock mass in the 1960s. Interestingly, the CSIR noted in the report that from the measurements they could deduce that closure on the reef elevation was composed of approximately 60% hangingwall movement ('sag') and 40% footwall rise. Estimated contours of closure lines were derived from the measurement points. These are given in Figure 6, and this is noteworthy as it probably was the first contour plot of closure in a gold mine stope.

Leeman (1958) conducted extensive measurements of closure and ride in the 64E stope, Angelo Section, at East Rand Proprietary Mines (ERPM). The depth below surface was approximately 2700 m. These experiments were conducted to investigate if there was a relationship between closure behaviour and rockbursts. The mine layout in those years and the experimental site are shown in Figure 7. The instruments used were a 'plumb-bob' closure and ride meter and the CSIR closure

Figure 7—Locality of the longwall stope at ERPM where continuous closure measurements were recorded (area 9) (after Leeman, 1958). The longwall is shown at the bottom

recorder. These instruments are shown in Figure 8. Characteristic data from the closure recorders is given in Figure 9. Leeman emphasised the ongoing closure, even in the absence in blasting, and referred to this as 'gradual closure'.

Leeman found that the closure decreased as the measurement position moved away from the face (Figure 10). This figure illustrates the significant contribution made by the 'gradual closure' to the total closure measured. In his conclusions, he made the comment that '*the closure is probably nothing more than the gradual subsidence of a mass of fractured rock in the hanging-wall plus the "squeezing" upwards in the footwall of a similar mass of fractured rock*.' He could not find any relationship

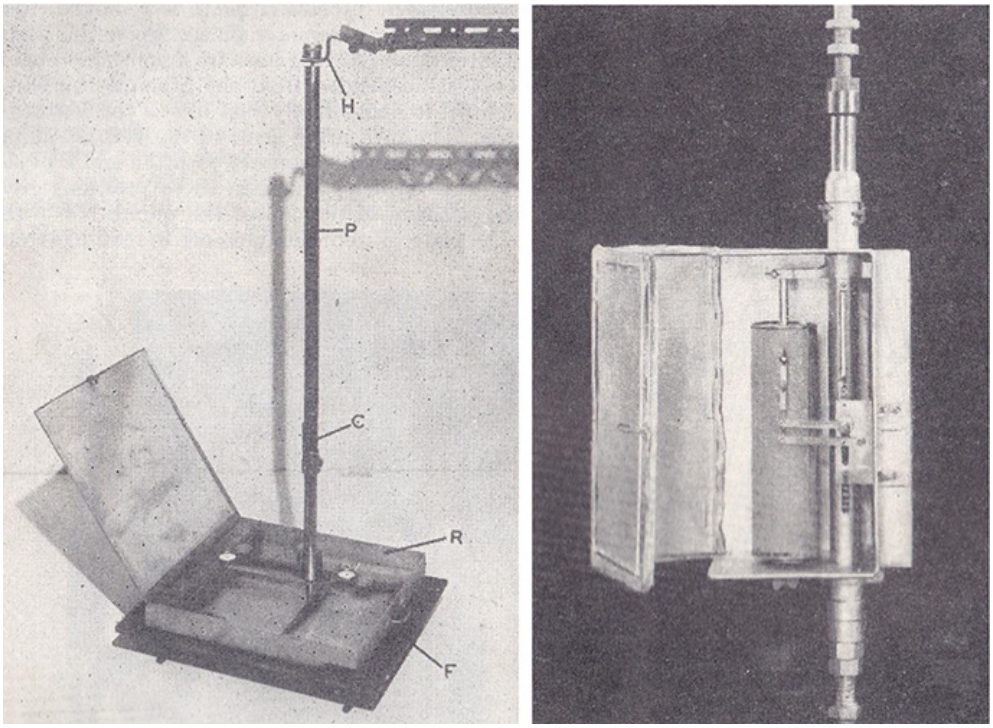

Figure 8—Type of closure instruments used. A plumb-bob closure and ride meter is shown on the left and a CSIR closure recorder on the right (after Leeman, 1958)

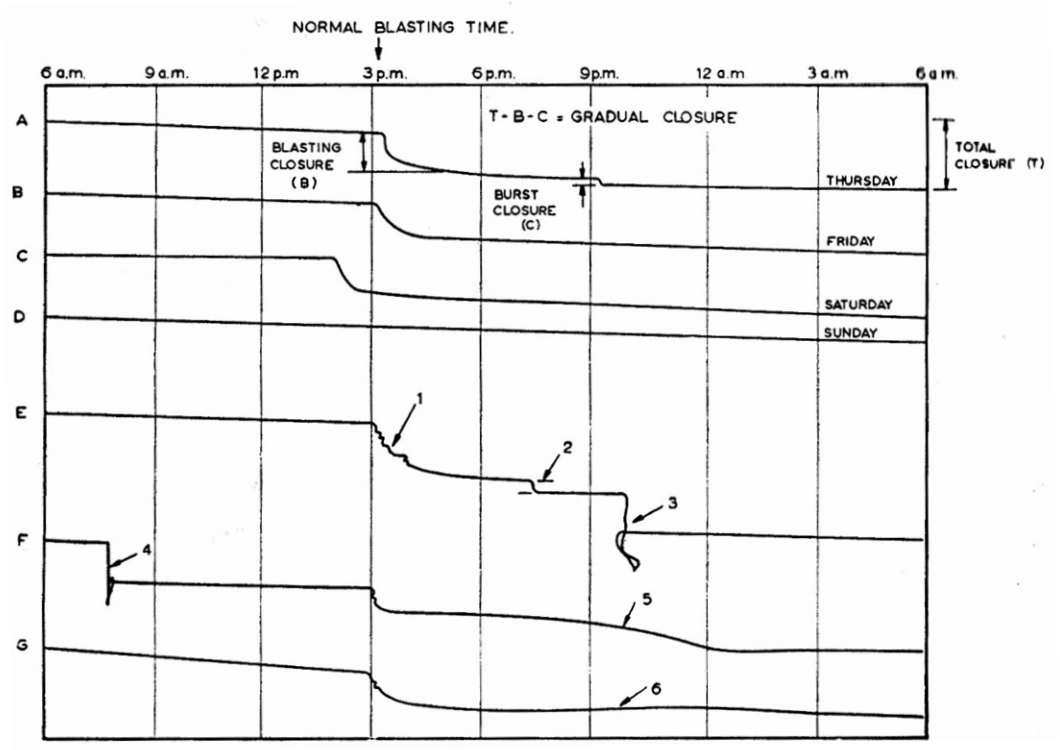

Figure 9—Characteristic closure curves recorded by the continuous closure recorders. Note the ongoing 'gradual closure' during Sunday, when no blasting occurred (after Leeman, 1958)

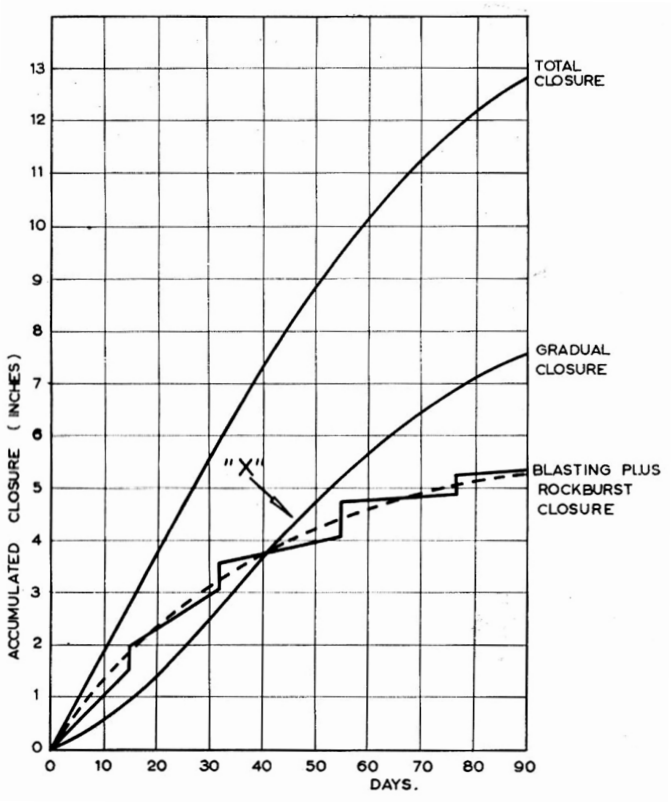

Figure 10—Characteristic closure curves recorded in the stope as the measurement point moved further away from the face into the back area (after Leeman, 1958)

between closure behaviour and rockbursts. The rate of gradual closure was a minimum on Sundays when no blasting occurred and he concluded '*the effect of blasting is to accelerate the gradual closure in a stope*.'

It is significant that the Leeman (1958) paper illustrated very clearly that the fractured rock mass surrounding the stopes results in time-dependent closure behaviour when measuring in a continuous fashion between the footwall and hangingwall of the stope. Evidence of the fractured rock mass, consisting of a hard brittle material, behaving in a creep-like fashion was a major discovery. Creep behaviour is more usually associated with soft rocks such as salt and potash. Surprisingly, this important finding was ignored after 1958 and the Leeman paper gathered dust for the next three decades.

Systematic continuous closure measurements and the time-dependent nature of the rock mass were only recorded again in the 1990s as described by Malan, Napier, and Janse van Rensburg (2007). The reason for this was probably that elastic theory was already deeply entrenched by the 1960s, as described in the next section.

Deformation measurements and elastic theory

Hoek (2006) wrote that '*Much of the early work in rock mechanics applied to mining was focused on the problem of rockbursts and this work is dominated by theoretical solutions which assume isotropic elastic rock and which make no provision for the role of structural discontinuities. In the first edition of Jaeger and Cook's book, Fundamentals of Rock Mechanics (1969), mention of structural discontinuities occurs on about a dozen of the 500 pages of the book. This comment does not imply criticism of this outstanding book but it illustrates the dominance of elastic theory in the approach to rock mechanics associated with deep-level mining problems*.' It seems as if the adoption of elastic theory to describe the behaviour of the rock mass had already gained momentum in the 1950s. Roux and Denkhaus (1954) describe the approach of assuming an elastic, homogeneous, and isotropic rock mass to predict the distribution and magnitude of stress around mining excavations. In the paper, they gave solutions for the stress distribution around circular and elliptical openings. For more complex mining geometries, such as the tabular-shaped stopes, they recommended that photo-elastic methods be used and they illustrated the stress distribution around a slot in a plate subjected to vertical pressure. Denkhaus (1958) published a seminal paper with the title: '*The application of the mathematical theory of elasticity to problems of stress in hard rock at great depth*.' This paper is rarely quoted by the rock engineering fraternity in modern times, but it is a key source illustrating the early adoption of elastic theory for analysis in the South African mining industry. Figure 11, for example, illustrates Denkhaus' proposal to use the principle of superposition and the analytical solutions for the stress around circular and elliptical openings to illustrate the elevated stress in the 'remnant' between the two openings.

Regarding who should be credited with first proposing elastic theory for use in the South African mining industry, Denkhaus, Hill, and Roux (1958) note that in 1952 the Central Mining – Rand Mines Group commissioned a research team from the CSIR to investigate the rock stress problem at depth. This initiative proved to be so successful that that in 1956 the Transvaal and Orange Free State Chamber of Mines agreed to assume sponsorship of the research programme. To oversee the work, a 'Rockburst and Strata Movement Research Committee' composed of members from the Chamber of Mines, the CSIR, and mining groups was established. A key task of the research team was to investigate if the stress around mining excavations can be determined by mathematical analysis. A major driver for the research team's proposal to use elastic theory was that laboratory compression tests on rock specimens from the Witwatersrand indicated that rock behaves essentially elastically up to the point of failure. Denkhaus (1958) referred to earlier papers from other countries that applied elastic theory to mining problems, such as Terzaghi and Richart (1952). Regarding the fracture zone, Denkhaus admitted that '*Obviously this fracture zone, which does not necessarily extend up to surface, cannot be regarded as a continuous elastic solid body to which the theory of elasticity*

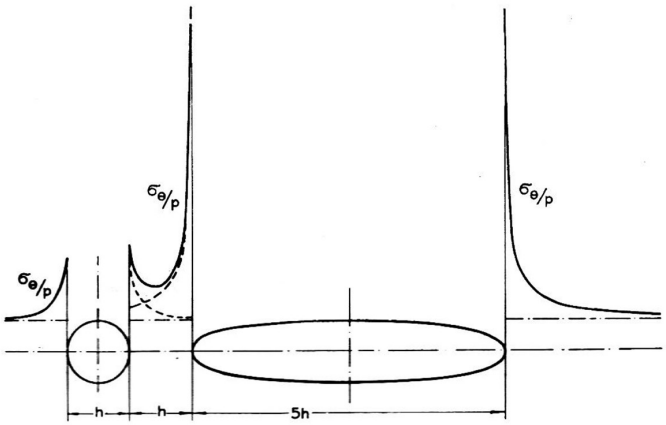

Figure 11—Stress distribution in the rock between a circular and elliptical opening subjected to a uniaxial vertical load (after Denkhaus, 1958)

can be applied. The stress in the solid rock surrounding the fracture zone, particularly the stress at the boundary of the fracture zone, can be determined by means of the theory of elasticity, however.' Interestingly, he also admitted that the effect of creep is beyond the scope of elastic theory, as he must have been aware of the time-dependent closure measurements that his colleague Leeman collected.

It is of interest to note that at the same time as these studies were carried out a number of breakthroughs were achieved in coal mine design. A significant early contribution was the publication of the paper by Hackett in 1959 in which a parallel-sided panel geometry was suggested to be analogous to a crack in an elastic medium, with the important distinction that the opposing faces of the crack could interpenetrate one another in the same manner as the roof and floor of a mine excavation. Hackett used this model to explore the distribution of the stress state and displacements near a parallel-sided panel excavation. He found that predicted displacements were in good qualitative agreement with available field measurements. It is of great interest that Hackett acknowledges the contributions of R. Hill for his technical support of the suggested approach. This pioneering work was followed by a series of ground-breaking papers by Berry (1960, 1964) and Berry and Sales (1961, 1964) which laid the theoretical foundation for the numerical technique now commonly referred to as the Displacement Discontinuity Method (DDM). Berry (1960) makes the following explicit acknowledgement: '*The author is grateful for much helpful discussion on various aspects of the problem to his colleagues, Mr. T.W. Sales, Dr. P. Hackett, Professor F.B. Hinsley and particularly to Professor R. Hill who was responsible for the fundamental idea of the excavation as a dislocation*.' It is not commonly realized that the basic concept of representing a narrow tabular mine excavation as a 'crack' is apparently due to R. Hill, who is known more widely for his seminal text on plasticity theory (Hill, 1950). It is of interest as well that the time-dependent nature of ground movements near coal mine excavations was also recognized in the paper by Berry (1964), which includes a section on the representation of the host medium as a viscoelastic material.

The description of the tabular excavation model as a 'displacement discontinuity' is used several times by Berry (1960, 1964) and by Berry and Sales (1961, 1964). The same concept was introduced in the early foundational papers written by Salamon (1963, 1964a, 1964b, 1965) and was termed by him the 'Face Element Principle'. Salamon also introduced two further models to describe rock strata flexure in addition to the isotropic elastic and transverse isotropic elastic models. These novel alternatives include the so-called 'frictionless laminated model' comprising a quasi-continuum derived from the vertical response of a stack of contiguous, horizontal elastic plates and the 'multi-membrane model' in which bedded strata are approximated by a large number of horizontal membranes (which do not support bending moments) connected by a large number of vertical springs.

The displacement discontinuity technique was formulated in numerical computer codes in the late 1960s using then newly available mainframe computers. Early examples of these efforts were presented by Starfield and Fairhurst (1968) and by Plewman, Deist, and Ortlepp (1969). A description of the popular South African tabular mine design tool, known as MINSIM, which was developed at the Chamber of Mines of South Africa Research Organisation (COMRO) was published by Deist, Georgiadis, and Moris (1972).

The displacement discontinuity method, however, only became recognized as an identifiable numerical technique analogous to the finite element method following the publication of papers by Crouch (1976) and the subsequent publication of the now iconic textbook by Crouch and Starfield in 1983. The technique is exhibited in this text in a much more general setting than as a specialized tool for tabular mine excavation analysis and has been used extensively for the analysis of geological fault mechanics, fracture mechanics and fracture growth, and notably for the analysis of fluid-driven hydraulic fracture propagation.

The adoption of the elastic concept was reinforced by another set of famous deformation measurements conducted early in the 1960s. Ryder and Officer (1964) measured the rock mass deformation in the hangingwall and footwall near the K and L longwalls at ERPM from 1961 to 1963 (Figure 12). The 58 haulage in the hangingwall and the 68 haulage in the footwall provided access to regions remote from the stopes and away from the fracture zone (Figure 13).

Vertical displacements were measured in the haulages using accurate surveying techniques and a number of benchmark points spaced along the haulages. The measurement points were anchored 8 feet into the rock to avoid the influence of local fractured material. The results obtained for the 68 haulage are shown in Figure 14. The longwall mined over this footwall haulage and the upward movement of the haulage is shown. These results are compared to the displacement predicted by a 2D analytical elastic solution of an inclined slit (to represent the stope). The results for the 58 haulage are shown in Figure 15. As this haulage was in the hangingwall, the parts being undermined moved downwards. In both cases the agreement between the measured and theoretical displacements was good, in spite of the fact that a 2D analytical solution was used. These graphs are historically significant as the study was the first to compare theoretical elastic displacements in the rock mass with actual movements observed in the vicinity of a deep-level longwall (it was the first comparison between movements and elastic theory as confirmed by Ortlepp and Nicoll, 1964).

Based on this good fit, the authors concluded that the observed displacements in the rock mass remote from mining excavations are essentially in agreement with elastic theory. It was also found that the elastic constants determined from small specimens appear to be a good estimate of the properties of the rock mass underground. The values used in this study were a Young's modulus of 80 GPa and a Poisson's ratio of 0.16.

Ortlepp and Cook (1964) used a similar simplified 2D elastic solution to compare measurements close to a longwall at Harmony Gold Mine with elastic theory. Ortlepp and Nicoll (1964) extended the work of Ryder and Officer (1964) by using an electrical analogue to simulate the rock movements at Harmony Gold Mine and ERPM. This analogue could account for the complex geometry. This work confirmed the earlier simplified elastic analyses and validated the concept of elastic behaviour for the rocks in the South African gold mines. The updated fit for the 58 hangingwall haulage at ERPM is shown in Figure 16.

Based on this flurry of publications using elastic theory to predict far field rock mass movements, significant effort was dedicated in the years that followed to develop further techniques to simulate complex 3D layout geometries (*e.g.* Salamon, 1963, 1964a, 1964b). As this required a significant effort, it

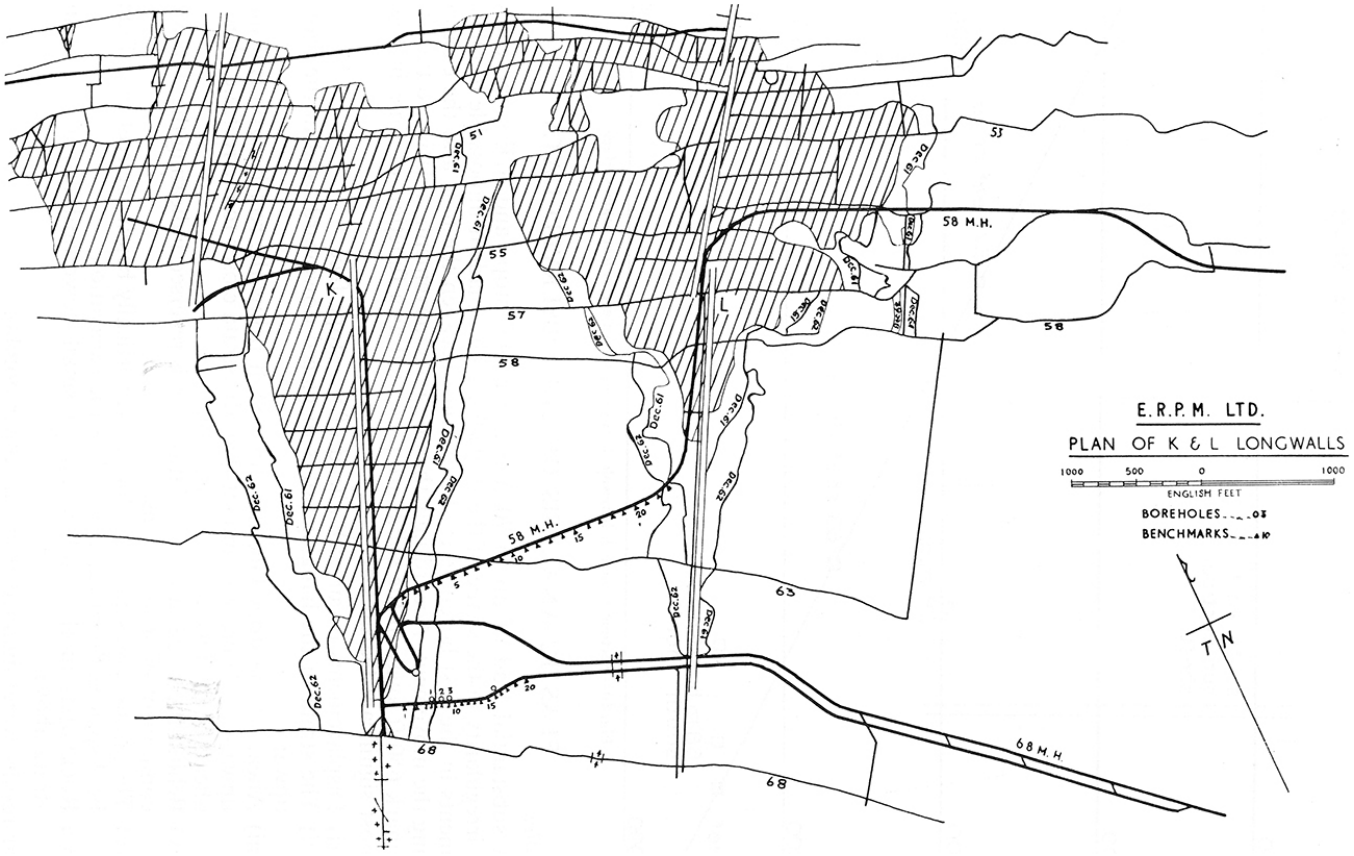

Figure 12—Mining geometry at the start of the deformation monitoring experiment at the K and L longwalls at ERPM (after Ryder and Officer, 1964)

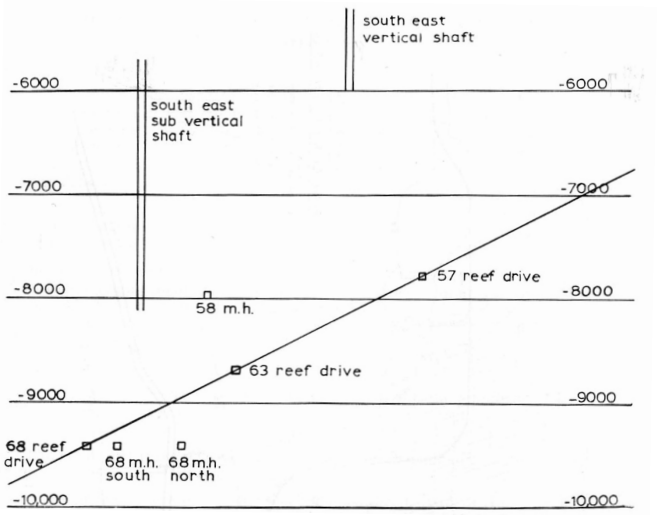

Figure 13—Section through the K longwall at ERPM showing the elevations of the 58 haulage and 68 haulage (after Ryder and Officer, 1964)

is hypothesised that the behaviour of the fracture zone and associated time-dependent behaviour recorded earlier by Leeman (1958) was not given the necessary attention.

Early work on the time-dependent behaviour of the rock mass

Roux and Denkhaus (1954) already hypothesised that the rock mass behaves in a time-dependent fashion, as rockbursts frequently occurred several hours after blasting when no changes in geometry occurred that could affect the stress field. They conducted creep tests on quartzite specimens and illustrated that time-dependent behaviour was observed for these specimens. Hodgson (1967) referred to the successful use of elastic theory to describe the far field rock mass behaviour and the design criteria proposed on the basis of this, but noted that '*The behaviour of the rock in the region between the elastic solid and the excavation is of the most immediate concern to mining practice but has been inadequately formulated.*' He suggested that if continuous measurements of closure are recorded, an estimate can be made of the proportions of energy change associated with

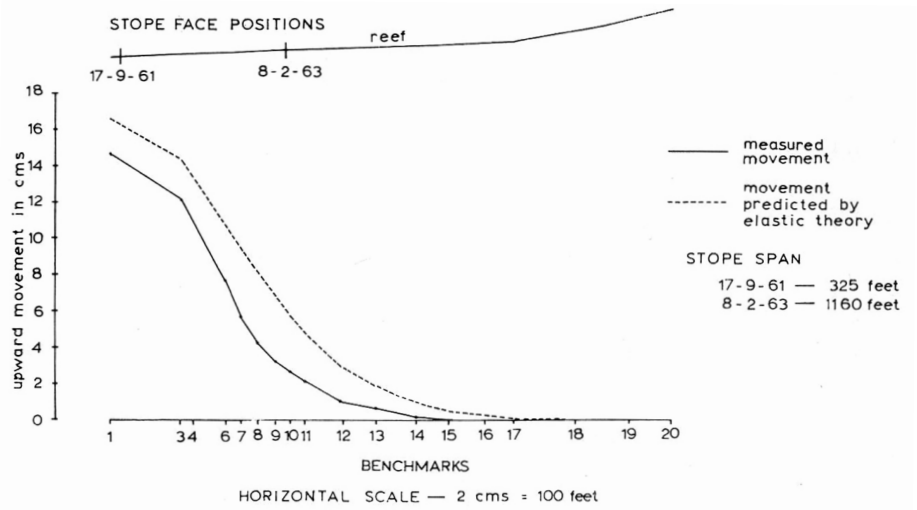

Figure 14—Comparison between the measured and theoretical 2D elastic displacement of the 68 footwall haulage at ERPM between 1961 and 1963 (after Ryder and Officer, 1964)

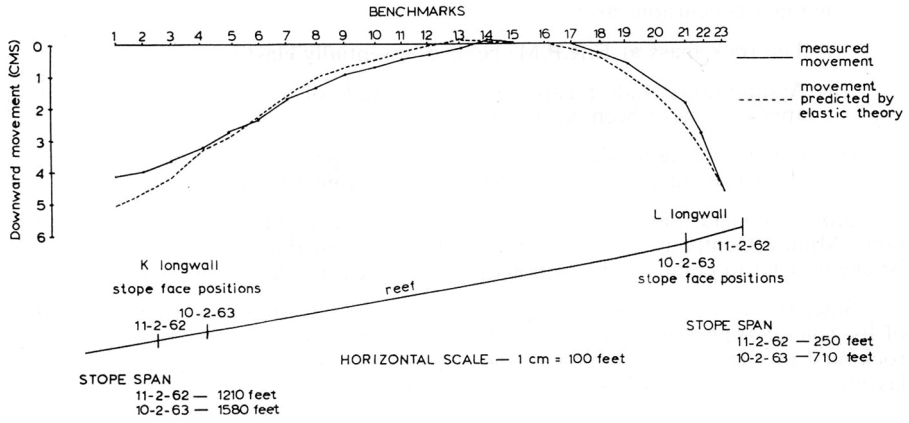

Figure 15—Comparison between the measured and theoretical 2D elastic displacement of the 58 hangingwall haulage at ERPM beween 1961 and 1963 (after Ryder and Officer, 1964)

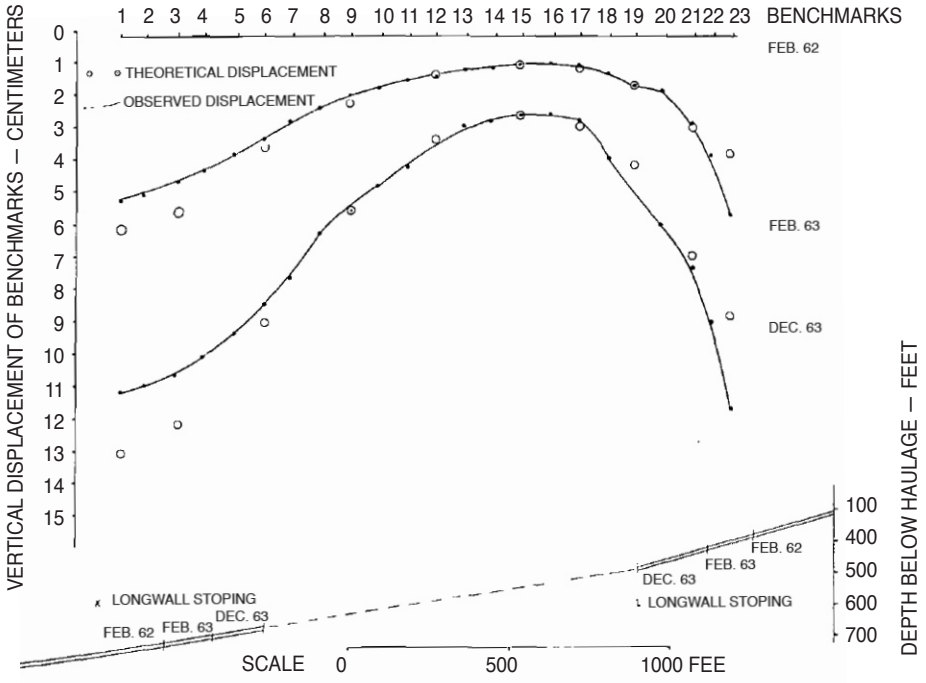

Figure 16—Comparison between the measured and theoretical 3D elastic simulation of the 58 hangingwall haulage at ERPM (after Ortlepp and Nicoll, 1964)

violent and non-violent energy release. Hodgson collected data in the K and L longwalls at ERPM. The convergence meter was a nickel-chrome wire anchored in a borehole at a depth of 50 feet in the hangingwall, which extended through the stope into the crosscut below, 50 feet into the footwall, and was tensioned by springs. The instrument is shown in Figure 17. An LVDT was used to record the displacement of the wire on a continuous basis.

Hodgson found that the long-term total convergence was in agreement with the elastic displacements from stope geometry changes, but there was a time-dependent component controlled by the behaviour of the failed rock near the face. He examined the energy balance proposed by Cook *et al.* (1966) and proposed that the time-dependent convergence has implications for mining cycles, rates of face advance, and stope support. He proposed a model – a migrating fracture zone to account for the observed closure behaviour (Figure 18). Based on this model, he suggested that the rockburst hazard will increase if too high a face advance rate is attempted.

Hodgson concluded by stating that '*The observations have shown that the most important property of the failed zone is time-dependent behaviour and that this behaviour is of direct concern to practical problems of designing support, face advance per blast and frequency of blasting so as to minimize the rockburst problem or, at least avoid aggravating it.*'

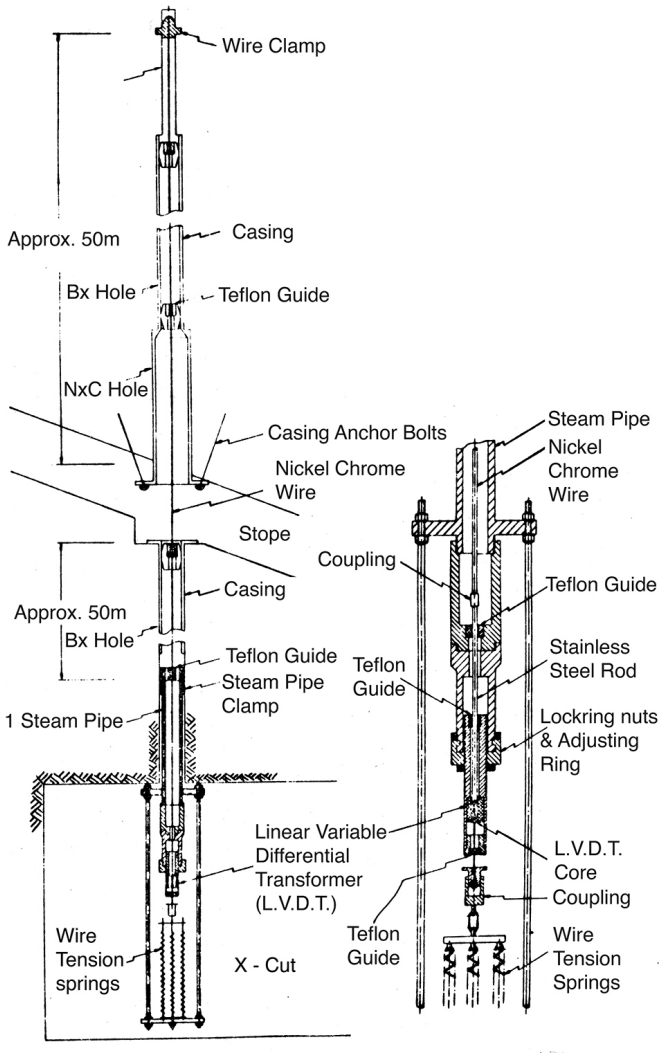

Figure 17—Convergence meter used by Hodgson (1967)

This was a profound statement, but unfortunately this important work was not considered again until the 1990s (Malan, 1999, 2002).

In-situ tests on large rock specimens

Although not related to closure measurements, this section is included to illustrate the elaborate underground measurements that were conducted on large coal specimens in the early 1970s. This is a useful illustration of what can be achieved with appropriate planning and the value that can be gained from these tests. It unfortunately also demonstrates that once concepts in rock engineering become entrenched, it is very difficult to displace them, even if good experimental results are obtained that indicate possible better solutions.

Cook, Hodgson, and Hojen (1971) describe the use of a 100 MN jacking system to test coal pillars underground. This was an important test of the empirical relationship (Equation [1]) proposed by Salamon and Munro (1967) and it is surprising that this paper by Cook is almost never quoted in the literature. A motivation for this study was that ever-larger coal pillars are required as the depth of mining increases (similar to the current problem faced by the platinum industry). One suggested solution was the use of barrier pillars and smaller yield pillars between these barriers. The complete load-deformation curves for the pillars were required. A system of jacks was developed to load pillars with a cross-section of 2 m × 2 m in the underground workings. The jacks were installed in a horizontal slot along the central plane of symmetry of a pillar. A photograph available to the author of these kinds of experiments by the Chamber of Mines is shown in Figure 19. The work by Cook, Hodgson, and Hojen (1971) is shown in Figure 20. The agreement between these test results and the empirical equation developed by Salamon and Munro (1967) is shown in the figure.

Bieniawski and van Heerden (1975) gave an overview of large-scale *in-situ* tests done throughout the world. Bieniawski himself was involved with the testing of 66 large coal specimens in underground mines. Based on this work, Bieniawski proposed

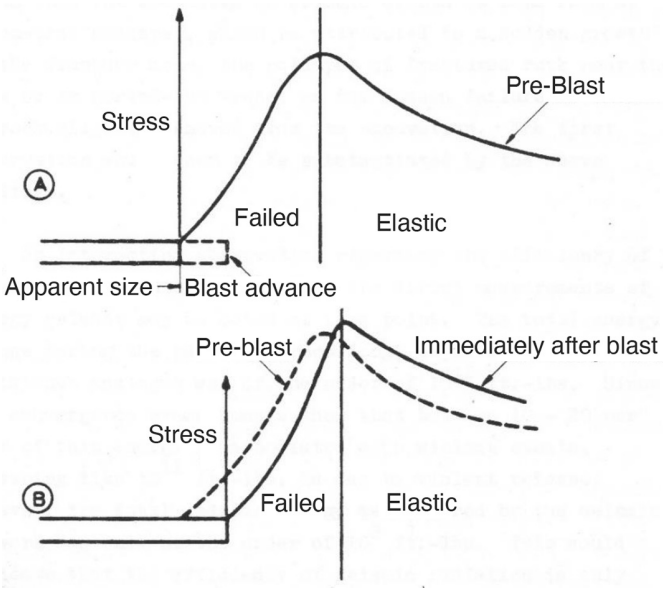

Figure 18—Migration of the fracture zone as proposed by Hodgson (1967). He suggested this migration occurs in a time-dependent fashion to account for the observed closure behaviour

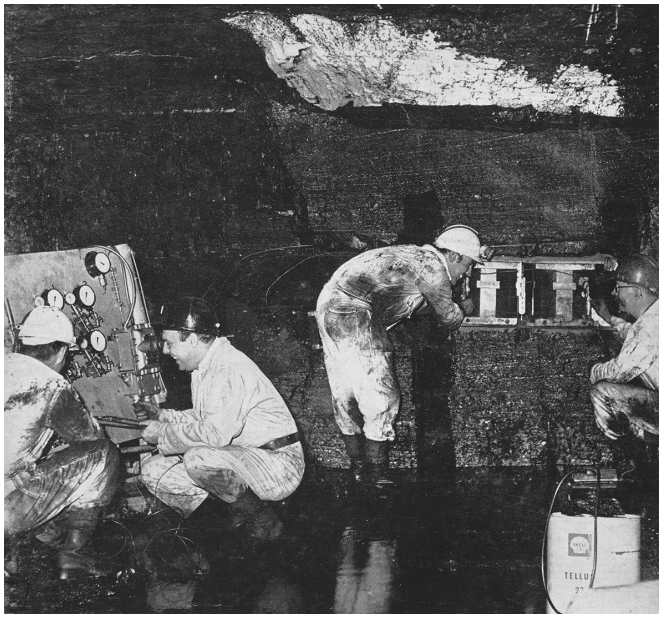

Figure 19—Loading of a coal pillar by jacks installed in a slot cut in the pillar

that the linear formula given in Equation [3] is preferable for describing the strength of coal pillars (Figure 21).

In spite of the disagreement regarding the most appropriate empirical strength formula to use, the underground coal experiments further increased the confidence in coal pillar strength. In contrast, appropriate experimentation was never done on the platinum mines to verify the formulae used and the uncertainty regarding pillar strength remains to this day.

Problems caused by the adoption of elastic theory

As noted by Hoek (2006), in the book by Jaeger and Cook, Fundamentals of Rock Mechanics (1969), structural discontinuities are described on only approximately a dozen of the 500 pages of the book. This illustrated the dominance of elastic theory in the approach to rock mechanics associated with deep-level mining in the early years. By the 1980s, elastic theory was firmly entrenched in the design of layouts and the application of the associated ERR criterion was a key aspect of the strategy to control rockbursts (see, *e.g.* Heunis, 1980). As stated by Heunis: '*Irrespective of the method used, the effectiveness of reducing the energy released by mining depends strictly on the prevention of elastic closure and ride in the mined out area*'. The focus on

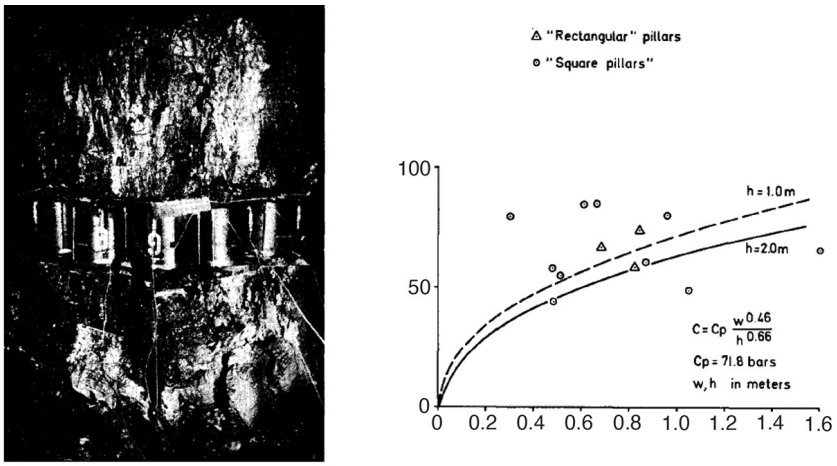

Figure 20—Experimental work conducted to test the *in-situ* strength of coal pillars (after Cook, Hodgson, and Hojen, 1971). The graph on the right illustrates the predicted strengths using the power law strength formula and the test results of all the pillars tested

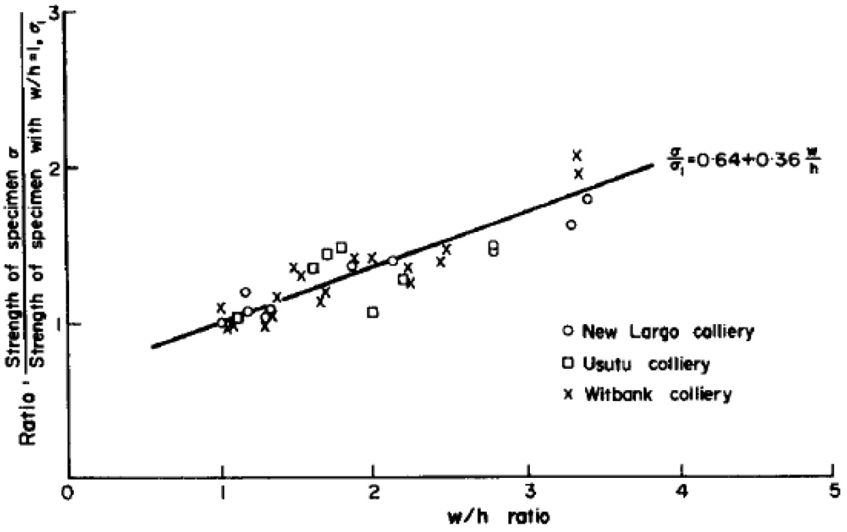

Figure 21—Results from the large-scale tests conducted underground, and a fit using Equation [3] (after Bieniawski and van Heerden, 1975)

elastic closure resulted in difficulties when researchers attempted to analyse detailed measurements of stope closure, as illustrated below.

Walsh *et al.* (1977) conducted closure measurements at West Driefontein Gold Mine. Data from four closure stations at a distance of less than 15 m from the face showed that convergence and ride are significantly larger than predicted by elastic theory. They suggested that '*Slip on cracks in the hangingwall and footwall apparently controls deformation in this region*.' Gurtunca and Adams (1991) published a paper with a proposal to determine the *in-situ* modulus of the rock mass by using backfill measurements. They measured convergence in stopes supported by backfill and found that the closure is significantly higher than that predicted by elastic theory when using the MINSIMD modelling package and a Young's modulus of 70 GPa (Figure 22). They recommended a reduction in the Young's modulus to more accurately simulate the closure, and values between 40 GPa and 70 GPa were deemed more appropriate. They mentioned that it is difficult to separate the magnitudes of inelastic closure from the elastic convergence, but recognized that the inelastic behaviour of the rock mass caused by the fracture zone around these stopes is responsible for the unexpectedly large closure measured in the backfill. They proposed that '*The use of an in situ modulus provides an effective interim solution until a new computer model that allows for joints, different layers, and inelastic closures becomes generally available*.'

Stacey (1991), in his response to the Gurtunca and Adams (1991) paper, felt that this interim solution should not be used as a downgraded elastic modulus is no more correct than any other modulus that has been used. What is required is greater engineering understanding and interpretation by rock engineers when using the existing tools.

These controversies arose as a suitable model to simulate the inelastic stope closure and the prominent time-dependent stope closure, recorded as long ago as 1935, was never developed. Elastic theory and numerical modelling techniques made the simulation of stress and displacement for irregular geometries on a stope-wide scale possible. This was such a huge step forward that ignoring the effect of the fracture zone was deemed acceptable.

Recent measurements of time-dependent rock deformation

The early time-dependent closure results from Leeman (1958) and hypotheses of mining rate behaviour by Hodgson (1967) were further investigated by Malan, Napier, and Janse van Rensburg (2007). Malan conducted extensive measurements of continuous closure in a number of gold mines and profiles similar to that illustrated in Figure 9 were obtained. It was also discovered for the first time that the closure behaviour of crush pillar layouts in the intermediate depth platinum mines also contain a significant time-dependent component (Figure 23). The closure data was found to be a wonderful diagnostic for rock mass response.

Malan, Napier, and Janse van Rensburg (2007) found that the closure measurements contained a significant time-dependent component in spite of the brittle nature of the rock. Time-dependent rates as high as 1 mm/h were measured in extreme cases. The time-dependent closure component appears to be ubiquitous in the gold mines and intermediate depth platinum mines and is even observed in very brittle environments such as Ventersdorp Contact Reef stopes with a Ventersdorp lava hangingwall. Various approaches to simulate the time-dependent closure have been investigated since this work was initiated. Plane strain analytical solutions for the convergence of stopes where the rock behaves as a Burgers viscoelastic material in distortion were derived (Malan, 2002). These models gave a reasonable fit to data recorded underground. Although viscoelastic theory therefore appears to be able to simulate time-dependent closure behaviour, there are subtle problems with the use of this theory as it cannot simulate the failure processes in the rock and care should be exercised when attempting to use these models. To overcome these problems, continuum and discontinuum elasto-viscoplastic models have been developed. Discontinuum models have the advantage of being able to simulate the creep behaviour of prominent discontinuities. The development of these models has provided useful insights into rock mass deformation and has enabled the simulation of parameters such as rate of mining to be conducted for the first time.

By recording the time-dependent closure behaviour, a number of practical applications for the mining industry became available. Among these are the delineation of geotechnical areas using closure data, use of the data as a hazard indicator, and to give warning of large collapses in the platinum mines (Figure 24), identification of areas in need of preconditioning in the gold mines, measurement of the effectiveness of preconditioning, and improved data for support design to include the effect of mining rate. Additional detail is given in Malan, Napier, and Janse van Rensburg (2007).

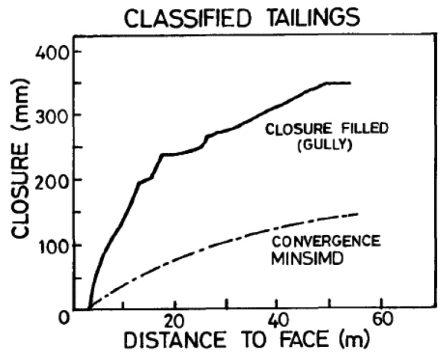

Figure 22—Difference between closure measured in a backfilled stope and elastic modelling (MINSIMD) (after Gurtunca and Adams, 1991)

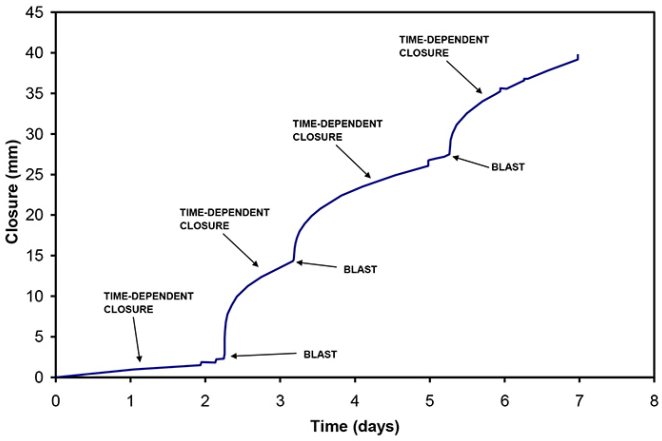

Figure 23—Typical continuous closure behaviour in a deep Merensky Reef stope (after Malan, Napier, and Janse van Rensburg, 2007).

Malan and Napier (2018) investigated the use of a time-dependent limit equilibrium model to simulate the historical time-dependent closure profiles collected in the South African mining industry. Earlier work indicated that a viscoelastic creep model is not suitable for replicating the spatial behaviour of the closure recorded underground. The time-dependent limit equilibrium model appears to be a useful alternative as it can explicitly simulate the on-reef time-dependent failure of the reef. A key finding in this paper is that the model gives a better qualitative agreement with the underground closure measurements (Figure 25). For both the model and actual data, the rate of time-dependent closure decreases into the back area. Explicit simulation of the fracture zone in the face appears to be a better approach to simulating the time-dependent behaviour in deep hard-rock stopes. The calibration of the limit equilibrium model nevertheless remains a difficult problem. Using this model, Napier and Malan (2018) simulated the effect of mining rate. Figure 26 illustrates the effect of different mining rates and sequences for two hypothetical adjacent 25 m panels. The total area mined is equal to 1500 m^2. For the fast mining, both panels are advanced every day with an increment length of 1 m; for the slow rate, the mining cycles between the panels, and for the 0.5 m increment, both panels are mined together. The effect of mining rate on energy released is shown in the figure and it appears that the model is at least qualitatively able to simulate what has been suspected about mining rates in industry for a long time.

It has been recognized for many years that time-dependent deformations are often a prominent feature of the observed behaviour of coal mine workings. This plays an important role in determining the long-term stability of pillar layouts. The early pillar design formula established by Salamon and Munro (1967), and subsequently extended by Madden (1991) to include pillars having a large width to height ratio, did not contain any explicit incorporation of time-dependent strength decay. Subsequent work by Salamon, Ozbay, and Madden (1998) included a proposed pillar edge scaling model to describe the long-term stability of pillars. A detailed critique of the merits of the squat pillar formula has been published recently by Mathey and van der Merwe (2016). A number of empirical relationships have been proposed by van der Merwe (2012, 2016a, 2016b) to enable

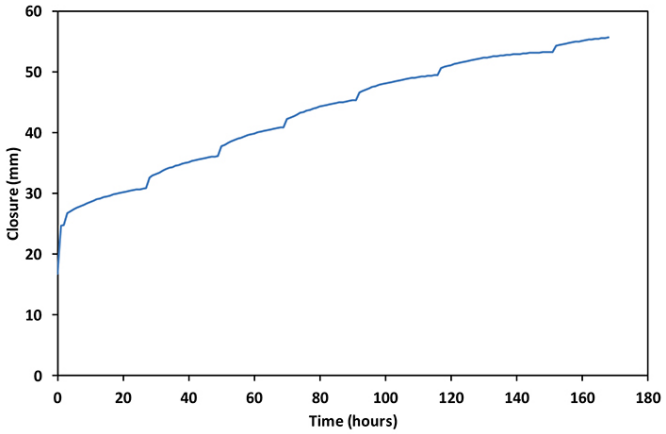

Figure 25—Simulated time-dependent closure curve for a number of mining steps (after Malan and Napier, 2018)

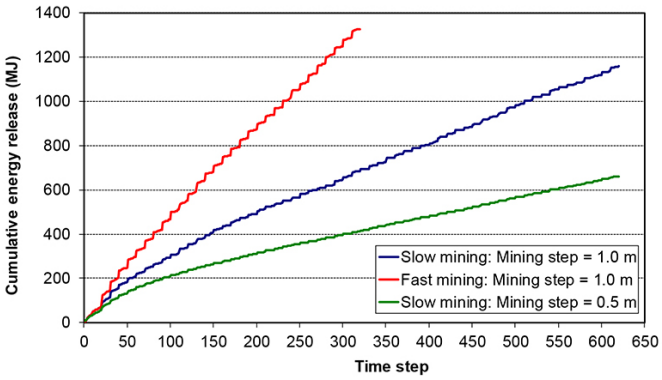

Figure 26—Accelerated closure recorded before a massive collapse in a UG2 panel (after Malan, Napier, and Janse van Rensburg, 2007)

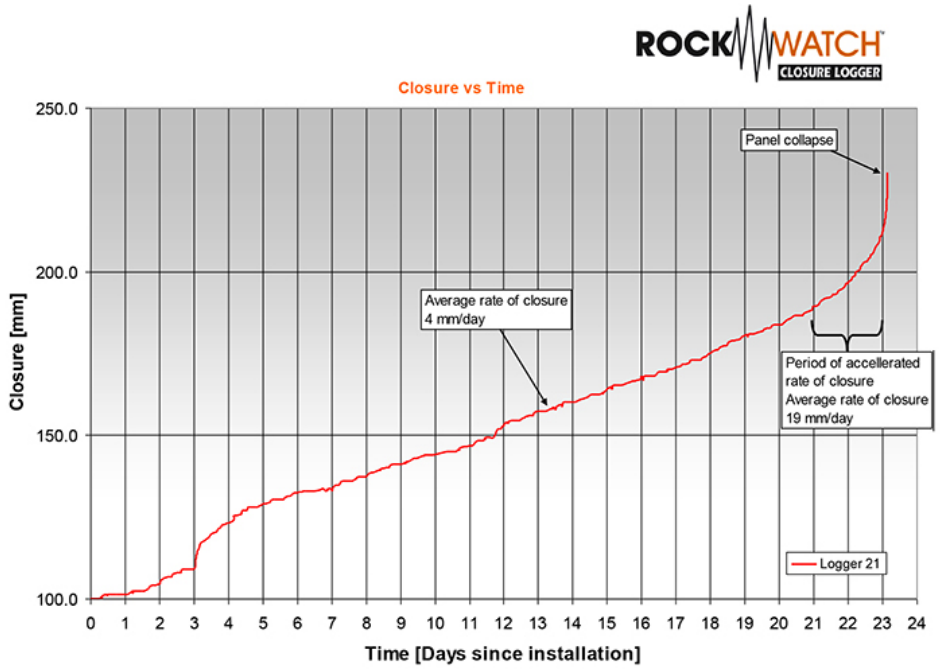

Figure 24—Accelerated closure recorded before a massive collapse in a UG2 panel (after Malan, Napier, and Janse van Rensburg, 2007)

firmer design predictions of the strength properties for the life of coal pillars. This is particularly important in coal mine operations where the workings may be at a shallow depth and the long-term collapse of the original pillar system can lead to severe surface infrastructure damage up to several decades after the cessation of mining activity. It would seem that in this case there is a critical need for numerical modelling design tools to incorporate time-dependent pillar scaling and damage mechanisms.

Conclusions

This paper has described some interesting aspects associated with historical underground measurements in South African gold and coal mines. Elastic theory was introduced in the 1950s and deformation measurements were used to confirm the applicability of elastic theory to simulate the rock mass behaviour in the 1960s. Although the prominent time-dependent component of stope closure was measured as early as 1934, it was conveniently ignored owing to the benefit of adopting simple elastic theory. Ignoring the time-dependent response of the rock for many decades resulted in important aspects such as the effect of mining rate, the effect of advance per blast, and the need for enhanced design criteria being neglected in the gold mines. Only recently was work started to address this gap in knowledge. Continuous closure measurements may possibly be a good diagnostic measure of the stress acting on remnants. This hypothesis needs to be carefully tested. In the platinum mines, time-dependent closure data is a good indication of effective pillar crushing. Absence of crushing may lead to pillar bursting and closure measurements may possibly be used to identify these areas. This also needs to be researched in more detail. A key lesson to be learnt from history is that monitoring data may reveal unexpected rock mass behaviour that does not fit with preconceived ideas. Any anomalous behaviour must not be ignored as it may contain diagnostic information that will assist with the development of safe mining practices and stable excavations.

The *in-situ* measurements of large coal specimens in the 1960s and 1970s indicated that a linear formula may be a better approximation of coal pillar strengths. This alternative formulation was never adopted, however, as the power law strength formula was already deeply entrenched in the industry at that stage. In spite of these apparent failures, a key lesson learnt from these historical measurements is that major advances in the field of rock mechanics will not be possible without careful monitoring of the rock mass behaviour in experimental sites. Appropriate strength formulae for pillars in the Bushveld Complex and enhanced design criteria for the gold mines can only be developed using extensive underground monitoring programmes.

Acknowledgements

This work forms part of research conducted in the Harmony Gold Chair of Rock Engineering and the authors would like to thank Harmony Gold for their kind support.

References

Altson, B.T. 1933. Remarks on sand-filling. *Papers of the Association of Mine Managers of South Africa*, 1931–1936. pp. 429–432.

Barcza, M. and von Willich, G.P.R. 1958. Strata movement measurements at Harmony Gold Mine. *Papers of the Association of Mine Managers of South Africa*, 1958–1959. pp. 447–464.

Berry, D.S. 1960. An elastic treatment of ground movement due to mining I. Isotropic ground. *Journal of the Mechanics and Physics of Solids*, vol. 8. pp. 280–292.

Berry, D.S. and Sales, T.W. 1961. An elastic treatment of ground movement due to mining II. Transversely isotropic ground. *Journal of the Mechanics and Physics of Solids*, vol. 9, pp. 52–62.

Berry, D.S. and Sales, T.W. 1964. An elastic treatment of ground movement due to mining III. Three dimensional problem, transversely isotropic ground. *Journal of the Mechanics and Physics of Solids*, vol. 9. pp. 73–8352–62.

Berry, D.S. 1964. The ground considered as a transversely isotropic material. *International Journal of Rock Mechanics and Mining Sciences*. vol. 1. pp. 159–167.

Bieniawski, Z.T. and van Heerden, W.L. 1975. The significance of in situ tests on large rock specimens. *International Journal of Rock Mechanics and Mining Sciences and Geomechanical Abstracts*, vol. 12. pp. 101–113.

Bieniawski, Z.T. 1992. A method revisited: coal pillar strength formula based on field investigations. *Proceedings of the Workshop on Coal Pillar Mechanics and Design*. IC 9315. US Bureau of Mines.

Cook, N.G.W., Hoek, E., Pretorius, J.P.G., Ortlepp, W.D., and Salamon, M.D.G. 1966. Rock mechanics applied to the study of rockbursts. *Journal of the South African Institute of Mining and Metallurgy*, vol. 66. pp. 435–528.

Cook, N G.W., Hodgson, K., and Hojem J.P.M. 1971. A 100-MN jacking system for testing coal pillars underground. *Journal of the South African Institute of Mining and Metallurgy*, vol. 71. pp. 215–224.

CSIR. 1958. Second report on strata movement – Analyses of the results of strata movement measurements at Harmony goldmine during the year 1957. National Mechanical Engineering Research Institute, CSIR, Pretoria.

Crouch, S.L. 1976. Solution of plane elasticity problems by the displacement discontinuity method. *International Journal for Numerical Methods in Engineering*, vol. 10. pp. 301–343.

Crouch, S.L. and Starfield, A.M. 1983. Boundary Element Methods in Solid Mechanics. George Allen & Unwin, London.

Deist, F.H., Georgiadis, E., and Moris, J.P.E. 1972. Computer applications in rock mechanics. *Journal of the South African Institute of Mining and Metallurgy*, vol. 72. pp. 265–272.

Denkhaus, H.G. 1958. The application of the mathematical theory of elasticity to problems of stress in hard rock at great depth. *Papers of the Association of Mine Managers of South Africa*, 1958–1959. pp. 271–310.

Denkhaus, H.G., Hill, F.G., and Roux, A.J.A. 1958. A review of recent research into rockbursts and strata movement in deep-level mining in South Africa. *Papers of the Association of Mine Managers of South Africa*, 1958–1959. pp. 245–269.

Durrheim R.J. 2010/ Mitigating the risk of rockbursts in the deep hard rock mines of South Africa: 100 years of research. *Extracting the Science: A Century of Mining Research*. Society for Mining, Metallurgy, and Exploration, Inc., Phoenix, Arizona. pp. 156-171.

Gurtunca, R.E. and Adams D.J. 1991. Determination of the in situ modulus of the rockmass by the use of backfill measurements. *Journal of the South African Institute of Mining and Metallurgy,* vol. 91, no. 3. pp. 81–88.

Hackett, P. 1959. An elastic analysis of rock movements caused by mining. *Transactions of the Institution of Mining Engineering,* vol. 118. pp. 421–435.

Hedley, D.G.F. and Grant, F. 1972. Stope-and-pillar design for Elliot Lake Uranium Mines. *Bulletin of the Canadian Institute of Mining and Metallurgy*, vol. 65. pp. 37-44.

Heunis, R. 1980. The development of rock-burst control strategies for South African gold mines. *Journal of the South African Institute of Mining and Metallurgy*, vol. 80. pp 139-150.

Hill, R. 1950. The Mathematical Theory of Plasticity. Oxford University Press, Oxford.

Hodgson, K. 1967. Report on the behaviour of the failed zone ahead of a face, as indicated by continuous seismic and convergence measurements. *Research Report* no. 31/67. Transvaal and Orange Free State Chamber of Mines Research Organisation. April 1967.

Hoek, E. 2006. Practical Rock Engineering. https://www.rocscience.com/learning/hoeks-corner/course-notes-books

Jaeger, J.C. and Cook, N.G.W. 1969. Fundamentals of Rock Mechanics. Chapman and Hall, London.

Jooste, Y. and Malan, D.F. 2020. The need for improved layout design criteria for deep tabular stopes. *Journal of the Southern African Institute of Mining and Metallurgy*, vol. 120, no. 1. pp 23–32.

Leeman, E.R. 1958. Some measurements of closure and ride in a stope of the East Rand Proprietary Mines. *Papers of the Association of Mine Managers of South Africa*, 1958–1959. pp. 385–404.

Madden, B.J. 1991. A re-assessment of coal pillar design. *Journal of the South African Institute of Mining and Metallurgy*, vol. 91. pp. 27–37.

Malan, D.F. 1999. Time-dependent behaviour of deep level tabular excavations in hard rock. *Rock Mechanics and Rock Engineering*, vol. 32, no. 2. pp. 123-155.

Malan, D.F. 2003. Manuel Rocha Medal Recipient: Simulating the time-dependent behaviour of excavations in hard rock. *Rock Mechanics and Rock Engineering*, vol. 35, no. 4.

Malan, D.F. and Napier, J.A.L. 2011. The design of stable pillars in the Bushveld mines: A problem solved? *Journal of the Southern African Institute of Mining and Metallurgy*, vol. 111. pp 821–836.

Malan, D.F. and Napier, J.A.L. 2018. Reassessing continuous stope closure data using a limit equilibrium displacement discontinuity model. *Journal of the Southern African Institute of Mining and Metallurgy*, vol. 118, no. 3. pp. 227–234.

Malan, D.F. Napier, J.A.L, and Janse van Rensburg, A.L. 2007. Stope deformation measurements as a diagnostic measure of rock behaviour: A decade of research. *Journal of the Southern African Institute of Mining and Metallurgy*, vol. 107, no. 11. pp. 743–765.

Mathey, M. and van der Merwe, J.N. 2016. Critique of the South African squat coal pillar strength formula. *Journal of the Southern African Institute of Mining and Metallurgy*, vol. 116, no. 3. pp. 291–299.

Mickel, R.E. 1935. Pressure bursts. *Papers of the Association of Mine Managers of South Africa*, 1931–1936. pp. 394–428.

Napier, J.A.L. and Malan D.F. 2018. Simulation of tabular mine face advance rates using a simplified fracture zone model. *International Journal of Rock Mechanics and Mining Sciences*, vol. 109. pp. 105–114.

Ortlepp, W.D . and Cook, N.G.W. 1964. The measurement and analysis of the deformation around deep, hard-rock excavations. *Proceedings of the International Conference on Strata Mechanics*, Columbia University, New York, May 1964. Columbia University.

Ortlepp, W.D. and Nicoll, A. 1964. The elastic analysis of observed strata movement by means of an electrical analogue. *Journal of the South African Institute of Mining and Metallurg*, November 1964. pp. 214–235.

Roux, A.J.A. and Denkhaus, H.G. 1954. An investigation into the problem of rockbursts. An operational research project: Part II: An analysis of the problem of rockbursts in deep-level mining. *Journal of the Chemical, Metallurgical and Mining Society of South Africa*, vol. 55. pp. 103–124.

Plewman, R.P., Deist, F.H., and Ortlepp, W.D. 1969. The development and application of a digital computer method for the solution of strata control problems. *Journal of the South African Institute of Mining and Metallurgy*, vol. 70. pp. 33–44.

Ryder, J.A. and Jager, A.J. 2002. Rock Mechanics for Tabular Hard Rock Mines. Safety in Mines Research Advisory Committee, Johannesburg.

Ryder, J.A. and Officer, N.C. 1964. An elastic analysis of strata movement observed in the vicinity of inclined excavations. *Journal of the South African Institute of Mining and Metalluryg*, vol. 64, no. 6. pp. 219–244.

Ryder, J.A., Watson, B.P., and Kataka, M. 2005. PlatMine 1.2: Estimation of UG2 and Merensky Reef pillar strengths through back-analyses. PlatMine report, March 2005. Miningtek Division of CSIR, Johannesburg.

Salamon, M.D.G. 1963. Elastic analysis of displacements and stresses induced by the mining of seam or reef deposits – Part I: Fundamental principles and basic solutions as derived from idealised models. *Journal of the South African Institute of Mining and Metallurgy*, vol. 63. pp. 128–149.

Salamon, M.D.G. 1964a. Elastic analysis of displacements and stresses induced by the mining of seam or reef deposits – Part II: Practical methods of determining displacement, strain and stress components from a given mining geometry. *Journal of the South African Institute of Mining and Metallurgy*, vol. 64, no. . pp. 197-218.

Salamon, M.D.G. 1964b. Elastic analysis of displacements and stresses induced by the mining of seam or reef deposits – Part III: An application of the elastic theory: Protection of surface installations by underground pillars. *Journal of the South African Institute of Mining and Metallurgy*, vol. 64. pp. 468–500.

Salamon, M.D.G. 1965. Elastic analysis of displacements and stresses induced by the mining of seam or reef deposits – Part IV: Inclined reef. *Journal of the South African Institute of Mining and Metallurgy,* vol. 65. pp. 319-338.

Salamon, M.D.G. and Munro, A.H. 1967. A study of the strength of coal pillars. *Journal of the South African Institute of Mining and Metallurgy*, vol. 68. pp 56–67.

Salamon, M.D.G., Ozbay, M.U., and Madden, B.J. 1998. Life and design of bord-and-pillar workings affected by pillar scaling. *Journal of the South African Institute of Mining and Metallurg*, vol. 98. pp. 135–145.

Stacey, T.R. 1991. Written contribution on the paper by Gurtunca, R.E. and Adams, D.J. 1991. Determination of the in situ modulus of the rockmass by the use of backfill measurements. *Journal of the South African Institute of Mining and Metallurgy*, vol. 91, no. 8. pp. 286–288.

Starfield, A.M. and Fairhurst, C. 1968. How high-speed computers advance design of practical mine pillar systems. *Engineering and Mining Journal*, vol. 169. pp. 78–84.

Szwedzicki, T. 1989. Geotechnical assessment deficiencies in underground mining. *Mining Science and Technology*, vol. 9. pp. 23–37.

Terzaghi, K. and Richart, F.E. 1952. Stresses in rock about cavities. *Geotechnique*, vol. 3. pp. 57–90.

Van der Merwe, J.N. 2012. Rock engineering method to pre-evaluate old, small coal pillars for secondary mining. *Journal of the Southern African Institute of Mining and Metallurgy*, vol. 111, no. 1. pp. 1–6.

Van der Merwe, J.N. 2016a. Review of coal pillar lifespan prediction for the Witbank and Highveld coal seams. *Journal of the Southern African Institute of Mining and Metallurgy*, vol. 116, no. 11. pp. 1083–1090.

Van der Merwe, J.N. 2016b. A three-tier method of stability evaluation for coal mines in the Witbank and Highveld coalfields. *Journal of the Southern African Institute of Mining and Metallurgy*, vol. 116, no. 12. pp. 1189–1194.

Van der Merwe, J.N. 2019. Coal pillar strength analysis based on size at the time of failure. *Journal of the Southern African Institute of Mining and Metallurgy*, vol. 119, no. 7. pp. 681–692.

Walsh, J.B., Leyde, E.E., White A.J.A., and Carragher B.L. 1977. Stope closure studies at West Driefontein Gold Mine. *International Journal of Rock Mechanics and Mining Sciences and Geomechanical Abstracts,* vol. 14. pp. 277–281.

Watson, B.P., Ryder, J.A., Kataka M.O., Kuijpers, J.S., and Leteane F.P. 2008. Merensky pillar strength formulae based on back-analysis of pillar failures at Impala Platinum. *Journal of the Southern African Institute of Mining and Metallurgy*, vol. 108, no. . pp. 449–61. ◆

Projectification in the South African mining industry

W.A. Smith[1], M.C. Bekker[1], and C. Marnewick[2]

Affiliation:
[1] Graduate School of Technology Management, University of Pretoria.
[2] University of Johannesburg.

Correspondence to:
G. Bekker

Email:
giel.bekker@up.ac.za

Dates:
Received: 2 Oct. 2019
Revised: 26 Jan. 2021
Accepted: 23 Feb. 2021
Published: May 2021

How to cite:
Smith, W.A., Bekker, M.C., and Marnewick, C. 2021 Projectification in the South African mining industry. Journal of the Southern African Institute of Mining and Metallurgy, vol. 121, no. 5, pp. 217–226.

DOI ID:
http://dx.doi.org/10.17159/2411-9717/950/2021

ORCID
G. Bekker
https://orchid.org/0000-0002-4837-2677

C. Marnewick
https://orchid.org/0000-0002-2340-8215

Synopsis

Projects or project-orientated approaches have become a common form of work in nearly all sectors of economies. This has led to concepts such as 'projectified' and 'project orientated' organizations. By defining projectification of a company, industry, or economy as the share of project work in total work, one can reasonably determine the impact that project management, and by default projectification, has had on that company, industry, or economy in terms of staff optimization and allocation.

This paper presents the results for such a projectification study of the South African mining industry. This sector has long been a significant contributor to the country's economy from a gross value added (GVA) and employment point of view. Understanding the impact of projectification and the project management way of work on this industry may potentially add significant value to both the mining and project management knowledge areas.

We show that although the mining industry is considered by some to operate in archaic ways, the level of projectification has increased over time, and now represents approximately one third of all work conducted.

Keywords
rojectification, mining projects, project management, project management office.

Introduction

The mining industry in South Africa has long been a significant contributor to the economy from a gross value added (GVA) and employment point of view. The mining industry in South Africa includes quarrying, underground, and open pit, as well as hard and soft rock mining operations. These different types of operations are divided into the following categories by commodity:

- Energy minerals
- Ferrous metals
- Industrial minerals
- Nonferrous metals and minerals,
- Precious metals and minerals.

For the purposes of this paper, the mining industry in South Africa is considered as mining companies that are typically production orientated. This definition excludes consulting and construction companies, original equipment manufacturers (OEMs), and other equipment suppliers and service providers. The intent was to review what approach is taken to conduct work by production orientated businesses in the mining environment, and this was encapsulated by information received. The impact of the abovementioned sectors is important but was deliberately excluded at this time to isolate mining companies. However, the intent is to follow-up this study with a paper covering the other disciplines in the mining environment and their impact on global projectization of the full value chain of mining.

Mining operations can also be divided into a two 'spheres of technology' application; first where some organizations insist on digitalization drives that increase the automation of work, and second where others do as little as possible to drive change towards digital applications. The drive for digitalization and expansion in mining in South Africa may be seen as a catalyst for the projectification of the South African mining industry. The improvement in technology is providing the opportunity for changes in operational philosophy and thus the commissioning of an increasing number of projects.

According to ISO 21500 (2012) a 'project' can be defined as a 'unique set of processes consisting of coordinated and controlled activities with start and end dates, performed to achieve project objectives'. In the mining sector projects are more than the development of a new mining reserve, processing plants, materials handling, or other capital infrastructure. Projects in this sector, as with other capital-intensive industries, also include information technology, business optimization, stay-in-business, safety, environmental, and other compliance-related initiatives.

Projectification in the South African mining industry

A project includes various management activities and therefore project orientated approaches have become a common form of work in nearly all sectors of economies. This has led to concepts such as 'projectified' and 'project orientated' organizations (Schoper *et al.*, 2018). Brenin and Soderlund (2006) defined 'projectification' as a 'general development process in which firms to a greater extent focus their operations on projects, project management and various types of project-like structures'. Projects, and the management thereof, are often centralized in project management offices (PMOs). However, the extent of projectification in mining organizations in comparison to the regular way of work has, as far as the authors are aware and based on a literature survey, never been systematically examined. The lack of projectification research in the mining industry could be due to its production- and maintenance-orientated nature. Understanding the impact of projectification on budgeting, human resources, and organizational structures may provide valuable insights into the level of projectification that can or should be allowed in an organization. Projectification is not fully understood in the mining industry in South Africa. Clarification on the level of projectification can address resource allocation issues that may occur in the industry.

The research objective is to understand the functional and operational activities of organizations in the mining industry in South Africa, specifically related to project work. Based on these definitions, the levels of projectification in organizations can be measured by obtaining information on the time and capital spent in the project environment. To fully comprehend the levels of projectification in the South African mining context, this publication attempts to answer the following questions:

1. Do mining companies have formal project structures such as project management offices (PMOs)?
2. What percentage of the company's working time is used for projects?
3. What percentage of the South African mining industry can be regarded as projectized?
4. How does South Africa compare with developed economies in this regard?

Literature survey

In order to contextualize the content of this paper, some project-related definitions need to be clarified. Adding to the ISO 21500 definition, Nicholas and Steyn (2017) defined a project as a unique activity, conducted by a temporary organization with a specific set of desired deliverables that must be achieved within a fixed time frame to realize specific benefits Projects are initiated and managed within an organizational environment and therefore a project-based organization is defined as one that conducts its main external and internal activities by means of projects (de Rooij, Janowicz-Panjaitan, and Mannak, 2019). Project management is the application of knowledge, skills, tools, and techniques to execute project activities to achieve project goals as per the project definition (Nicholas and Steyn, 2017). The project management process can be divided into five stages: namely initiation, planning, execution, monitoring/control, and closure. This leads to the magnitude of projectification being considered as the share of project work in an organization with respect to the total amount of work done. (Schoper *et al.*, 2018)

The origin of project management theory

Weaver (2006) traces the inception of project management philosophy back to the 15th century when the Protestants, later referred to as Puritans, presented the ideas of reductionism, individualism, and the Protestant work ethic (PWE), which reverberates significantly in modern project management theories as Puritanism (Whitty and Schulz, 2007). The definitions of and differences between these concepts are provided in the following paragraphs.

According to Weaver (2006), reductionism in project management places emphasis on the removal of redundant or unnecessary elements within a specific process as a means of formulating an understanding of its functionality. Reductionism therefore refers to a practical approach through which a phenomenon is understood by reducing it to simpler individual constituents. Whitty (2009) agrees that reductionism is 'heuristically useful' and emphasises that in a traditional sense, project management is executed by means of a 'conscious initiative' where reductionism is actively applied to make sense of project environments.

Individualism, according to Weaver (2006) 'assumes that we are active, independent agents who can manage risks and create ideas'. The ideas generated through individualism are subsequently transformed into action, which as noted by Altinkaya (2006) is more prevalent in modern developed economies.

The third theoretical concept that shaped Puritanism is that of the PWE. According to Whitty and Schulz (2007), prior to the initiation of the PWE, developed societies perceived their role in the work force as a 'necessary evil' rather than a 'calling'. The transformation associated with the PWE contributed to the success of early economic development and capitalism and is known as a value-based work ethic that believes in the moral benefit of work and its ability to enhance character.

From an evolutionary perspective, the theologies that have shaped Puritanism throughout history have been further incorporated into two key philosophies namely, liberalism and Newtonianism (Weaver, 2006).

Liberalism has transformed project management theory through renewed teachings of Puritanism that sparked a work ethic that drives the economic traits of capitalism (Whitty and Schulz, 2007).

In conjunction with liberalism, Newtonianism initiated the era of scientific enquiry where scientific observations provided vital insight in terms of various phenomena. Both liberalism and Newtonianism philosophies have influenced the scientific management theory of Taylor, a vital influencer on modern project management known as Taylorism (Figure 1).

The inception of modern project management is strongly linked to the development of scientific management theory by Frederick W. Taylor, later referred to as Taylorism. Taylor (Shenhar and Dvir, 2004; Drob, 2009) hypothesised around scientific management principles and applied scientific reasoning to the application of labour analysis and improvements on the elementary components associated with it.

According to Whitty and Schulz (2007), Taylorism 'marked an era of efficiency. From a corporate perspective; work was to be systemised, efficiency glorified, and the managerialism doctrine would complete the foundation for the spirit of project management'. Taylor's management system brought on project management innovations in the field of industrial engineering when his influential swork (The Principles of Scientific Management, published in 1911) led to dramatic improvements

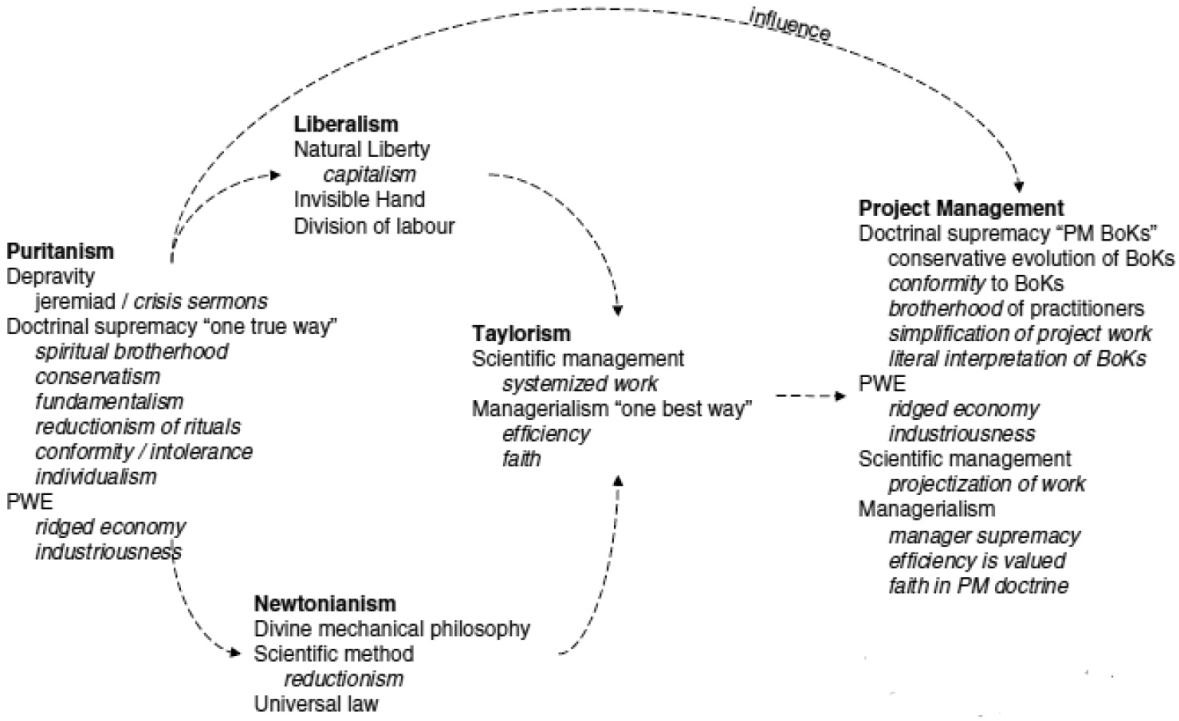

Figure 1—Evolution of Puritanism (Whitty and Schulz, 2007)

in productivity. Taylor's research was largely motivated by the need for greater competence and efficiency. This is the cornerstone of project management as a field of study.

Although the idea of project execution as an arranged activity can be found in almost every civilization in history, aspects associated with the evolution of project management theories and its buildup towards a modernized practice were first implemented in the USA in the twentieth century (Drob, 2009). The prevalence of project management application and theory became increasingly significant as a result of the benefits realized through organizing work based on projects and understanding the need to 'communicate and integrate work across multiple departments and professions' (Shenhar and Dvir, 2004).

Cicmil, Lindgren, and Packendorff (2016) state that project-based companies in modern society often employ Taylorist strategies to improve human performance, labour utilization, and productivity. Furthermore, Metcalfe (1997) emphasises that project management practices facilitate greater managerial control within modern organizations. To further comprehend these concepts, it is necessary to understand classification of projects, and how this influences the type of PMO and eventually the levels of projectification in an organization and industry.

Classification of projects

The classification of projects is necessary to understand the vast project management realm. Crawford, Hobbs, and Turner (2006) identified three groups of project classifications:

- Size, risk, or complexity
- Strategic importance, stage of the life cycle, or sector
- Contract form, payment terms, or risk ownership.

Various reasons exist for each classification or group classification like resource management practises, strategic importance, organizational structure management, and financial investment selections. For the purpose of this research, the monetary value of projects is important and therefore the classification based on the capital value approach by Payne and Turner (1999) was used (Table I).

Table I

Payne and Turner (1999) project classification by size

Classification	Cost as % of company turnover
Small	0.1%
Medium	1%
Large	10%
Major	Company turnover

This classification of projects has an impact on the management style of projects. The set-up of managementstructures and/or temporary organizations to manage projects of different classes changes the value proposition of such projects. The classification of different projects is imperative to the management thereof and the eventual impact on projectification of organizations.

Project management office and the value added

According to Aubry, Hobbs, and Thullier (2007), the most common reaction to the management of multiple projects in organizations is to implement a PMO. Cooke-Davies, Schlichter, and Bredillet (2001) emphasised that 'there is a growing recognition that project management involves more than the skillful and competent management of individual projects. It also requires a set of systems, processes, structures, and capabilities that enable an organisation to undertake the right projects and to support them organisationally.' Therefore, the role of a PMO in an organization and the development of that PMO in any organization must be closely linked to the type of business and the generic rules and practices of that industry.

According to van der Linde and Steyn (2016) the value added to organizations by PMOs, or project management as an action, can be attributed to three areas:

- Where the PMO fulfils the purpose of adding value to the organization through formal project management practices
- The level of value-creating capability the PMO has in an organization
- The level of key performance indicator (KPI) improvement due to PMO involvement in projects.

Similarly, Crawford and Pennypacker (2001) found that implementing PMOs adds significant value to an organization. The average improvements claimed are:

- 54% in financial performance
- 50% in project/process execution
- 36% in customer satisfaction
- 30% in employee satisfaction.

It is accepted that the value added by a PMO of the right composition and type in an organization can have a positive impact on project performance in terms of time, cost, and quality of the product, facility, or service. The PMO could also determine the level of projectification of an organzation by influencing the strategic decision-making processes.

Projectification

The term projectification first appeared in the literature in 1995 when Midler (1995) conducted a case study into the organizational changes at Renault. Bredin and Söderlund (2011) define projectification as a move from repetitive production to non-routine work processes and the use of temporary projects. Schoper *et al.* (2018) define projectification as the share of project work in an organization's activities.

Together with the earlier definition of Brenin (2006), projectification can be considered as the conducting of work, either routine or unique, in the form of a project. This is contradictory to the definition of a project as a unique process (Lester, 2017) or task. However, projectification has considerably changed the definition of what is deemed a project, way beyond the definitions given in the literature (Maylor *et al.*, 2006).

Projectification in organizations passes through four phases, identified by Midler (1995) as:

- Starting as a functional organization with informal project coordination
- Establishing centralized project coordination and project coordinator roles
- Establishment of project management structures through empowerment and autonomy of project managers
- Finally, a transformation of organizational processes, practices, incentive systems *etc.* into a balance between functional and project work.

Projectification thus goes further than pure organizational changes; it concerns a fundamental organizational transformation from the point of view where project work is a tool to achieve organizational goals.

The projectification of an organization is based on the view that organizational structure changes will provide solutions for certain types of tasks. This phenomenon can be linked to the Organization Theory in the context of scientific management. This theory refers to the need to handle non-routine and specialized tasks differently from standard production-type tasks (Packendorff and Lindgren, 2014).

Maylor *et al.* (2006) revealed that the increase in restructurings relates to or indicates an increase in projects being executed. They also refer to the increased reliance on standardization of operational frameworks and the increased prevalence of PMOs. The performance of these offices is directly linked to the perception of performance of the organization. Drawing on the conclusions made by Schoper *et al.* (2018) and the assumption that the links between industries, their contribution to economies, and the level of projectification are correct, it could be expected that similar results can be achieved in the South African context.

Mining industry operational model

In the mining industry projects are clustered in several categories to satisfy the different areas of operation. Mining operations, engineering operations, beneficiation plants, information management, and new business development all launch projects from time to time to ensure continuous production. The addition of PMOs in large organizations, in this case mining organizations, has significantly contributed to the success of projects and the organizations at large (Aubry, Hobbs, and Thiollier, 2009).

Different project management methodologies have also been tested in the South African mining industry. Phillis and Gumede (2009) tested the effectiveness of the critical chain project methodology in a mining application with relative success, and the work by Nelwamondo and Pretorius (2018) illustrated that project management methodologies can be employed to 'break the boundaries of traditional management'. This testing of the project way of work, the implementation of PMOs, and by definition the projectification of the mining industry warranted further research into the impact it has on the sector.

To understand the impact of projectification in the South African mining industry, it is important to understand the different organizational structures and projectification as a process or structure change. It also important to understand what is considered project work.

The typical functional organizational structure of a production environment, is compartmentalized into functional and skill-based departments (Midler, 1995). Each department has a function to perform and does not venture outside the boundaries or mandate of that department. Figure 2 depicts this typical functional organization.

With increased emphasis on working safer, cleaner, and more effectively, cross-functional performance of work is required to execute more complex tasks or essential projects. Most firms operating in such a multi-project environment have adopted a matrix organizational structure for the fast and cost-effective execution of such projects (van Staden, Steyn, and Schnetler, 2015). In a production environment this remains a challenge, with responsibility conflicts that are created when daily production goals are meshed with project-orientated goals. Figure 3 graphically represents such an organization.

The functioning of a matrix organization does present some challenges regarding the roles and responsibilities of personnel (Kuprenas, 2003). The most significant challenge is that of balancing responsibility between functional and allocated project work (van Staden, Steyn, and Schnetler, 2015). To address the potentially constraining effect that the matrix-type organizational design has on the execution of work in the mining industry, the

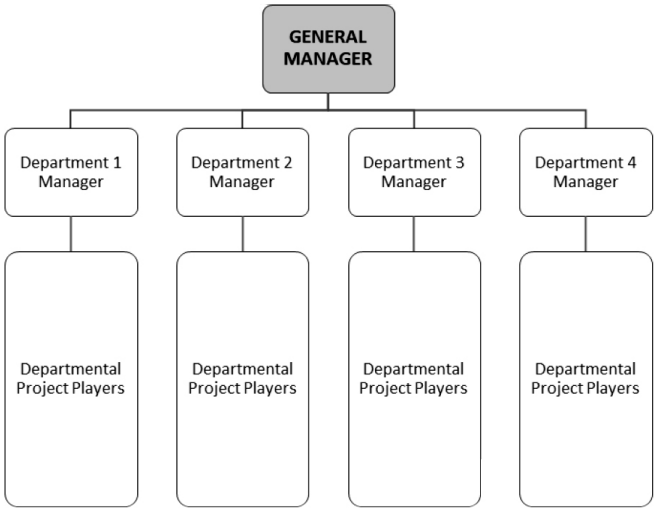

Figure 2—The functional structure (adapted from Midler, 1995)

life-cycle characteristics and fluctuating workload of a project need to be considered and incorporated (Turner and Müller, 2003).

Research methodology

This research project is deemed to be of the natural paradigm type and thus the decision, or inclination, toward the paradigm of positivist ontology. Positivist ontology, or positivism, holds that the world is external and that there is a single objective reality to any research phenomenon or situation regardless of the researcher's perspective or belief (Hudson and Ozanne, 1988).

Answering the research questions required analyses of data gathered from a survey and thus is inherently quantitative. The South African mining industry is the setting for this research. The setting is expanded to include companies listed on the Johannesburg Stock Exchange (JSE) or that employ more than 150 people. This selection of companies provides a setting where project management duties are generally part of the organization, whether internally or externally sourced.

Figures 4 and 5 illustrate where the research took place in the South African economy and what components of the project management landscape were addressed.

A purposive sampling technique, also referred to as non-probability sampling, was used in this research. According to Etikan, Musa, and Alkassim (2016), purposive sampling (judgment sampling) is the deliberate choice of a participant due to the qualities the participant possesses. It is a non-random technique that does not need underlying theories or a set number of participants. For this research, the intent was to ensure that the data collected is representative of the largest contributors to the South Africa economy via the South Africa mining industry. In this way the projectification factor can be linked to the economy of the mining industry and the country. The specific sampling was done by retrieving information from Statistics South Africa (STATSSA) on the highest grossing, in terms of turnover, mining companies in South Africa and retrieving data from that population. The threshold for selection was determined

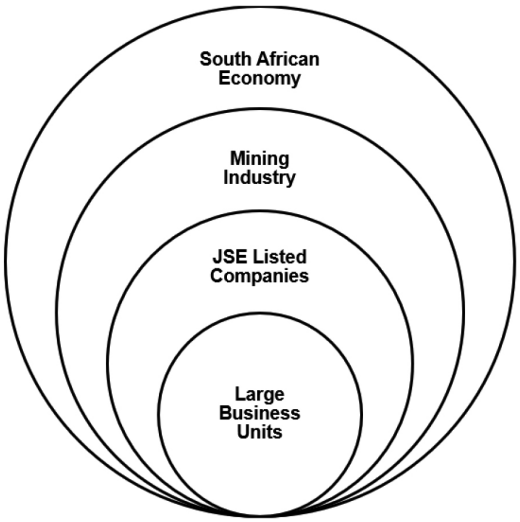

Figure 4—Mining industry and large business units

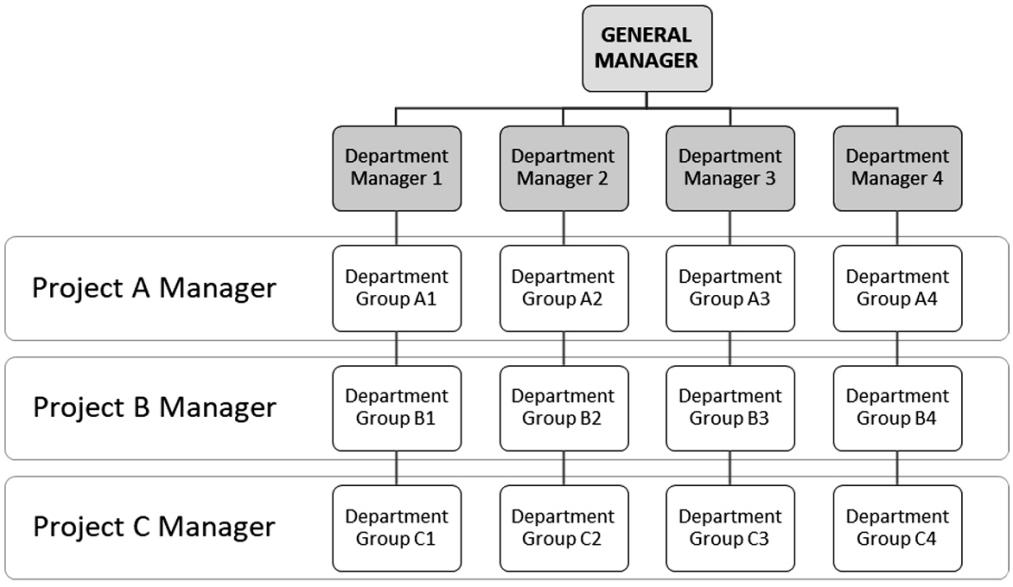

Figure 3—Typical matrix organization

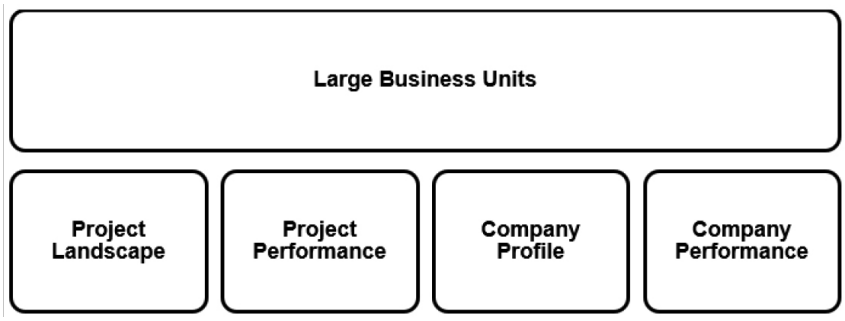

Figure 5—Components addressed in the selected industry

Table II

Attributes to be tested for validity

Attribute	Verification questions
Internal validity	• What bias exists in the selection of respondents, if any? • Did the system of measurement change during research? • Do any of the respondents have a reason to make the study fail?
External validity	• Was the survey biased with reference to respondent type? • Is the sample representative of the population?
Reliability	• Can the same results be obtained if the research is repeated by the same researcher?
Objectivity	• Can the same results be obtained by a different researcher? • Is there a conflict of interest from the researcher?

by JSE listing, employee numbers, or overall contribution in monetary value. In South Africa, the highest grossing mining companies are those in the diamond, gold, and platinum sectors.

Data collection

The data for this research was gathered by way of an online survey sent to as many potential participants as possible *via* email. The survey was structured as follows:

- Company details (size, manpower *etc.*)
- Internal company project landscape, which included all projects and project-related work
- Project and company performance
- Participant details (role in company *etc.*)

Descriptive statistical analysis was used to analyse the gathered data. Due to the different type of projects conducted in the mining industry, the analysis was based on the Schoper *et al.* (2018) definition of projectification.

Ensuring the reliability and validity of the data collected is imperative to the success of any research. An attempt to ensure quality of data was made by selecting the person to complete the survey as a person of some authority in an organization. The assumption was that such a person will be well informed on the questions asked and thus a quality response may be expected. Table II describes the attributes and the verification questions that were asked for each question.

The survey process requested respondents to answer each of the questions. There should be high level of confidence that the approach selected is appropriate.

Assumptions and limitations

Using the same approach as Schoper *et al.* (2018) to determine the level of projectification in the South African mining industry will result in similar limitations regarding the value added by project work. Because the work input is not equated to a value output in all cases (data to this effect is not necessarily available), the estimation of value added by projects is not exact. For example, mining houses carry out replacement of equipment through projects. Over the lifespan of a haul truck, for example, there is no quantifiable benefit for such a replacement other than sustainability. Some of these projects run into billions of rands.

The assumption that the person selected to do the survey will be well informed to answer the questions correctly may influence the results. Ideally one would have more than one person in one organization do the survey for validity, but the anonymous nature of the survey doesn't allow this kind of verification. This limitation may put data validity at risk; however, the approach taken for validation of data would have addressed this.

Results

The population of companies that fit the profile described and that were selected for this research is 43. Only 20 of these companies responded, some only partly. This gives a response rate of 46.5%. Some respondents did not complete all the questions, and the zero response questions were excluded from the analysis. Although all the companies contacted are known entities and the specific persons can be identified as the point of contact, the feedback is entirely anonymous. The research questions were answered individually in subsections to clearly separate the details and also to clarify different instances where projectification and project management have an impact.

- *Research Question 1:* Do mining companies have dedicated project management office (PMO) structures?
  The 20 respondents' results showed a 55:45 spilt between a positive and a negative answer to this question. The correlation between the 'yes' and 'no' answers and the time and money dedicated to projects in the organizations is clear. The dedicated PMO set-up in an organization is

clearly dependent on the time and effort (both human and monetary capital) required to execute work. The importance of managing the project process correctly, or at least the perception of good project management, can be created by having a dedicated, specialist team to conduct project activities.

- *Research Question 2*: What percentage of company's working time is used for projects?
  A total of 17 responses were received on this question. The data to answer this question was sourced by including a direct question for the hours worked *vs* project hours worked in the survey. Future and past hours allocated to the project environment were also included to understand where the respondent is coming from and where their institution is heading. Figure 6 shows the changes in project work proportions for the respective organizations in the years 2014, 2019, and projected for 2024. The different respondents are annotated by the Rx value on the x-axis and the percentage of work done in project form for that respondent on the y-axis.

The general feedback indicates that the portion of project work in companies is increasing or is expected to increase towards 2024. Projectification, it seems, is on the rise in these mining organizations. Now, generalizing this information for the entire mining industry in South Africa requires understanding that not all mining is equal. The company that does all its work in the project form will typically be an exploration-type mining operation that uses consultants and contractors. The entity in itself does not necessarily perform any work other than managing projects in the mining space. It may be the holder of the rights to mining activities without running the operations.

Figure 7 illustrates the feedback from respondents in an alternative manner. Each year is represented in a pie chart that indicates the percentage of respondents that conduct work in a project-orientated manner. For example, in 2014 only 6% of respondents spent between more than 75% of their hours on project work. The data indicates that project work is likely to increase in future.

In summary; the current level of projectification and the future prospect of projectification in the mining industry in South Africa seems to be somewhat stable. Although less than 30% of the time spent during a day is employed in project work, the general feedback from respondents indicates that this will increase through 2024. The slow adoption of the project way of work up to 2019 can be attributed to the production target orientation, attention to immediate, short-term activities to support the targets, and functional structure employed in the South African mining sector.

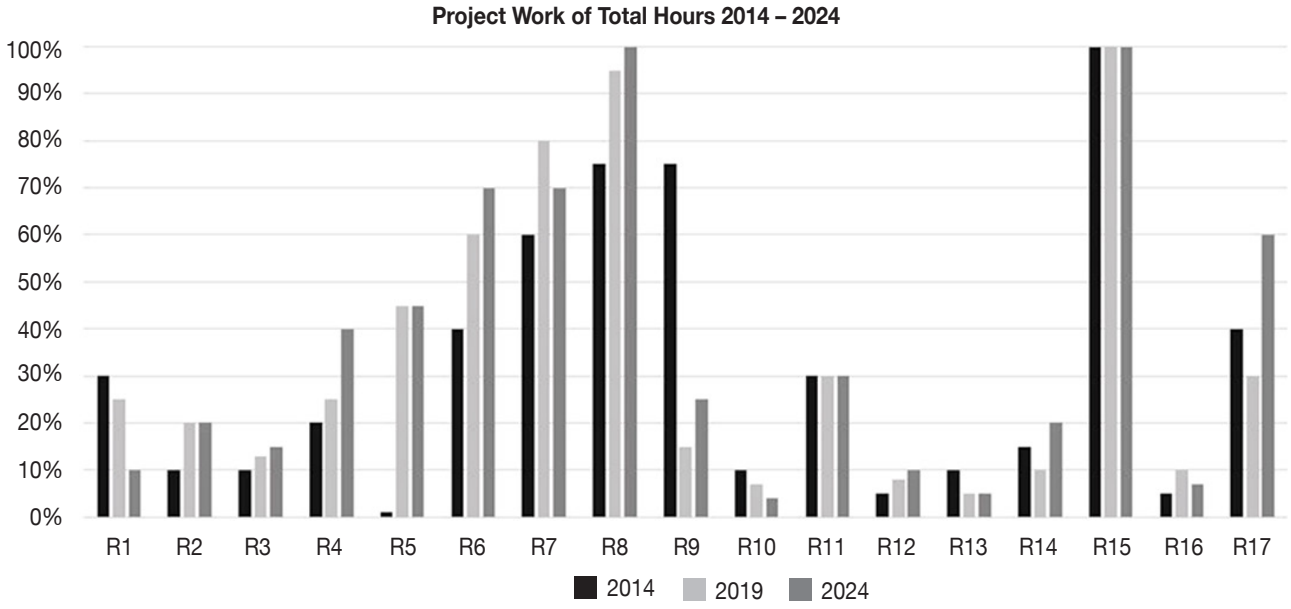

Figure 6—Proportion of project work in an organization

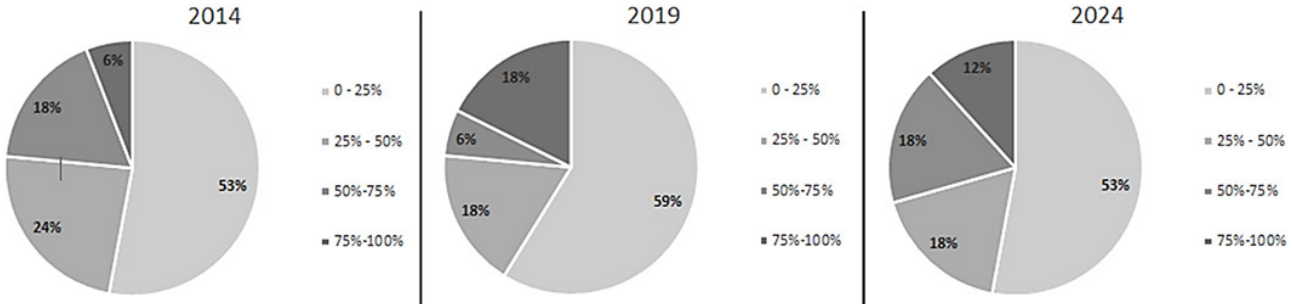

Figure 7—Percentage work hours to overall hours per respondent

- *Research Question 3*: What percentage of the South African mining industry can be defined as project orientated?
  Being project orientated entails that one focuses on projects as a result of the value that is realized by those projects. To determine what percentage of the South African mining industry is project orientated, one can look at the value generated by projects for the respective companies. One can also investigate the operational characteristics in the companies evaluated. To do so, five statements made in the survey were aimed at obtaining clarity regarding the prevalence of temporary structures, the amount of work invested in projects, and the importance assigned to temporary work. The five statements on which responses were requested are listed below:
  ST1 - Our firm is characterized by a high level of temporariness
  ST2 - Most of the activities in our firm are conducted within projects
  ST3 - Most of the work in our firm is invested in projects
  ST4 - Much of the work done in our firm is attributable to temporary organizations
  ST5 - Temporary work has in general a high importance in our firm.

The respondents were requested to evaluate each statement on a Likert scale with seven options from 'strongly disagree' to 'strongly agree'. The analysis of Likert data is a contentious issue because the data is not continuous. Nonparametric tests need to be applied to determine an effect in the ordinal data, but there is also a concern that the probability of detection of such an effect is limited because of spasmodic data. In this case, no comparisons will be done between data-sets and therefore the probability of success in applying nonparametric tests like the Mann-Whitney or t-test is reduced.

Based on this, the decision was made to present the percentage of project orientation in the mining industry in South Africa as the percentage of results in the positive side of the Likert scale. Figure 8 depicts the responses in a stacked bar graph to illustrate the negative and positive responses from the respondents. The black vertical centre line indicates the zero value in the scale where the disagree options have been assigned negative numbers and the agree options positive numbers. The 'neither agree nor disagree' option has been divided between positive and negative sides of the zero line.

It is clear that the bulk of the responses are on the negative side of the neutral line. The negative to positive ratio is 60:40 and is based on the sum of the number of responses to each statement (for example, Statement 1 had 12 negative responses (–12) and 7 positive responses). This indicates that there is a low percentage or level of project orientated organizations in the South African mining industry. This low number can be attributed to the issues described earlier. Mining in South Africa is not yet completely developed in the project space and one can understand the lower projectification values as described here.

- *Research Question 4*: How does South Africa compare with developed economies?
  The comparison to developed economies was done by comparing the South African mining industry with the the economies of Germany, Norway, and Iceland (Schoper *et al.*, 2018). This comparison is shown in Figure 9.

The South African mining industry compares well with the findings for the developed economies. The comparison with the developed nations aims to support the evidence that projectification, as it is now understood, is on the rise in the South African mining industry and that this is a current trend in large industries and economies. A steady growth in project-type

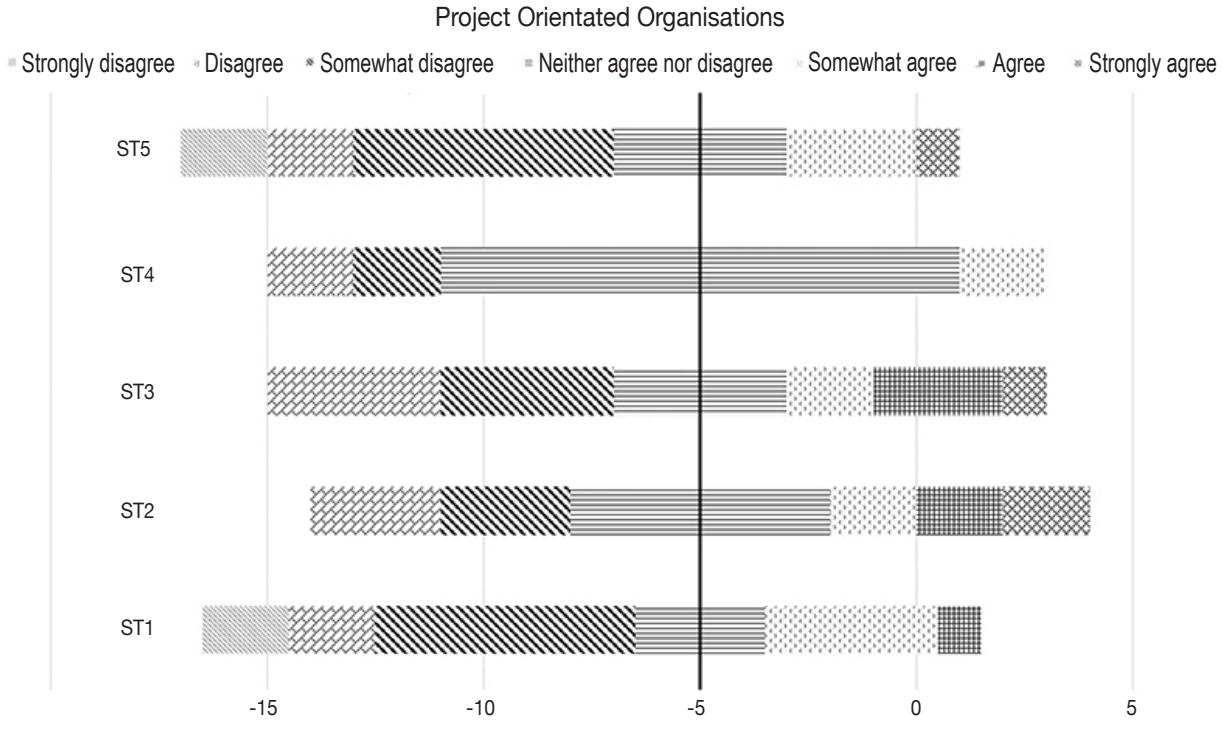

Figure 8—Percentage project orientation in the South African mining industry

work in all industries in the developed economies is expected, as is the case in the surveyed companies for the mining industry. The growth in technology and the need to control outcomes more precisely in an actively changing environment has necessitated the project approach in all walks of life. The trends depicted in Figure 9 are synonymous with the conclusions reached by Schoper *et al.* (2018), Midler (1995), and Jensen, Thuesen, and Geraldi (2016). Projectification is a 'human condition' that can be found in all industries and across all economies. Some environments take longer to become projectified than others, as is the case with the South African mining industry.

Conclusions

Considering the broad impact that mining has on the South African economy, a deeper investigation needs to be done on the impact projectification can have on the industry. From the surveyed responses it can be concluded that the level of projectification has not reached that observed in the telecommunication industry, which has higher project turnaround times.

Mining houses traditionally manage projects as part of their operational processes and these projects are not necessarily reflected in the answers provided in the survey. The value of some expansions in underground works, for example, may be in the medium project size classification and not be recorded in this survey feedback. This *modus operandi* limits the exposure that project management as a field of study has in the mining industry. The authors, having conducted projects with the some of the largest mining companies in South Africa, can relate to this shortcoming. The formal application of project management principles and thus the overall projectification in the mining industry in South Africa is not yet as refined as may be the case in other industries.

The majority of the respondents have dedicated PMOs (55%), but the application thereof may be where the detail should be analysed further. The types of projects that these PMOs execute are mainly in the HR and marketing space. Pure technical work seems to be outsourced more than handled internally. Although the type of projects the PMO executes is not really relevant in the projectification space *per se*, it is significant in the mining industry. The levels of projectification will definitely be impacted if internal PMOs conduct more mining-related or technical projects.

In reviewing the level of projectification in the mining industry in South Africa, it became clear that the current status and outlook for future projectification looks to be stable. The Schoper *et al.* (2018) definition was used to determine the level of projectification and it is clear that projectification in the mining industry has grown in the last five years. It may be concluded that the level of projectification in the mining industry can be linked to the performance of the industry as a whole. It can also be concluded from the results that projectification in this industry is likely to decline if the decline in the overall industry and the associated economy continues. The current stable outlook for projectification is heavily dependent on the optimism of the respondent.

The projectification level and the project orientation of the mining industry are directly linked. The prevalence of temporary organizations and importance of temporary work are directly linked to the levels of projectification in the organization. Project orientation can be linked to the ability of the mining industry to expand and grow. In the ten years covered in this study, the South African economy has not grown and the mining industry has contracted significantly. Thus, it can be concluded that the percentage project orientation in the mining industry will follow the same growth curve as projectification.

The South African mining industry compares well with findings for the developed economies. Although the overall projectification is low, some growth is expected. This growth may be attributed to changes in operational approach to manage the effects of a slowing economy and other factors that impact mining operations daily. The comparison with developed economies needs to be further investigated to understand the overall projectification of the South African economy. The mining industry alone does not provide a holistic view of the levels of projectification in the country. One must also consider the inherent differences between the developed and developing economies.

This study covers the projectification of one-tenth of the South African economy. It adds value to the project management

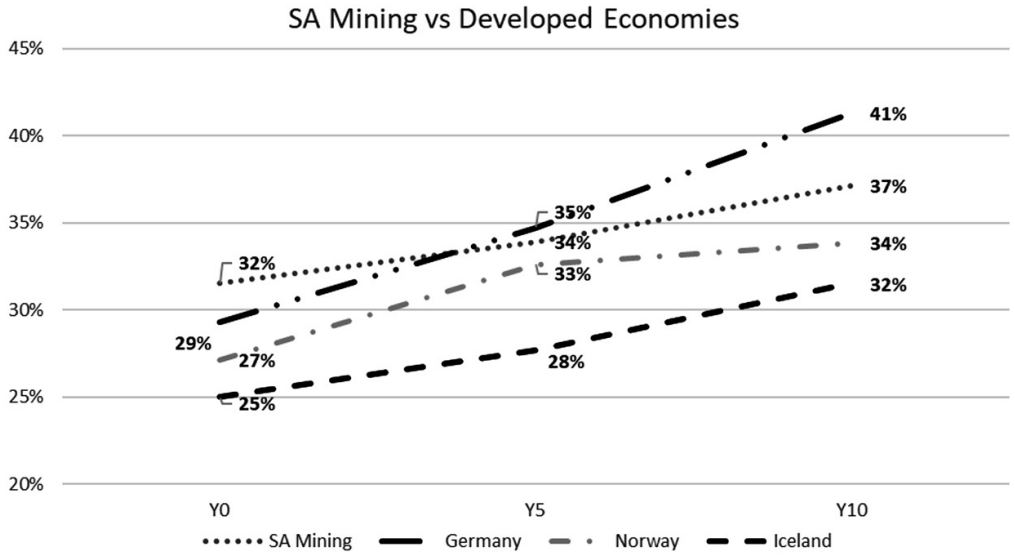

Figure 9—Projectification; South African mining *vs* developed economies over 10 years

knowledge area but excludes a significant part of the entire picture. It is recommended that a complete projectification study is done on the economy as a whole. This will better explain the impact project management has on the way work is done and what the approach to company structures, both from a human and other resource points of view, should be. As regards the mining industry; further study at a business unit level may provide more detailed results for projectification as viewed or perceived from a micro level and not from a corporate level.

By understanding the level of projectification in a specific economy, industry and/or business unit; decisions regarding resource allocation, in all forms and shapes, can be made to impact the work performance of those resources and essentially the bottom line of economy, industry and/or business unit. For example; projectification impacts the way organizations are structured, the way finances are structured and the effectiveness of delivering a service or a product. Knowing to what level an organization is projectified will benefit that organization in all these areas of decision-making.

References

Altinkaya, A. 2006. Cultural differences in international projects. A research study at Ericsson. MSc dissertation, Chalmers University of Technology, Gothenburg, Sweden. http://publications.lib.chalmers.se/records/fulltext/25690.pdf

Analysis Project. Not dated. Ethics in public administration | Code of conduct in public administration. http://analysisproject.blogspot.com/ [accessed 4 August 2018].

Aubry, M., Hobbs, B., and Thuillier, D. 2007. A new framework for understanding organisational project management through the PMO. *International Journal of Project Management*, vol. 25, no. 4. pp. 328-336.

Aubry, M., Hobbs, B., and Thuillier, D. 2009. The contribution of the project management office to organisational performance. *International Journal of Managing Projects in Business*, vol. 2, no. 1. pp. 141–148.

Bredin, K. and Soderlund, J. 2006. Perspectives on human resource management: an explorative study of the consequences of projectiffication in four firms. *International Journal of Human Resources Development and Management*, vol. 6, no. 1 pp. 92–113.

Bredin, K. and Soderlund, J. 2011. The HR quadriad: A framework for the analysis of HRM in project-based organizations. *International Journal of Human Resource Management*, vol. 22, no. 10. pp. 2202-2221.

Cicmil, S., Lindgren, M., and Packendorff, J. 2016. The project (management) discourse and its consequences: on vulnerability and unsustainability in project-based work. *New Technology, Work and Employment*, vol. 31, no. 1. pp. 58–76.

Cooke-Davies, T., Schlichter, J., and Bredillet, C. 2001. Beyond the PMBOK guide. *Proceedings of the 32nd Annual Project Management Institute 2001 Seminars and Symposium*, Nashville, TN. The Project Management Institute, Newtown Square, PA.

Crawford, J.K. and Pennypacker, J.S. 2001. The value of project management: Proof at last. *Proceedings of the PMI 2001 Seminars & Symposium*, 2001. The Project Management Institute, Newtown Square, PA. pp. 1–10.

Crawford, L., Hobbs, B., and Turner, J.R. 2006. Aligning capability with strategy: Categorizing projects to do the right projects and to do them right. *Project Management Journal*, vol. 37, no. 2. pp. 38–50.

De Rooij, M.M.G., Janowicz-Panjaitan, M., and Mannak, R.S. 2019. A configurational explanation for performance management systems' design in project-based organizations. *International Journal of Project Management*, vol. 37, no. 5. pp. 616–630.

Drob, C. 2009. The evolution of the project management. *Studies and Scientific Researches. Economic Edition*, no. 14. pp. 31–34.

Etikan, I., Musa, S.A., and Alkassim, R.S. 2016, Comparison of convenience sampling and purposive sampling. *American Journal of Theoretical and Applied Statistics,* vol. 5, no. 1. pp. 1–4.

Hudson, L., and Ozanne, J. 1988. Alternative ways of seeking knowledge in consumer research. *Journal of Consumer Research*, vol. 14, no. 4. pp. 508–521.

ISO 21500. 2012. Guidance on project management, 1st edn. International Organization for Standardization, Geneva.

Jensen, A., Thuesen, C., and Geraldi, J. 2016. The projectification of everything: Projects as a human condition. *Project Management Journal*, vol. 47, no. 3. pp. 21–34.

Kuprenas, J.A. 2003. Implementation and performance of a matrix organization structure. *International Journal of Project Management*, vol. 21, no. 1. pp. 51–62.

Lester, E.I.A. 2017. Project definition. *Project Management, Planning and Control. 7th edn*. Butterworth-Heinemann. pp. 1-5.

Maylor, H., Brady, T., Cooke-Davies, T., and Hodgson, D. 2006. From projectification to programmification. *International Journal of Project Management*, vol. 24, no. 8. pp. 663-674.

Metcalfe, B. 1997. Project management system design: A social and organisational analysis. *International Journal of Production Economics*, vol. 52, no. 3. pp. 305–316.

Midler, C. 1995. "Projectification" of the firm: The Renault case. *Scandinavian Journal of Management*, vol. 11, no. 4. pp. 363–375.

Nicholas, J. and Steyn, H. 2017. Project Management for Engineering, Business and Technology. 5th edn. Routledge.

Nelwamondo, P. and Pretorius, J. 2018. Application of the event chain project management methodology to a mining stope. *Journal of the Southern African Institute of Mining and Metallurgy*, vol. 118, no. 12. pp. 1233–1242.

Packendorff, J. and Lindgren, M. 2014. Projectification and its consequences: Narrow and broad conceptualisations. *South African Journal of Economic and Management Sciences*, vol. 17, no. 1. pp. 7–21.

Payne, J.H. and Turner, J.R. 1999. Company-wide project management: the planning and control of programmes of projects of different type. *International Journal of Project Management*, vol. 17, no. 1. pp. 55–59.

Phillis, R. and Gumede, H. 2011. A case study on stoping shift buffering at Impala Platinum: A critical chain project management perspective. *Journal of the Southern African Institute of Mining and Metallurgy*, vol. 111, no. 11. pp. 793–800.

Schoper, Y.-G., Wald, A., Ingason, H.T., and Fridgeirsson, T.V. 2018. Projectification in developed economies: A comparative study of Germany, Norway and Iceland. *International Journal of Project Management*, vol. 36, no. 1. pp. 71–82.

Shenhar, A.J. and Dvir, D. Project management evolution: Past history and future research directions. *Proceedings of the PMI Research Conference, 2004.* Project Management Institute, Newtown Square, PA:. pp.11–14.

Statistics South Africa. 2018. Mining: Winners and losers of 2017. http://www.statssa.gov.za/?p=10963 [accessed 5 August 2018].

Turner, J.R. and Müller, R. 2003. On the nature of the project as a temporary organization. *International Journal of Project Management*, vol. 21, no. 1. pp. 1–8.

USC Libraries. Not dated. Organizing your social sciences research paper: Quantitative methods. University of Southern California. https://libguides.usc.edu/writingguide/quantitative [Accessed 29 August 2018].

Van der Linde, J. and Steyn, H. 2016. The effect of a project management office on project and organisational performance: A case study. *South African Journal of Industrial Engineering*, vol. 27, no. 1. http://sajie.journals.ac.za/pub/article/view/1114/672

Van Staden, P.J., Steyn, H., and Schnetler, R. 2015. Characteristics of matrix structures, and their effects on project success. *South African Journal of Industrial Engineering*, vol. 26, no. 1. pp. 11–26.

Weaver, P. 2006. A brief history of project management. *APM Project*, vol. 19, no. 11. https://mosaicprojects.com.au/PDF_Papers/P061a_A_Brief_History_of_Project_Management.pdf

Whitty, S.J. 2009. New philosophy of project management: An investigation into the prevalence of modern project management by means of an evolutionary framework. PhD dissertation, University of Queensland.

Whitty, S.J. and Schulz, M.F. 2007. The impact of Puritan ideology on aspects of project management. *International Journal of Project Management*, vol. 25, no. 1. pp. 10–20. ◆

Density – A contentious issue in the evaluation and determination of Resources and Reserves in coal deposits

L. Roux[1]

Affiliation:
[1] Leon Roux
Retired from Exxaro's Grootegeluk Coal Mine and continued with the Clean Coal Research Group at the University of the Witwatersrand during his research years preparing for this paper.
Post Humous.

Correspondence to:
L. Roux

Email:
rouleo@outlook.com

Dates:
Received: 8 Mar. 2019
Revised: 6 Aug. 2020
Accepted: 24 Feb. 2021
Published: May 2021

How to cite:
Roux, L. 2021
Density – A contentious issue in the evaluation and determination of Resources and Reserves in coal deposits.
Journal of the Southern African Institute of Mining and Metallurgy, vol. 121, no. 5, pp. 227–250.

DOI ID:
http://dx.doi.org/10.17159/2411-9717/17386/2021

Synopsis

The initial evaluation of a coal deposit often raises uncertainty with regard to the accuracy of the reported Resources and Reserves. Reconciliation of results from mining and beneficiation with the original raw field data highlights deficiencies in original estimations. Credible Resource and Reserve estimation forms the basis on which an entire mining enterprise is motivated, initiated, funded, and established as a commercially viable proposition. This is required for sustainable extraction purposes and to support vital downstream industries such as power generation.

Accurate determination of the density of the matrix of the material being evaluated is the key to credible values being obtained for Resources and Reserves. Losses between 15% and 20% of the Resource/Reserve can be realized if incorrect densities are applied to the tonnage derivation. Coal plies and particles have different relative densities, determined by the maceral composition, rank, and mineral and moisture content. These factors in turn contribute to the moisture, volatile matter, ash and carbon contents of a coal, which affect the overall density of the raw coal. More specifically, the relationship of ash to density and the effective matrix porosity were found to be critical in solving the greater majority of the problems in predictive calculations.

A major deficiency identified is the inability to determine effective porosity, allowing absorption of adventitious moisture and altering the mass of the core sample. Although the volume of the raw material is altered through crushing, the change in mass after controlled air-drying, used with the original geometrical volume of the raw material, provides a credible air-dry density and allows the determination of the volumetric change related to effective porosity. This parameter can be validated through the evaluation of proximate ash using the ash-adjusted algorithm and a correction for the inherent moisture applied to also give a credible relative density value for an air-dried sample.

A combination of theoretical, empirical, and reconciliatory evaluations of the available data, taken from the exploration phase through the mining process to final production, has shown that an integrated approach using the ash-adjusted density (AAD) methodology, in conjunction with other evaluative techniques, provides credible results with a considerably higher degree of accuracy than is currently possible.

Keywords
coal, deposit evaluation, Resources, Reserves, density determination, ash-adjusted density.

Introduction

The evaluation of coal deposits from exploration through Resources and Reserves classification, mining and prediction of grades, application of interpretive measures in the overall evaluation of coal deposits, the behaviour of the raw feed material in the beneficiation process, and the final mass accounting of saleable products may be enhanced through the application of the ash-adjusted density (AAD) methodology (Roux, 2012)

Many uncertainties affect budgetary and forecasting purposes and the definition and quantification of saleable reserves. This is problematic in most coal deposits, particularly those related to specialized products with very strict quality specifications in newly developing coalfields or previously unexplored regions, which could be far more variable and difficult to assess than deposits in conventionally mined areas where a wealth of data has already been accumulated over time. Basic information that has been used historically for the determination of Resources and Reserves may be instrumental in portraying misleading results relating to either under- or overestimation of Resources and Reserves, especially in relation to tonnage estimations.

The crux of the matter relates to the accuracy of the density of the material being evaluated. Density *per se* underpins all Resource and Reserve estimations as well as reconciliation after mining. An in-depth study is required of not only the methods of density determination, but including variations with regard to the geology of the deposit, specifically the composition of the coal, the composition of its solid

matrix, its rank, type, and grade, and pore fluids or gases, which all have an effect on the *in-situ* as well as air-dry or absolute density of the matrix material.

Preston and Sanders (2005) very aptly describe the situation relevant to probably one of the more important aspects at the beginning of the value chain. Density is a contentious issue. 'The relative density of coal is a fundamental physical parameter which should be well understood by geologists, who need to know the *in situ* relative density of coal for use in reserve calculations.' This, according to the authors, appears to be poorly understood and unfortunately also poorly documented, with virtually no practical definitive work having been done, apart from that of Smith (1991). Thus, the application of relative density in Reserve calculations is uncertain, or at worst incorrect. Quality Coal Consulting conducted a study for Pacific Coal (Preston and Sanders, 2005) to address this problem, with primary consideration being given to the relationships between coal density, coal porosity, and moisture. A prerequisite of any evaluation is the validation of the basic information from the original source. Uncertainty here could have far-reaching effects on the eventual evaluation of the deposit, especially with regard to its economic viability and sustainability.

In South Africa, all Coal Resources and Coal Reserves are classified according to the SAMREC Code and SANS10320:2004, which outline the standard method of reporting of Coal Resources and Coal Reserves through the application of the various technical parameters, and specifically the determination of GTIS (gross tons *in situ*), TTIS (total tons *in situ*) and MTIS (mineable tons *in situ*). Venmyn Deloitte found considerable inconsistency in the reporting of Coal Resources in the minerals industry, and particularly among South Africans and Australians. Some companies used GTIS, some used TTIS, and others used MTIS, with some reporting on all of these values in the interest of clarity. Note that the evaluation done here is based on information from the only currently operating mine in the Waterberg Coalfield in South Africa.

The JORC Code and the Australian Guideline for Estimating and Reporting are not as prescriptive, although the Guideline states that, 'Coal resources should be estimated and reported for individual seams or seam groupings within a deposit. They should also be subdivided and reported on the basis of key variables, such as thickness, depth range, strip ratio, coal quality parameters, geographic constraints and geological or technical considerations. The key variables and assumptions for each deposit should be clearly stated in order to ensure clarity and transparency of the report.' However, in a South African scenario, the use of different reporting standards for Coal Resources was found to be particularly problematic.

One particular scenario raising concern with regard to Coal Resource reporting highlighted by Venmyn Deloitte refers to the Waterberg Coalfield, where multiple seam deposits with intercalated shales occur in the Volksrust Formation. The multiple seams are delineated into sedimentary depositional zones, and sampling of these zones in some cases does not separate the coal from the interlaminated shale portions. The zones are modelled and the tonnages calculated, and Resource statements have quoted the tonnages pertaining to the whole zone rather than only the coal portion, which according to Venmyn can be misleading.

Venmyn Deloitte noted that the coal industry in South Africa is attempting to standardize one method of reporting. This has led to a re-assessment and re-writing of the SANS Code, which is currently underway. Revisions proposed have been used in this paper and the most critical initial values have been singled out for evaluation.

Considering the SAMREC Code and proposed revisions of SANS 10320; 2004, ***Mineable Tonnes In Situ Coal Resource*** refers to the tonnage and coal quality, contained in the coal seam, or section of the coal seam proposed to be mined, at the theoretical mining height, adjusted by *geological loss factors* and specific mining methods after the relevant minimum and maximum mineable thickness cut-offs and relevant coal quality cut-off parameters have been applied. For Public Reporting purposes all Coal Resource tonnages and coal quality must be reported ***as a Mineable Tonnes in situ Coal Resource (MTIS basis***), with associated yield, coal quality and moisture content.

Coal Reserve reporting refers to, *the Coal Reserve that is the economically mineable part of a Measured and / or Indicated Coal Resource, which includes diluting and contaminating materials and allowances for losses, which may occur when the material is mined or processed and is defined by studies at Pre-feasibility or Feasibility level, as appropriate, that include application of Modifying Factors and such studies which demonstrate that, at the time of reporting, extraction could reasonably be justified.*

Key issues for the derivation of primary tonnage estimates are:

1. The ***in situ density*** of the coal adjusted from the laboratory determined relative density taking analyzed moisture content related to the *in situ* bed moisture content into account.
2. ***Geological loss factors*** applied to resource tonnages.
3. Theoretical mining height of the coal seam, or the optimal selected part of the coal seam that is expected to be mined, based on a geological assessment
4. The Resource that will be upgraded by washing in a coal processing plant, quantified by washed coal quality data for quality points of observation
5. The theoretical product yield being the laboratory estimate of the yield of the target product at a specific coal quality, or at a specific cut-point density, on an undiluted and uncontaminated basis.

Another point that could be added refers to the type of coal deposit.

6. A thick inter-bedded seam deposit or a multiple seam deposit.

The credibility of Coal Resource and Reserve estimations currently and conventionally obtained is questionable.

This relates to actual mined data being irreconcilable with the original raw data obtained from basic field evaluations during exploration. This is specifically applicable when *in-situ* raw density obtained through the application of the Archimedes principle in the determination of SG is used for tonnage estimations in geological modelling, mine planning, scheduling, budgeting, and production.

Problems experienced in correct tonnage estimations are largely due to the inability of the processes applied to establish an appropriate and verifiable reconciliation of material from Resource through the value chain of extraction, beneficiation, to production, including product tonnage prediction. Pre-determined predicted Resources and Reserves are essential for planning and

scheduling of appropriate feed material to be supplied from the mine to the beneficiation plant and ultimately for the production of specified saleable products. This problem is further exacerbated by limitations with regard to accurate physical measurements that are needed to validate the results. Therefore, measurement, monitoring, and correct estimation are key issues in question.

Review

An assessment of tonnages extracted and compared to the original planned and budgeted figures, as well as attempts at reconciling the final data with the original basic data used for the determination of Resources and Reserves, has highlighted critical deficiencies in the entire process. These deficiencies are related to both the initial evaluation methods and the mining process (Roux, 2010).

To begin the assessment, the suggested addition of the type of coal deposit will be reviewed before the issues highlighted in the SANS proposed changes.

The type of coal deposit

The Volksrust Formation, classified as a thick interbedded seam deposit and which forms the upper part of the coal deposit, comprises intercalated shale and bright coal layers with an average thickness of about 60 m (Figure 1). It displays such a well-developed repetition of coal-shale assemblages that it can be divided into seven major sedimentary cycles or zones. Smaller sub-cycles ('samples') are contained within these zones; these were sampled individually during exploration of the deposit. The terms '*zone*' and '*sample*' are used at Grootegeluk instead of '*seam*' and '*ply*' due to the site-specific intercalated nature of the coal and shale.

The Volksrust Formation zones typically start with bright coal at the base, with the ratio of coal to shale decreasing from the base of each zone upwards. The Basal Zone is the exception because the coal is more evenly distributed throughout this zone. The shales of the Volksrust Formation show an increase in carbon content with depth and range from a massive bluish-grey mudstone at the top to carbonaceous shales towards the Basal Zone.

Although the thickness and coal quality of the Volksrust Formation zones are reasonably constant across the coalfield, a large variation in the yield of semi-soft coking coal occurs vertically in the coal succession.

The mineralogy of the Volksrust Formation is dominated by kaolinite, quartz, and minor amounts of apatite in the lower portion while the upper portion is dominated by quartz, kaolinite, and minor amounts of montmorillonite, illite, and microcline. Calcite lenses occur predominantly in the upper half of the Volksrust Formation and have been interpreted as being syndepositional. Diagenetic globular pyrite and spherulitic siderite occur in the coals and organic-rich mudstones. The mineralogy of the mudstones and trace element concentrations suggest deposition in fresh water rather than marine waters. (Faure *et al.*, 2002).

At Grootegeluk the zones were subdivided into sub-cycles (samples). The individual samples from the Volksrust Formation were further subdivided into a coal and shale component for stringers thicker than 1 cm. Stringers of less than 1 cm thickness were included in the overriding lithology, *i.e.* coal stringers in shale less than 1 cm were retained in the shale samples, while the same applies to shale stringers in coal samples. The coal and the shale components were analysed separately to enhance grade control functionality. The reasoning behind this was that if part of a recognized sample was left in the floor, or conversely mined out previously, this could be taken into account when compiling the mined vertical sequence and an adjustment pertinent to the actual material could be made.

The analytical results for the individual components were then composited to obtain values for the entire sample, including both the shale and coal components. Unfortunately, a Resource value for only the coal component (as suggested by Venmyn Deloitte) was not feasible due to the intercalated nature of the coal and shale components. The Resource would have to be beneficiated in order to extract economically viable coal, thus the shale component of these sub-cycles (samples) needs to be recognized as part of the Resource.

The Vryheid Formation (approximately 55 m thick) forms the lower part of the coal deposit and comprises carbonaceous shale and sandstone with interbedded dull coal seams varying in thickness from 1.5 m to 9 m (Figure 2). The Vryheid Formation is classed as a '*Multiple Seam Deposit Type*' according to the SAMREC Code. There are five coal seams or zones in the Vryheid Formation, all of which are composed predominantly of dull coal with some bright coal developed at the base of zones 2, 3, and 4. Due to lateral facies changes and changes in the depositional environment, these zones are characterized by a large variation in thickness and quality.

Zone 3 is the best-developed dull coal zone within the mine lease area, reaching a maximum thickness of 8.9 m. The basal portion of this zone yields a small fraction that has semi-soft coking coal properties.

Zone 2 is, on average, 4 m thick and reaches a maximum thickness of 6 m in the mine lease area. The basal portion of this zone also yields a fraction that has semi-soft coking coal properties. This zone is the most constant of all the Vryheid

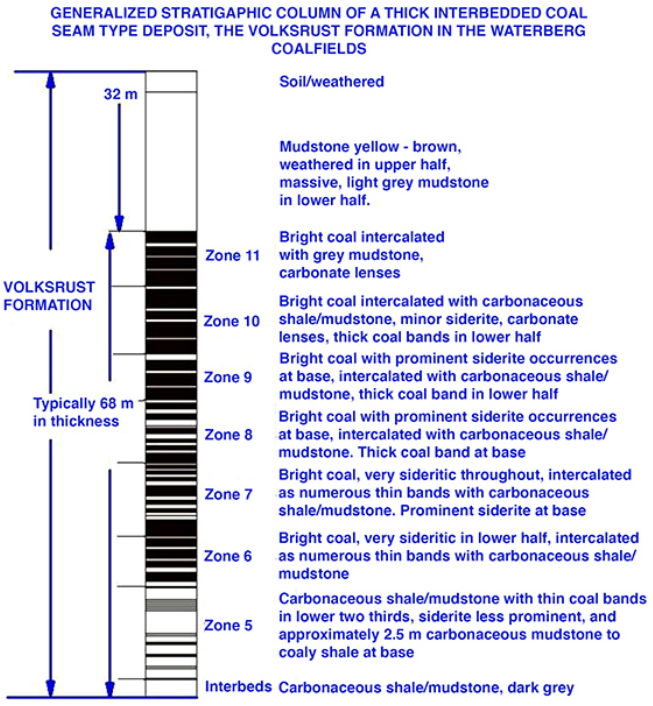

Figure 1—Generalized stratigraphic column of thick interbedded coal seam type deposit of the Volksrust Formation at Grootegeluk Coal Mine, indicating zonal delineation

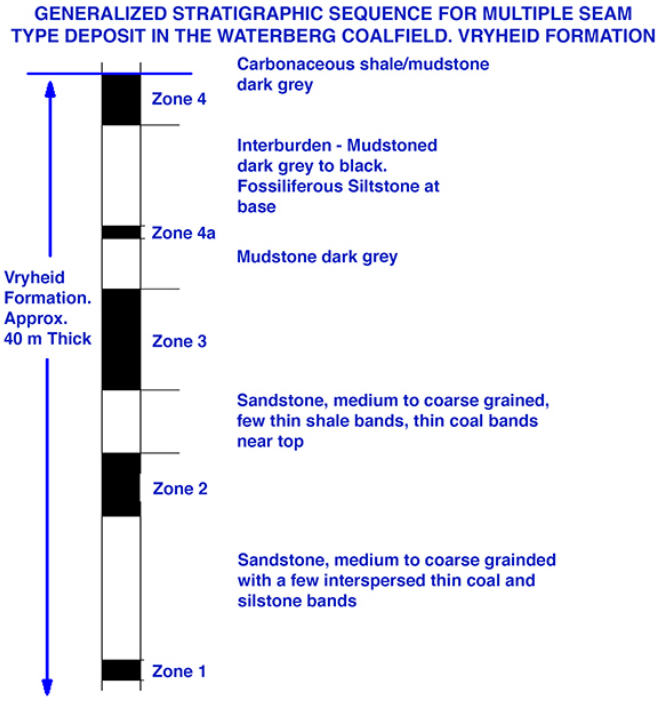

Figure 2—Cyclic sedimentary subdivision of coal sequence for the Vryheid Formation

Formation coal zones across the entire Waterberg Coalfield regarding thickness.

Zone 1, the basal Vryheid coal zone, has an average thickness of 1.5 m, but varies quite rapidly being the lowermost coal layer in the sequence.

The distinct differentiation between the Volksrust Formation and the Vryheid Formation illustrates two different depositional environments, the Volksrust Formation being representative of an autochthonous deposit, while the Vryheid Formation is typically an allochthonous deposit.

The Vryheid formation is defined as a multiple seam deposit although also subdivided into sub-cycles for the individual seams. Each seam is treated as a single entity, coal only, therefore the Resources representing the seam are relevant to coal only.

In-situ density

Before one can consider determining the *in-situ* density of the coal an in-depth understanding of the matrix within the volume of the coal sample is required. Which properties of the matrix would have the greatest influence on the determined density of the coal? Would it be the volume occupied by the matrix, its mineral content, its moisture content, or its void content (porosity), also taking its permeability into account? The most basic definition of density refers to the mass per unit volume of the material being assessed.

Density = Mass/Volume

The volumetric component is the most complex property in the determination of the density of the material being evaluated.

The typical definition of volume in most dictionaries is given vaguely as 'the space occupied by an object'. McGraw-Hill's Dictionary of Scientific and Technical Terms (1984) does not say much more, their definition merely relates the object to three-dimensional space: '*A measure of the size of a body or definite region in three dimensional space …*' In order to appreciate the various conditions under which volume is defined, particle technology's lexicon used for these definitions can be found in the British Standards Institute (BSI,1991) and the American Society for Testing and Materials (ASTM,1994) documents. Here the 'volume' of a material is described as the summation of several rigorously defined elemental volumes.

A cylindrical length of rock core can be used as an example of an object that contains all types of elemental volumes and differences in material volume according to the measurement technique, measurement method, and conditions under which the measurements are performed.

The rock core, obviously, is solid material with a volume that can be calculated after measuring its length and its diameter, from which its cross-section can be determined. However, it also contains surface irregularities, small fractures, fissures, and pores that both communicate with the surface and pores that are isolated within the structure. Voids that connect to the surface are referred to as open pores while interior voids inaccessible from the surface are referred to as closed pores. Surface irregularities compose another type of void volume. For example, assume the bulk volume of the core is determined from linear measurements of its length and cross-section. The value of volume determined in this way is limited in accuracy because the surfaces are not perfect. If a perfect plane were to be laid on one of the surfaces of the core, there would be many voids sandwiched between the two surfaces (Figure 3).

For lack of a standard definition, this can be referred to as 'external void volume' and will refer to the void volume between a solid surface and that of a closely fitting envelope surrounding the object. It does not include pores that penetrate the interior of the particle. The meaning of the term is admittedly vague, but this volume can be determined or estimated under certain analytical conditions and can provide an indication of surface rugosity. When a solid material is in granular or powdered form, the bulk contains another type of void: interparticle space. The total volume of interparticle voids depends on the size and shape of the individual particles, their sorting, and packing. (Webb, 2001)

The complexity of the term volume is highlighted by the following definitions:

- *Absolute powder volume*: (also called absolute volume): The volume of the solid matter after exclusion of all the spaces (pores and voids) (BSI).

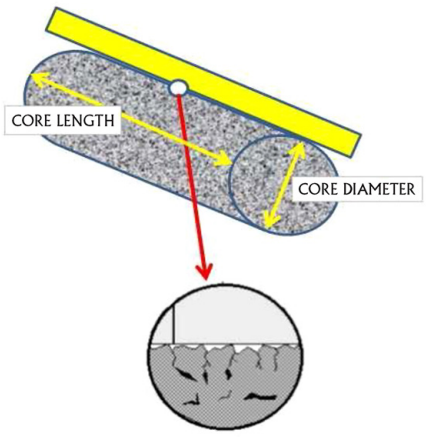

Figure 3—A straight edge placed along the outside edge of the length of core demonstrating the concept of 'external volume', the volume contained by virtue of surface irregularities (Micromeritics Instrument Corp., 2000)

- *Apparent particle volume*: The total volume of the particle, excluding open pores, but including closed pores (BSI).
- *Apparent powder volume*: The total volume of solid matter, open pores, and closed pores and interstices (BSI).
- *Bulk volume*: The volumes of the solids in each piece, the voids within the pieces, and the voids among the pieces of the particular collection (implied by ASTM D3766).
- *Envelope volume*: The external volume of a particle, powder, or monolith such as would be obtained by tightly shrinking a film to contain it (BSI). The sum of the volumes of the solid in each piece and the voids within each piece that is, within close-fitting imaginary envelopes completely surrounding each piece (implied by ASTM D3766).
- *Geometric volume*: The volumes of a material calculated from measurements of its physical dimensions.
- *Skeletal volume*: The sum of the volumes of the solid material and closed (or blind) pores within the pieces (implied by ASTM D3766).
- *True volume*: Volume excluding open and closed pores (implied by BSI).
- *Void*: Space between particles in a bed (BSI).

If particle characteristics as shown in Figure 4 are re-evaluated, the envelope volume (Figure 5) can be considered as being representative of a cross-section of the core sample retrieved from the borehole. It represents the geometric volume derived from the product of the cross-section of the core and its length, not taking rugosity shown in the figure into account and assuming that the core is an absolute solid.

Density derived from this would then simply be determined by the mass of the core divided by its bulk volume. No free moisture content is known since the core was not impeccably preserved on recovery and no moisture determination was done.

In the next case, reflecting probable skeletal volume, the core is subjected to Archimedes principle for SG determination and assuming saturation of the core, its mass in air divided by the difference between the mass in air and the mass in water gives a specific gravity for the entire sample, which is greater than the original density determined on the core as received. This is the result of water ingress during the procedure (Figure 6).

The core dispatched to an accredited laboratory is weighed on receipt, crushed, and screened to –13 mm +0.5 mm, air-dried under controlled conditions, and re-weighed before float/sink analyses are done. The air-dry mass is substantially less than the recovery mass; using this mass and the original envelope volume of the core results in a density substantially lower than the first two values obtained. This, however, is not representative of the true air-dry mass of the sample because the mass of the –0.5 mm fraction after screening is not reported or shown in the geological database. This –0.5 mm material is, however, used for a raw proximate analysis of the sample. The density value obtained cannot be deemed representative of the air-dry density and as such cannot be used to derive an accurate estimate of air-dry skeletal volume (Figure 7) of the matrix.

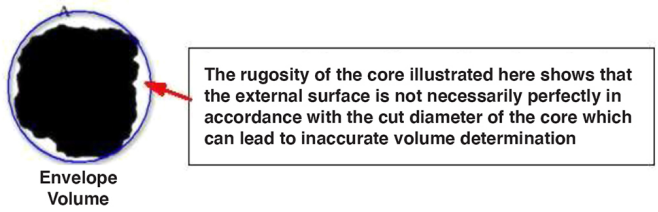

Figure 5—Envelope volume

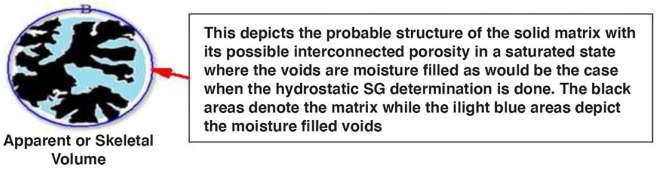

Figure 6—Apparent moisture-saturated skeletal volume

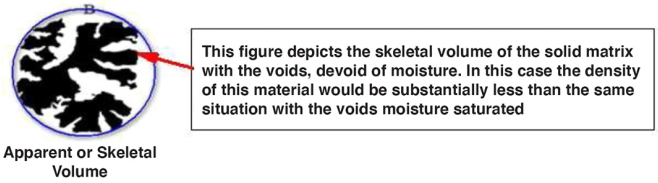

Figure 7—Air-dry skeletal volume

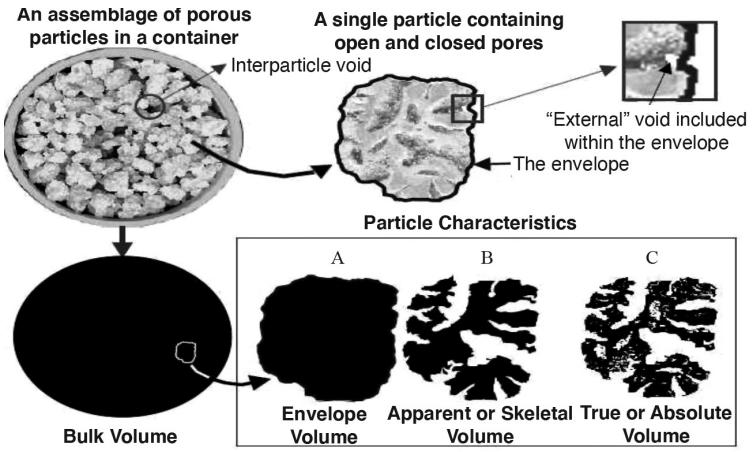

Figure 4—Illustrations of various volume types. At the top left is a container of individual particles illustrating the characteristics of bulk volume in which interparticle and 'external' voids are included, at the top right is a single porous particle from the bulk. The particle cross-section is shown surrounded by an enveloping band. In the illustrations at the bottom, black areas are analogous to volume. The three illustrations at the right represent the particle. A is the volume within the envelope, B is the same volume minus the 'external' volume and volume of open pores, and C is the volume within the envelope minus both open and closed pores (Webb, 2001)

In order to determine the solid matrix percentage, the core needs to be absolutely air dry, its mass determined, and then submerged in water for the Archimedes determination of SG. If the Archimedes SG determination is conducted properly, allowing for complete saturation so that no air bubbles are observed during the submerged phase, the SG can be used to determine the volume capable of supporting that density for the air-dried mass of the core. This in turn can be subtracted from the original volume and the result expressed as a percentage of the original volume representing voids in the matrix. This percentage subtracted from 100% would be representative of the solid matrix of the core.

The last scenario, shown in Figure 8, depicts the absolute volume; here both interconnected porosity and closed porosity are shown. The closed porosity may contain gas, air, or moisture. The moisture may be representative of the inherent moisture, which can be released only during combustion. If the absolute dry density can be determined and the mineral volatile content, including inherent moisture, is known or determined, the air-dry density of the sample can be determined.

Considering the requirements for Coal Resource tonnage reporting and the stipulation that these tonnages are reported as 'mineable tonnes *in situ*' raises another problem if the *in-situ* moisture content of the coal beds is unknown. Groundwater levels, porosity, and permeability would greatly influence the *in-situ* density of the material being assessed. Consider two scenarios sketched in Figure 9, the first illustrating an exploration borehole intersecting a coal sequence under the groundwater table, the probability of the core retaining the moisture when it is recovered is relatively good. This core should, however, be immediately sealed to prevent moisture loss, sent to the laboratory and the moisture content determined. This moisture content would represent the *in-situ* moisture of the core. In the second example, in a purported dry borehole, the core may still contain some moisture, relating initially to interstitially trapped water and secondly to structural or inherent moisture. These values should also be ascertained since they will influence the overall apparent relative density of the material.

A third scenario to consider, sketched in Figure 10, is an exploration borehole that may have been drilled several years earlier, prior to any mining activities, but is now in a position where an opencast mining operation has advanced closer to the specific exploration borehole from which the original determinations were done. Groundwater, having drained from this area into the mine's sump over the years, is now at a level below some of the coal seams and the mining benches have been exposed to natural atmospheric and climatic conditions for several years, thus rendering them effectively dry.

Information with regard to *in-situ* densities determined during the exploration phase, used for mineable tons *in situ* determinations, is no longer valid since the moisture content in the subsurface environment has changed over time.

Consider what the *in-situ* moisture content of this material would be. Assuming this is the same borehole shown in the first scenario (Figure 9, left), the moisture content in the upper benches may be the same as for the borehole drilled through a dry area, similar to the one shown in Figure 9, right. Surely it is no longer feasible to use the values initially obtained for an apparent relative density, especially if they were derived using the Archimedes principle method?

The most logical value to use would be representative of the air-dry relative density, which at least partially conforms to the material being mined. This value would allow more credible Resource and Reserve tonnage estimation and an improved planned volume of material to be extracted in order to satisfy budgetary predictions. Planned mining extraction should rather be based on volumes to be extracted in order to produce the required tonnages of matrix material.

Density and porosity

Traditionally, the basic method of determining the relative density of an assumed solid, such as coal, is to weigh it in air, then immerse it in water and weigh it again, the relative density being equal to the ratio of the weight in air to the loss of weight in water.

True or Absolute Volume

This figure depicts both the interconnected voids as well as voids within the matrix that are not interconnected and may contain trapped moisture or air/gas. The black skeletal structure represents the solid matrix and as such, less than the previous figure. This material would represent the absolute volume of the matrix material

Figure 8—Absolute volume

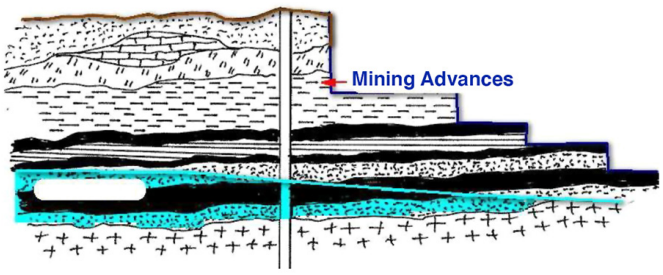

Figure 10—Opencast mining approaches the exploration borehole, illustrating the effect of the drainage of groundwater over time

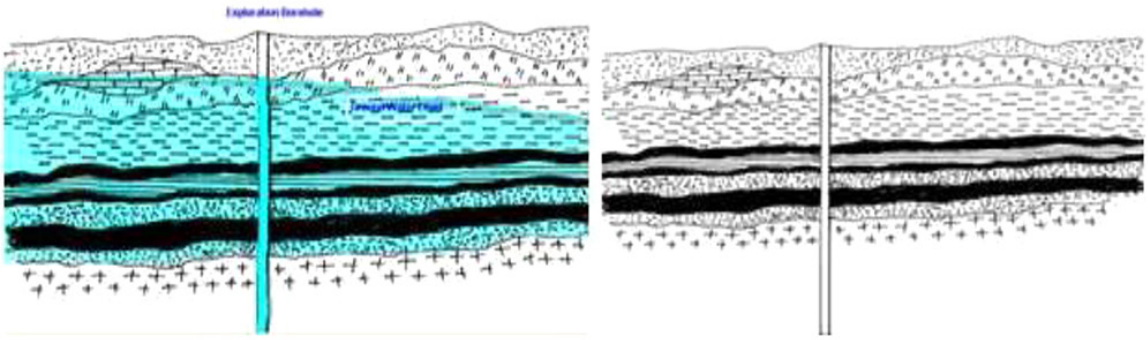

Figure 9—(Left) Coal measures below groundwater level, (right) coal measures essentially dry – no groundwater influence

Analyses done by the University of Illinois as early as 1916 on relative density (at that time referred to as specific gravity) under varying conditions of moisture content add a whole new perspective to density determinations (Nebal, 1916).

The American Society for Testing and Materials book of standard definitions lists no less than 40 definitions for density based on mass per unit volume. The British Standards Institute reduces this to 14. The determination of the mass of an object is relatively straightforward; the determination of the volume, however, is complex. The volume of a solid object, whether it is a single piece or a mass of finely divided powder, is a concept that cannot be ascribed to a single, neat definition.

A more specific definition of relative density (RD)

At a temperature of 5°C the density of water is 1.0 g/cm^3, thus the relative density of a material is its density relative to the density of water at 5°C. This property is a ratio, thus dimensionless, and is numerically equivalent to the density of the material. All relative density determinations require the mass and the volume of the material to be measured. The mass determination is simple; the volume determination however, as discussed earlier, both in regard to measurement and understanding in heterogeneous materials such as coal, is complex. This relates primarily to the porosity of coal and the variable degree to which different methods cope with this aspect of the determination. Since coal is porous, most of the contained moisture is held physically in its pores. The pores may be interconnected or isolated. Interconnected pores contribute to permeability thus, when coal is dried, its permeability allows some of the moisture to leave the pores, which become filled with air. If the dry coal is placed in water, the air in the pores is displaced by the water, and the coal becomes saturated. Under such circumstances the length of time that the coal is immersed before it is weighed affects the value obtained for the relative density.

True (or absolute) relative density should only be used to describe the relative density of a volume of pore-free coal, which by implication means that whichever method is used in determining the volume of the sample, the medium used must occupy all the pores, which in practice is very difficult. Helium, being the smallest atom, has the best probability of penetrating the greatest number of pores, thus the helium density method is the recognized method for determining this parameter. The availability of consistently reliable true or absolute relative density values for coal would make the estimation of *in-situ* relative density a straightforward process.

Apparent (or coal particle) relative density describes the relative density of lump coal which may contain pores, fissures, and moisture, the persistence of which in the actual sample may be variable, tending to give unreliable results when density is determined by the Archimedes method. A more precise determination can be obtained by use of the mercury density method, but similar to the helium method, the equipment required is not always available.

In-situ relative density

In-situ relative density refers to the relative density of the coal in the ground. The coal under confining pressure contains pores and fissures filled with water and dissolved gases. The relative density measurement of the coal *in situ* is the value that is used for the estimation of Coal Resources. This value may be calculated from the coal thickness (*in situ*), the core diameter, and the mass of impeccably preserved core lengths. The Australian Standard method of determining coal density is most commonly used, and although the method is cheap and easy to apply, the state of the sample when tested does not simulate the *in-situ* condition of the coal because the sample is ground to –212 µm, removing fissures and some pores. It is also air-dried, retaining its inherent moisture. The moisture thus retained is representative of the inherent moisture of the coal sample as determined by proximate analysis on the same sample.

The method involves measuring the liquid displacement, in either a density bottle or a volumetric flask, thus determining the volume of the ground coal sample; this is then related to the original weighed mass. The major problem with the method is the inability of the liquid to occupy all pores within the coal and thus displace all air and water. The result gives neither absolute relative density nor an *in-situ* relative density, although it is probably closer to the absolute relative density. Under rigorously controlled conditions, the standard density bottle method may give results closely approximating the true or absolute relative density for coal expressed on the air-dry basis.

This standard method does not replicate the conditions required for determination of *in-situ* relative density since the values obtained are tested on an air-dry basis, whereas the resources of coal *in situ* are not; the use of standard relative density in Resource and Reserve calculations is thought to result in an overestimation of Reserves. In order to convert the standard relative density to an *in-situ* relative density, the sample needs to be reconstructed to simulate original conditions, especially with relevance to the original volume, restoring the pores and fissures destroyed in the grinding process. The reduction in volume of the sample has a greater effect on the relative density than the loss of mass held in that volume.

If the voids are restored to their original state and refilled with water, both the volume and mass will increase. The volume, however, will increase at a rate higher than the mass and thus the sample density will decrease, trending towards unity, the relative density of water. The most critical information required here relates to the *in-situ* moisture content of the sample, since this would be essential for the calculation of densities, Reserves, coal handling mass calculations, and the estimation of product coal total moisture. To assess the *in-situ* moisture content of the samples, cores should be promptly bagged and sealed so that the total moisture retained can be determined by a laboratory.

Research at the University of Illinois in 1916 on the effects of coal porosity illustrated the fact that the voids were air-filled as a result of being air-dried, the air being expelled when the sample was submerged in water for the density determination. This indicated the inherent problems that could be expected in determining the relative density of coal. It also indicated the differences in the specific gravity values obtained for purported fresh coal as opposed to the 'true' specific gravity of air-dried coal and the moisture contents of these coals. Several experiments were conducted to determine the effect on specific gravity of the expulsion of air through the replacement of water in the voids in an air-dried coal, as well as the time required for the expulsion of the air from interconnected voids. One of the interesting experiments in this range compared the specific gravity of fresh coal and that of the same dry coal. A range of samples were allowed to dry in the laboratory under constant temperature for 60 days. The specific gravity of the fresh coal averaged 1.28 g/cm^3 while that of the air-dried coals was 1.19 g/cm^3. The same samples were then subjected to boiling water in order

to dispel air and the voids, now filled with water, raised the SG to 1.31 g/cm³. From this it was deduced that the moisture loss of the fresh coal was dependent on the original moisture content of the coal, the porosity of the coal, the humidity in the air to which the coal was exposed, and the final loss dependent on the period of time that the coal was exposed to air. Subsequent experiments were then done to ascertain the density of coal samples from an air-dry condition to probable full saturation, and the concomitant changes in apparent density over time. It is interesting to note that the greatest change took place within the first two hours, as shown in Figure 11.

The experiment was repeated with the values being determined over shorter time periods to assess the rate of change within the first 2 hours. This is shown in Figure 12. Here again the greater part of the change was noted within the first hour of immersion, the specific gravity increasing from 1.16 g/cm³ to approximately 1.30 g/cm³, and eventually to 1.32 g/cm³ after two hours.

This early experimental work highlights the possible error with regard to so-called relative density and the effect on the relative density as a result of, the porosity of the medium and whether the pores are air- or water-filled. The effective porosity or moisture-holding capacity would have to be taken into account when considering which value of 'relative density' should be used in Resource and Reserve tonnage determination.

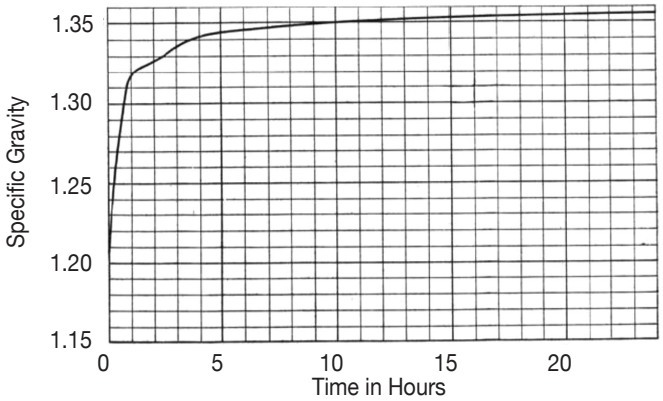

Figure 11—Graphical representation of the increase in specific gravity over 24 hours in a coal sample submerged in water at room temperature (Nebal, 1916)

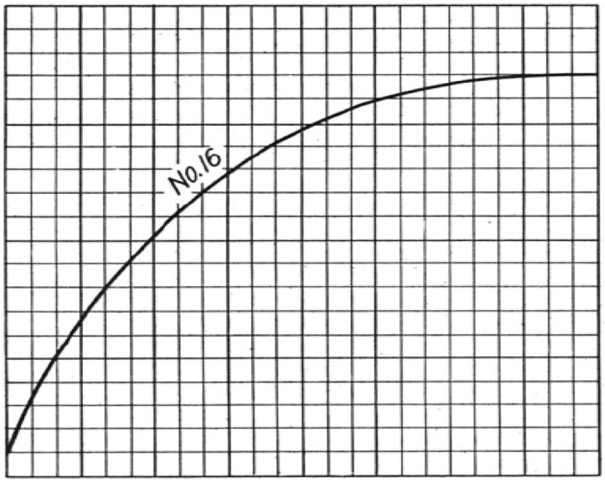

Figure 12—The change in specific gravity of coal samples immersed in water at room temperature (Nebal, 1916)

Considering values obtained in the field, such as relative density determined by the Archimedes principle, and the availability of appropriate information, it is extremely difficult to assess the relevant *in-situ* density of the coal from data obtained at the exploration site. These initial values, however, can be partially validated when the laboratory results are received.

Literature studies and personal communication with experts in the field (Pinheiro, pers. comm.) has revealed the most common methods of determining *in-situ* relative density are by the Archimedes principle and by pycnometry through the application of the Australian Standard method (AS1038.21 Item 4). The value obtained from the Australian Standard method should not be used for Reserve calculations since the values obtained are on an air-dry basis and coal Resource/Reserve calculations are not – they are based on *in-situ* values. The sample used for this determination, after preparation, is no longer representative of its original state with regard to volume and moisture content and can therefore result in an overstatement of Reserves (Preston and Sanders, 2005), Such values can be compensated to reflect the probable *in-situ* density by applying a change of basis equation converting coal relative density from one moisture basis to another, provided that the appropriate inputs with regard to moisture content are known.

The equation used for this is:

$$RD_2 = RD_1 \times (100 - M_1) / (100 + (RD_1 \times (M_2 - M_1) - M_2))$$

where

RD_1 = old RD, which is the RD determined *via* the density bottle

M_1 = Old moisture, which is moisture content determined from the original core sample as sealed and preserved in the field on extraction from the core barrel

RD_2 = new RD

M_2 = new moisture (which is moisture retained in the pulverized sample, probably representative of the inherent moisture.

This change of basis equation will enable the relative density of coal to be converted from one basis to another provided that the information used is reliable. If no information relating to the core's adventitious moisture content in the field is available, this method cannot be used.

Example:

RD from density bottle 1.93 g/cm³

Moisture content of core sample 20%

Inherent moisture from proximate analysis 2% $RD_2 = RD_1 \times (100 - M_1) / (100 + (RD_1 \times (M_2 - M1) - M_2))$

$= 1.93 \times (100 - 20)/(100+(1.93 \times (2-20) - 2)$

$= 154.4/81.93$

= 1.88 g/cm³ relative *in-situ* RD

A different approach to the estimation of *in-situ* relative density was developed by Peabody Energy (Robeck and Huo, 2015). The mineral matter content is used with relative to estimate pure coal and mineral densities for given data-sets on a dry basis. A hyperbolic regression is then used with known *in-situ* moisture values to predict *in-situ* relative density for all raw samples.

Robeck and Huo's approach was to provide a solution for the contentious problem related to Resource and Reserve tonnage estimations through a fully deterministic RD *vs.* ash relationship. Their approach determining mineral matter content

was applied because ash, although representing the indestructible mineral matter, is considered a combustion product and thus not representative of the original mineral matter content. The reason for this being that mineral volatiles such as H_2O of hydration, CO_2, SO_2, salts (*e.g.*, Cl), carbonates, and sulphides are lost during combustion (Ward, 1984) and the remaining solid residue (ash) is less than the original mineral matter (Figure 13).

Complications due to (a) mineral composition, (b) coal maceral distribution, and (c) the presence of water- and air-filled pores detract from the simplistic two-phase mixture of coal and rock. Primary and secondary mineral composition may vary widely, and coal maceral content is determined by a number of factors, including rank, vegetation type, and environment of deposition (Renton, 1982).

Densities and mineral matter ratio values are shown for a few of the most common minerals in Table I. The ratio (r) is directly related to the percentage mass loss. This relates to the mineral volatiles percentage lost. Individual mineral densities vary and most distributions average between 2.5 and 2.8 g/cm^3. The ratio can range from 1 to almost 2 depending on the mineral constituents. Similarly, the density of coal macerals can range from 1.03 to 1.70 g/cm^3.

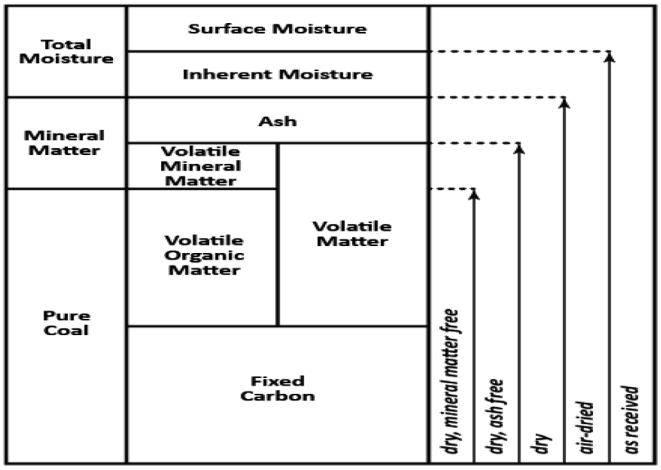

Figure 13— Relationship between the various constituents of coal and reporting bases (Ward, 1984)

Although coal density is a function of rank, increasing with degree of lithification (Smith, 1991; Sanders, 2003), maceral composition contributes to the variability of densities within the same rank. The influence of rank is attributed to changes that occur as rank increases and volatile elements (H, N, and O) are lost.

Several different models, formulations, and methods applied by various authors were evaluated by Robeck and Huo and used in the formulation of their proposed new approach correlating density to mineral matter, which would improve their predictions. The authors do, however, recognize the influence of unsaturated *in-situ* porosity and acknowledge that it has not been addressed in this method because void porosity is a volumetric percentage while the relative concentrations of coal, mineral matter, and moisture are mass weighted percentages. They claim that the amount of air-filled porosity (free gas) is small in high-rank coals and can safely be ignored in saturated coal seams. This may be true for high ranking coals, but lower ranking coals have greater effective porosity and moisture holding capacity.

Unless sampled core is impeccably preserved (sealed) on recovery so that the true moisture saturation can be determined and related to its *in-situ* state, the percentage of saturation and voids play a major role in varying determined densities for the samples. The volumetric component therefore makes a far greater contribution than mineral volatiles lost upon combustion. The authors also admit that the single greatest source of error in density estimations is the choice of *in-situ* moisture values.

Empirical formulae derived by Fletcher and Saunders (2003) based on a range of black coals (and not necessarily applicable to all basins or coal types) may have found applicability in both Australia and North America. No moisture holding capacity or equilibrium moisture data was available for their work. Their study attempted to use an empirical multivariate equation developed by Meyers *et al.* (2004). This equation proved unsuccessful so the authors used an assumed constant moisture value for coal and mineral matter that was consistent with earlier analytical work and JORC reports.

Porosity

Coal moisture content plays an integral part in contributing to

Table I

Mineral matter densities (ρ_m) and ratios (r) for common minerals in coal (Ryan, 1990; Vassilev *et al.*, 2010)

Mineral	Chemical composition	Abundance (%)	ρ_m (g/cm^3)	r	Mass loss (%)
Quartz	SiO_2	11–56	2.65	1.00	0
Kaolinite	$Al_2Si_2O_5(OH)_4$	14–42	2.16–2.68	1.16	14.0
Illite	$KAl_4(AlSi_7O_{20})(OH)_4$	3–13	2.6-2.9	1.05	4.5
Montmor-illonite (smectite)	$(½Ca,Na)_{0.7}(Al,Mg,Fe)_4[(Si,Al)_4\ O_{10}]_2\ (OH)_4 \cdot nH_2O$	0–4	1.7–2.0	1.05	5.0
Chlorite	$(Mg,Al,Fe)_{12}[(Si,Al)_8O_{20}](OH)_{16}$	2–6	2.6-3.3	1.26	20.4
Pyrite/marcasite	FeS_2	0.5–12	4.88–5.01	1.50	33
Calcite	$CaCO_3$	1–22	2.71	1.79	44
Siderite	$FeCO_3$	0–2	3.96	1.61	38
Ankerite	$Ca(Mg,Fe,Mn)(CO_3)_2$	0–3	3.05	1.79*	44
Dolomite	$CaMg(CO_3)_2$	0–6	2.84	1.91	48
Gypsum	$CaSO_4 \cdot 2H_2O$	0–13	2.31	1.26	20.9
Plagio- clase	$NaAlSi_3O_8$ - $CaAl_2Si_2O_8$	1–11	2.62–2.76	1.00	0
K-feldspar	$KAlSi_3O_8$	0.5–5	2.55–2.63	1.00	0

* Assumes an average ankerite composition of 54% Ca, 24% Mg, 20% Fe, and 2% Mn

changes in relative density. Porosity *per se* provides the capacity for moisture or gas storage and is also an integral part in the overall structural composition of the materials matrix, and depending on the nature of the fluid or gas that may be contained within the pores will have an effect on the density of the material. Porosity by definition in the geological sense is the volume of the non-solid portion of the rock filled with fluids or gases, divided by the total volume of the rock, and is defined by the ratio (Anderson,1975).

$$\emptyset = \frac{V_V}{V_T}$$

where V_V is the volume of void space (such as fluids) and V_T is the total or bulk volume of material, including the solid and void components. Porosity is a fraction between 0 and 1, typically ranging from less than 0.01 for solid granite to more than 0.5 for peat and clay. It may also be represented in percentage terms.

The highest porosity normally anticipated in rocks is 47.6% (Crain, 2010). A more probable porosity is in the mid-twenties range. The normal range of porosities in granular systems is 5% to 35%. In general, porosities tend to be lower in deeper and older rocks, due primarily to overburden stresses on the rock (compaction) and cementation.

Porosity in coal can be a combination of both primary and secondary porosity, the latter referring to an enhancement of overall porosity as a result of chemical leaching of minerals or the development of fractures associated with stress in the system. This can replace the primary porosity or coexist with it. Porosity can be further subdivided into effective porosity (interconnected porosity), referring to the fraction of the total volume in which fluid flow can effectively take place, and closed porosity, referring to the fraction of the total volume with fluids or gases confined within the matrix (impermeable).

Understanding the morphology of the porosity is thus very important for groundwater, petroleum flow, and in the case of coal, surface and inherent moisture content entrapped in coal. It is a well establi-shed fact that coal is a porous substance and that both the pore size distribution and total pore volume vary, depending on a number of factors.

Various systems of classification of the pores have been proposed by different authors (van Krevelen, 1993). Consensus has been reached with regard to classifications resulting from high-resolution electron microscopy, where coal is characterized by a dual porosity consisting of macropore and micropore systems.

The micropore system consists of pores less than 2 nm in diameter and which occur as part of the matrix, while the macropore system is related to the fracture network designated by the cleat system, bedding planes, and surfaces (van Krevelen, 1993). Macroporosity refers to pores that are greater than 50 nm in diameter. Flow-through macroporosity is described by bulk diffusion. Mesoporosity refers to pores that have a diameter between 2 nm and 50 nm. Microporosity refers to pores that are smaller than 2 nm in diameter. Movement in micropores is by activated diffusion.

Lower rank high-volatile bituminous coals and sub-bituminous coals have a relatively high total porosity and a high proportion of intermediate pore sizes. High-rank bituminous coals have no intermediate sized pores and appreciably lower microporosity, while lignites on the other hand have high levels of macroporosity. Figure 14 illustrates the effect of coal rank on porosity. Macropores predominate in the lower ranks, while geophysical factors relating to compaction and water expulsion gradually reduce the porosity in the higher ranks. The development of secondary porosity begins with the formation of micro- and mesopores at approximately the low-volatile bituminous coal rank designation, implying an increase in porosity due to progressive changes in the molecular structure through the higher ranks.

Porosity is related to the maceral composition, where microporous content is found predominantly in the vitrinite content and meso- to macroporous content predominates in inertinite (Gan *et al*,, 1972; Unsworth, Fowler, and Jones, 1989; Lamberson and Bustin, 1993; Levine 1993).

Coal porosity is also associated with cleats within the coal seams. Cleats are natural opening-mode fractures in coal beds. They usually occur in two sets that are, in most instances, mutually perpendicular and also perpendicular to the bedding. These fracture sets, and partings along bedding planes, impart a blocky character to coal (Figures 15 and 16). Cleats account for the predominant natural porosity and permeability paths in coal seams. Coal cleats are extensional fractures that formed, especially in the vitrain layers, as a result of active coalification processes and fluid pressure exerted during tectonic events (Close, 1991).

Vitrain/non-vitrain interbeds, which have different mechanical properties, were subjected to different strain magnitudes during these tectonic episodes, which also favoured fracture genesis. In the light of the effects of coalification on cleat development, Levine (1993) noted that porosity of coal is a function of molecular interactions. Levine's study suggested that cleat porosity is related to the compositional constituents, namely the macerals and minerals, as well as the maturity of the coal, which changes with the coalification process.

The relationship between porosity and carbon content was determined using laboratory tests on coal samples (Ettinger, 1960). The results showed that minimum porosity occurred at a carbon content of approximately 70 to 80%, representative of low-volatile bituminous to medium-volatile bituminous coal. Jones *et al.* (1988) found that the mechanical properties governing the apertures and frequency of cleats were related to coal type and rank. More recent work, however, has shown

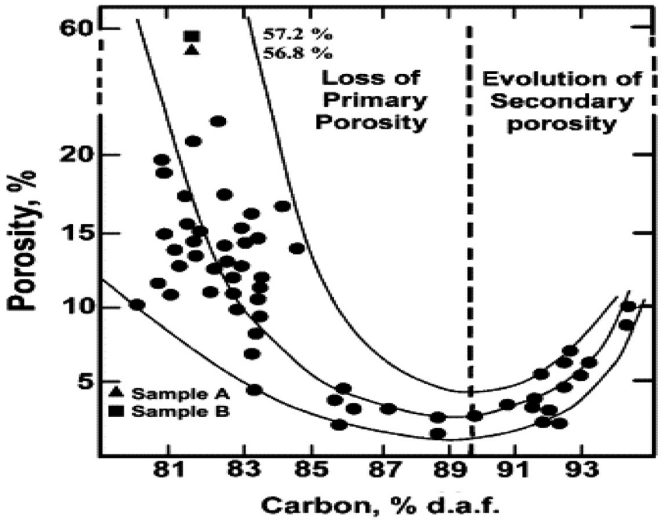

Figure 14—Relationship between coal porosity and coal rank (Gan, 1977; King and Wilkins, 1944; Levine, 1993)

that the lowest porosity occurs at a dry mineral matter-free fixed carbon content of approximately 89%, as shown in Figure 14 (King and Wilkins, 1944; Levine, 1993).

The cleats, however, contribute to the moisture storage capacity of the coals in addition to moisture storage within the micro- through macropores related to coal type maceral composition and rank.

One remarkable attribute of cleat formation is the extent to which they are developed in many coal beds of nearly all ranks in maturity. Cleats are typically much more intensely developed than fractures in adjacent non-coal rocks. Bright coal lithotypes (vitrain) generally have closer spaced cleats than dull coal lithotypes (durain).

Coals with low ash content tend to have smaller cleat spacings than coals with high ash content. Organic-rich shales also commonly have closely spaced fractures that resemble cleats. (Close,1993) On a more diminutive scale, the sketches in Figure 18 shows examples of cleat formation and an indication of the extent of cleat formation in some hand samples.

It is evident that coal porosity, and as such relative permeability, can be highly variable. The movement of or saturation by moisture would in many instances be by diffusion, thus a reasonable amount of moisture would be retained in such a structure even if the large specimen were exposed to natural drying. This moisture is additional to the structurally bound moisture.

An interesting study was conducted by Wang (2007) on the influence of coal quality factors on seam permeability associated with coal bed methane production and cleat studies, which illustrates the reality of the cleat formation perfectly. The emphasis of this study was on the major cleats and involved the reduction of coal core samples to 40 mm cubes, which were treated with silicone gel in order to harden and preserve the samples. The cubes were then polished, removing the rough surfaces and resulting in a smooth shining surface on which the major cleats, spacing, length and apertures could be measured (Figure 19). This was illustrative of the major cleats regarded as connective and providing a major contribution to seam permeability as well as contributing to increased porosity.

It is against this background that the research was undertaken as it is believed that every effort should be made to obtain the correct information with regard to the true density of coal in order to establish a realistic evaluation of a given coal deposit.

Figure 15—Photograph of a 2.5 m mining horizon section illustrating the nature of the face and formation of cleats on a macro scale

Figure 16—Photograph of a hand sample illustrating cleats, especially noticeable in the vitrain layers of bright coal; note the blocky nature as a result of these smaller cleats

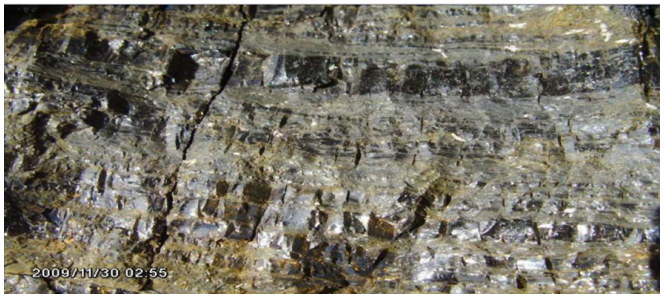

Figure 17—Vertical fissures and cleats

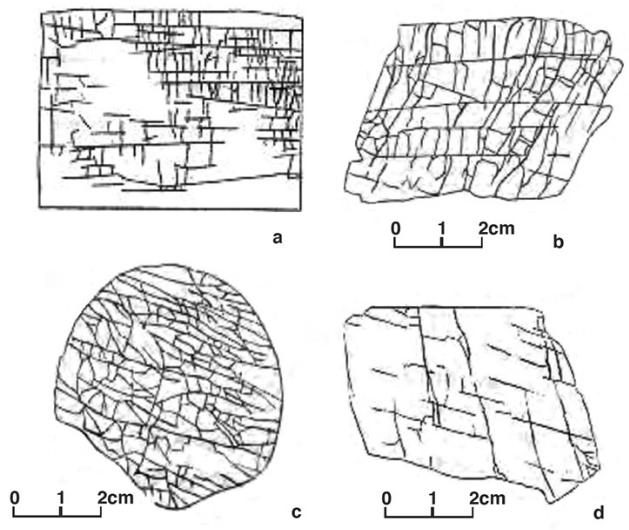

Figure 18—Sketches showing (a) parallel face cleats with general continuity and occasional discontinuity, (b) face cleats parallel and continuous, (c) a high-density cleat system in various directions, and (d) low-density parallel cleats (Fan, 1997)

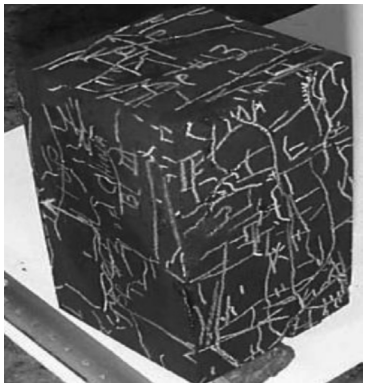

Figure 19—Photograph of a 40 mm coal cube displaying the major cleats infilled with silicone to contrast against the coal background and also to strengthen and retain the coal sample intact (Wang, 2007)

Geological losses

From the foregoing review of density, porosity, and moisture content, the major geological losses are related to porosity and moisture content of the matrix material. Quantification of these losses would enable a more accurate estimation of resource tonnages.

An evaluation of predicted product yields and the differences noted between the predicted values and actual plant production *via* the application of ash-adjusted density (AAD) initiated research concentrating mainly on the beneficiation aspects and in-house determined correlation factors that were applied to specific regions in the mine. This was based on the optimal yield and cut density prediction for semi-soft coking coal and power station middlings coal in the Waterberg Coalfield, Limpopo (Roux. 2012).

The results obtained allowed the negation of a collection of different correlation factors relating to the origin of the raw feedstock material. These factors were reduced to a single correlation factor specific to a particular beneficiation process. It was based on the beneficiation plant's capabilities and efficiency, the physical nature of the run-of-mine material, its reduction to a specific top size before processing, and the actual results obtained, irrespective of the origin of the material. The implementation of this methodology after the plant-specific correlation factor had been applied to the theoretically determined product yields improved the predicted values to such an extent that the beneficiation plant's products were conforming with the predicted values. (Roux, 2012).

The probability that the correlation factor could be removed entirely still existed, however, since the correlation factor, although plant-specific, was based on plant production results, and a deficiency equivalent to the difference between the plant-specific correlation factor and a 100% theoretical yield value determined from the cumulative wash table remained. This difference at the time was approximately 17.82%.

If this difference could be accommodated and negated then the reconciliation loop would be complete and it would support the values obtained from the geological model, resulting in increased confidence in the credibility of the data. Paramount in this evaluation was consideration of the relationships between coal density and porosity, with porosity and interrelated permeability playing a major role in varying densities for the same volume of material.

Methodology

Three approaches to validate the determination of credible density values, namely, the revised AAD methodology (Roux, 2012), the evaluation of pure coal and mineral matter (Robeck and Huo, 2015), and the Australian Standard method (pycnometer or density bottle) were used.

Ash-adjusted density

The original theory with regard to the AAD methodology as outlined by Roux (2012) was based on distribution and cumulative frequencies of the float fraction values from a 31 000 sample data-set. This resulted in a linear regression for the ash/density relationship where RD = 0.0136 × Ash% + 1.198, giving an R^2 value of 0.99.

The sample data-set was re-evaluated by deriving descriptive statistics for each sample float fraction and regressions on the mean, median, and mode values to complement and enhance the earlier work on the data-set. The re-evaluated statistics for the ash content at the coal float fractions are presented in Table II.

The revised regression based on the median values (Figure 20) is:

$$\text{Absolute dry RD} = 0.0130 \times \text{Ash\%} + 1.2384$$

This gives a better result than the previously determined regression since the derived equation validates the petrophysical matrix density of bituminous coal as published by Schlumberger, where a matrix density for bituminous coal is given as 1.24 g/cm³, for anthracite 1.47 g/cm³, and lignite 1.19 g/cm³.

The first part of the equation represents the incremental indestructible mineral content of the sample, with the intercept being represented by a constant equivalent to the matrix density of a bituminous coal. The AAD value represents the absolute dry density of the float fraction. The expected air-dry density was approximated by including the effect of the inherent moisture content derived from proximate analysis.

The resultant density value was found to be slightly higher than the AAD value determined.

A reconstruction of the sample to *in-situ* relative density could then be calculated, provided that the free moisture content

Table II

Descriptive statistics results for float fractions analysed

	Ash 1.35 g/cm³	Ash 1.40 g/cm³	Ash 1.50 g/cm³	Ash 1.60 g/cm³	Ash 1.70 g/cm³	Ash 1.80 g/cm³	Ash 1.90 g/cm³	Ash 2.00 g/cm³	Ash 2.10 g/cm³
Mean	7.34	13.51	20.22	28.48	35.96	42.32	48.15	53.32	57.08
Standard error	0.05	0.08	0.09	0.10	0.09	0.09	0.10	0.10	0.12
Median	6.99	14.06	21.00	29.20	36.41	42.61	48.60	53.70	57.67
Mode	6.10	16.00	21.70	29.90	37.60	44.00	51.00	52.70	59.10
Standard deviation	2.09	3.62	4.14	4.23	4.14	4.16	4.33	4.48	5.12
Sample variance	4.36	13.07	17.14	17.89	17.16	17.29	18.77	20.09	26.22
Kurtosis	3.03	0.52	0.14	–0.23	–0.30	–0.19	0.04	0.36	0.12
Skewness	1.29	0.17	–0.31	–0.26	–0.13	–0.15	–0.38	–0.46	–0.50
Range	17.22	26.23	25.40	27.50	27.96	30.70	29.10	31.80	31.61
Minumum	3.28	4.47	8.70	15.90	23.74	27.20	32.70	36.30	39.09
Maximum	20.50	30.70	34.10	43.40	51.70	57.90	61.80	68.10	70.70
Sum	14156.60	26103.04	39170.81	55259.82	69800.52	82064.53	92059.22	100987.23	107816.41
Count	1928	1932	1937	1940	1941	1939	1912	1894	1889
95% Confidence level	0.09	0.16	0.18	0.19	0.18	0.19	0.19	0.20	0.23

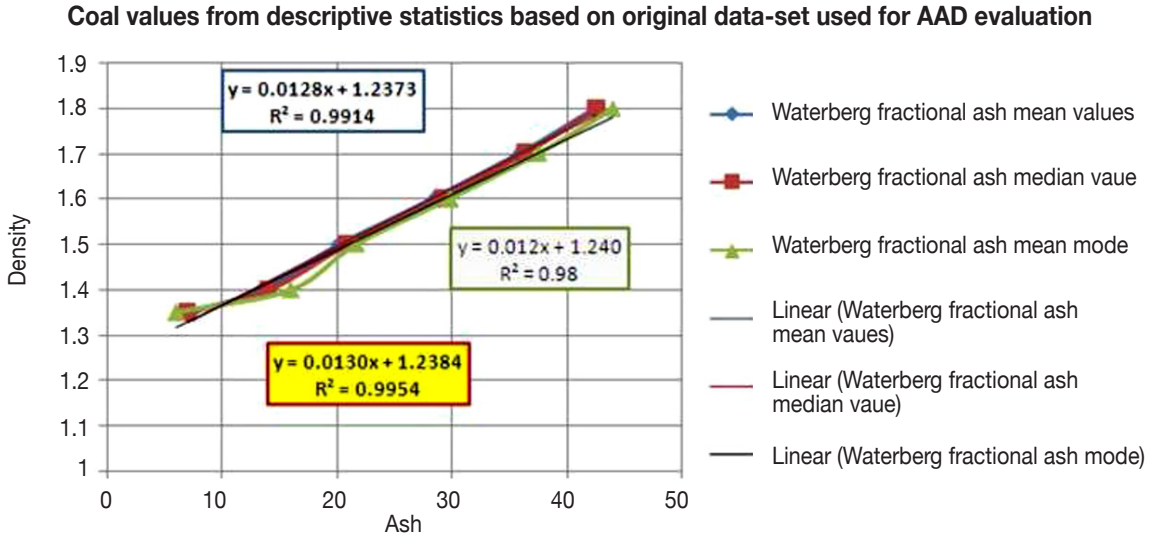

Figure 20—The revised regression based on descriptive statistic results obtained for each float fraction from the original data-set

and air- or gas-filled voids of an impeccably preserved sample are known.

Evaluation of pure coal and mineral matter for in-situ density determination (Robeck and Huo, 2015) - the Gray method

The proposed evaluation requires an estimation of mineral matter content, and the most commonly used method is the Parr formula (Rees, 1966).

$$M_d = 1.08\ Ad + 0.55\ S_{tot}$$

where S_{tot} = total sulphur (dry)

and the mineral matter ratio is determined by

$$r = \frac{1.08Ad + 0.55S_{tat}}{Ad}$$

An alternative, the Gray method in which M_d cannot exceed 100%, accounts for a wider range of mineral volatiles and reveals changes in mineral content with increasing ash.

This only requires specific energy (CV) and ash, and is the most robust, particularly for high-ash samples. The relationship between dry CV and mineral matter is given by:

$$E_d = E_{dmmf}\frac{100 - M_d}{100}$$

where

E_d = Specific energy, dry, expressed in MJ/Kg

E_{dmmf} = Specific energy, dry mineral matter free The mineral matter ratio is determined by

$$r = \frac{100\ (E_{dmmf} - E_d)}{E_{dmmf}Ad}$$

The dry mineral matter-free CV is determined by:

$$E_{dmmf} = \frac{100\ *(CV - 0.155)}{(100 * (\mathrm{Min}h + 1.08) * (Ad + 0.555))}$$

Mineral matter content is then derived by:

$Md = rAd$

The determination of the air-dry density of the sample is then obtained from the equation:

$$\rho_{est} = \frac{100}{(a + \ ) * M_d}$$

where coefficients a and b are determined by:

$$a = \left(\frac{\mathrm{Min}h}{\rho_w}\right) + 100 - \left(\frac{\mathrm{Min}h}{\rho_c}\right)$$

where ρ_c represents the matrix density of bituminous coal, 1.2384 g/cm³c and ρ_w is the density of water at 5°C, 1.0 g/cm³.

$$a = 100 - \left(\frac{\mathrm{Min}h}{100}\right) * \left(\frac{\rho_c - \rho_m}{\rho_c * \rho_m}\right)$$

where ρ_m = density of the mineral matter (here 2.53 g/cm³ was used for Waterberg coals).

The individual densities of the samples can then be obtained from the following equations.

$$\rho_c = \frac{100}{a}$$

and

$$\rho_m = \frac{100}{a + (100 * \ )}$$

Australian Standard method (AS1038.21 Item 4)

The most common method used is the Australian Standard method (AS1038.21 Item 4) where the coal sample is pulverized to –212 µm, thereby removing fissures and some pores. It is then air-dried, retaining some (but not all) of its *in-situ* moisture, weighed, and submerged in a density bottle or volumetric flask. The amount of water displaced relates to the volume of the ground material, which is then divided by the mass to obtain the relative density, referred to as the standard relative density.

Research and evaluation results

Ash-adjusted density validated against laboratory-determined density

An exploration borehole, sampled and dispatched for analyses,

was treated in the normal way according to the standards followed by the accredited laboratory responsible for the analyses. In addition to the normal float/sink and proximate analyses, it was requested that the true relative density of each float fraction be determined using the density bottle method (Australian Standard method) at the same laboratory. These values were compared with AAD values obtained by application of the derived algorithm to ascertain the accuracy of the algorithm. The two sets of results, *i.e.* laboratory true density and AAD values, were found to be very close.

The 'true relative densities' of 741 float and sink fractions were determined according to the Australian Standard method, AS1038.21 Item 4. In the process of converting a coal sample to a ground, air-dried state the greatest change is noted in the volume, which has a greater effect on the relative density than the loss of mass. In this situation, the density trend would approximate the absolute density of the coal.

The float and sink wash data for the individual coal and shale samples from the exploration borehole was evaluated. The coal and shale samples were combined for the separate stratigraphic units' AAD-derived densities and the re-determined laboratory densities were compared and statistically evaluated at a 99.9% confidence level. The cumulative probability of the difference between the two measured data-sets showed a very positive result. The coal and shale sample data was then combined and re-evaluated statistically. The individual coal and shale results, as well as a combination of coal and shale results, are shown in Figure 21.

All three sets of values obtained at various confidence levels indicate a high level of accuracy. Since this evaluation is based on a comparison between AAD calculated values and laboratory-determined values, it is apparent that the AAD methodology can be used confidently for predictions of dry densities in coal assessments. Minor differences between the two data-sets (the AAD results and the density bottle results) are attributable to the inherent moisture content of the samples. The AAD values had not been corrected to accommodate the inherent moisture content, thus they represent an absolute dry matrix density, and if this correction is applied the values would be comparable with an air-dry density.

This research was confined to the crushed, air-dried –13 + 0.5 mm material that was sink/float separated to obtain a range of fractions for further analysis. The values pertinent to the true density of the matrix material were assessed by re-determination of the relative density through the application of the ash-adjusted density algorithm and then compared.

The samples require reconstruction to resemble the raw material prior to crushing. This needs the restoration of the sample to its original volume, which can be achieved by considering properties such as moisture content and porosity, both of which were altered during sample preparation when the sample was pulverized to –212 µm for the pycnometer density determination.

Evaluation of pure coal and mineral matter for in-situ density determination (Robeck and Huo, 2015)

The air-dry relative density values for the exploration borehole samples were obtained by applying the Gray method. This pertained to the air-dry density of the samples because information on the free moisture content was not available. This approach was comparable to the AAD methodology since the AAD results refer to the absolute dry density of the samples (density excluding inherent moisture).

A chart similar to the 'Fish Diagram' developed by Robeck and Huo (2015) was populated with Waterberg coal data derived using both the Gray and Parr methods. As *r* increases on the y axis, the amount of mineral volatiles also increases (Figure 22). The relative position between zero and the 100% limit indicates the relative coal/mineral content. The area to the right of the 100% line is indicative of the amount of inorganic volatile matter (Robeck and Huo, 2015). Values below approximately 23% ash content are less reliable and may be approximated by the average of the Parr data-set at 1.12; the mean for the Gray data-set is 1.20.

Note that the Waterberg samples exhibit an abundance of kaolinite with minor silicates. Three sets of data – values derived from the AAD method, values from the Gray adapted method, and lastly the laboratory-determined density bottle values – were then plotted for comparative purposes.

The values determined from the AAD and Gray methods represent absolute dry (for AAD values) and air-dry densities. The AAD values have been adjusted from an absolute dry basis to an air-dry basis based on the inherent moisture content for a 100% yield so that all three data-sets are now comparable. Note that the matrix density of bituminous coal at 1.24 g/cm^3 and that of the mineral content at 2.53 g/cm^3 are the same as the values used in the AAD evaluation, and have been used in the Gray method. Trends established by the AAD and Gray methods correlate almost perfectly, with a slight divergence in the higher ash regimes, as shown in Figures 23, 24, and 25.

Note that the laboratory values up to 2.0 g/cm^3 are generally lower than both sets of calculated values. Although these

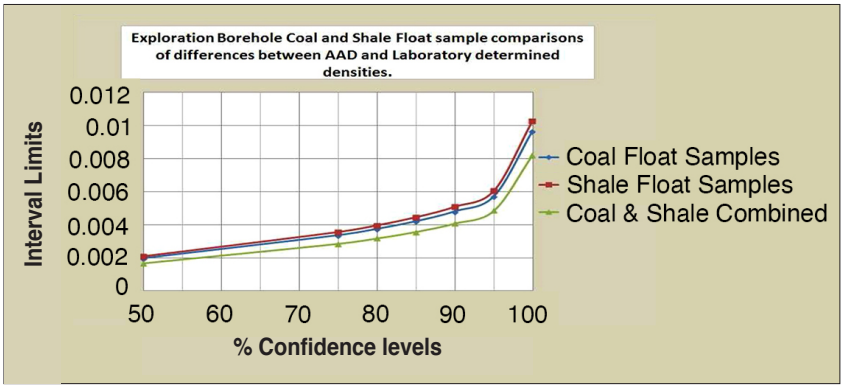

Figure 21—Confidence level accuracies for coal, shale, and coal-shale combination

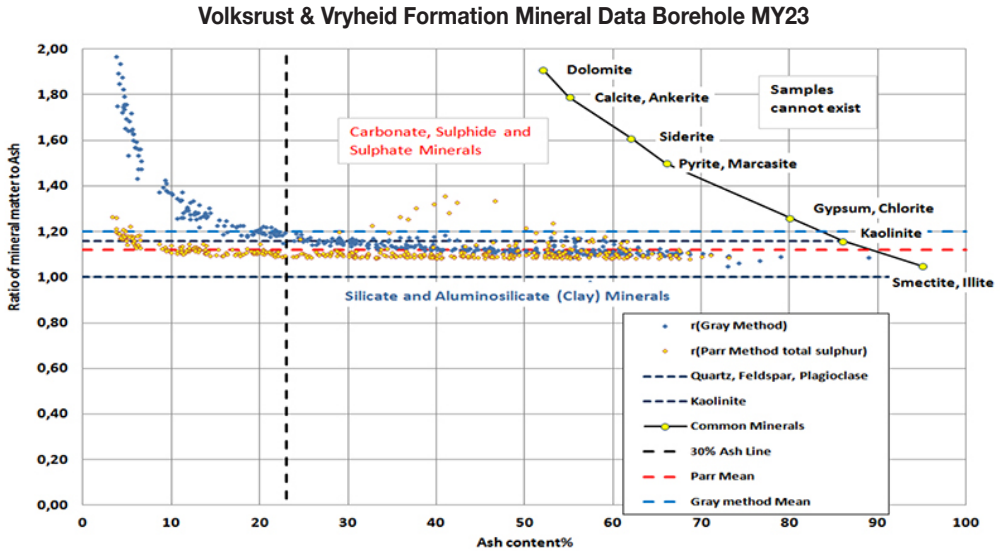

Figure 22—Diagram illustrating the ratio of mineral matter to ash *vs.* sample ash

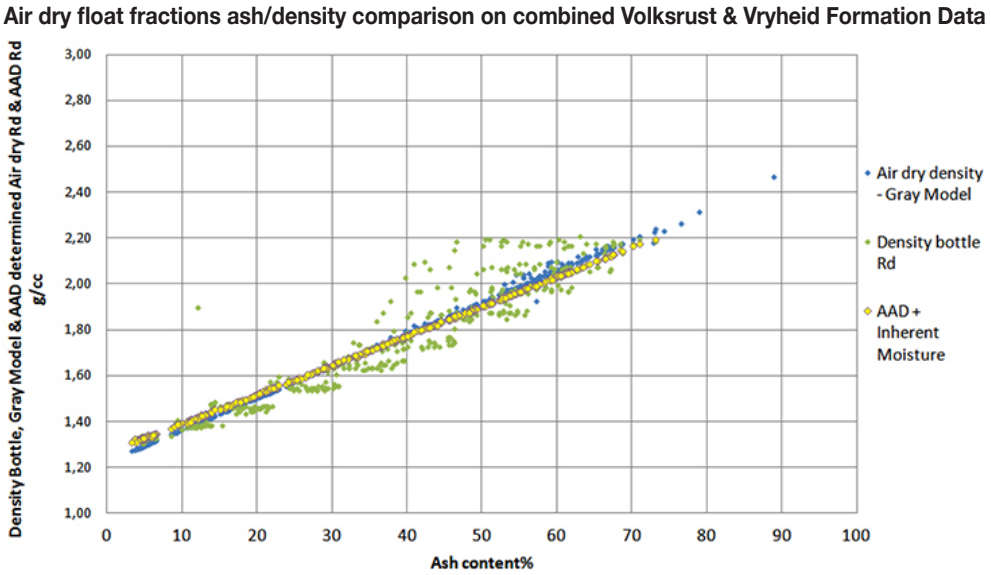

Figure 23—Plot of inherent moisture-adjusted AAD RD, Gray Method RD, and laboratory density bottle RD

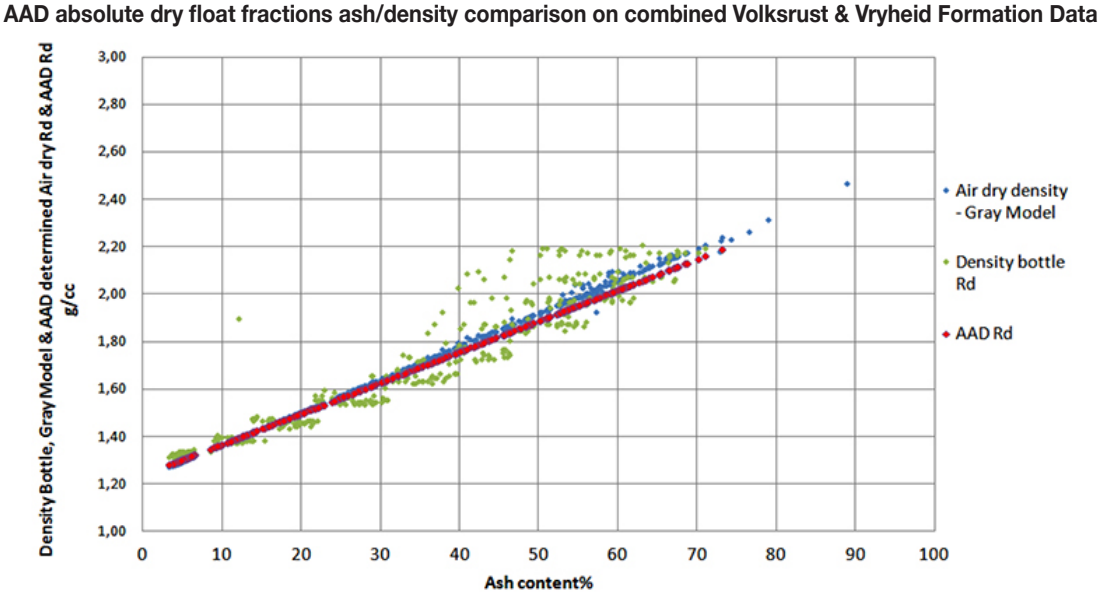

Figure 24—Plot of absolute dry density obtained from AAD against the Gray model and density bottle densities

Diff between Gray and AAD moist adjusted Rd	
Mean	-0,014
Standard Error	0,001
Median	-0,013
Mode	0,000
Standard Deviation	0,016
Sample Variance	0,000
Kurtosis	-0,946
Skewness	-0,141
Range	0,075
Minimum	-0,051
Maximum	0,024
Sum	-5,766
Count	416
Confidence Level(95,0%)	0,002

Diff between Gray method and AAD Rd	
Mean	0,005
Standard Error	0,001
Median	0,002
Mode	0,000
Standard Deviation	0,011
Sample Variance	0,000
Kurtosis	-0,697
Skewness	0,456
Range	0,049
Minimum	-0,014
Maximum	0,035
Sum	1,909
Count	416
Confidence Level(95,0	0,001

Figure 25—Descriptive statistics for the differences between the Gray method and AAD moist-adjusted, as well as between Gray method and AAD

samples are air-dry, containing their inherent moisture, they are less dense than the calculated equivalents, implying an air-filled volumetric difference contributing to the lower density.

The calculations did not include estimations of *in-situ* moisture and the final estimation for an *in-situ* relative density. The absence of any data relevant to moisture content of the cores on recovery led to the determinations being terminated at an air-dry equivalent.

Variability of densities

In order to illustrate the variability of densities over a period of time a further set of samples was taken randomly from a borehole in the deeper part of the Waterberg Coalfield where the entire succession was well below the regional groundwater table. The purpose was specifically to test various density determinations, as well as helium pycnometry, in an attempt to justify the decision to terminate evaluations at an air-dry equivalent value.

The results are portrayed in Table III. The samples were not impeccably preserved; they had been exposed to atmospheric conditions for about two weeks after recovery from drilling and thus were partially dry. The field mass would therefore have been partially dry. The samples were sent to an external laboratory for specified relative density determinations, but this could not be done and the samples were returned and stored for approximately 7 months before being sent to another laboratory for helium pycnometry.

The first set of data was derived on an as-received basis. The samples were then dried at 105°C for 24 hours and re-tested, giving more representative air-dry results. The final set of data was determined after the samples had been re-submerged in water for 48 hours, presenting a different set of results.

This illustrates the susceptibility of the samples to moisture absorption from the ambient atmosphere and raises doubt with respect to densities other than air-dried densities for Reserve calculations. The variability of results obtained is directly related to the effective porosity of the samples and the ambient environmental and atmospheric conditions.

An example, following the practice with known and derived values evaluated for each of the mentioned methods, follows. In this case a sample of exploration core, 257 cm long with a cross-section of 117.81 cm^2, weighing 46.440 g on recovery, was used.

The initial data available was the mass in air, mass in water, and the calculated bulk (geometric) volume. There was no data relevant to total free moisture content since the core had not been impeccably preserved on recovery. A field specific gravity determination by the Archimedes principle was then done prior to the core being dispatched to an accredited laboratory for further analysis. The SG value obtained was used to represent the *in-situ* density of the core and in the determination of resource tonnages.

Returning to basic concepts in order to assess the differences, the basic equation of Density = Mass/Volume and variations of this equation were utilized to determine different values dependent on given variables.

The recovered mass of the core sample was 46.440 g and its bulk volume was 30 227 cm^3, which gave a density of 1.53 g/cm^3. The Archimedes-determined SG was 1.68 g/cm^3. The most significant change here related to the mass of the sample; applying the density derived *via* Archimedes resulted in a calculated mass of 50.177 g, a 3.737 g difference. This is equivalent to approximately 7.5%, which can only be attributed to the moisture absorbed by the core during the hydrostatic determination. The difference in calculated volume and the original geometrical volume is also approximately 7.5%. Neither of these densities is suitable to use as an *in-situ* density value because the adventitious moisture content on retrieval is unknown.

The core was then dispatched to an accredited laboratory for further analysis. On reception the core was again weighed and the mass received recorded. It was then crushed to a –13 mm top size and screened to include the –13 mm and the +0.5 mm particles. The crushed material was air-dried under controlled conditions of temperature and humidity and once again weighed before float/sink analysis was done on the crushed material. The mass thus obtained was used in conjunction with the original volume, producing yet another density value, substantially less than the previously determined densities. In this case the air-dried mass of the –13 mm +0.5 mm material was 41.113 g (the calculated equivalent mass was 41.109 g) and the derived density was 1.36 g/cm^3. This density was still not representative of the solid matrix because no mention was made of the –0.5 mm fraction after the screening had been done. This fraction's mass should have been included for the mass to be representative of the solid matrix within the overall measured volume of the core. Fortunately this value was available for this sample. The –0.5 mm mass was 2.990 g, thus taking the total to 44.103 g representing the air-dry mass of the material on which float and sink and proximate analyses were done. The revised density using the above mass would then be 1.46 g/cm^3. If this density represents the particulate solid material of the matrix then its equivalent volume within the total core can be determined. Table IV illustrates the initial field and preliminary laboratory evaluation of mass, volume, and density.

The equivalent volume for an air-dry density is represented by 87% solids and 13% voids for this sample measured against the Archimedes-determined SG, assuming that the core was entirely saturated. Float/sink analysis at fixed density values ranging from 1.35 g/cm^3, 1.40 g/cm^3, and then at 0.1 g/cm^3 intervals to a 2.20 g/cm^3 float with a final sink value greater than 2.20 g/cm^3 were then done. Each float fraction was then pulverized to –212 µm for the density bottle RD determination according to procedure AS1038.21 Item 4 and subsequent proximate analyses of each float fraction. The results are shown in Table V.

Table III

Results of randomly selected samples, illustrating the effects of absorption of atmospheric moisture, drying, and re-wetting through submergence in waters

Original data prior to submission to Anglo Lab for pycnometry										
Sample name	*In-situ* mass (kg)	*In-situ* mass (g)	Length (cm^3)	Geometric volume (cm cubed)	Dry mass (kg)	Dry mass (g)	Field RD	RD gram/^{3} cubic cm^3	Geometric volume (cm cubed)	Volume from pycnometry
Sample 1 (5)	1.527	1 527.00	36	1 134.00	1.5250	1 525.00	1.36	1.34	1134.00	1 133.33
Sample 2 (9)	1.283	1 283.00	29.5	929.25	1.2780	1 278.00	1.38	1.38	929.25	954.55
Sample 3 (9	2.006	2 006.00	34	1 071.00	2.0040	2004.00	1.87	1.87	1 071.00	1 032.29
Sample 4 (1 ME)	1.671	1 671.00	29	913.50	1.6690	1669.00	1.83	1.83	913.50	1 039.87
Sample (5)	1.656	1 656.00	34	1 071.00	1.6540	1 654.00	1.5	1.54	1 071.00	993.90
Sample 1 (6)	0.919	919.00	17.5	551.26	0.9200	920.00	1.67	1.67	551.25	520.00

First set of data from Anglo Lab on samples received (untouched for period from June 2014 to January 2015)				
Folder No.	REPLNR	Order No	Sample name	Bulk relative density (g/cm^3)
187482	1	4362144_1	Sample 1 (5)	1.4
187482	1	4362145_1	Sample 2 (9)	1.43
187482	1	4362146_1	Sample 3 (9)	1.96
187482	1	4362147_1	Sample 4 (1ME)	1.61
187482	1	4362148_1	Sample 5	1.64
187482	1	4362149_1	Sample 6	1.75
187482	2	4362149_2	Sample 6R	1.73

First set of data from Anglo Lab on samples received (untouched for period from June 2014 to January 2015							
Folder No.	REPL NR	Order No	Sample name	Dry mass	Relative density (g/cm^3)	Relative density (g/cm^3)	Volume from pycnometry
187482	1	4362144_1	Sample 1 (5)	1 496	1.4	1.32	1 133.33
187482	1	4362145_1	Sample 2 (9)	1 260	1.43	1.32	954.55
187482	1	4362146_1	Sample 3 (9)	1 982	1.96	1.92	1032.29
187482	1	4362147_1	Sample 4 (1ME)	1 643	1.61	1.58	1 039.87
187482	1	4362148_1	Sample 5	1 630	1.64	1.64	993.90
187482	1	4362149_1	Sample 6	910	1.75	1.75	520.00
187482	2	4362149_2	Sample 6R	910	1.73	1.74	522.99

Samples submerged for 48+ hours, mass recorded after no dripping noted from samples							
Folder No.	REPL NR	Sample No	Sample name	Dry mass	Wet mass (g/cm^3)	Nett mass (g/cm^3)	
187482	1						
187482	1	4362144	Sample 1 (5)	1 510	1 560	50	
187482	1	4362145	Sample 2 (9)	1 270.1	1 310	39.9	
187482	1	4362146	Sample 3 (9)	1 996	2 040	44	
187482	1	4362147	Sample 4 (1ME)	1 654.1	1 716	61.9	
187482	1	4362148	Sample 5	1 643.3	1 684	40.7	
187482	2	4362149	Sample 6	915.8	934	18.2	

Comparatvie table from dry to saturation after 48 hours							
Sample name	Dry mass	Wet mass	Difference	Volume	Dry Rd	Wet Rd	Moisture absorbed
Sample 1 (5)	1 496	1 569	64	1 133.33	1.32	1.38	4.10%
Sample 2 (9)	1 260	1 310	50	954.55	1.32	1.37	3.82%
Sample 3 (9)	1 982	2 040	58	1 032.29	1.92	1.98	2.84%
Sample 4 (1ME)	1 643	1 716	73	1 039.87	1.58	1.65	4.25%
Sample 5	1 630	1 684	54	993.90	1.64	1.69	3.21%
Sample 6	910	934	24	520.00	1.75	1.80	2.57%

Table IV

Initial field evaluation of sample 14 from MY23

Sample No.	Lab mass	–13 mm mass	Total < 0.5 mm mass	Arch. SG	Thickness (cm)	Core volume	Field mass SG	Lab mass SG	–13 mm mass SG
Coal									
14	34620	30620	2387	1.58	202	23798	1.45	1.45	1.29
< 13 mm + < 0.5 mm mass		33007				23798	Air dry SG		1.39
Shale									
14S	11654	10493	603	1.98	55	6480	1.81	1.80	1.62
< 13 mm + < 0.5 mm mass		11096				6480	Air dry SG		1.71
Combined coal and shale –13 mm + 0.5 mm screened air dry material									
14	46274	41113	2990	1.68	257	30277	1.53	1.53	1.36
Combined coal and shale including –0.5 mm material									
14 Actual air dry mass incl < 0.5 mm	46274 44103	41113	2990	1.68	257	30277	1.53	1.53	1.36 1.46

Table V

Float/sink and proximate analyses results for the two separate components, coal and shale for Sample 14

Borehole BH ID	Sample	Type	Fraction type	RD 1	RD 2	Yield	Moisture	Ash	Volatiles	Sulphur	CV	Pycn. RD	AAD RD	–13 mm mass contribution	< –0.5 mm mass
Float/sink and other analyses performed on coal and shale portions of Sample 14 MY23															
Sample 14 MY23 Coal															
MY311LQ23	14	Coal	F	0	1.35	9.52	3.45	4.11	36.48	0.69	30.99	1.33	1.29	2916	
MY311LQ23	14	Coal	F	1.35	1.4	5.51	2.76	11.01	35.28	0.79	28.54	1.39	1.38	1687	
MY311LQ23	14	Coal	F	1.4	1.5	19.17	2.33	19.66	32.46	0.82	25.66	1.46	1.50	5868	
MY311LQ23	14	Coal	F	1.5	1.6	19.84	1.97	27.21	29.80	0.79	22.79	1.54	1.59	6076	
MY311LQ23	14	Coal	F	1.6	1.7	14.63	1.79	35.85	26.47	0.9	19.76	1.64	1.71	4478	
MY311LQ23	14	Coal	F	1.7	1.8	11.09	1.87	41.98	24.13	0.78	17.17	1.72	1.79	3395	
MY311LQ23	14	Coal	F	1.8	1.9	7.28	1.67	51.22	22.37	0.93	13.32	1.88	1.91	2229	
MY311LQ23	14	Coal	F	1.9	2	4.34	1.48	53.77	24.61	1.1	12.08	1.97	1.94	1330	
MY311LQ23	14	Coal	F	2	2.1	1.84	1.54	53.38	30.10	1.83	11.61	2.08	1.93	563	
MY311LQ23	14	Coal	F	2.1	2.2	1.48	1.90	52.57	31.66	4.18	11.25	2.17	1.92	454	
MY311LQ23	14	Coal	R		0.5		2.15	23.39	32.25	1.13	23.53		1.54		2387
MY311LQ23	14	Coal	S	2.2	9.99	5.30	2.05	56.53	31.68	13.16	9.22	2.63	1.97	1622	
														30620	
Sample 14 MY23 shale															
MY311LQ23	14	Shale	F	0	1.5	4.94	2.77	16.59	31.69	0.8	26.83	1.42	1.46	519	
MY311LQ23	14	Shale	F	1.5	1.6	3.40	2.29	30.92	26.59	0.68	21.71	1.57	1.64	357	
MY311LQ23	14	Shale	F	1.6	1.7	5.03	2.34	39.71	23.04	0.55	18.36	1.70	1.76	528	
MY311LQ23	14	Shale	F	1.7	1.8	6.32	2.10	47.65	20.91	0.4	15.45	1.79	1.86	663	
MY311LQ23	14	Shale	F	1.8	1.9	8.84	2.14	54.55	17.76	0.31	12.63	1.90	1.95	928	
MY311LQ23	14	Shale	F	1.9	2	8.68	2.21	60.17	16.25	0.29	10.19	2.00	2.02	911	
MY311LQ23	14	Shale	F	2	2.1	10.37	2.06	65.65	14.29	0.25	8.05	2.10	2.09	1089	
MY311LQ23	14	Shale	F	2.1	2.2	16.24	1.87	71.94	12.49	0.18	5.85	2.21	2.18	1704	
MY311LQ23	14	Shale	R		0.5		1.74	50.77	19.79	0.69	14.53		1.90	0	603
MY311LQ23	14	Shale	S	2.2	9.99	36.16	1.39	79.82	10.29	1.06	2.72	2.4	2.28	3794	
														10493	
Borehole BH ID	**Sample**	**Type**	**Fraction type**	**RD 1**	**RD 2**	**Yield**	**Moisture**	**Ash**	**Volatiles**	**Sulphur**	**CV**	**Pycn. RD**	**AAD absolute dry RD**	**AAD air dry RD**	**Mass contribution**
Coal and shale cumulative of Sample 14															
MY311LQ23	14	C&S Comp.	F	0	1.35	7.12	2.58	3.08	27.29	0.52	23.19	1.00	1.28	1.31	2929
MY311LQ23	14	C&S Comp.	F	1.35	1.4	4.12	2.06	8.23	26.40	0.59	21.35	1.04	1.35	1.38	1695
MY311LQ23	14	C&S Comp.	F	1.4	1.5	15.58	2.44	18.89	32.27	0.81	25.95	1.45	1.49	1.52	6407
MY311LQ23	14	C&S Comp.	F	1.5	1.6	15.70	2.05	28.15	28.99	0.76	22.52	1.55	1.61	1.64	6456
MY311LQ23	14	C&S Comp.	F	1.6	1.7	12.21	1.93	36.82	25.60	0.81	19.41	1.65	1.72	1.75	5019
MY311LQ23	14	C&S Comp.	F	1.7	1.8	9.89	1.93	43.41	23.32	0.68	16.74	1.74	1.80	1.84	4065
MY311LQ23	14	C&S Comp.	F	1.8	1.9	7.67	1.79	52.06	21.21	0.77	13.15	1.88	1.92	1.95	3155
MY311LQ23	14	C&S Comp.	F	1.9	2	5.44	1.67	55.38	22.51	0.90	11.60	1.98	1.96	1.99	2235
MY311LQ23	14	C&S Comp.	F	2	2.1	3.99	1.67	56.47	26.12	1.43	10.71	2.09	1.97	2.01	1639
MY311LQ23	14	C&S Comp.	F	2.1	2.2	5.20	1.89	57.45	26.84	3.17	9.89	2.18	1.99	2.03	2138
MY311LQ23	14	C&S Comp.	S	2.2	9.99	13.07	1.88	62.39	26.29	10.11	7.58	2.57	2.05	2.09	5374
															41113
MY311LQ23	14	C&S Comp.	R		0.5	0.00	2.05	30.29	29.11	1.02	21.26		1.63	1.67	2990
											Total air dry mass Sample 14				44103
Borehole BH ID	**Sample**	**Type**	**Fraction type**	**RD 1**	**RD 2**	**Yield**	**Moisture**	**Ash**	**Volatiles**	**Sulphur**	**CV**	**Pycn. RD**	**AAD absolute dry RD**	**AAD air dry RD**	
Coal and shale cumulative of Sample 14															
MY311LQ23	14	C&S Comp.	F	0	1.35	7.12	2.58	3.08	27.29	0.52	23.19	1.00	1.28	1.31	
MY311LQ23	14	C&S Comp.	F	1.35	1.4	11.25	2.39	4.97	26.96	0.54	21.51	1.01	1.30	1.34	
MY311LQ23	14	C&S Comp.	F	1.4	1.5	26.83	2.42	13.05	30.04	0.70	24.51	1.27	1.41	1.44	
MY311LQ23	14	C&S Comp.	F	1.5	1.6	42.53	2.28	18.62	29.65	0.72	23.78	1.37	1.48	1.52	
MY311LQ23	14	C&S Comp.	F	1.6	1.7	54.74	2.20	22.68	28.75	0.74	22.80	1.44	1.53	1.57	
MY311LQ23	14	C&S Comp.	F	1.7	1.8	64.63	2.16	25.85	27.92	0.73	21.87	1.48	1.58	1.61	
MY311LQ23	14	C&S Comp.	F	1.8	1.9	72.30	2.12	28.63	27.21	0.74	20.95	1.52	1.61	1.65	
MY311LQ23	14	C&S Comp.	F	1.9	2	77.74	2.09	30.51	26.88	0.75	20.29	1.56	1.64	1.67	
MY311LQ23	14	C&S Comp.	F	2	2.1	81.73	2.07	31.77	26.84	0.78	19.83	1.58	1.65	1.69	
MY311LQ23	14	C&S Comp.	F	2.1	2.2	86.93	2.06	33.31	26.84	0.93	19.23	1.62	1.67	1.71	
MY311LQ23	14	C&S Comp.	S	2.2	9.99	100.00	2.04	37.11	26.77	2.13	17.71	1.74	1.72	1.76	
MY311LQ23	14	C&S Comp.	R		0.5	0.00	2.05	30.29	29.11	1.02	21.26		1.63	1.67	

The proximate analyses shown in Table V were composited into a representative wash table of coal and shale combined. This was then cumulated to represent the effect of each additional yield from the basic 1.35 g/cm³ through to the 2.20 g/cm³ sink value. The AAD algorithm was applied to each float fraction to determine the absolute dry density and then corrected to an air-dry density by taking the inherent moist content into account. The density bottle values were also included in the wash tables for comparative evaluation. A summary of the masses, volumes, densities, and perceived percentage solids and voids for the varying densities determined is displayed in Table VI.

From the foregoing, very little difference is evident between the methods utilizing the analytical data. Densities of 1.45 g/cm³ to 1.46 g/cm³ were obtained using an average correction factor of 0.83 for the solid matrix, which implies that the effective porosity of this sample is approximately 17%.

Figure 26 shows the volumetric differences by the different methods applied. The first three, namely field mass, Archimedes, and laboratory air-dried densities, are all based on the original bulk volume of the core sample and show very little to no variation, whereas the values derived from AAD on raw analysis, AAD on cumulative density, pycnometry (density bottle), and finally the Gray method are on average 17% lower than the geometrical volume.

If the original laboratory mass of 46.274 g and the determined air-dry density of 1.46 g/cm³ are taken into account, the volume to support this density would be 31.695 cm³, which is 1.418 cm³ greater than the original geometric volume (30.277 cm³) and by implication suggests more core than the original. The original core length was 257 cm and the cross-section117.81 cm², therefore the extra volume would represent approximately 12 cm more core, increasing the original length to 269 cm. Since the core cannot stretch or grow, the only logical explanation is that the additional volume represents the voids/porosity of the solid matrix and that the solid matrix within the confines of the geometric volume is therefore equivalent to 100% less the depicted void volume, in this case 17%, thus the solid matrix is only 83% of the total volume (Figure 27).

Table VI

Perceived percentage solids and voids based on various density determination methods. Combined coal and shale

Determination method	Mass g	Volume cm³	Density g/cm³	Perceived % solids	Possible % voids	Mass loss from original field mass to other measured masses
Field and preliminary laboratory evaluation of perceived solids and voids						
Archimeded	46300	27560	1.68	0.91	0.09	
Field mass/volume	46300	30277	1.529			
Lab mass./volume	46274		1.528			26
Determination method	**Mass g**	**Volume cm³**	**RD**	**% Solids**	**Possible % voids matrix**	
Laboratory sample preparation evaluation of perceived solids and voids						
–13 mm – 0.5 mm mass/volume	41113	30277	1.358	0.81	0.19	5187
Air dry mass including < 0.5 mm/volume	44103		1.46	0.87	0.13	2197
Determination method	**Mass g**	**Volume cm³**	**RD**	**% Solids**	**Possible % voids matrix**	**Air-dry RD derived from RD x % solid matrix**
Validation of solid matric RD based on pycnometer, AAD results and grey method						
Pycnometer RD1111.74	44103	25347	1.74	0.84	0.16	1.457
Absolute dry AAd RD			1.72	0.85	0.15	1.457
Air dry AAD RD			1.76	0.83	0.17	1.457
Gray method RD			1.75	0.83	0.17	1.460

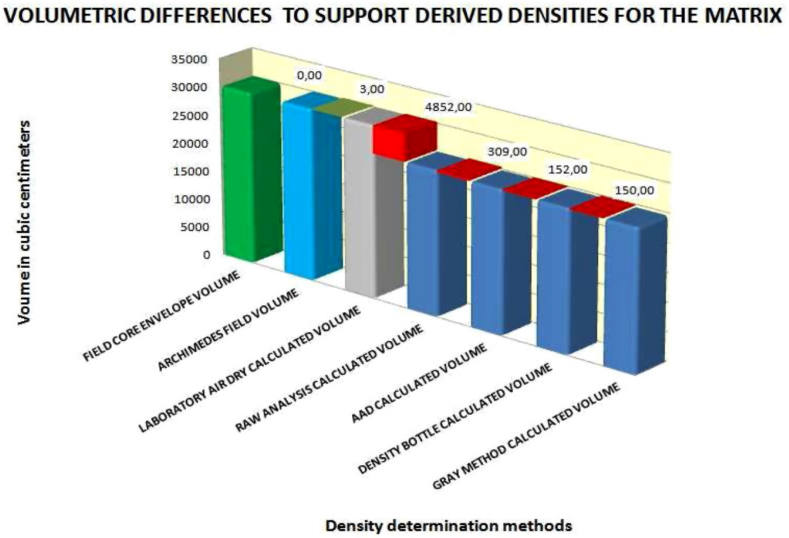

Figure 26—Volumetric differences based on the densities obtained from the different methods

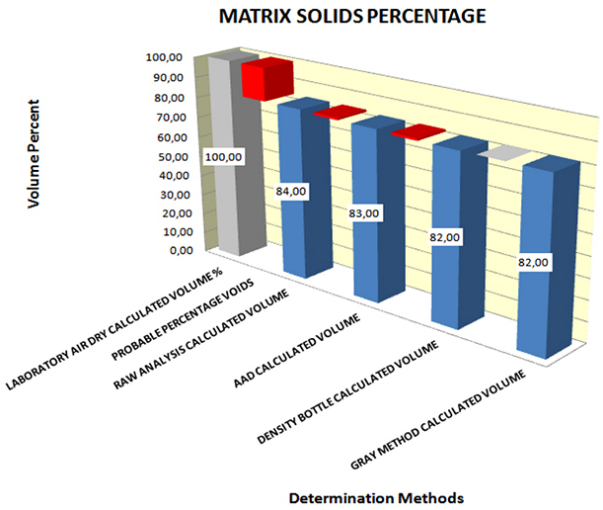

Figure 27—Solid matrix representation of values derived from the displayed determination methods

If the densities determined from the various methods were, however, used to calculate *in-situ* tonnages without corrections related to possible geological losses as determined by the volumetric evaluations applied, the net result would be substantially overestimated values (Table VII).

The overestimation is determined by the final percentage by which the calculated value exceeds the mass of the measured air-dry material, *i.e.* the Archimedes-calculated mass of 50.865 g measured against 44.103 g results in an overestimation of 15.07%. It is also apparent that the field mass volume contains a fair percentage of moisture.

It is of paramount importance that the methods under consideration are fully understood and that the AAD evaluation on the proximate analytical values needs to be adjusted to account for the inherent moisture of the coal, since the AAD gives an absolute dry density for the coal. The inherent moisture content determined for Waterberg coals is between 1.5% and 2.5%, which taken into account will slightly increase the determined density values, making them comparable with both the density bottle values and the Gray determinations. The sample then needs to be restored to its original volume and the void to solid ratio determined in order to get a representative air-dry relative density.

Production reconciliation

From a mining production and reconciliation perspective two examples, one from the Volksrust Formation and the second from the Vryheid formation, were dealt with. These two scenarios are depicted in the locality map shown in Figure 28, showing the positions of the mining strips, blocks, and surrounding exploration boreholes from which the basic information with regard to mining block densities and expected run of mine tonnages were obtained.

The same approach using the basic density equation was used in this evaluation. The masses relate to tonnages, the volumes in cubic metres to the material mined, and the initial densities allocated to the areas as well as the derived densities represented by the surveyed volumes and reported tonnages. Table VIII represents data from mining horizon bench 3 which is in the Volksrust Formation. Material from this bench is beneficiated for both a semi-soft coking coal and a power station product.

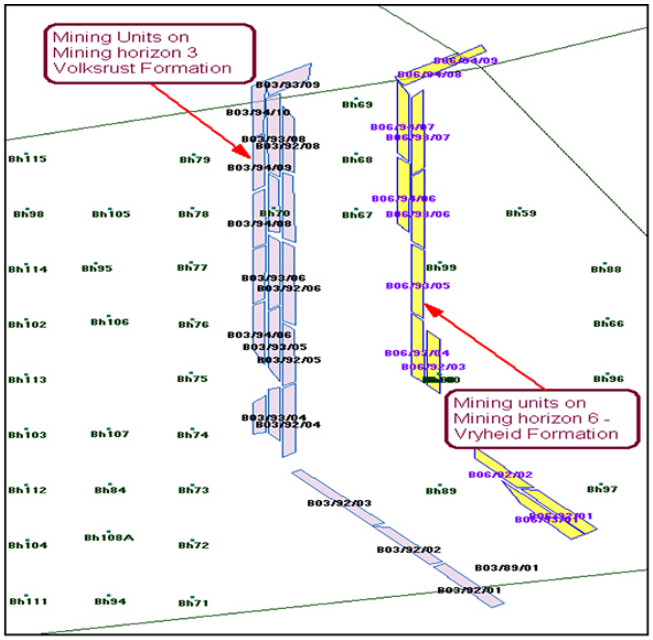

Figure 28—Locality map illustrating the respective mining strips, mining units, and mining horizons evaluated with locations of boreholes spread over the entire area

Table VII

Overestimation of core mass as a result of solid to void ratios

Determination method	Density g/cm³	Volume cm³	Actual solids volume cm³	Voids volume cm³	% voids	
Air dry mass including < 0.5 mm/volume	**1.46**		**25251**	**5026**	**16.60%**	**Based on average calc values from pycnometer, AAD and Gray methods. RD**
Pycnometer RD	1.74	30277	25347	4930	16.28%	
Air dry AAD RD	1.76		25130	5147	17.00%	
Gray method RD	1.75		25130	5147	17.00%	
Average for calculated values	1.75		25130	5147	17.00%	
Determination method	**Density g/cm³**	**Volume cc**	**Mass in grams = RD x volume**	**% Over estimation**		
Archimedes	1.68	30277	50865.36	15.07%		
Air dry mass including < 0.5 mm/volume	1.46		44204.42			

Table VIII

Mining blocks on bench 3 (Volksrust Formation) with model-assigned areas, volumes, and predicted tonnages based on raw density values allocated to the various blocks as well as the information pertinent to these blocks when they were staked for drilling and blasting prior to mining

Block No.	Seam	Model area	Model thick	Model volume	Raw RD	Model report *In-situ* tons	Survey staked area	Seam thickness	Staked volume	Survey RD	Survey staked tons
B03/92/01w	B3	12 536.00	17.07	213 989.52	1.84	393 663.00	12 044.00	16.46	198 286.41	1.84	364 847.00
B03/92/02	B3	10 866.00	16.53	179 614.98	1.83	328 962.00	11 285.00	17.19	193 967.76	1.83	354 961.00
B03/92/03	B3	15 701.00	16.14	253 414.14	1.83	462 557.00	16 390.00	16.68	273 312.57	1.83	500 162.00
B03/92/04	B3	11 903.00	16.41	195 328.23	1.88	366 843.00	14 980.00	16.06	240 594.15	1.88	452 317.00
B03/92/05	B3	12 923.00	16.22	209 611.06	1.88	393 827.00	12 269.00	16.49	202 369.68	1.88	380 455.00
B03/92/06	B3	15 102.00	16.79	253 562.58	1.87	474 963.00	16 835.00	16.73	281 675.94	1.87	526 734.00
B03/93/04	B3	9 958.00	16.35	162 813.30	1.88	305 877.00	10 352.00	15.19	157 197.86	1.87	293 960.00
B03/93/05	B3	13 529.00	16.64	225 122.56	1.88	423 671.00	13 922.00	16.28	226 670.21	1.88	426 140.00
B03/93/06	B3	13 448.00	16.60	223 236.80	1.86	415 800.00	14 861.00	16.67	247 722.46	1.87	463 241.00
B03/93/07	B3	13 447.00	16.32	219 455.04	1.86	407 429.00	12 136.00	17.15	208 161.62	1.85	385 099.00
B03/93/08	B3	17 009.00	12.56	213 633.04	1.82	387 763.00	16 273.00	15.28	248 676.67	1.80	447 618.00
B03/93/09	B3	10 618.00	15.32	162 667.76	1.81	293 717.00	10 797.00	14.20	153 329.44	1.80	275 993.00
B03/94/04	B3	7 284.00	16.43	119 676.12	1.88	225 131.00	7 219.00	14.42	104 123..94	1.88	195 753.00
B03/94/06	B3	11 218.00	16.73	187 677.14	1.88	353 566.00	11 645.00	15.37	179 025.00	1.88	336 567.00
B03/94/07	B3	11 218.00	16.59	186 106.62	1.86	346 646.00	11 429.00	15.85	181 136.56	1.86	336 914.00
B03/94/08	B3	11 218.00	16.40	183 975.20	1.86	341 774.00	11 429.00	16.35	186 856.45	1.86	347 553.00
B03/94/09	B3	11 218.00	12.42	139 327.56	1.85	257 126.00	11 297.00	15.14	170 982.70	1.85	316 398.00
B03/94/010	B3	11 218.00	14.67	164 568.06	1.81	297 585.00	10 673.00	15.45	164 919.89	1.81	298 505.00
		220 414.00	15.85	3 493 779.71	1.85	6 476 900.00	225 836.00	16.02	3 619 009.31	1.85	6 703 137.00

Table IX

The same blocks as in Table VIII with as-mined values and the final survey reported results

Block No.	SEAM	As mined values at same basis					Survey measured data			
		As-mined area	As mined bench thickness	As mined volume	Equivalent as-mined *in-situ* tons	Model raw RD	Surveyed area	Survey thickness	Survey volume	Surveyed tons
B03/92/01	B3	11 348.64	16.46	186 838.38	343 782.62	1.84	10 945.42	17.07	186 838.38	274 173.58
B03/92/02	B3	8 155.14	17.29	140 986.92	258 006.07	1.83	8 529.15	16.53	140 986.92	223 129.73
B03/92/03	B3	19 037.82	16.38	311 755.13	570 511.88	1.83	19 315.68	16.14	311 755.13	478 641.71
B03/92/04	B3	14 423. 51	16.66	240 310.45	451 783.64	1.88	14 644.15	16.41	240 310.45	379 294.56
B03/92/05	B3	9 794.55	16.19	158 616.71	298 199.41	1.88	9 779.08	16.22	158 616.71	246 191.78
B03/92/06	B3	13 455.32	16.13	217 055.40	405 893.59	1.87	12 927.66	16.79	217 055.40	322 471.29
B03/93/04	B3	6 693.13	15.09	100 967.70	189 819.27	1.88	6 175.39	16.35	100 967.70	144 819.98
B03/93/05	B3	17 134.02	15.98	273 826.30	514 793.45	1.88	16 455.91	16.64	273 826.30	408 835.50
B03/93/06	B3	13 487.42	16.27	219 430.95	408 141.56	1.86	13 218.73	16.60	219 430.95	330 768.83
B03/93/07	B3	1 108.46	16.65	18 458.52	34 332.84	1.86	1 131.04	16.32	18 458.52	28 968.07
B03/93/08	B3	1 064.31	14.98	15 944.98	29 019.86	1.82	1 269.50	12.56	15 944.98	28 623.02
B03/93/09	B3	1 463.42	14.30	20 928.50	37 880.58	1.81	1 366.09	15.32	20 928.50	29 240.23
B03/94/04	B3	1 074.37	13.82	14 851.66	27 921.12	1.88	903.94	16.43	14 851.66	19 425.37
B03/94/06	B3	8 223.62	15.27	125 603.81	236 135.17	1.88	7507.70	16.73	125 603.81	178 261.57
B03/94/07	B3	7 958.93	15.95	126 935.76	236 100.51	1.86	7 651.34	16.59	126 935.76	187 686.50
B03/94/08	B3	5 000.76	16.45	82 259.17	153 002.05	1.86	5 015.80	16.40	82 259.17	126 897.93
B03/94/09	B3	4 941.20	15.34	75 774.38	140 182.61	1.85	6 101.00	12.42	75 774.38	143 125.12
B03/94/10	B3	6 493.27	15.95	103 581.04	187 481 69	1.81	7 060.74	14.67	103 581.04	168 577.13
		150 857.88	16.14	2 434 125.76	4 522 987.95	1.86	149 998.33	16.23	2 434 125.76	3 719 131.90

In Table X, overestimation percentages are attributable to completely different areas, bench thicknesses, densities, and volumes planned and staked as opposed to the raw material actually mined. The most important fact, however, lies between the as-mined data and the surveyed data. In Table XI the areas, volumes, bench thicknesses, and relative densities for the model, staked, and as-mined scenarios have been equalized in order to compare the four scenarios on the same basis. The only difference is in the tonnage for the surveyed material and its resultant density. This shows a difference of 17.41%, which could be attributable to the voids in the matrix, implying that the solid matrix contributing to the final density is only 82.59%.

The second evaluation represents data from bench 6 in the Vryheid Formation. This material is mined, crushed and screened, and dispatched directly as a power station product.

Summary

Basic field and preliminary laboratory density determinations are valueless unless the core is impeccably preserved and its moisture content determined. If this has not been done the air-dry density should be validated through the evaluation of alternative methods, including pycnometry, application of AAD, and the Gray method. When using the Gray method it is advisable to use the inherent moisture content determined through proximate

analysis, the reason behind this being that Robeck and Hoe (2015) used averaged total moisture content in their evaluations. This may be from actual analyses on impeccably preserved core where moisture determinations were done.

Density determinations on the selected sample chosen for the theoretical evaluation after the –13 mm +0.5 mm and the –.5 mm air-dry mass divided by original geometric volume include:

- Australian Standard method, AS1038.21 Item 4
- The Gray method (Robeck and Huo, 2015)
- Ash-adjusted density (Roux, 2012).

These three methods all require the pulverization of the air-dried sample to –212 µm, leading to a significant loss in volume. Results obtained from the Gray method (using proximate analyses results for inherent moisture content) displayed a 0.01 g/cm³ density difference, slightly higher than the pycnometer and AAD results. Applying the same principle with regard to changing volumes, factors for the solid matrix were on average 0.83 (83% of the total sample) and voids 0.17 or 17%. These factors applied to the determined densities gave an air-dry density of 1.46 g/cm³ for the sample evaluated. This volumetric difference is a geological loss as a result of the matrix porosity of the material.

From a physical mining perspective, where more than a single sample was composited to represent a mining horizon bench, the reconciliation of tonnages hauled and the volumes of material extracted for the two scenarios evaluated also gave results within the same range as those obtained from laboratory and theoretical evaluations.

The first scenario, based on bench 3 production, shows a difference of 17.41% attributable to the voids in the matrix, which implies that the solid matrix contributing to the final density is only 82.59%. The second scenario, bench 6, resulted in a void percentage of 17.89% and a solid matrix percentage of 82.11%.

It is thus considered that a change of volume equation, given reliable input, will enable the determination of a more credible air-dry density of coal which can then be adjusted to accommodate adventitious moisture representative of *in-situ* conditions if accurate moisture determinations are done on impeccably preserved samples. Alternatively, the laboratory air-dry density should be used for Resource and Reserve calculations. This air-dry value should include both the mass of the screened –13 +0.5 mm as well as the mass of the –0.5 mm material.

Table X

Summaries of the weighted averages for the four data-sets relevant to the foregoing mining units, depicting tonnage differences and overestimation percentages

	Summary of initial reported values				
	Area	Thick	RD	Volume	Tonnage
Model	220 414.00	15.84	1.85	3 491 357.76	6 459 011.86
Staked	225 836.00	16.02	1.85	3 617 892.72	6 693 101.53
As mined	150 858.00	16.14	1.86	2 434 848.12	4 522 987.95
Surveyed	149 998.00	16.23	1.53	2 434 125.76	3 719 131.91
Model to surveyed tonnage difference Model % overestimation					2 739 879.95 60.84%
Staked to surveyed tonnage difference Staked % overestimiation					2 973 969.63 44.43%
A-mined tonnage difference As-mined % overestimation					803 856.04 17.77%

Table XI

Comparison of planning, survey, and mining data-sets on the same basis

	Calculated values for surveyed area and volume				
	Area	Thick	RD	Volume	Tonnage
Model	149 998.33	16.23	1.85	2 434 125.76	4 503 132.66
Staked	149 998.33	16.23	1.85	2 434 125.76	4 503 132.66
As mined	149 998.33	16.23	1.85	2 434 125.76	4 503 132.66
Surveyed	149 998.33	16.23	1.53	2 434 125.76	3 719 131.90
As-mined tonnage difference As-mined % overestimation					784 000.76 17.41%

Conclusions and recommendations

Field samples

1. If samples are not sealed and impeccably preserved in order

Table XII

Mining blocks on bench 6 (Vryheid Formation) with model-assigned areas, volumes, and predicted tonnages based on raw density values allocated to the various blocks as well as the information pertinent to these blocks when they were staked for drilling and blasting prior to mining

Block No.	Geological model allocated values						Survey staked data				
	Model area	Model thick	Model PS coal yield	Model volume	Model report *in-situ* tons	Archimedes raw RD	Survey staked area	Survey staked tons	Survey RD	Calculated thickness	Staked volume
B06/92/01	13 651	4.22	100	57 607.22	95 964	1.67	12 400	78 881	1.67	3.81	47 234
B06/92/02	10 222	4.01	100	40 990.22	67 541	1.65	10 491	64 340	1.65	3.72	38 994
B06/92/03	12 746	4.03	100	51 366.38	84 734	1.65	11 282	54 038	1.65	2.90	32 750
B06/93/01	14 030	4.17	100	58 505.1	97 144	1.66	13 849	84 206	1.66	3.66	50 727
B06/93/04	14 285	4.02	100	57 425.7	94 216	1.64	12 892	69 008	1.63	3.28	42 336
B06/93/05	14 285	4.01	100	57 282.85	93 793	1.64	14 336	90 889	1.64	3.87	55 420
B06/93/06	14 285	4.04	100	57 711.4	93 645	1.62	15 095	89 224	1.62	3.65	55 077
B06/93/07	14 281	4.07	100	58 123.67	94 639	1.63	16 128	97 345	1.63	3.70	59 721
B06/93/08	5 216	3.94	100	20 551.04	33 624	1.64	2 819	17 546	1.64	3.80	10 699
B06/94/06	14 285	4.04	100	57 771.4	93 832	1.63	14 432	107 375	1.63	4.56	65 874
B06/94/07	14 281	3.96	100	56 552.76	92 410	1.63	14 684	98 621	1.63	4.12	60 504
B06/94/08	8 987	3.97	100	35 678.39	58 352	1.63	11 112	69 594	1.63	3.84	42 696
B06/94/09	7 500	4	100	30 000	48 860	1.63	5 715	26 638	1.63	2.86	16 342

Table XIII

Bench 6 blocks with as-mined reported values as well as the final survey results

Block No.	As mined reported datsModel					Model	Survey measured data		Despatch reported tonnages		
	Seam	As-mined area	As-mined bench thick	As-mined volume	Equivalent as-mined *in-situ* tons	Archimedes raw RD	Surveyed volume	Surveyed tons	GG3	GG2	Toal despatch tons
B06/92/01	Bench 6	12 049	3.51	42 284	70 614	1.67	42 284	70 614	109 727	489	110 217
B06/92/02		10 926	3.92	42 797	70 614	1.65	42 797	70 614	82 095	1 309	83 404
B06/92/03		3 256	2.70	8 800	14 520	1.65	8 800	14 520	91 196	1 476	92 672
B06/93/01		31 934	3.56	113 775	188 867	1.66	113 775	188 867	56 746	813	57 559
B06/93/04		15 018	3.18	47 815	78 417	1.64	47 815	77 938	57 176	1 151	58 328
B06/93/05		10 751	3.47	37 261	61 108	1.64	37 261	61 108	70 092	1 633	71 725
B06/93/06		36 800	2.85	104 832	169 828	1.62	104 832	169 828	75 194	661	75 855
B06/93/07		15 273	3.10	47 390	77 246	1.63	47 390	77 246	77 423	1 194	78 616
B06/93/08		1 241	3.20	3 964	6 501	1.64	3 964	6 501	100 049	1 194	101 242
B06/94/06		69 319	2.26	1 569 70	255 861	1.63	156 970	255 861	51 522	3 447	54 968
B06/94/07		5 791	2.82	16 332	26 621	1.63	16 332	26 621	51 522	1 799	53 321

Table XIV

Comparison of planning, survey, and mining data-sets

	Summary of reported values				
	Area	Thick	RD	Volume	Tonnage
Model	15 805 4	4.05	1.64	63 950 6	10 487 24
Staked	15 523 5	3.73	1.64	57 837 3	94 770 5
As mined	21 235 7	2.93	1.64	62 222 0	102 019 6
Surveyed	21 236 2	2.93	1.64	62 222 0	10 197 18
Despatch					
Probable voides			17.89%		
Solid matrix			82 11%		

to retain the free moisture neither Archimedes nor field mass/volume density determinations are suitable for Resource and Reserve determinations based on so-called *in-situ* conditions. Moisture loss or gain as a result of exposure to atmospheric conditions or absorption during hydrostatic testing for SG determination will lead to erroneous results not representative of the sample in its *in-situ* state. If the sample is sealed on recovery, the densities determined by these methods should be almost identical. Corrections to convert to an air-dry density can then be done when the free moisture content has been determined.

2. The mass of the initial laboratory-crushed air-dried state, including both the –13 +0.5 mm fraction and the –0.5 mm fraction, can be used over the original geometric volume to give an indication of the probable air-dry density of the sample, provided that the crushed material has been properly air-dried under controlled temperature and humidity, ensuring a credible value for the air-dried material.

Laboratory-prepared samples

1 The density of float/sink fractions, air-dried, and pulverized to –212 µm determined by applying the Australian Standard method AS1038.21 Item 4 can be composited to give a representative air-dry density of the sample from the particles in the solid matrix.

2 The AAD methodology can be applied to the proximate ash content data to determine an absolute dry density of the sample, which should then be adjusted to take the inherent moisture content into consideration to provide an equivalent air-dry density.

3 The Gray method, proposed by Robeck and Huo, can also be used to determine an equivalent air-dry density for the sample. Robeck and Huo, however, oppose the use of the ash component since it is a product of combustion and excludes possible mineral volatiles. These mineral volatiles include H_2O of hydration, CO_2, SO_2, salts (*e.g.*, Cl), carbonates, and sulphides (Ward, 1984). As a result, the remaining ash (solid residue) underrepresents the original mineral matter. For this reason, sample ash almost never reaches 100%, even in samples lacking carbonaceous material.

4 The greatest loss of mineral volatiles relates to water loss as a result of vaporization coupled with minor amounts of the aforementioned volatiles.

5 The density values obtained from these laboratory procedures all need to be related to the original geometric or envelope (bulk) volume, because the total volume of the sample has been dramatically reduced as a result of pulverization. The mass of sample if properly air-dried, however, should remain the same.

6 Ash-adjusted density with a correction applied to account for inherent moisture and then reconstructed to be accommodated within the original volume gives a reliable air-dry density and requires the least analytical data to acquire the desired result. These values have all been found to be within the 95–99% confidence range.

It is recommended that *Resource and Reserve tonnages be reported on an air-dry basis. Water and voids do not generate revenue*. The air-dry density gives credible results with respect to the actual resource material. If the moisture content in the matrix of the resource material is higher, the budgeted tonnages calculated on the air-dry basis would be more conservative, negating the possibility of overestimation of the actual Resource.

Resource and Reserve values can be adjusted to reflect an averaged free moisture content, enhancing planning and scheduling with regard to probable tonnages *in situ* in the specific environment being evaluated. This may be accomplished through the evaluation of downhole geophysical logs, specifically the density log. After correlation to identify the zones and samples, comparisons of log densities with AAD densities for the same samples can be made. The differences noted would be indicative of the probable moisture or void content in the samples.

One of the biggest influences with regard to fluctuating tonnages and varying *in-situ* densities can be attributed to

the movement of groundwater in relation to the material being evaluated. Depleting groundwater levels will result in lower tonnages as the groundwater drains from the porous material, while increased groundwater levels could saturate the material through absorption thereby greatly increasing the *in-situ* tons of raw material.

The use of air-dry densities in order to derive Resource and Reserve tonnages allows a very conservative approach. It is also the basis on which product data extraction is calculatedone, therefore any excesses measured in a mining operation can be adjusted to accommodate possible increases in free moisture content of the material being mined. This can be accommodated in the mining loss/gain factors applied to mineable tonnages.

References

American Society for Testing and Materials. 1994, Compilation of ASTM Standard Definitions. 8th edn. West Conshohocken, PA.

Anderson, G. 1975. Coring and Core Analysis Handbook. Petroleum Publishing Company, Tulsa, AZ.

British Standard BS 2955. 1991. Glossary of Terms Relating to Particle Technology. British Standards Institution, London.

Close, J. 1993. Natural fractures in coal. *Hydrocarbons from Coal*, Law, B.E. and Rice, D.D. (eds). AAPG Studies in Geology, vol. 38. pp. 119–132.

Crain, R. 2003. The new role of petrophysics in geophysical interpretation. *CSEG Recorder*, vol. 28, no. 7. https://csegrecorder.com/articles/view/the-new-role-of-petrophysics-in-geophysical-interpretation

Crain, R. 2010. Petrophysical Handbook. Rocky Mountain House, AB, Canada.

Dreyer, J.C. 1991. Waterberg Coalfield: Geology, resources, mining and products. (Abstr.). *Proceedings of the Conference on South Africa's Coal Resources*, Witbank, 6-9 November. Geological Society of South Africa, Johannesburg.

Dreyer, J.C. 1994. Total utilization of the coal resource: The Grootegeluk experience. *Journal of the South African Institute of Mining and Metallurgy*, vol. 94. pp. 153-164.

Falcon, L.M. 1987. The complexities of coal. *Review; Gold Fields of South Africa*. pp. 64-67.

Falcon, R.M.S. 1986. Classification of coals in Southern Africa. *Mineral Deposits of Southern Africa*, vol. 2. Anhaeusser, C.R..and Maske, S. (eds.). Geological Society of South Africa, Johannesburg. pp. 1899-1921.

Gan, H., Nandi, S.P., and Walker, P.L. 1972. Nature of the porosity in American coals. *Fuel*, vol. 51. pp 272–277.

Gearhart Owen Industries. 1975. Formation evaluation data handbook. Fort Worth. TX.

Gray, V.R. 1983. A formula for the mineral matter to ash ratio for low rank coals. *Fuel*, vol. 62. pp. 94–97.

Huang, H., Wang, K., Bodily, D.M., and Hucka, V.J. 1995. Density measurements of Argonne Premium coal samples. *Energy & Fuels*, vol. 9. pp. 20–24.

King, J.G. and Wilkins, E.T. 1944. The internal structure of coal. *Proceedings of the Conference on Ultra-fine Structure of Coals and Cokes*, London, 1943. British Coal Utilization Research Association, London. pp. 46–56.

Laubach, S.E., Marrett, R.A., Olson, J.E., and Scott, A.R. 1998. Characteristics and origins of coal cleat: A review. *International Journal of Coal Geology*, vol. 35. pp. 175–207

Levine, J.R. 1993. Exploring coalbed methane reservoir. Short Course, Institut Francais di Petrole, Rueil-Malmaison. 265 pp.

McEnaney, B. and Mays, T.J. 1989. Porosity in carbons and graphites. *Introduction to Carbon Science*. Marsh, H. (ed.), Butterworths, London. pp. 153–196.

McGraw-Hill. 1984. Dictionary of Scientific and Technical Terms. 3rd edn. New York.

Meyers, A., Clarkson, C., Wex, T., and Leach, B. 2004. Estimation of *in-situ* density of coal and relative density analyses: *Final Report for ACARP Project C10042*. Australian Coal Association Research Programme, Brisbane.

Morley, C. 2003. Beyond reconciliation – A proactive approach to using mining data. *Proceedings of the Fifth Large Open Pit Conference*, Kalgoorlie, 3–5 November 2003. Australasian Institute of Mining and Metallurgy, Melbourne. pp 185–191.

Nebel,M.L. 1916. Specific gravity studies of Illinois coal. University of Illinois *Bulletin*, vol. XIII, no. 44. Engineering Experiment Station, July 1916. Urbana, IL.

Noppé, M. 2004. Reconciliation: importance of good sampling and data QAQC. *Proceedings of the Mining and Resource Geology Symposium*. XYZ, EGRU Contribution no. 62.

Preston, K. 2005, Estimating the *in situ* relative density of coal – Old favourites and new developments. *Proceedings of the Bowen Basin Symposium 2005. The Future for Coal – Fuel for Thought*, Beeston, J.W. (ed.). Geological Society of Australia, Coal Geology Group and the Bowen Basin Geologists Group, Yeppoon, Queensland. pp. 13–22.

Preston, K. and Sanders, R. 2005. Calculating reserves - A matter of some gravity. A study by Quality Coal Consulting Pty Ltd for Pacific Coal Pty Ltd.

Preston, K B. and Sanders, R.H. 1993, Estimating the *in-situ* relative density of coal. *Australian Coal Geology,* vol. 9, May. pp. 22–26.

Rees, O.W. 1966, Chemistry, uses and limitations of coal analyses. *Report of Investigations 220*. Illinois State Geological Survey. 55 pp.

Robeck , E. and Huo, D. 2015. Pure coal and mineral matter properties: A practical foundation for *in situ* density estimation. Peabody Energy, St. Louis, MO.

Rodrigues, C.F. and Lemos de Sousa, M.J. 2002. The measurement of coal porosity with different gases. *International Journal of Coal Geology*, vol. 48. pp. 245–251.

Roux. L. 2012. Optimal yield and cut density prediction of semi soft coking coal and powerstation coal in the Waterberg Coalfield, Limpopo Province. MSc dissertation, University of the Witwatersrand, Johannesburg.

Roux. L. 2017. The application of ash adjused density in the evaluation of coal deposits. PhD thesis, University of the Witwatersrand, Johannesburg.

Smith G.G. 1991. Theoretical estimation of *in-situ* bulk density of coal. *CIM Bulletin*, vol. 84, no. 949. pp. 49–52.

Unsworth, J.F., Fowler, C.S., and Jones, L.F. 1989. Moisture in coal: 2. Maceral effects on pore structure. *Fuel,* vol. 69. pp 18–26.

Van Krevelen, D.W. 1993. Coal: Typology–Physics–Chemistry–Constitution. 3rd edn. Elsevier, Amsterdam. 979 pp.

Wang, X. 2007. Influence of coal quality factors on seam permeability associated with coal bed methane production. PhD thesis, Faculty of Science, University of New South Wales.

Ward. C.R. (ed.). 1984. Coal Geology and Coal Technology. Blackwell Scientific, Melbourne. 345 pp.

Ward C.R. 2002. Analysis and significance of mineral matter in coal seams. *International Journal of Coal Geology*, vol. 46. pp. 67–82.

Webb, P.A. 2001. Volume and density determinations for particle technologists. Micromeritics Instrument Corp., Norcross, GA. ◆

A critical investigation into spontaneous combustion in coal storage bunkers

S. Govender[1], J.J.L. du Plessis[2], and R.C.W. Webber-Youngman[3]

Affiliation:
[1] Grootegeluk Mine, Exxaro Resources, Pretoria, South Africa.
[2] Department of Mining Engineering, University of Pretoria, South Africa.
[3] Head of Department, Department of Mining Engineering, University of Pretoria, Pretoria, South Africa.

Correspondence to:
S. Govender

Email:
Mervin.Govender@exxaro.com

Dates:
Received: 14 Jul. 2016
Revised: 1 Oct. 2019
Accepted: 23 Feb. 2021
Published: May 2021

How to cite:
Govender, S., du Plessis, J.J.L., and Webber-Youngman, R.C.W. 2021
A critical investigation into spontaneous combustion in coal storage bunkers.
Journal of the Southern African Institute of Mining and Metallurgy, vol. 121, no. 5, pp. 251–260.

DOI ID:
http://dx.doi.org/10.17159/2411-9717/16-478/2021

ORCID
R.C.W Webber-Youngman
https://orchid.org/0000-0002-0101-7125

Synopsis

Spontaneous combustion (SC) is a cold oxidation reaction that generates heat, causing a temperature rise of the reactant and leading, with limited heat dissipation, to self-ignition of the reactant, which occurs without an external heat source. Although not limited to coal, the most significant hazard of SC are the fires that occur in coal mining operations around the world. These fires pose a serious risk to the safety of workers in the mines as well as adverse effects on the environment, and can affect the quality of life for current and future generations. We investigated the occurrence of SC in raw coal storage bunkers with the purpose of compiling a decision analyser for engineers designing or working with coal storage bunkers. Specific experts were interviewed from different backgrounds and companies, followed by field research at a coal mine. The important factors affecting the possibility of SC occurring were the type of coal supplied to the bunker, the mining practice, and physical conditions around the bunker. The information presented here will assist in reducing the SC risk in raw coal storage bunkers. These findings, together with the systematic decision analyser developed, will assist design engineers and mine personnel to take early preventative steps in managing SC. The decision analyser was tested for many different scenarios and gave good guidance on how to minimize and prevent SC in bunkers.

Keywords
bunkers, coal storage, spontaneous combustion.

Introduction

In coal mining, spontaneous combustion (SC) can occur in many areas such as product or run-of-mine stockpiles, underground workings, waste dumps, coal faces, in-pit ramps, and backfill areas. Extensive research was done by Phillips, Uludag, and Chabedi (2011) on SC in coal stockpiles, dumps, and coal faces. SC is when an oxidation reaction occurs without an external heat source. Heat is generated spontaneously within an oxidized substance when dissipation of the heat generated is limited or cannot take place. This study investigated the occurrence of SC in coal storage bunkers, and established that there was no single research report available that addresses the problem adequately. The decision analyser steps that were developed in this investigation will assist towards a possible solution to problems associated with SC. The process described will assist personnel in understanding, preventing, and managing SC.

Background

In a surface mine, it is frequent practice to have haul trucks dumping material into a tipping bin in a continuous sequence, or from a stockpile of coal when it is positioned close to the tip. Storage bins or bunkers are frequently used to facilitate continuous feed to processing plants. At Grootegeluk Mine, two coal processing plants are fed from two raw coal storage bunkers in series (Figure 1) with storage capacities of 17.5 kt and 30.5 kt. This capacity allows for 8 hours of continuous plant operation.

During the commissioning of the bunkesr and plants in 2012, SC occurred in the storage bunkers. A risk assessment was done using a 5-by-5 risk matrix to assess the current SC problem as part of the normal course of operations. An initial risk rating of 22 was achieved, which is deemed to be extremely high. The implementation of additional known control measures reduced the risk rating to 15, which was still considered to be too high.

One of the proposed control solutions was that the bunker should be loaded from a shuttle car moving in sequence from right to left on one side and from left to right on the other side. The bunker should be kept at between 73 and 79% capacity, but should never exceed 85%. However, due to problems experienced with the shuttle car and the need to ensure that coal covers all draw-off points to prevent oxygen from entering the bunker, this sequence of loading could not be realized (Gerber, 2014). Figure 2 shows a side view of the storage bunker.

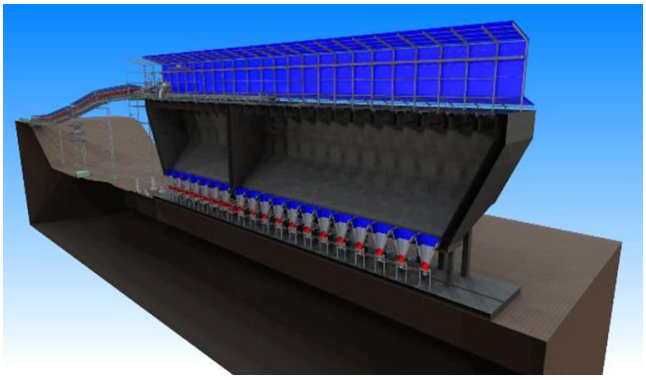

Figure 1—Section of coal storage bunker (Moolman, 2010)

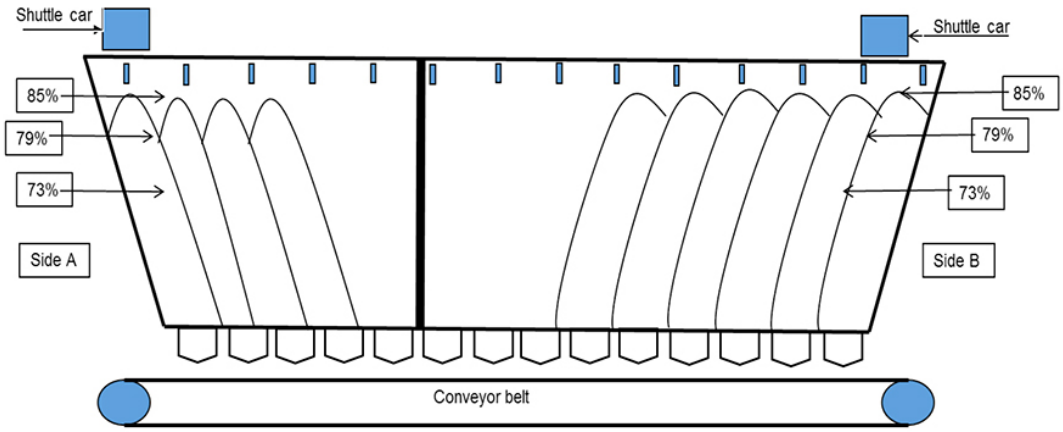

Figure 2—Side view of the coal storage bunker (Gerber, 2012)

Due to the magnitude of the SC problem, further studies were necessary to find a more permanent solution to prevent and control SC. The proposed solution developed and presented in this paper provides design engineers with a decision analyser for evaluating the risk factors leading to potential SC in storage bunkers and assisting in designing preventative measures.

The main factors that cause and/or determine the extent or severity of SC are the type of coal, the mining practice, and the physical conditions around the bunker. The grade, rank, sulphur content, and petrographic composition of the coal determine how the coal will react. Mining practice influences the average standing time of the coal in loose cubic metres (LCM) on the mining benches, the temperature of the coal when it is fed into the bunker, and the broken coal loading and cleaning practices. The physical conditions in and around the bunker include the ambient temperature, layout of the bunker with respect to the wind direction, and dead spots in the bunker structure.

Type of coal mined and supplied to a bunker

Coal analysis is based on the international classification of in-seam coals. In terms of this classification, four characteristics of coal were examined, namely the grade, the rank, the sulphur content, and petrographic composition.

Grade, rank, and sulphur content

The grade of the coal fed to the bunker ranges from very low to a carbonaceous rock grade coal. The ash content, which is important in determining the grade, ranges from 19.8–50% AD. Kaymakci and Didari (2002) posited that high-grade coals have a lower tendency to self-heat, while low-grade coals have a higher tendency to self-heat due to the higher volatile content and reactants, mostly vitrinite. A high ash content decreases the propensity of a coal to heat spontaneously. However, certain constituents of the ash (lime, soda, and iron compounds) may accelerate heating, whereas other constituents (alumina and silica) could have a retarding effect. Therefore, some components of ash promote combustion, while others inhibit it. The size distribution and permeability of the bunker feed also affect the risk of SC.

The rank of a coal refers to the degree of maturity of the coal. It is dependent on the degree of metamorphism, *i.e.* the properties of vitrinite, which is largely responsible for the coking properties of a coal. The greater the vitrinite content, the better the coking properties of the coal. Vitrinite reflectance is a direct measure of the rank of a coal, which is obtained through petrographic analysis.

Coal benches have different rank, grade, and sulphur ranges. For example, bench 2 could have a very low grade coal with a rank which is a high-volatile bituminous low rank C and a sulphur average of 1.4%. Bench 3 could have a carbonaceous rock grade coal with a rank corresponding to a high-volatile bituminous low rank C and a sulphur average of 1.26%. To establish the rank, grade, and sulphur range, a statistical analysis was done using information from the mine's geographic information system (GIS). This study could also have been conducted using the data from exploration boreholes. The data was separated into the different benches with their respective ash contents and calorific and sulphur values.

Phillips, Uludag, and Chabedi (2011) found that the rank of coal is one of the chemical factors that contribute to SC. Kaymakci and Didari (2002) state that it is widely recognized in the coal industry that lower-ranking coals are more susceptible to SC than higher-ranking coals. According to Adamski (2003), as the rank decreases towards lignite, the tendency for coal to self-heat increases, *i.e.* the lowest-ranked coal is more likely to self-heat under the same set of conditions.

Phillips, Uludag and Chabedi (2011) suggested that organic sulphur and the presence of pyrite contribute to SC. Kaymakci and Didari (2002) explain how the chemical factors such as pyrite content may accelerate SC. According to Panigrahi *et al.* (2005), at one mine coal with a sulphur content of 0.5% started to burn within two weeks of exposure. Guney (1968) concluded that the pyrite in coal may accelerate spontaneous heating due to the increased sulphur content. Guney further concluded that the pyrite must be present in a concentration greater than 2% before it can have any effect. However, SC can occur when sulphur or pyrite is present. The key factor is the size of the pyrite nodules and their exposure. The large nodules on their own, when exposed to oxidizing conditions or wetting after a dry period, can generate heat ten times faster than coal. This initiates 'hot spots' which then develop further into SC. Furthermore, pyrite oxidation is highly exothermic and could become autothermic/self-sustaining depending on the balance of supply of reagents, reaction rate, rate of heat transfer, and accumulation of heat. A sufficient increase in temperature could trigger SC. A window of conditions is required for this to happen.

Petrographic composition

To better understand the variations in the physical and chemical properties of the coal at a mine a petrographic analysis is performed to confirm expectations of the coals and to assess their utilization potential (ALS Coal Technology, 2015). Petrographic analysis provides information that is used to establish how the coal will react under different conditions. ALS Coal Technology (2015) indicates that the greater the percentage of vitrinite and liptinite in the composition, the greater the reactivity, and the greater the percentage of inertinite, the lower the reactivity of the coal.

In summary, if the ash values for the coal are high and it is a lower-grade coal then it is prone to SC. This is further dependent on the coal bench being mined and the amount of heat accelerators and retarders in the ash content of the coal. The lower the rank of coal the greater the tendency to SC. A high percentage of sulphur in the orebody could also give rise to SC.

Mining practice

The geological setting of the coal seam to be mined must be checked for faulting and faulted zones, which contribute to the dangers of SC by allowing air ingress into the coal mass (Kaymakci and Didari, 2002). The US Department of Energy (1994) claims that in opencast mines, the main factors responsible for mine bench fires due to SC are the presence of micro- and macro-cracks in the bench walls, which allow the entry of air, extended exposure of the bench walls to the open atmosphere, and accumulation of loose coal on the bench floor.

Standing time of loose cubic metres on the benches

The short-term production schedule for the case study coal mine indicated that broken coal fed to the plants had a standing time on the benches of about 6 days to 2 weeks on average, during which it is exposed to ambient environmental conditions. This allows for air ingress that can lead to oxidation and heating of the coal. If left unattended the coal will self-ignite once it reaches the critical SC point.

According to de Korte (2014), the time taken for heating to occur varies considerably. Product stockpiles and coal inventory in the mine should not be left longer than the incipient heating period. Both run-of-mine (ROM) and saleable product coal have been known to be susceptible to SC. A layer of coarse particles at the base and edges of the stockpile may result in increased ventilation. The situation is exacerbated by prevailing hot, moist winds and rain, which may increase the risk of SC in the summer months.

The US Department of Energy (1994), Adamski (2003), Phillips, Uludag and Chabedi (2011), and Humphreys (2004) reached similar conclusions, that freshly extracted coal absorbs oxygen more quickly than coal mined earlier. The oxygen absorption rate is a function of the coal's age, and fresh coal is more reactive than aged coal or coal that has been exposed to oxygen for longer periods. The reactivity decreases with exposure and oxidation over time. According to the US Department of Energy (1994), hot spots may not be present for the first one to two months. The heat transfer within the pile is controlled largely by the air flow through the coal, and will be less significant at very low flow rates. The surface temperature of the pile controls the convective heat loss at the pile's surface. These heat transfer processes are dependent on the temperature distribution and geometry of the reacting coal pile.

Phillips, Uludag, and Chabedi (2011) stated that when rainfall erodes the coal stockpiles, it exposes more coal to oxygen and, depending on the properties of the coal, heating of broken coal left in stockpiles in the pit or elsewhere on the mine can occur after a certain period of time.

Kaymakci and Didari (2002) concluded that the moisture content has an influence on the propensity of coal to self-heat, whereas Lyman and Volkmer (2001) established that the wetting and drying of coal provides an opportunity for heat transfer to occur in coal stockpiles. According to Lyman and Volkmer (2001), increases or decreases in heat affect the moisture content and oxidation rate, which explains most of the heat generated in the coal. The critical issue here is that when coal has been dried below its natural inherent moisture content, and then is exposed to moisture again, an exothermic process, termed 'heats of wetting', takes place, which generates sufficient heat to create a trigger point that in turn initiates hot spots. The coal dries out in winter and when exposed to rain or high humidity in spring, hot spots occur in places where just enough air passes through the coal bed to allow heats of wetting to occur, which then proceeds to oxidation and SC. Too much water or rain would swamp the process and too great an air flow would carry the heat away. So, the prime 'spot' for heating to start is where the conditions are optimal for heating to take place which is not dissipated. Therefore, porosity and size are key factors here.

Adamski (2003) and Grossman, Davidi, and Cohen (1995) drew similar conclusions, namely that where oxygen is in contact with the coal and oxidation starts to produce heat, and if this heat cannot dissipate, SC is initiated. Extra heat due to the condensation of moisture can lead to runaway self-heating if a coal pile is at a critical temperature point and oxygen is available. If the stockpile temperature increases above 30°C, then the moisture content of the coal vaporizes and carbon

dioxide and hydrocarbons of lower molecular weight are emitted. The vaporization and emission rates of gases decrease with temperature, as vaporization is an endothermic process. However, the moisture is transferred by diffusion to drier parts of the stockpile, causing condensation and an increase in temperature, since condensation is an exothermic process. These processes can decrease or increase the ignition point of the coal in different parts of the stockpile. The autogenous heating of stockpiled coal is restricted to small distinct areas, referred to as hot spots, which are characterized by good oxygen diffusion and insufficient heat dissipation. The oxidation-induced autogenous heating of coal causes a loss in calorific value and can also lead to safety and handling problems.

Evidence suggests that coal stockpiles should not be left on the mining benches for longer than is necessary for loading, and this time period should be determined through a risk assessment process for each bench. The mixing of freshly mined coal and aged coal should be avoided to minimize spontaneous heating, since. when old oxidized, weathered and dry coal is in contact with to wet fresh coal, self-heating occurs through heats of wetting once again. This is a dangerous situation as hot spots form all along the interface of the two lots of coal. This can occur in many situations, including when old coal is mixed with fresh coal when being loaded on board ships as well as on stockpiles.

Physical conditions at the storage bunker

Detailed information on the physical conditions around the bunker operation that may contribute to SC was obtained, including the fines ratio, temperatures in and around the bunker, and wind velocity. Monthly average wind speeds, wind direction, temperatures, pressure, and humidity data were obtained from a local weather station. Figure 3 shows the various physical measurements taken around the bunker.

To establish the impact of particle size on SC, samples were taken before the coal was fed into the ROM bunker and at the exit from the bunker. This was done to establish the change in coarse to fines ratio as the particles flow through the bunker. To obtain the best results it was critical to ensure that the bunker was empty and at its lowest level when the samples were taken. The coal height will drop a maximum of about 22 m during operations. The samples were screened at apertures from 0 to 150 mm.

The results indicated that 14.8% of the material fed into the bunker is –4 mm, increasing to 20% –4 mm at the discharge end. The reason for this test was to ascertain whether the ratio of coarse to fine material can affect the flow of air in the bunker. According to Itay, Hill, and Glasser (1989) the most important factor contributing to SC is particle size. Very fine coal does not burn due to a shortage of oxygen, whereas coarse does not burn easily as the rapid and easy passage of air through the body of the coal dissipates any heat generated. There is a critical middle size range where the air flow is just enough for oxidation and therefore heat production, but not fast enough to dissipate the heat. The most dangerous combination is a mixture of fine and coarse material, which increase the permeability of the mixture. However, the air velocity measurements taken at the discharge point of the bunker indicated that a reasonable proportion of fine and coarse coal particles minimizes the flow of air entering into the bunker.

The ambient conditions around a coal mine, in particular the daily temperature and the weather patterns, influence the temperature of the coal entering the bunker. If the wind direction is in line with the bunker, air could be forced into the bunker thereby allowing the entry of oxygen, resulting in SC. It therefore becomes important to position the bunker loading and exit chutes out of the direct line of the prevailing wind direction.

The presence of 'dead spots' in the bunker could result in coal standing and oxidizing at these points, thereby creating hot spots (Figure 4), which could damage the structure of the bumker.

Results

The coal type, mining practice, and physical conditions around the bunker have an impact on the occurrence of SC. A diagrammatic plan view of an opencast mine is depicted in Figure 5, showing the pit layout, the loading area, the crushers, and the storage bunker.

The geological setting is an important contributor, especially if the coal seam is prone to faulting. SC is influenced by the type of coal being mined in terms grade and heat accelerators in the ash content. The high vitrinite and liptinite in the coal and low rank result in an increased oxidation rate and heating, which leads to a possibility of SC. A high content of organic and pyritic sulphur in the coal also increases the possibility of SC.

The standing time of the coal LCM on the mining benches and the possibility of it undergoing SC is influenced by many factors such as loading and cleaning cycles, ambient temperature, and exposure to moisture.

High temperatures in and around the bunker increase the likelihood of SC. If coal is found to be hot at the crusher it should be rerouted to the hot coal stockpile for cooling and disposal, as shown in Figure 5. This coal should not be fed to the bunker.

The loading and exit chutes of the bunker should be out of the direct line of the prevailing wind direction to avoid air being forced into the bunker, resulting in SC. An appropriate ratio of fine to coarse material should be maintained to minimize air

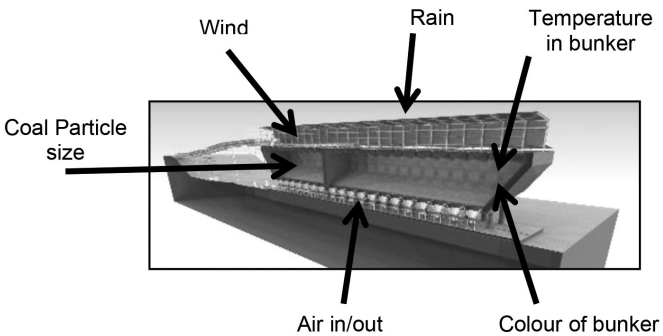

Figure 3—Raw coal storage bunker with external factors

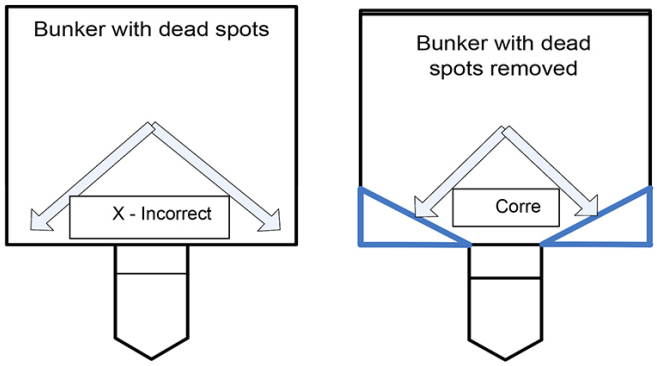

Figure 4—Bunker with and without dead spots

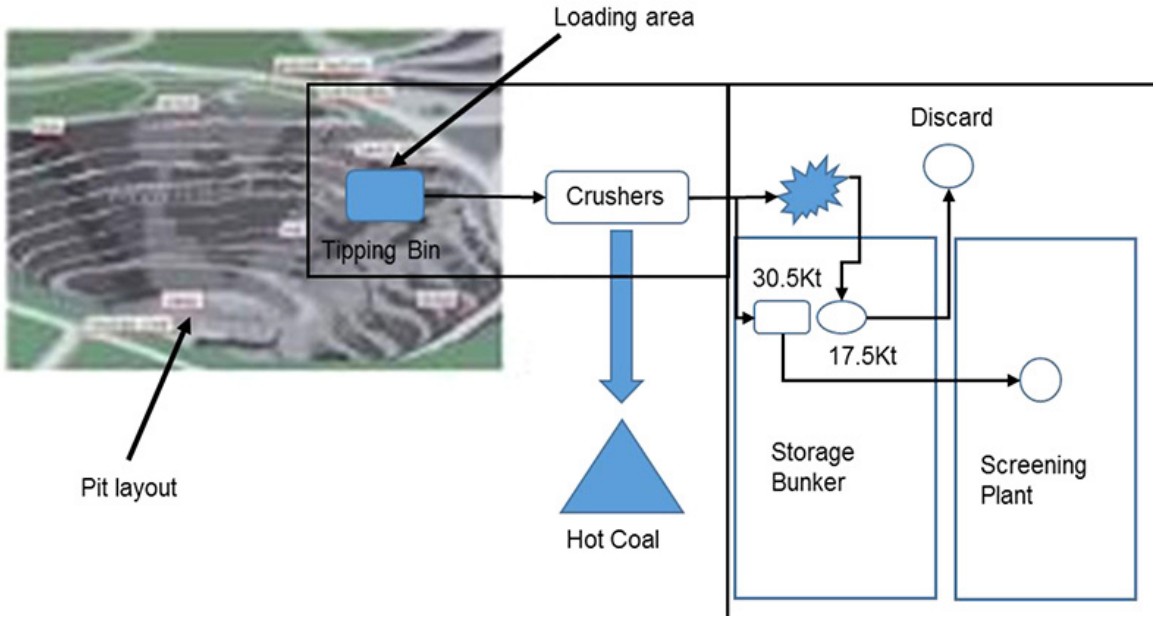

Figure 5—Plan view of coal movement from the mine to the bunker

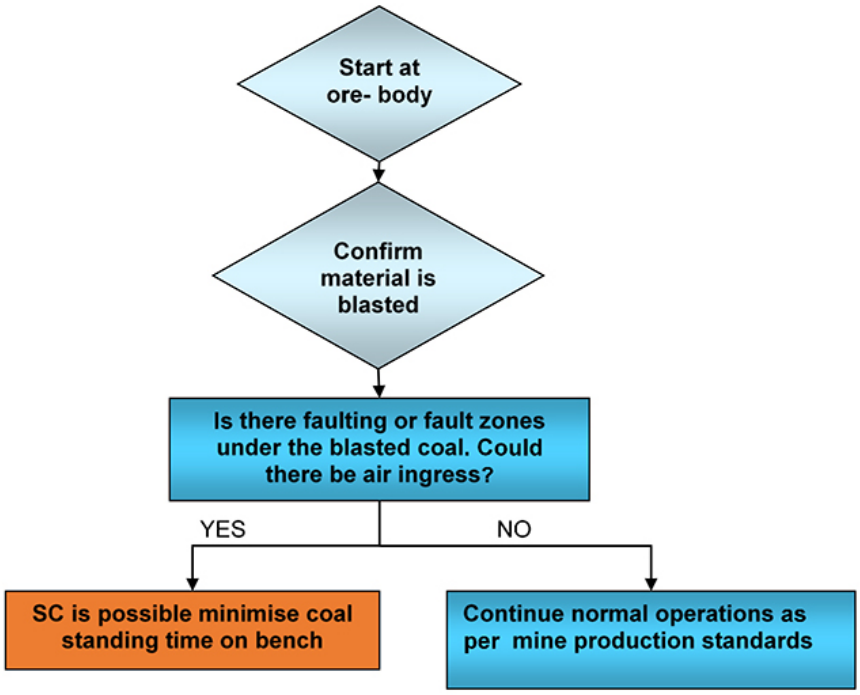

Figure 6—Impact of faulting and fault zones

ingress and decrease the possibility of SC. The presence of 'dead spots' in the bunker could result in coal standing and oxidizing at these points, thereby creating hot spots and resulting in SC.

The assessment of the factors influencing SC was utilized to develop a decision analyser that can be used to assist mine personnel in understanding the potential causes of SC. The decision analyser was split into six simple steps that address the possibility of SC from the orebody to the bunker. These steps involve determining the impact of faulting and fault zones, the grade, reactivity, rank, and of the coal, confirming the sulphur content of the coal, the coal standing time on the benches, and the physical conditions at the bunker.

Step 1: Impact of faulting and fault zones

The decision process starts once the coal has been blasted (Figure 6). It is important to establish whether the blasted material is lying on a fault or in a fault zone that could allow air ingress into the stockpile, leading to oxidation and heating. If this is not the case, normal mining operations can continue using the mine's standards and procedures. The standing time of the coal on the mine bench must be minimized, and the coal should be moved or processed as soon as possible.

Step 2: Confirm grade of coal

This step deals with understanding the impact of coal properties

on SC. It starts with establishing the grade of coal present (Figure 7). This is determined by the ash content – the higher the ash content the lower the grade. Once the grade has been established, the presence of heat accelerators must be established. If the ash contains a high amount of lime, soda, or iron, then SC is possible, whereas high amounts of alumina or silica reduce the possibility of SC. Once it has been established that SC is possible, measures must be put in place to manage the risk and monitor the coal temperature in the operations. These measures could include reducing the standing time of coal on the benches, by ensuring that heat is dissipated from the stockpile, or taking steps to block air ingress into the stockpile.

Step 3: Confirm reactivity and rank of coal

The next step is to establish the reactivity of the coal, since the reactivity is a direct measure of the rank. A high content of vitrinite and liptinite results in higher reactivity, which increases the oxidation rate and results in heating of the coal (Figure 8). A low-rank coal is more prone to SC than a high-rank coal. Once it has been established that SC is probable, measures must be put in place to manage the risk and monitor the coal temperature.

Step 4: Impact of sulphur content of the coal

In this step the chemical properties must be confirmed, especially the sulphur content. The amount of organic and pyritic sulphur in the coal has an influence on SC (Figure 9). High amounts of organic and pyritic sulphur indicate a greater possibility of SC. If there is a possibility of SC, measures must be put in place to manage the risk and monitor the coal temperature.

Step 5: Determine coal standing time on the benches

To determine the coal standing time with low risk of SC on the benches it is important to consider the outcomes of steps 1–4. These outcomes, together with other influencing factors such as inadequate loading, poor cleaning cycles, coarse coal at the base of the stockpile, exposure of coal after rain, the wetting of coal and a high ambient temperature (Figure 10) will indicate whether SC is likely. Thereafter measures must be put in place to manage the risk at the source and to monitor the coal temperature regularly.

Step 6: Impact of physical conditions at the bunker

The last step in this decision process relates to where the coal has been loaded and is being transported to the bunker. If the coal has been loaded into the crusher and the monitoring equipment detects a high temperature, the coal must be redirected to a hot coal area or lay-down area for cooling and disposal (Figure 5). Such coal should not be transported to the bunker. It is advisable that temperature monitoring devices be installed in the transporting section to assist decision-making as to whether to load or redirect hot coal. This should be the first line of defence in order to prevent hot coal from entering the bunker. At the bunker (Figure 11), continuous monitoring is necessary to detect high-temperature areas. The following parameters need to be monitored: air ingress into the bunker, the fines content, and dead spots that could evolve into hot spots. If SC is detected in the bunker, the only option is to stop loading and remove coal from the affected area immediately. A gas monitoring device could be installed at the bunker to measure CO levels. If the CO level is found to be above 4%, the coal is self-heating in areas not often visible to the naked eye, devolatilizing gases are being emitted, and an explosion is possible, as the CO level has reached the lower explosive limit (LEL).

As the coal proceeds through the different steps the risk of SC increases. The first priority is therefore to put measures in place to prevent SC.

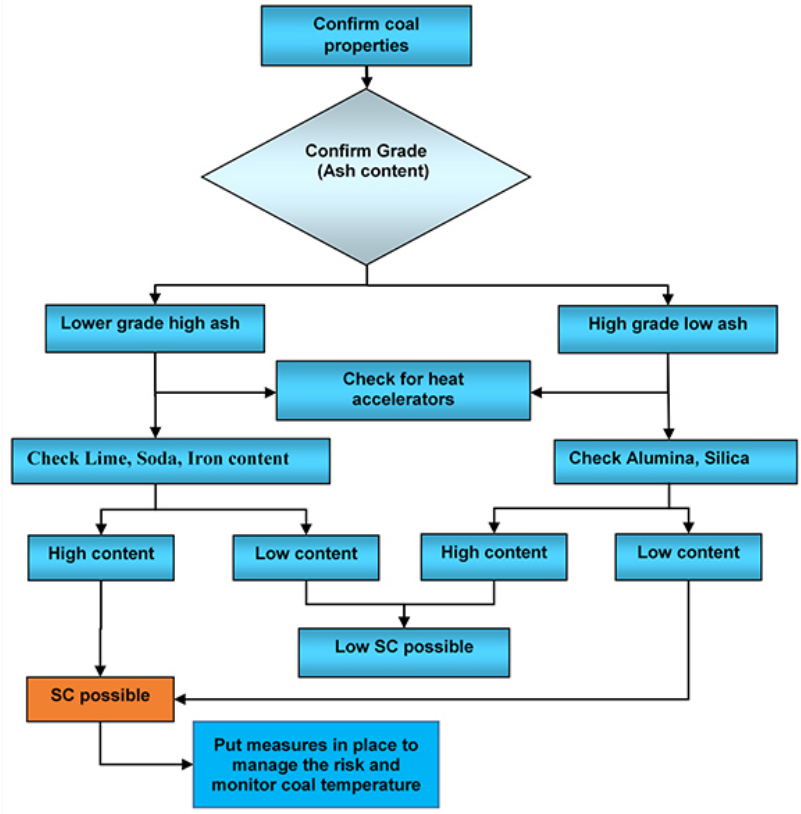

Figure 7—Confirm grade of coal

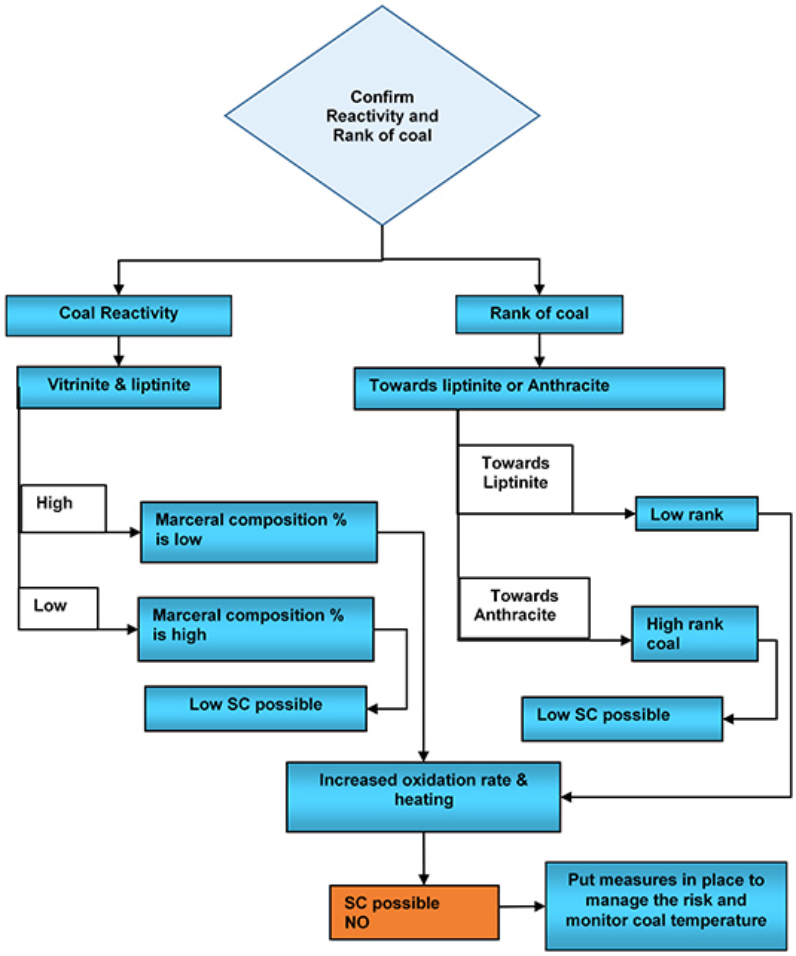

Figure 8—Confirm reactivity and rank of coal

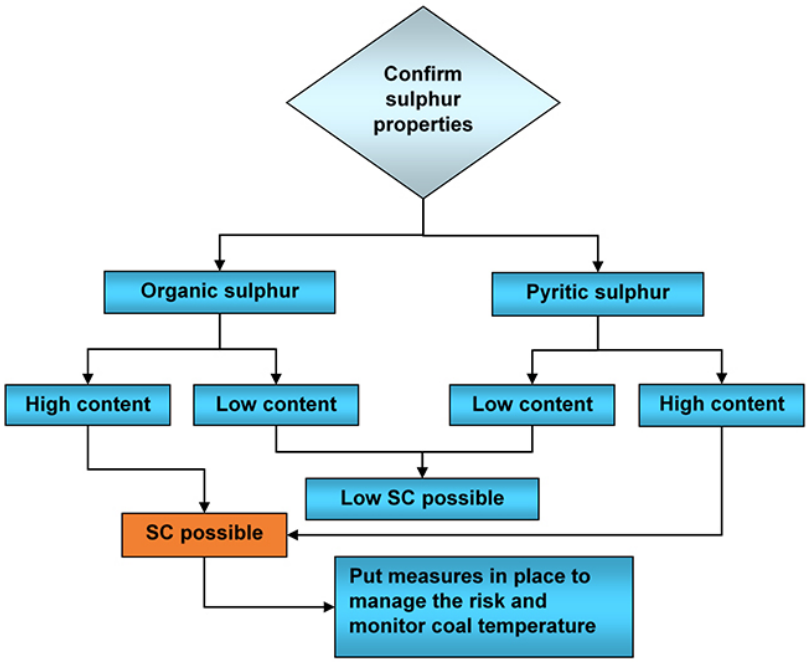

Figure 9—Impact of sulphur content of the coal

Control measures

The control measures can be broken up into two main areas: the bunker design and management control

Bunker design

The bunker must be so designed so as to prevent dead spots or areas where hotspots can form, as per Figure 4. A particle flow

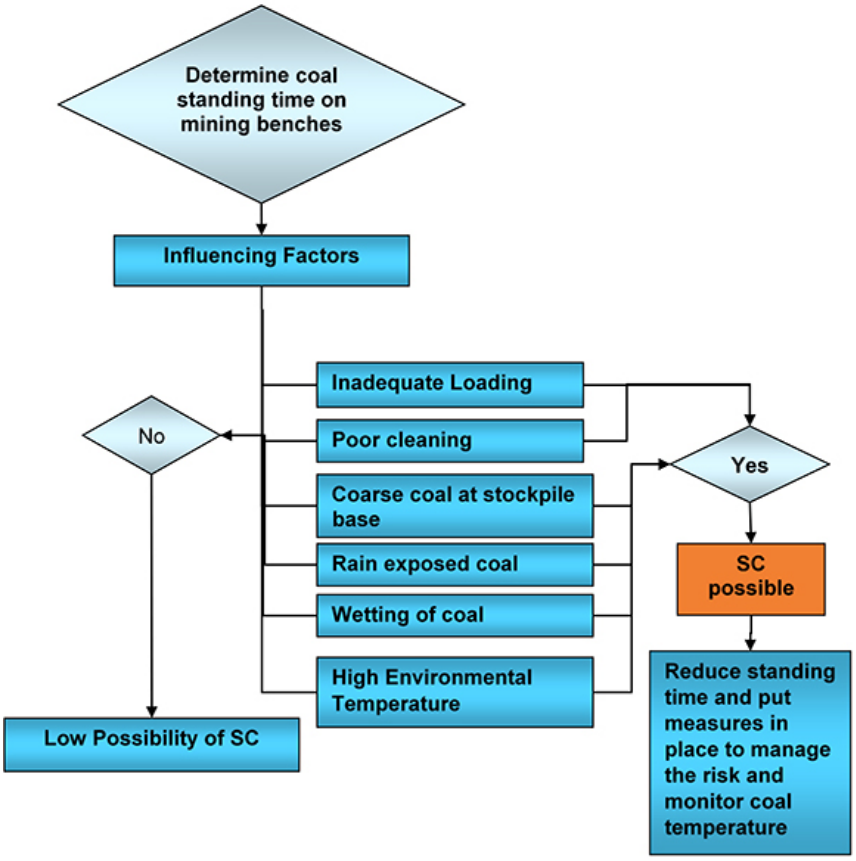

Figure 10—Determine coal standing time on benches

analysis can be done by using simple software or a discrete element method to simulate the flow of material in the bunker or silo. The simulation will provide insight into the mass flow/final flow, residence time/product degradation, rat-holing, bridging, blockage, dust formation, bunker/silo shape, cone shape, output dimension, and wall thickness calculations.

The designer must consider the static and dynamic operation of the mine. During normal production, breakdowns, planned maintenance, and scheduled routine inspections occur. At times, these could last for hours, during which time the coal is standing inside the bunker and most likely to combust spontaneously. The temperature of the coal should be monitored continuously during any such abnormal periods. If the coal temperature starts to increase above 50°C it is best to remove the coal from the bunker. Therefore, one can assume that a safe duration for the coal standing in the bunker is dependent on the temperature of the coal.

Thermal cameras or temperature probes should be installed to monitor the coal entering the crusher and bunker or silo. This will inform the operator if hot coal is being fed from the mine or source.

Air flow measurements must be taken in order to establish whether air is entering the bunker or silo. This will influence the oxidation rate of the coal. These measurements must be taken regularly by the mine hygiene specialist using a well-calibrated velocity meter.

If the bunker has a number of coal-extraction points, it becomes important to ensure that the sequence of loading coal into the bunker is designed in such a way as to minimize the quantity of air being drawn into the bunker. This will help to prevent oxidation and can be done by ensuring that there is always coal at all the extraction points or that they are sealed off. The process engineer needs to build in a standard operating procedure which will ensure that coal is not drawn off completely from the extraction point. This operating procedure can be applied by using simple instrumentation and programmable software, which will then trigger a warning to the operator when the extraction point is reaching a dangerously low level.

Depending on the amount of dust generated when the bunker or silo is loaded, it will be advisable to install explosion-proof equipment in that area or within that control zone. This dust is carbonaceous dust and if present the area is referred to as a Class II location. The ignition temperature, electrical conductivity, and thermal blanketing effect of the dust are all critical when dealing with heat-producing equipment such as lighting fixtures and motors.

Management and control

To address the issue of the standing time of coal on the benches, a risk assessment must be done and a standard operating procedure established as to how to manage the raw coal standing time on the benches. Training in this procedure must be provided to all mine personnel.

Mining best practices must be established to control and treat hot coal. If hot coal is detected, it should be moved to a safe location and allowed to burn out in a controlled environment. After it has been burnt out, it should be disposed of safely. The cause of the SC must be established and proactive measures put in place to prevent its reccurrence.

There should be a standard operating procedure for emptying the bunker in a controlled manner in the event of SC. This should follow from a risk assessment and adequate training of operating personnel.

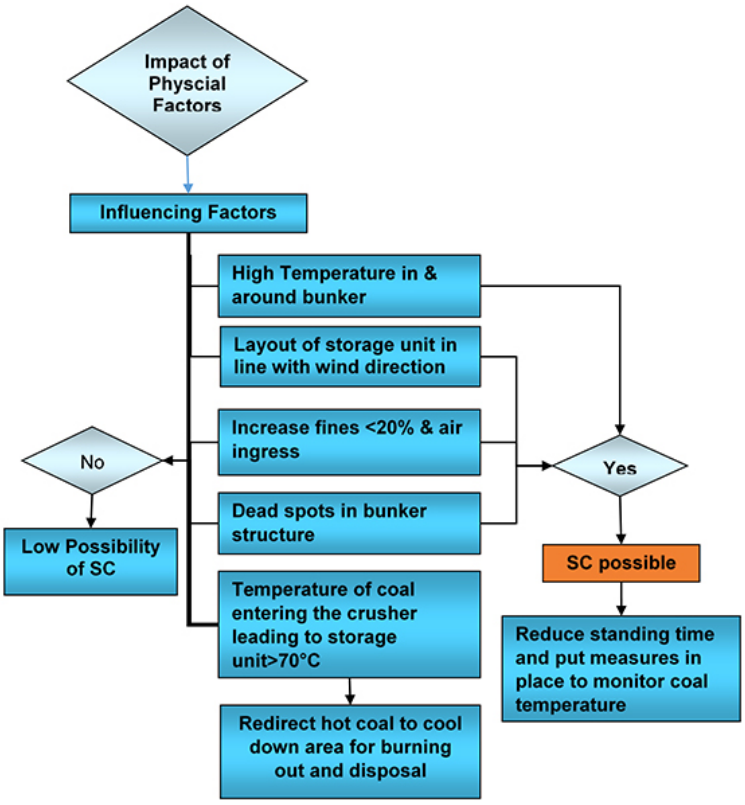

Figure 11—Impact of physical conditions at the bunke

Conclusions

This study examined the factors that could influence SC of coal at various stages from the mine (pit) to the storage bunker. It is evident that the type of coal mined and the mining practice play a major role in the management of the SC risk. The physical factors pertaining to the bunker, although less important, also influence the likelihood of SC occurring in the bunker. These findings, together with the systematic decision analyser presented, will assist mine personnel to take early preventative steps to manage and control the risk of SC in the bunker. This decision tool was tested for many different scenarios and gave good guidance on how to minimize and prevent SC in a bunker. The SC problem has been reduced to a bare minimum. The outcomes of this study can be applied to similar situations in other mines.

References

Adamski, S.A. 2003. Prevention of spontaneous combustion in back-filled waste material at Grootegeluk Coal Mine. PhD thesis, University of the Witwatersrand.

ALS Coal Technology. 2015. Petrography and imaging centre. http://www.alsglobal.com/~/media/Files/Divisions/Energy/Coal/Coal%20Resources/Capabilities-and-Services-Fact-Sheets/ALS-Coal-Petrography-and-Imaging-Centre-Fact-Sheet.pdf [accessed: 27 September 2015].

De Korte, J. 2014a. Managing spontaneous combustion of coal. Part 1: Causes, controls and case studies. *Proceedings of the Fossil Fuel Foundation Conference on Spontaneous Combustion*, Johannesburg, South Africa, 13–14 February 2014.

De Korte, J. 2014b. Managing spontaneous combustion of coal. Part 2: Tests to determine the spontaneous combustion propensity of coal. *Proceedings of the Fossil Fuel Foundation Conference on Spontaneous Combustion*, Johannesburg, South Africa, 13–14 February 2014.

Gerber, J. 2012. Operating philosophy – Grootegeluk Medupi Expansion Project. Grootegeluk Coal Mine, Operating Standards document No. MCG-B78-0000-0000-G-PHI-001. Lephalale, South Africa.

Gerber, J. 2014. Personal communication, 7 January. Grootegeluk Coal Mine, Lephalale, South Africa.

Grossman, S.L., Davidi, T.S., and Cohen, H. 1995. Explosion risks during the confined storage of bituminous coals. *Fuel*, vol. 74, no. 12. pp. 1772–1775.

Guney, M. 1968. Oxidation and spontaneous combustion of coal – Review of individual factors. *Colliery Guardian*, vol. 216. pp. 105–110 and 137–143.

Humphreys, D. 2004. The application of numerical modelling to the assessment of the potential for, and the detection of, spontaneous combustion in underground coal mines. PhD thesis, University of Queensland, Australia.

Itay, M., Hill, C.R., and Glasser, D. 1989. A study of the low temperature oxidation of coal. *Fuel Processing Technology*, vol. 21, no. 2. pp. 81–97.

Kaymakci, E. and Didari, V. 2002. Relations between coal properties and spontaneous combustion parameters. *Turkish Journal of Engineering & Environmental Sciences*, vol. 26. pp. 59–64.

Lyman, R.M. and Volkmer, J.E. 2001. Pyrophoricity (spontaneous combustion) of Powder River Basin coals: Considerations for coal bed methane development. Coal Report CR 01-1. Wyoming State Geological Survey, Laramie, WY.

Moolman, J. 2010. Grootegeluk Medupi Expansion Project – Detailed design – 3D design showcase. Grootgeluk Coal Mine, Lephalale, South Africa.

Panigrahi, D.C., Udaybhanu, G., Yadav, M.D., and Singh, R.S. 2005. Development of inhibitors to reduce the spontaneous heating susceptibility of Indian coals. *Proceedings of the Eighth International Mine Ventilation Congress*, Brisbane, Queensland, Australia, July 2005. Australasian Institute of Mining and Metallurgy, Melbourne.

Phillips, H., Uludag, S., and Chabedi, K. 2011. Prevention and control of spontaneous combustion. *Best Practice Guidelines for Surface Coal Mines in South Africa.* Coaltech Research Association, Johannesburg.

Department of Minerals and Energy. 2002. Guideline for the compilation of a mandatory code of practice for the prevention of flammable gas and coal dust explosions in collieries. DME 16/3/2/1-A1, 1 August 2002. Government Printer, Pretoria.

US Department of Energy. 1994. Primer on spontaneous heating and pyrophoricity. DOE Handbook FSC-6910, DOE-HDBK-1081-94, Washington, DC.http://energy.gov/sites/prod/files/2015/01/f19/DOE-HDBK-1081-2014.pdf [accessed: 15 November 2014]. ◆

BOOK REVIEW

Mining in Zimbabwe – From the 6th to the 21st Centuries

Edited by Martin Prendergast and John Hollaway

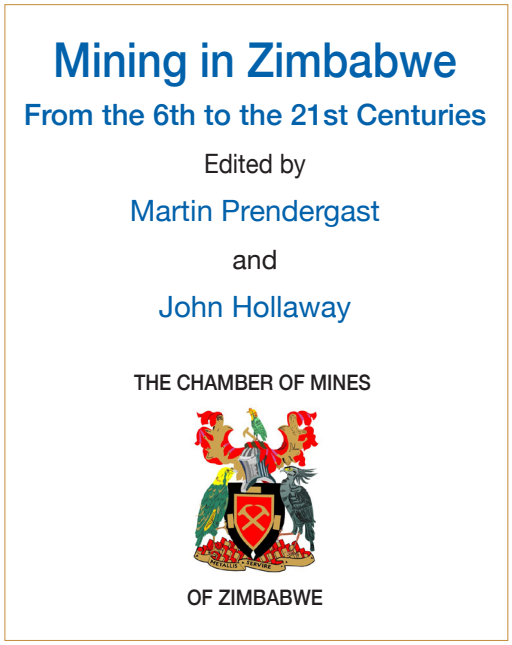

A truly remarkable book, outlining how Zimbabwe's professionals and entrepreneurs have developed their mining industry over the past 100 years. The book covers Zimbabwe's diverse mineral sectors – gold, coal, asbestos, chrome, copper, tin, iron and steel, nickel, diamonds, platinum group metals, industrial minerals, and minor minerals and metals – in the context of history, geology, exploration, historical and current mining methods, mineral processing, mine infrastructure, and production data. Each section, authored by experts in their sectors, is supported by photographs and illustrations that leave the reader well informed of this once-powerful industry.

The book covers the small, medium, and large mines, both past and present, in Zimbabwe. The reader is taken to the smaller hydrothermal underground gold mines near Bulawayo, the Shabani asbestos mine, the large mechanized coal mines in Hwange, the iron ore mines and steel mill of Redcliff, modern day underground platinum mines on the Great Dyke, the Empress nickel mine, the chrome mines of Gweru, to the tin mine of Kamative, and the chaotic and short-lived diamond mines of Marange.

Insights into the personalities of mining men in Zimbabwe, such as 'Tiny' Rowland, Norman Levin, Major John Hilton, and Kurt Kuhn, among, many others, bring additional life to the narrative.

One is drawn into, and astounded by, Zimbabwe's natural resources and the mines and mining-related infrastructure built meticulously by past mining professionals in the country. This book is a showcase of how mining was used for the greater benefit of society in terms of infrastructure, education, and skills development.

A great guide for any country intent on developing its mining industry, but also an illustration of the demise of a mining industry, when mineral policies, commodity cycles, and resource depletion work against it.

Although historical in its narration, this book can be used as a reference for the next generation of mining professionals when developing new mining projects in Zimbabwe or resurrecting old mines on the foundations laid by mining professionals of the past. It demonstrates that Zimbabwe, with all the strategic commodities required for future technologies, technical skills, and relatively intact infrastructure build by past mining generations, has many key ingredients to become yet again a successful mining country.

Dr Michael Seeger
Mining Engineer

The geometric axial surface profiles of granular flows in rotating drums

Elbasher M.E. Ahmed[1], I. Govender[1], and A. Mainza[2]

Affiliation:
[1] Department of Chemical Engineering, University of KwaZulu-Natal, South Africa.
[2] The Centre for Minerals Research, University of Cape Town, South Africa.

Correspondence to:
I. Govender

Email:
indresan.govender@gmail.com

Dates:
Received: 25 May 2020
Revised: 9 Nov. 2020
Accepted: 13 Jan. 2021
Published: May 2021

How to cite:
Ahmed, Elbasher M.E., Govender, I., and Mainza, A. 2021 The geometric axial surface profiles of granular flows in rotating drums.
Journal of the Southern African Institute of Mining and Metallurgy, vol. 121, no. 5, pp. 261–266.

DOI ID:
http://dx.doi.org/10.17159/2411-9717/1228/2021

Synopsis

A mechanistic description of axial segregation in rotating drum flows remains an open question. Consequently, optimal mixing of grinding balls and rocks for efficient breakage, maximum production of fines, and slurry transport is seldom achieved. Experimental and numerical studies of granular mixtures in rotating drums identify alternating axial bands that eventually coarsen in the long-term limit. Most models of axial segregation are limited to binary mixtures and cannot always predict the logarithmic coarsening effects observed experimentally. A key missing factor is a robust description of the axial free surface profile that is valid across a wide range of flow regimes. We present a practical model of the axial free surface profile by linking it to readily-derived geometric features of the cross-sectional S-shaped free surface profile. A parametric study shows good agreement with experimental measurements reported in the literature and heuristically valid trends.

Keywords
rotating drum, granular flow, axial profile, comminution, mixing, segregation.

Introduction

Over the past few decades, rotating drums have attracted considerable research effort by both the engineering and physics communities. The prototypical configuration of rotating drums is often favoured for its ability to display a wide range of granular flow phenomena such as avalanching, chaotic mixing, and segregation (Seiden and Thomas, 2011; Pignatel *et al.*, 2012). Consequently, the processes of blending, mixing, and grinding of materials such as cement, fertilizer, chemicals, and pharmaceuticals are commonly carried out in rotating cylinders (Perry and Green, 1984). In the chemical and process industries, rotating drums are extensively used as mixers, dryers, granulators, and reactors for processing granular materials (Santomaso *et al.*, 2003).

Rotating drum flows exhibit both azimuthal and axial flows with their interplay leading to complex multidirectional flow fields that resist a coherent theoretical description. While cross-sectional flow has been widely studied (Zik *et al.*, 1994; Rajchenbach, 1990); Yamane *et al.*, 1998; Taberlet *et al.*, 2006), axial flow and geometry is rarely discussed (Chou and Lee, 2009; Dury *et al.*, 1998). Chou and Lee (2009) experimentally studied cross-sectional and axial flow patterns of dry granular material in 2D and 3D rotating drums. They argued that sidewall and arching effects lead to a slightly arced axial surface profile and a relatively flat free surface profile in the rolling Froude regime. With increased rotational speeds, the axial surface curvature becomes significant while the free surface profile takes on a distinct S-shape.

Figure 1 is a schematic of the axial bed profile and S-shaped free surface for a drum operating in the cascading Froude regime. To quantify the axial profile of the bed, Chou and Lee (2009) proposed a semi-empirical formula that varies parabolically with axial position, and depends on both the elevation of the surface at axial midpoint y_c (see Figure 1) and a coefficient a_z that characterizes the axial surface curvature. Unfortunately, these coefficients render their formula impractical in the context of industrial systems that are opaque to visual measurement and too aggressive for sensitive *in-situ* measurement sensors.

Numerical simulation by the discrete element method (DEM) facilitated a similar study by Dury *et al.* (1998). To quantify the characteristic length of boundary effects ξ, Dury *et al.* (1998 used, in batch simulations with mono-sized spheres, abstract constants that can become very difficult, if not impossible, to quantify in realistic industrial systems like tumbling mills.. The numerically determined variation of the time-averaged axial repose angle with axial position was fitted to an exponential

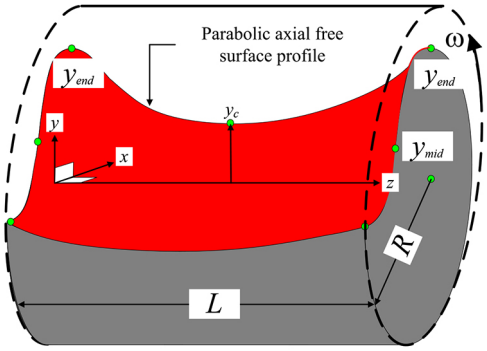

Figure 1—Schematic of axial surface profile (red surface) in a drum with length *L* and radius *R* rotating at angular speed ω. The shoulder y_{end} and midpoint y_{mid} located on the azimuthal free surface denote vertical heights that are used in the new model given by Equation [2]. We note that y_{end} and y_{mid} are easily extracted from the numerical solution of the free surface

function involving the bed repose angle at the axial midpoint and axial boundary wall, ξ, and drum length *L*. Notwithstanding the good agreement with DEM simulations, the model cannot be easily used outside of DEM or idealized experimental contexts where ξ is readily quantified. Noting the limitations of the models by Chou and Lee (2009) and Dury *et al.*, (1998), in the present work we propose a new formula that circumvents the need for abstract constants that can become very difficult, if not impossible, to quantify in realistic industrial systems like tumbling mills.

In the next section we describe the construction of the new axial surface profile model. A parametric study then follows, wherein we consider the influence of drum angular speed across the three dominant Froude regimes (rolling, cascading, and cataracting), drum length, and fill fraction on the axial free surface profile. Noting that our model naturally builds upon well-established azimuthal free surface profiles reported in the literature (Zik *et al.*, 1994), these are also included in the parametric study. Finally, the structural similarity between the model by Chou and Lee (2009) and ours allowed us to incorporate their experimentally verified model into the existing analysis by back-fitting the difficult-to-measure axial surface curvature a_z to our results.

Construction of the axial-profile

Chou and Lee (2009) developed a semi-empirical formula to describe the axial surface profiles as parabolic curves along the drum axis (z-axis). Their formula is given by:

$$y(z) = y_c + \frac{a_z}{2}\left(z - \frac{L}{2}\right)^2 \qquad [1]$$

where y_c is the surface height at the axial centre-line (see Figure. 1), a_z is the axial surface curvature (obtained by measurement), and L is the length of the drum. An obvious limitation relates to the difficulty in estimating the constants y_c and a_z in realistic scenarios, where measurement of these quantities is impractical due to the harsh and opaque environments typically encountered in industrial tumbling mills. To this end we propose a variation on their formula with a view to replacing these constants with simple and easy-to-calculate expressions based on the S-shaped free surface profile. The proposed modification circumvents the need for explicit knowledge of the axial surface curvature, a_z and gives the following result for the axial free surface profile.

$$y(z) = (y_{mid} + R) + \frac{y_{end} - y_{mid}}{A}\left(z - \frac{L}{2}\right)^2 \qquad [2]$$

where $A = 2\varpi RL$ is the azimuthal surface area of the drum with radius R. The underlying philosophy of our model is that values for y_{end} and y_{mid} (see Figure 2) can be obtained from a numerical solution of the differential equation governing the S-shape of the azimuthal free surface. In this regard, several models for the cross-sectional free surface profile exist (Zik *et al.*, 1994; Rajchenbach, 1990); Taberlet *et al.*, 2006). For example, the model of Zik *et al.* (1994) is given by

$$\Lambda\left[\frac{dY_{fs}}{dx} - \mu\right]\left[1 + \left(\frac{dY_{fs}}{dx}\right)^2\right] = 1 - \left[\left(\frac{x}{R}\right)^2 + \left(\frac{Y_{fs}}{R}\right)^2\right] \qquad [3]$$

where P_0 represents the lithostatic pressure at the bottom of flowing layer, (x, Y_{fs}) are the coordinates to the free surface, and Λ is a lumped parameter given by

$$\Lambda = \frac{2P_0^3}{3\eta\omega\rho^2 g^2 R^2} \qquad [4]$$

that depends on the granular viscosity η, angular speed of the drum ω, bulk density ρ, and drum radius R. Figure 2 illustrates a free surface solution for the parameters given in Table I.

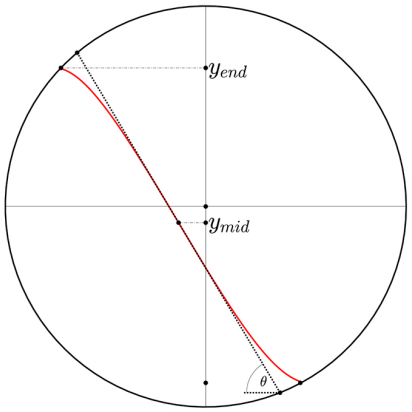

Figure 2—S-shaped free surface profile (red curve) based on the values in Table I. The shoulder position y_{end} and inflection point y_{mid}, obtained from this numerical solution, form the key inputs to the model given by Equation [2]. The origin of the (x, y) coordinate system is located at the centre of the drum

Table I

Input parameters employed for illustrating the azimuthal free profile model fit shown in Figure 2

Parameter	Description	SI Units
ρ = 2500	Density	$\frac{g}{m^3}$
g = 9:81	Local gravitational acceleration	$\frac{m}{s^2}$
R = 0:238	Drum radius	m
P_{crit} = 60	Percentage of critical speed	%
η= 6 10^{-3}	Granular viscosity	Pa · s
d = 3 10^{-3}	Particle diameter	m
h_0 = 1:3d	Depth of owing layer	m
ϕ = 0:58	Average solids fraction	[–]
θ = 40	Repose angle at depth h_0	deg
$P_0 = \rho\phi gh0\cos(\theta_0)$	Pressure at depth h0	Pa
α = 0:4	Fill fraction	[–]
$L = 2R$	Drum length	[m]
μ = 0:4	Mohr-Coulomb friction coecient	[–]

By exploiting the symmetry of the azimuthal free surface model, solutions to the inflection point y_{mid} = –1.92 cm and shoulder position y_{end} = 16.34 cm were obtained for the configuration depicted in Table I. Substitution into Equation [2] then yields the axial surface profile proposed in this paper. Figure 3 illustrates the axial surface profile using our model, Equation [2], and that of Chou and Lee (2009) Equation [1]. In the absence of measured values for the axial curvature parameters a_z and y_c required by the model of Chou and Lee (2009), we perform a least-squares fit of Equation [1] against our solution by treating a_z and y_c as the unknown constants to be fitted. The maximum vertical displacement of the axial surface, denoted V_{disp} in Figure 3, will serve as a proxy for quantifying the degree of curvature, *i.e.*, the larger V_{disp}, the higher the degree of curvature.

Result and discussion

Noting that our model is influence by the azimuthal free surface profile (which ultimately determines the values of y_{mid} and y_{end}) and the drum length, we perform a parametric study by varying the drum fill fraction α, drum length L and Froude number $Fr = \frac{\omega^2 g}{R}$.

Froude number

To ensure a wide Froude regime coverage, we tested drum speeds consistent with rolling (1% critical speed), cascading (40% critical speed), and cataracting (85% critical speed) modes.

Figure 4 shows the influence of drum speed, expressed as a percentage of the critical speed, on the azimuthal and axial free surface profiles. At 1% of critical speed (Figures. 4a and 4b), the azimuthal free surface is flat while the axial free surface is slightly curved with V_{disp} < 1 cm. At 40% critical speed (Figures 4c and 4d), an increase in the repose angle, a slightly S-shaped azimuthal free surface profile, and an increased curvature in the axial free surface profile are evident, with V_{disp} < 1.5 cm. At a fully cataracting speed corresponding to 85% of critical, (Figures 4e and 4f), the azimuthal free surface depicts the highest bed repose, a slightly more S-shaped azimuthal free surface than

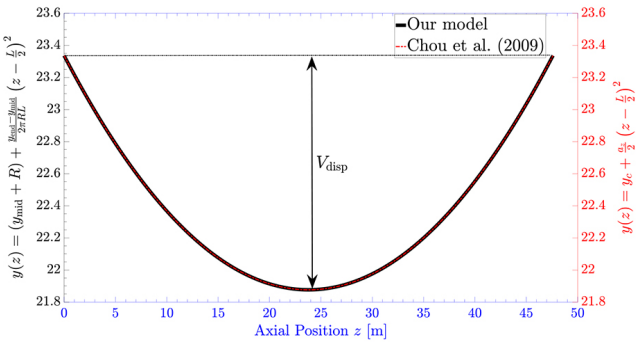

Figure 3—Axial surface profiles based on the data given in Table I. In the absence of measured values, y_c employed in Equation [1] is obtained using a least-squares fit of Equation [1] to the free surface profile in Figure 2

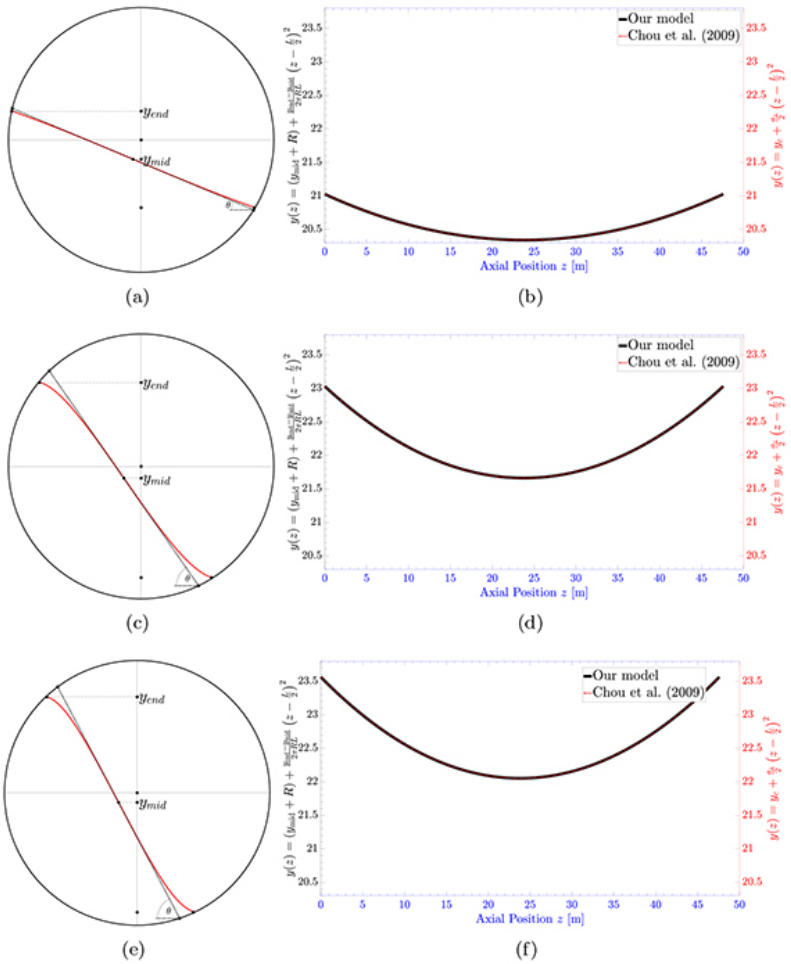

Figure 4—The effect of drum speed on the azimuthal and axial free surface profiles for the operating conditions specified in Table I. (a, b): 1% critical speed, (c, d): 40% critical speed, (e, f): 85% critical speed

the two lower speeds, and the highest curvature in the axial free surface, with V_{disp} = 1.5 cm. We also note that the trends found are very similar to the experimentally measured surface profiles by Chou and Lee (2009, see Figure. 22d in their paper).

Drum length

Using the configuration in Table I, we next varied the drum length in multiples of the drum radius – L = (R, 2R, 4R); see Figure 5. While the azimuthal free surface profile does not seem to vary much with drum length (Figures 5a, 5c, 5e), the axial free surface curvature definitely increases with increasing drum length (Figures 5b, 5d, 5f). Interestingly, V_{disp} doubles each time the drum length is doubled, suggesting a one-to-one doubling relationship between the drum length and V_{disp}. Consistent with the findings of Dury *et al.* (1998), when the drum is sufficiently long such that $L/2 > \xi$, the characteristic length of the boundary effects drops off sharply, leading to a slumped axial midsection of the bed that is characterized by a large value of V_{disp}. This might be the reason why the curvature follows a doubling relationship as opposed to a linear one.

Fill fraction

The final parametric study involves the drum fill fraction α. Again, using the configuration in Table I, the fill fraction was varied: α = 0.1, 0.2, 0.4, 0.8. The effect of increasing the drum fill fraction is to simply shift the axial free surface vertically upwards without much influence on V_{disp}. We note here that the insensitivity to fill fraction may be partly due to the limitations of the azimuthal free surface model.

Conclusion

A model of the axial free surface profile in a rotating drum was developed. While exhibiting a similar structure to the model of Chou and Lee (2009), the proposed model offers significant practical advantages over the former. In this regard, a well-chosen azimuthal free surface model is sufficient to numerically derive the key ingredients for the axial free surface model. A parametric study of the model considered variations in Froude regime, drum length, and fill fraction. The results appear consistent with the experimental findings of Chou and Lee (2009) and the numerical results obtained by Dury *et al.* (1998). The parametric study spanned operating conditions consistent with comminution practice in minerals processing as regards drum speed (< 85% of critical), drum aspect ratios (D:L = 2:1 – 1:2), and fill fractions (α = 0.2, 0.4); suggesting that the model can be used to complement understanding of segregation and transport in tumbling mills. On the rheological side, the realistic curvature response of the model to drum length suggests that the model inputs (y_{end} and y_{mid}) might be good proxies for the axial rheology that ultimately drives flow and shape in granular systems.

Future work will employ other azimuthal-free surface models (Rajchenbach, 1990); Yamane *et al.*, 1998; Taberlet *et al.*, 2006) in a similar parametric study. We also hope to incorporate measured free surface profiles *via* the technique of positron

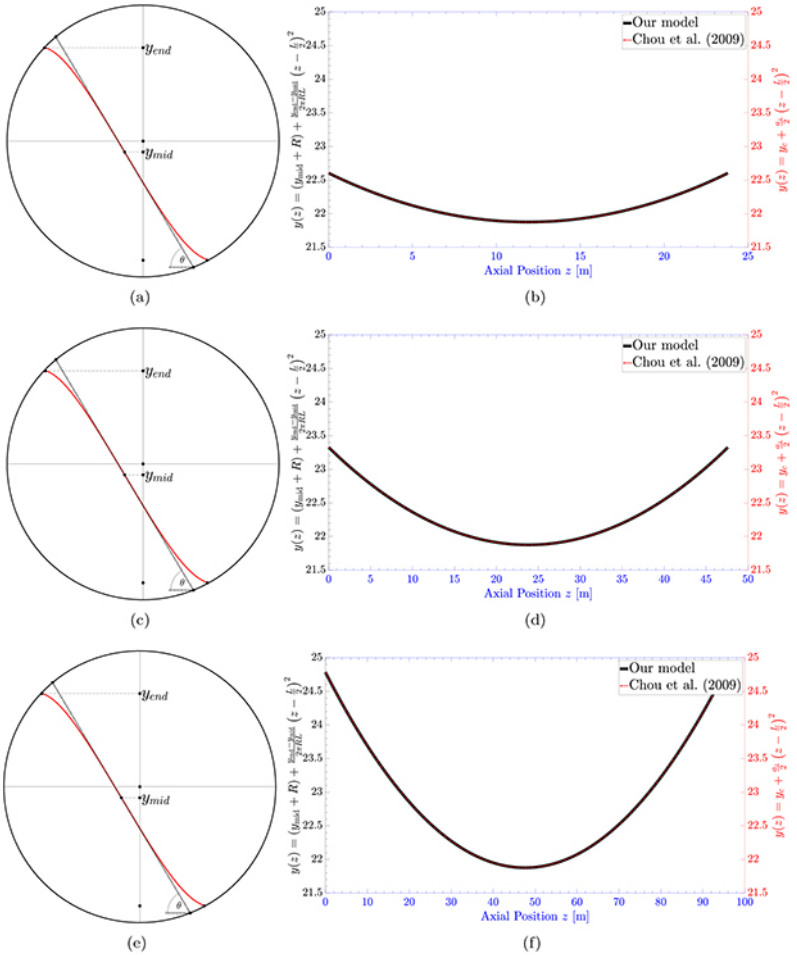

Figure 5—The effect of drum length L on the azimuthal and axial free surface profiles for the operating conditions specified in Table I. (a, b): L = R, (c, d): L = 2R, (e, f): L = 4R

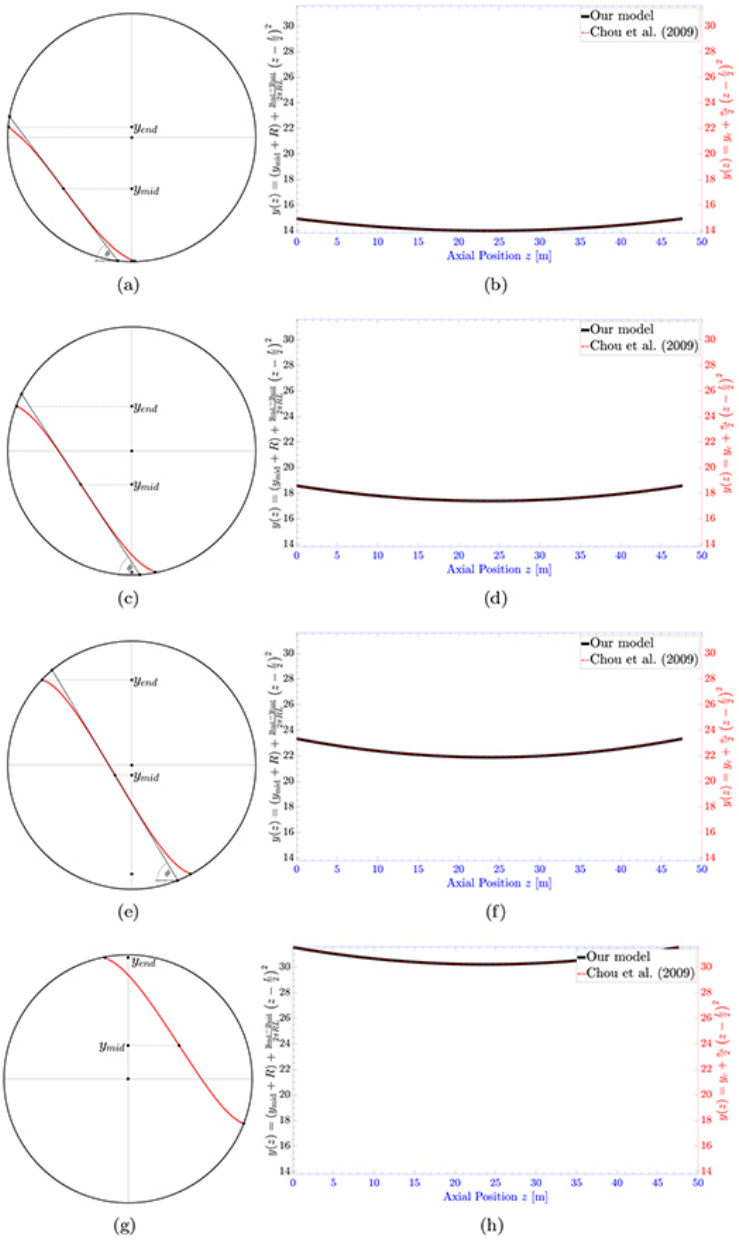

Figure 6—The effect of drum fill fraction α on the azimuthal and axial free surface profiles for the operating conditions specified in Table I. (a, b): α = 0.1, (c, d): α = 0.2, (e, f): α = 0.4, (g, h): α = 0.8

emission particle tracking and DEM with a view to building a semi-empirical formula that can be readily used to guide comminution transport optimization.

Acknowledgment

This work was supported by the Centre for Minerals Research (CMR) in the University of Cape Town Physics Department and the Department of Chemical Engineering at the University of KwaZulu-Natal.

References

Chou, H-T. and Lee, C-F. 2009. Cross-sectional and axial flow characteristics of dry granular material in rotating drums. *Granular Matter*, vol. 11, no. 1. pp. 3–32.

Dury, C.M., Ristow, G.H., Moss, J.M., and Nakagawa, M. 1998. Boundary effects on the angle of repose in rotating cylinders. *Physical Review E*, vol. 57. https://doi.org/10.1103/PhysRevE.57.4491

Perry, R.H. and Green, D.W. 1984. Perry's Handbook of Chemical Engineering. *Chemical Engineering Series*, McGraw Hill,New York.

Pignatel, F., Asselin, C., Krieger, L., Christov, I.C., Ottino, J.M., and Lueptow, R.M. 2012. Parameters and scalings for dry and immersed granular flowing layers in rotating tumblers. *Physical Review E*, vol. 86, no. 1. pp. 001304–12.

Rajchenbach, J. 1990. Flow in powders: From discrete avalanches to continuous regime. *Physical Review Letters,* vol. 65, no. 18. pp. 2221–2225.

Santomaso, A.C., Ding, Y.L., Lickiss, J.R., and York, D.W. 2003. Investigation of the granular behaviour in a rotating drum operated over a wide range of rotational speed. *Transactions of the Institute of Chemical Engineers*, vol. 81. pp. 936–945.

Seiden, G. and Thomas, P.J. 2011. Complexity, segregation, and pattern formaiton in rotating-drum flows. *Reviews of Modern Physics*, vol. 83. pp. 1323–1365.

Taberlet, N., Newey, M., Richard, P., and Losert, W. 2006. On axial segregation in a tumbler: An experimental and numerical study. *Journal of Statistical Mechanics: Theory and Experiment*, vol. 2006. P07013:041302.

Yamane, K., Nakagawa, M., Altobeli, S.A., Tanaka, T., and Tsuji, Y. 1998. Steady particulate flows in a horizontal rotating cylinder. *Physics of Fluids*, vol. 10. pp. 1419–1427.

Zik, O., Levine, D., Lipson, S.G., Shtrikman, S., and Stavans, J. 1994. Rotationally induced segregation of granular materials. *Physical Review Letters*, vol. 73. pp. 644–648. ◆

Obituary

Dennis Laubscher, Pioneer of block caving

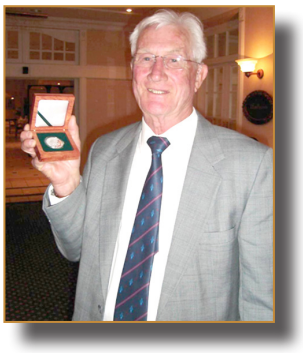

A legend in the mining industry, Dennis Laubscher, South Africa's and the world's foremost authority on block caving techniques, died 3 February at the age of 91 at Bushman's River Mouth, Eastern Cape. He is survived by four grown-up children (Susan Stampanoni, Dionne, Tessa, and Robert Laubscher) from his first marriage to Patricia May (nee Binnie) who died on 29 August, 2002; their elder son Carl having also passed away. On 27 February 2004, Dennis married Michelle (nee Broster).

Born in Tulbagh, Western Cape, on 1 October 1929, Dennis Laubscher earned a BSc (Eng.) in mining geology in 1952, and a PhD in 1964, both from the University of the Witwatersrand. His career was highlighted by numerous awards: the South Africa Institute of Mining and Metallurgy (SAIMM) Gold Medal in 1995; a Lifetime Achievement Award from the South African Institute of Rock Engineering in 1998; the De Beers Mass Mining Award at Massmin 2000; and the Brigadier Stokes Platinum Medal from SAIMM in 2007.

His career included a two-year stint as an exploration geologist with Bethlehem Steel and a 29-year career with African Associated Mines in Rhodesia (now Zimbabwe) as a mining geologist and geomechanics consultant. He joined Steffen Robertson and Kirsten, the forerunner of today's SRK Consulting, in Johannesburg in 1984.

Dennis founded his own consulting firm in 1987, and until shortly before his death he was active in Australia, Canada, Chile, Greece, Indonesia, Namibia, Papua New Guinea, Peru, the Philippines, South Africa, Swaziland, the USA, Zambia, and Zimbabwe.

In the 'seventies, while working on mines in Zimbabwe (Rhodesia), his first major contribution to the caving industry was the introduction of the Mining Rock Mass Rating system – MRMR. This classification system evolved from Z.T. Bieniawski's rock mass rating system (RMR) and was specifically designed for the caving mines and for mining practitioners to effectively communicate between disciplines and provide a tool for developing empirical guidelines for mining method selection, and cave design. Laubscher and Jakubec updated this classification system in 2000 and it is used successfully as a 'yardstick' in the industry today.

In 2000 the International Caving Study, the first comprehensive study on the subject, published a practical manual on block caving authored by Laubscher. This manual was not widely available, but demand for more information about the method was growing. So, in 2017, using the previous manual as background information, the Guidelines on Caving Mining Methods, co-authored by Dennis, Alan Guest, and Jarek Jakubec, was published by the University of Queensland in Australia.

As he travelled the world, Dennis made unique and lasting friendships while mentoring others. His colleagues around the world responded to news of his death with observations on his legacies. An 'uncompromising humanist,' he made an impact on people as well as projects. He has been called a 'titan' of the mining industry, a 'pioneer' of block caving, and 'the John Wayne of rock mechanics.'

The mining world has indeed lost a true original. Dennis Laubscher's contributions to the industry and its people will remain a stellar legacy.

NATIONAL & INTERNATIONAL ACTIVITIES

2021

9–10 June 2021 — **Diamonds – Source To Use — 2021 Hybrid Conference**
'Innovation And Technology'
The Canvas, Riversands, Fourways, South Africa
Contact: Camielah Jardine
Tel: +27 11 834-1273/7, Fax: +27 11 838-5923/833-8156
E-mail: camielah@saimm.co.za, Website: http://www.saimm.co.za

21–22 June 2021 — **Mandela Mining Precinct Virtual Symposium**
'Beneficiating Three Years' of Research, Development and Innovation'
Contact: Camielah Jardine
Tel: +27 11 834-1273/7, Fax: +27 11 838-5923/833-8156
E-mail: camielah@saimm.co.za, Website: http://www.saimm.co.za

23–25 June 2021 — **ROLLS6 2021**
London, UK
Contact: Chelsea Wallis
Tel: +44 (0)207 451 7302

24–26 June 2021 — **AGROMIN II AGRO-Mining Convention - Agriculture and Mining joined by Nature**
Trujillo, Peru
Contact: (51-1) 989-590-328
E-mail: informes@agrominperu.com, peru.agromin@gmail.com

27–30 June 2021 — **European Metallurgical Conference, EMC 2021**
Salzburg, Austria
Tel: +49 (5323) 93 79-0
E-Mail: verein@gdmb.de, Website: https://emc.gdmb.de/contact/

28–30 June 2021 — **Renewable Solutions for an Energy Intensive Industry Hybrid Conference 2021**
Mintek, Randburg, South Africa
Contact: Camielah Jardine
Tel: +27 11 834-1273/7, Fax: +27 11 838-5923/833-8156
E-mail: camielah@saimm.co.za, Website: http://www.saimm.co.za

1–2 July 2021 — **The Mine Waste & Tailings Stewardship Conference 2021**
Brisbane, Australia
Website: https://www.ausimm.com/conferences-and-events/mine-waste-and-tailings/

13–16 July 2021 — **Copper Cobalt Africa** *Incorporating* **The 10th Southern African Base Metals Conference**
Avani Victoria Falls Resort, Livingstone, Zambia
Contact: Camielah Jardine
Tel: +27 11 834-1273/7, Fax: +27 11 838-5923/833-8156
E-mail: camielah@saimm.co.za, Website: http://www.saimm.co.za

28 July – 22 September 2021 — **5th Mineral Project Valuation Hybrid Colloquium**
The Canvas Riversands, Fourways, Johannesburg
Contact: Gugu Charlie
Tel: +27 11 834-1273/7, Fax: +27 11 838-5923/833-8156
E-mail: gugu@saimm.co.za, Website: http://www.saimm.co.za

3–4 August 2021 — **DIMI (Diversity and Inclusion in the Minerals Industry) Hybrid Conference 2021**
'Empowering the African minerals industry through diversity and inclusion'
The Canvas, Riversands, Fourways, South Africa
Contact: Camielah Jardine
Tel: +27 11 834-1273/7, Fax: +27 11 838-5923/833-8156
E-mail: camielah@saimm.co.za, Website: http://www.saimm.co.za

16–17 August 2021 — **Worldgold Online Conference 2021**
Misty Hills Conference Centre, Muldersdrift, Johannesburg, South Africa
Contact: Camielah Jardine
Tel: +27 11 834-1273/7, Fax: +27 11 838-5923/833-8156
E-mail: camielah@saimm.co.za, Website: http://www.saimm.co.za

29 August–2 September 2021 — **APCOM 2021 Minerals Industry Hybrid Conference**
'The next digital transformation in mining'
Misty Hills Conference Centre, Muldersdrift, Johannesburg, South Africa
Contact: Camielah Jardine
Tel: +27 11 834-1273/7, Fax: +27 11 838-5923/833-8156
E-mail: camielah@saimm.co.za, Website: http://www.saimm.co.za

21–22 September 2021 — **5th Young Professionals Hybrid Conference 2021**
'A Showcase of Emerging Research and Innovation in the Minerals Industry'
The Canvas, Riversands, Fourways, South Africa
Contact: Gugu Charlie
Tel: +27 11 834-1273/7, Fax: +27 11 838-5923/833-8156
E-mail: gugu@saimm.co.za, Website: http://www.saimm.co.za

23–24 September 2021 — **3rd Global Engineering Online Symposium**
'Bridging the gap between research (academia) and industry while transitioning into 4IR'
Contact: Gugu Charlie
Tel: +27 11 834-1273/7, Fax: +27 11 838-5923/833-8156
E-mail: gugu@saimm.co.za,Website: http://www.saimm.co.za

26–29 September 2021 — **The 16th International Ferroalloys Congress (INFACON XVI)**
Clarion Hotel & Congress, Trondheim, Norway
infacon2021@videre.ntnu.no

18–19 October 2021 — **Southern African Rare Earths International Conference 2021**
Misty Hills Conference Venue, Muldersdrift, Johannesburg, South Africa
Contact: Camielah Jardine
Tel: +27 11 834-1273/7, Fax: +27 11 838-5923/833-8156
E-mail: camielah@saimm.co.za, Website: http://www.saimm.co.za

26–27 October 2021 — **SAMCODES Conference 2021**
'Good Practice and Lessons Learnt'
The Canvas Riversands, Fourways, South Africa
Contact: Gugu Charlie
Tel: +27 11 834-1273/7, Fax: +27 11 838-5923/833-8156
E-mail: gugu@saimm.co.za, Website: http://www.saimm.co.za

15–17 November 2021 — **Global Tailings Standards and Opportunities Hybrid Conference 2021**
'For the Mine of the Future'
Misty Hills Conference Venue, Muldersdrift, Johannesburg, South Africa
Contact: Gugu Charlie
Tel: +27 11 834-1273/7, Fax: +27 11 838-5923/833-8156
E-mail: gugu@saimm.co.za, Website: http://www.saimm.co.za

Company affiliates

The following organizations have been admitted to the Institute as Company Affiliates

3M South Africa (Pty) Limited
AECOM SA (Pty) Ltd
AEL Mining Services Limited
African Pegmatite (Pty) Ltd
Air Liquide (Pty) Ltd
Alexander Proudfoot Africa (Pty) Ltd
AMEC Foster Wheeler
AMIRA International Africa (Pty) Ltd
ANDRITZ Delkor(pty) Ltd
Anglo Operations Proprietary Limited
Anglogold Ashanti Ltd
Arcus Gibb (Pty) Ltd
ASPASA
Aurecon South Africa (Pty) Ltd
Aveng Engineering
Aveng Mining Shafts and Underground
Axiom Chemlab Supplies (Pty) Ltd
Axis House (Pty) Ltd
Bafokeng Rasimone Platinum Mine
Barloworld Equipment -Mining
BASF Holdings SA (Pty) Ltd
BCL Limited
Becker Mining (Pty) Ltd
BedRock Mining Support (Pty) Ltd
BHP Billiton Energy Coal SA Ltd
Blue Cube Systems (Pty) Ltd
Bluhm Burton Engineering (Pty) Ltd
Bond Equipment (Pty) Ltd
Bouygues Travaux Publics
Castle Lead Works
CDM Group
CGG Services SA
Coalmin Process Technologies CC
Concor Opencast Mining
Concor Technicrete
Council for Geoscience Library
CRONIMET Mining Processing SA (Pty) Ltd
CSIR Natural Resources and the Environment (NRE)
Data Mine SA
Digby Wells and Associates
DRA Mineral Projects (Pty) Ltd
DTP Mining - Bouygues Construction
Duraset
Elbroc Mining Products (Pty) Ltd
eThekwini Municipality
Ex Mente Technologies (Pty) Ltd
Expectra 2004 (Pty) Ltd
Exxaro Coal (Pty) Ltd
Exxaro Resources Limited
Filtaquip (Pty) Ltd
FLSmidth Minerals (Pty) Ltd
Fluor Daniel SA (Pty) Ltd
Franki Africa (Pty) Ltd-JHB
Fraser Alexander (Pty) Ltd
G H H Mining Machines (Pty) Ltd
Geobrugg Southern Africa (Pty) Ltd
Glencore
Gravitas Minerals (Pty) Ltd
Hall Core Drilling (Pty) Ltd
Hatch (Pty) Ltd
Herrenknecht AG
HPE Hydro Power Equipment (Pty) Ltd
Immersive Technologies
IMS Engineering (Pty) Ltd
Ingwenya Mineral Processing (Pty) Ltd
Ivanhoe Mines SA
Joy Global Inc.(Africa)
Kudumane Manganese Resources
Leica Geosystems (Pty) Ltd
Longyear South Africa (Pty) Ltd
Lull Storm Trading (Pty) Ltd
Maccaferri SA (Pty) Ltd
Magnetech (Pty) Ltd
MAGOTTEAUX (PTY) LTD
Malvern Panalytical (Pty) Ltd
Maptek (Pty) Ltd
Maxam Dantex (Pty) Ltd
MBE Minerals SA Pty Ltd
MCC Contracts (Pty) Ltd
MD Mineral Technologies SA (Pty) Ltd
MDM Technical Africa (Pty) Ltd
Metalock Engineering RSA (Pty) Ltd
Metorex Limited
Metso Minerals (South Africa) Pty Ltd
Micromine Africa (Pty) Ltd
MineARC South Africa (Pty) Ltd
Minerals Council of South Africa
Minerals Operations Executive (Pty) Ltd
MineRP Holding (Pty) Ltd
Mining Projections Concepts
Mintek
MIP Process Technologies (Pty) Ltd
MLB Investment CC
Modular Mining Systems Africa (Pty) Ltd
MSA Group (Pty) Ltd
Multotec (Pty) Ltd
Murray and Roberts Cementation
Nalco Africa (Pty) Ltd
Namakwa Sands (Pty) Ltd
Ncamiso Trading (Pty) Ltd
New Concept Mining (Pty) Ltd
Northam Platinum Ltd - Zondereinde
Opermin Operational Excellence
OPTRON (Pty) Ltd
Paterson & Cooke Consulting Engineers (Pty) Ltd
Perkinelmer
Polysius A Division Of Thyssenkrupp Industrial Sol
Precious Metals Refiners
Rams Mining Technologies
Rand Refinery Limited
Redpath Mining (South Africa) (Pty) Ltd
Rocbolt Technologies
Rosond (Pty) Ltd
Royal Bafokeng Platinum
Roytec Global (Pty) Ltd
RungePincockMinarco Limited
Rustenburg Platinum Mines Limited
Salene Mining (Pty) Ltd
Sandvik Mining and Construction Delmas (Pty) Ltd
Sandvik Mining and Construction RSA (Pty) Ltd
SANIRE
Schauenburg (Pty) Ltd
Sebilo Resources (Pty) Ltd
SENET (Pty) Ltd
Senmin International (Pty) Ltd
SISA Inspection (Pty) Ltd
Smec South Africa
Sound Mining Solution (Pty) Ltd
SRK Consulting SA (Pty) Ltd
Time Mining and Processing (Pty) Ltd
Timrite Pty Ltd
Tomra (Pty) Ltd
Ukwazi Mining Solutions (Pty) Ltd
Umgeni Water
Webber Wentzel
Weir Minerals Africa
Welding Alloys South Africa
Worley

SAIMM ONLINE

COLLOQUIUM

17TH ANNUAL STUDENT COLLOQUIUM

11 NOVEMBER 2021

The Southern African Institute of Mining and Metallurgy has been organizing and presenting the annual Student Colloquium since 2002, to afford the best final-year mining and metallurgical students an opportunity to present their final year projects to an audience of mining and metallurgical industry experts.

These students are our future young professionals and will be fundamentally affected by how the industry operates. We have to support and assist our future young professionals! As Nelson Mandela observed: 'Education is the most powerful weapon which you can use to change the world'.

The SAIMM cordially invites our experts in the field to meet the fine calibre of young professionals who are about to embark on their careers in industry. There are 11 mining and 11 metallurgical presentations planned for the event, to be held at Johannesburg on 11 November 2021 . The top five in each discipline will have the opportunity to be published in the prestigious SAIMM Journal in April 2022. The presentations selected will be required to be submitted in the form of draft papers before 12 October 2021.

Our strategy is: To contribute to the nurturing of prosperous and empowered young professionals.

SUPPORTED BY

NWU North-West University Noordwes-Universiteit Yunibesithi ya Bokone-Bophirima

Tshwane University of Technology — We empower people

VUT — Vaal University of Technology — Your world to a better future

UNAM University of Namibia

Namibia University of Science and Technology

Universiteit van Pretoria — University of Pretoria — Yunibesithi ya Pretoria

University of the Witwatersrand, Johannesburg

The University of Zambia — Service and Excellence

FOR FURTHER INFORMATION, CONTACT:

Gugu Charlie,
Conference Co-ordinator

E-mail: gugu@saimm.co.za
Tel: +27 11 834-1273/7
Web: www.saimm.co.za

YPC SAIMM Young Professionals Council

SAIMM The Southern African Institute of Mining and Metallurgy

SAIMM HYBRID CONFERENCE

YOUNG PROFESSIONALS COUNCIL

5TH YOUNG PROFESSIONALS CONFERENCE

A SHOWCASE OF EMERGING RESEARCH AND INNOVATION IN THE MINERALS INDUSTRY

21-22 SEPTEMBER 2021

THE CANVAS, RIVERSANDS, FOURWAYS

2 CPD POINTS

Innovation and research into mining technology is necessary to position Africa as a world leader in minerals production and beneficiation. The Young Professionals Council is pleased to host a unique, two-day conference that will showcase a broad range of emerging research and innovation from young professionals in the metals and minerals industry. Presentations will focus on new technology, tools and techniques relevant to exploiting Africa's mineral resources safely, competitively and sustainably.

OBJECTIVES

- a broad range of topics covering the entire mining value-chain will give a quick sense of developments in the field of mining and metallurgy
- a large body of research at Masters, PhD and Post-doctoral level will give insights into emerging themes and advances in the minerals and metals knowledge-areas
- a focus on innovative practices, technological applications and case-studies from mining operations and research institutions will give the practicing professional an opportunity to learn about new tools and techniques relevant to their work
- a gathering of diverse professionals within the metals and minerals community will give delegates an opportunity to obtain exposure, build reputations, further their careers and network with peers and leaders in the African Minerals Industry

WHO SHOULD ATTEND

This conference should be of value to all professionals across the entire minerals industry value chain, including:

- All metallurgical fields
- Exploration
- Geology
- Geotechnical engineering
- Leadership/management/government/community
- Mining
- Occupational Hygiene and SHE practitioners
- ICT experts
- Mechanical, electrical/electronic engineers
- Mineralogy

EXHIBITION/SPONSORSHIP

Sponsorship opportunities are available. Companies wishing to sponsor or exhibit should contact the Conference Co-ordinator.

EVENT FORMAT

At this point in time, the event is planned as a hybrid conference. However, as we are still in lock down as a result of COVID-19, this will be constantly reviewed, and if it appears that the effects of the pandemic are still such as to pose a threat to the health and safety of delegates, this will be changed to a digital event.

Please advise on your submission if you will be presenting in person or virtually. Virtual presentations will be streamed live or pre-recorded.

Please continue to submit your abstracts and check www.saimm.co.za regularly for updates.

FOR FURTHER INFORMATION, CONTACT:

Gugu Charlie,
Conference Co-ordinator

E-mail: gugu@saimm.co.za
Tel: +27 11 834-1273/7
Web: www.saimm.co.za